(BIS)PHOSPHONATE FUNCTIONALIZED POLYMERIC MATERIALS FOR BIOMEDICAL APPLICATIONS

by

Merve Seçkin Altuncu

B.S., Chemistry, Middle East Technical University, 2012

M.S., Chemistry, Boğaziçi University, 2015

Submitted to the Institute for Graduate Studies in

Science and Engineering in partial fulfillment of

the requirements for the degree of

Doctor of Philosophy

Graduate Program in Chemistry

Boğaziçi University

2022

ACKNOWLEDGEMENTS

I would wish to express my gratitude and thanks to my thesis supervisor Prof. Duygu Avcı Semiz for her endless attention, guidance and support throughout this work. It was a great pleasure to do research under her supervision. I have learned many valuable lessons from her that I will keep with me for the rest of my career.

I would like to express my appreciation to Prof. André Laschewsky for giving me the opportunity to take part in his research group at Potsdam University and enlarge my vision with his guidance. I would also wish to express my thanks to Prof. Havva Yağcı Acar and Prof. Oğuz Okay for their fruitful collaboration and recommendations to my graduate studies. I also want to extend my thanks to my examining committee Assoc. Prof. Ali Ersin Acar, Assist. Prof. Sesil Çınar, Prof. Nihan Nugay for their constructive review of the final manuscript of the thesis.

I would also like to thank Dr. Ayla Türkekul Bıyık, Dr. Bilge Gedik Uluocak for characterization of my samples through NMR and SEM; Asst. Prof. Ümit Gülyüz for his help in uniaxial compression measurements; Dr. Fatma Demir Duman and Gözde Demirci for their contribution in cytotoxicity studies, Assoc. Prof. Keziban Olcay for her help in dental sample preparation.

I would like to acknowledge The Scientific and Technological Research Council of Turkey (TÜBİTAK) for 2214-A International Research Fellowship Programme for PhD Students. Financial support for research and scientific activities through TÜBİTAK (117Z330 and 114Z926) is also acknowledged.

My special thank goes to my current and former labmates Melek, Türkan, Tuğçe, Betül, Burcu, Neslihan and Simay for their friendship, support and creating a pleasant working environment. I also want to thank Prof. Laschewsky's group members, Michelle,

Cristiane and Alejandro, for giving me a friendly working environment. I am thankful to all members of Chemistry Department, especially Özge Akdeniz for her endless motivation.

I would like to thank Fatma Hakkıoğlu, Kübra Kaytancı, Kübra Toka and Hazal Şenses for being my second family in İstanbul. I am grateful for their endless support and all memories we shared during my graduate years.

Last but not least, my deepest gratitude goes to my family for their endless love and support. I am grateful to my mother for teaching me not to give up which helped me a lot throughout this journey. I would like to thank my father for believing in me sometimes more than I do and making me feel that everything will be alright. I am thankful to my sister Sema for being my closest friend. I dedicate this thesis to my family, especially to my little sunshine Elif Su for giving me happiness and energy whenever I need.

ABSTRACT

(BIS)PHOSPHONATE FUNCTIONALIZED POLYMERIC MATERIALS FOR BIOMEDICAL APPLICATIONS

This work describes synthesis, characterization, and evaluation of (bis)phosphonate functionalized monomers, macromers and crosslinkers as well as their polymers and crosslinked networks for biomedical applications such as tissue engineering scaffolds, dental materials and targeted drug delivery. Various synthetic approaches were explored for incorporation of (bis)phosphonate functionality and tailoring of these materials' properties such as degradation rate, mechanical moduli, mineralization ability, water solubility and hydroxyapatite affinity. In the first part, three novel phosphonate/phosphonic acid functionalized poly (β-amino ester) (PBAE) macromers with varying levels of hydophilicity were synthesized and homo- and copolymerized with poly(ethylene glycol) diacrylate (PEGDA) to fabricate networks with tunable degradation and mechanical properties. The second part reports synthesis of three novel phosphonic acid containing poly (amido amine) macromers and their homo- and copolymerization with 2-hydroxyethyl methacrylate to obtain hydrogels showing composition-dependent swelling, degradation and mineralization. In the third part, two different types of bisphosphonate/bisphosphonic acid functional thermoresponsive polymers were synthesized (i) by copolymerization of three novel bisphosphonate functionalized acrylamide monomers containing different alkyl chains with N-isopropyl acrylamide, (ii) alendronate functionalization of a copolymer of NIPAM and 6-acrylamidohexanoic acid. In the last part, alendronate was incorporated into two carboxylic acid containing polymers (ibuprofen functionalized alkyl α-hydroxymethacrylate and 6-acrylamidohexanoic acid based polymers) via covalent and non-covalent interactions to enhance their hydroxyapatite affinity.

The materials synthesized here have potential for (mostly bone-related) biomedical applications such as tissue engineering and targeted controlled drug delivery; and the methods can be used to fabricate more such materials, tailoring their properties to fit the desired application.

ÖZET

BİYOMEDİKAL UYGULAMALAR İÇİN (BİS)FOSFONAT FONKSİYONLANDIRILMIŞ POLİMERİK MALZEMELER

Bu çalışma, (bis)fosfonat fonksiyonlandırılmış monomerlerin, makromerlerin, çapraz bağlayıcıların ilaveten bunların polimerlerinin ve çapraz bağlı polimerlerin sentezini, karakterizasyonunu ve değerlendirilmesini raporlamaktadır. (Bis)fosfonat fonksiyonel grubunu eklemek ve malzemelerin bozunma hızı, mekanik modülleri, mineralizasyon yeteneği, suda çözünürlük ve hidroksiapatit ile etkileşim eğilimini kontrol edebilmek için çeşitli sentetik yaklaşımlar araştırılmıştır. İlk bölümde, farklı hidrofilik özellikte üç yeni fosfonat/fosfonik asit fonksiyonlu poli(β-aminoester) makromer sentezlendi ve ayarlanabilir bozunma ve mekanik özelliklere sahip jeller elde etmek için homopolimerleştirildi ve poli(etilen glikol) diakrilat (PEGDA) ile kopolimerleştirildi. İkinci bölümde, fosfonik asit içeren üç yeni poli (amido amin) makromerin sentezi ve şişme, bozunma ve mineralizasyonları kompozisyona bağlı hidrojeller elde etmek amacıyla bu makromerlerin homo- ve 2-hidroksietil metakrilat ile kopolimerizasyonları raporlandı. Üçüncü bölümde, bisfosfonat/bisfosfonik asit fonksiyonlu iki farklı çeşit ısıya duyarlı polimer sentezlendi: (i) farklı alkil zincirlerine sahip bisfosfonat fonksiyonlu üç yeni akrilamid monomerinin N-izopropil akrilamid (NIPAM) ile kopolimerizasyonu, (ii) NIPAM ve 6-akrilamidohekzanoik asit kopolimerinin alendronat ile fonksiyonlandırılması. Son olarak, hidroksiapatit afinitelerini arttırmak için iki karboksilli asit içeren polimere (ibuprofen fonksiyonlu alkil α-hidroksimetakrilat ve 6-akrilamidohekzanoik asit bazlı polimerler) alendronat kovalent ve elektrostatik etkileşimler yoluyla eklenildi.

Bu tezde sentezlenen malzemeler doku mühendisliği ve hedefle yönelik kontrollü ilaç salımı gibi biyomedikal (daha çok kemik ile ilişkili) uygulamalar için kullanılma potansiyaline sahiptir. Kullanılan metodlar bu tür başka malzemelerin üretiminde ve bunların özelliklerini hedeflenen kullanıma uygun olarak ayarlayabilmekte kullanılabilir.

TABLE OF CONTENTS

LIST OF FIGURES

LIST OF TABLES

LIST OF SYMBOLS

σ_{nom}	Compressive stress
ν_2	Volume fraction
ν_e	Effective crosslink density
ε	Extinction coefficient and Strain
E	Young's modulus
J	Coupling constant
Q	Degree of swelling
M_n	Number average molecular weight
Hz	Hertz
pH	Power of hydrogen
pK_b	Base dissociation constant
T_g	Glass transition temperature

LIST OF ACRONYMS/ABBREVIATIONS

AIBN	2,2′-azobis(isobutyronitrile)
AEPA	2-aminoethyl phosphonic acid
ALN	Alendronate
AP	5-amino-1-pentanol
ATRP	Atom transfer radical polymerization
BDDA	1,4-butanediol diacrylate
BP	Bisphosphonate
Cat K	Cathepsin K enzyme
CTA	Chain transfer agent
DCM	Dicholoromethane
DMEM	Dulbecco’s modified eagle medium
DMPA	2,2-Dimethoxy-2-phenylacetophenone
DMSO	Dimethyl sulfoxide
DNA	Deoxyribonucleic acid
DOX	Doxorubicin
DSC	Differential scanning calorimetry
DTT	Dithiothreitol
EDC	N-(3-Dimethylaminopropyl)-N′-ethylcarbodiimide hydrochloride
EDTA	Ethylenediaminetetraacetic acid
EDX	Energy-dispersive X-ray spectroscopy
EPR	Enhanced permeability and retention

FBS	Fetal bovine serum
FRP	Free radical polymerization
FT-IR	Fourier transform infrared spectroscopy
GPC	Gel permeation chromatography
GSH	Glutathione
HAP	Hydroxyapatite
HDDA	1,6-Hexane diol diacrylate
HDEDA	1,6-hexanediol ethoxylate diacrylate
HEMA	2-Hydroxyethyl methacrylate
HEPES	4-(2-hydroxyethyl)-1-piperazineethanesulfonic acid
Irgacure 2959	2-Hydroxy-1-[4-(2-hydroxyethoxy)phenyl]-2-methyl-1-
LCST	Lower critical solution temperature
LRP	Living radical polymerization
MAM	More activated monomers
MBA	Methylene bisacrylamide
MDP	10-Methacryloyloxydecyl dihydrogen phosphate
MTT	Thiazolyl blue tetrazolium bromide
NHS	N-hydroxysuccinimide
NIH 3T3	Mouse embryonic fibroblast cells
NIPAM	N-isopropyl acrylamide
NMR	Nuclear magnetic resonance spectroscopy
PAA	Poly(amido amine)
PAMAM	Dendrimeric poly (amido amine)
PBAE	Poly(β-amino ester)

PBS	Phosphate buffered saline
PCG	Phosphorous containing groups
PDI	Polydispersity index
PEG	Poly(ethylene) glycol
PEGDA	Poly(ethylene glycol) diacrylate
PEGMA	Poly(ethyleneglycol) methyl ether methacrylate
PEI	Polyethylene imine
RAFT	Reversible addition-fragmentation chain transfer
RGD	Arginylglycylaspartic acid peptide
RPMI	Roswell Park Memorial Institute
Saos-2	Human osteogenic sarcoma cells
SBF	Simulated body fluid
SEC	Size exclusion chromatography
SEM	Scanning electron microscope
TEA	Triethylamine
TFA	Trifluoroacetic acid
TGA	Thermogravimetric analysis
THF	Tetrahydrofuran
TMS	Tetramethylsilane
TMSBr	Trimethylsilyl bromide
TMSP	Tris(trimethylsilyl)phosphite
UV	Ultraviolet
U-2 OS	Human bone osteosarcoma epithelial cells
XRD	X-ray diffraction

1. INTRODUCTION

1.1. Developments in Biomaterials

Biomaterials are defined as substances engineered to interface with biological systems to evaluate, treat, augment, or replace any tissue, organ, or function of the body [1]. Developing new biomaterials is important for improving the quality of living in a society where life expectancy is increasing. Biomaterial science which is the combination of medicine, biology, chemistry, tissue engineering and materials science, helps in the treatment of many illnesses caused by increase in the average lifetime. Cardiovascular applications such as artificial arteries and heart valve prostheses, and orthopedic implants dominate the market. In addition to that, technological advancements in the diagnosis of diseases or healing, and rising demand for plastic surgery are other driving forces in the growth of the biomaterials market [2]. According to a report prepared by Markets and Markets, the global biomaterials market is expected to reach USD 207 billion by 2024 which is almost two times bigger than the market size of 2019 [3].

The biomaterial concept is not new, it existed even in prehistorical times. For instance, in ancient Phoenicia carved dog or calf tooth was tied with gold wires to neighbouring teeth to mimic the lost one [4]. In the 1900s remarkable success was achieved thanks to the improvements in material science and surgical techniques (Figure 1.1). To give an example, the first total hip replacement prosthesis surgery was performed in 1938. Over the past few decades, biomaterials have broadened their applications from contact lenses and therapeutic medications to biosensors and medical equipment. Main application areas of biomaterials can be classified as orthopedic, dental, cardiovascular and ophthalmologic applications, tissue engineering, drug delivery, wound healing, organ implantations, bioelectrodes and sensors [5, 6]. Although the application area stays the same, materials are replaced with the newer ones to get better performance.

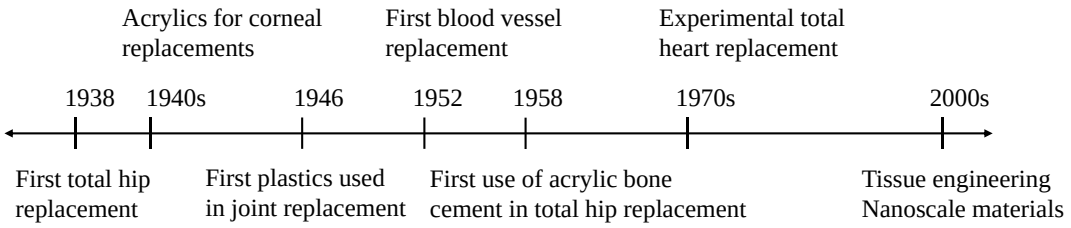

Figure 1.1. History of biomaterials. Adapted from [6].

The fundamental prerequisite of a material to function as a biomaterial is biocompatibility which can be defined as the ability to perform with an appropriate host response during a specific application [1]. In other words, a biomaterial should be nontoxic unless it is specifically designed to be so. The bio prefix of biomaterials remarks to biocompatible, rather than biological [7]. Furthermore, it is important to note that biocompatibility of a material depends on its surrounding tissue, hence the end-use application.

To meet the requirements of various applications, diversified materials such as metals, ceramics, composites, and polymers are utilized [8]. Different atomic arrangement and bonding of each substance cause different physical, chemical, and mechanical properties which are determinants to decide a material's role as a biomaterial. To give an example, a strong and rigid material that can be used as a hip joint is improper for heart valve leaflet which must flex 60 times per minute without tearing [8]. As seen from the Table 1.1, polymers which are long molecules synthesized by repeating of small units, have a wide range of application areas [9]. Flexibility in their synthesis enables them to have diverse physical, chemical and mechanical properties. Moreover, modification of polymers with functional groups is widely used to obtain smart, sophisticated, and multifunctional systems which are demanded in the last two decades.

Table 1.1. Advantages, disadvantages, and main application areas of materials. Adapted from [5,6].

Class of the Material	Advantages	Disadvantages	Main Application
Polymers			
Nylon, silicones, PTFE	*Resilient *Easy to fabricate	*Not strong *Deform with time	Reconstructive surgery, prosthesis in cardiovascular devices, opthalmology, wound healing, bioelectrodes, drug delivery
Metals			
Titanium, stainless steels, Co-Cr alloys, gold	*Strong *Tough *Ductile	*May corrode *High density	Orthopedic and dental implants, stents for cardiovascular surgeries
Composites			
Various combination	*Strong *Tailor-made	*Difficult to make	Hard tissue and joint replacement applications
Ceramics			
Aluminium oxide, carbon, hydroxyapatite	*Inert, *High modulus, *Compressive strength	*Brittle *Difficult to make *Poor fatigue resistance	Orthopedic and dental implants, musculosketal system, drug delivery

Other than chemical composition, biomaterials can be classified based on their interaction with the living body. During the 1960s and 1970s, biomaterials were preferred to be inert to prevent toxic reactions. The first generation of biomaterials only contributed structural support. After 1980s the knowledge regarding biological mechanisms has increased and the trend of choosing material has shifted from inert to active. Today materials are designed to interact with the body in a positive manner and even stimulate healing process [10]. Innovative smart biomaterials which are able to alter their properties in

response to stimuli offers many potential to broaden the boundaries of modern medicine [11]. Montoya et. al divided the materials into four categories which are inert, active, responsive, and autonomous regarding their interaction level with the environment and the ensuing biological responses (Figure 1.2). This classification represents how smart material is. Active materials can release a one-way bioactive therapy, but limited control on release might cause burst effect which is the main limitation of these materials. Responsive materials release specific therapeutic agents after sensing a stimulus such as mechanical stress, surface charge, temperature, pH level or a specific molecule. Autonomous materials, smartest ones, are self-sufficient. Such technologies are able to anticipate a defect at the earliest stage, communicate its presence outside of the body, and handle before observing any harmful outcome [12].

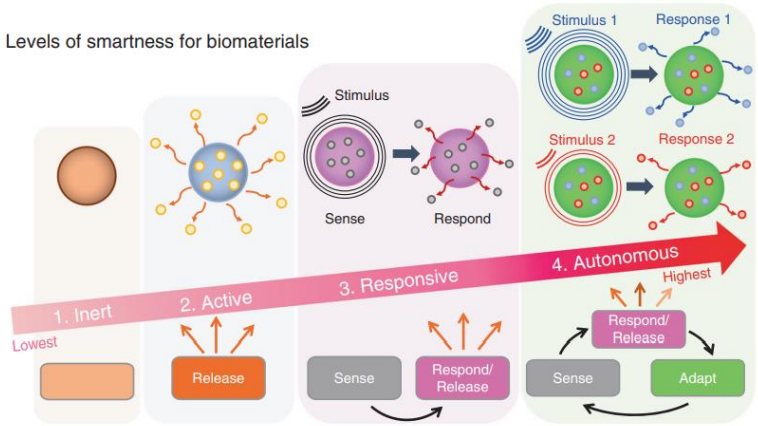

Figure 1.2. Four categories of materials regarding to their interactions. Reprinted from [12].

1.2. Poly(β-amino ester)s (PBAEs) and Poly(amido amine)s (PAAs)

1.2.1. Biodegradable Polymers

The evolution in biomedical technologies such as tissue engineering, regenerative medicine and drug delivery applications causes a shift from biostable biomaterials to biodegradable ones [1]. The long-term biocompatibility problems, which can be defined as

foreign body response, and the requirement for a second removal surgery of permanent biomaterials bring about an interest in the development of new biodegradable polymers. Biodegradable polymers whose degradation products are nontoxic have an active biocompatibility which must be proved over time. Moreover, the continuous changes in the properties of biodegradable polymer and degradation time should be in harmony with the healing or regeneration process [1,12]. The chemical, physical, mechanical and biological properties should match the requirements of the application. The wide scope of applications creates an urgency to develop custom designed polymers with tailored features for the desired function. Synthetic polymers have some advantages over natural polymers in flexibility in chemistry such as adjustable hydrophobicity, monomer type, degradation rate and time. On the other side, excellent biocompatibility and ability to mimic native cellular environments are the benefits of natural polymers [13].

Biodegradable polymers can be classified into hydrolytically and enzymatically degradable based on their cleavable bonds. Most of the natural polymers degrade in the presence of an enzyme. On the other hand, the polymers containing esters, anhydrides, carbonates, acetals, amides, urethanes and phosphates undergo hydrolysis. The characteristics of these polymeric families are shown in the Table 1.2. Degradation rates of these polymers can vary 12-fold from hydrolytically unstable (polyphosphazenes) to very stable (polyamides, rate constant 10^{-13} s^{-1}). Furthermore, degradation rate constant of polyanhydrides changes between 10^{-3} to 10^{-9} depending on polymer chemistry [14] . Erosion mechanism of the polymer family which is affected by water diffusion and monomer solubility has also an important impact on its function as a biomaterial [15]. To illustrate, bulk eroding materials in which fast water diffusion causes mass loss throughout the whole material are preferred for utilization in tissue engineering applications requiring porous structures, whereas surface erosion is promoted for drug delivery applications since the control of the release kinetics is easier when degradation occurs only at the surface [14].

Table 1.2. The properties of different polymer families. Reprinted from [14].

Polymer	Applications	Advantages	Disadvantages
Polyphosphazenes	Tissue engineering Vaccine adjuvant	Synthetic flexibility, Controllable mechanical properties	Complex synthesis
Polyanhydrides	Drug delivery Tissue engineering	Significant monomer flexibility, Controllable degradation rates	Low-molecular weights, Weak mechanical properties
Polyphosphoesters	Drug delivery Tissue engineering	Biomolecule compatibility, Highly biocompatible degradation products	Complex synthesis
Polycaprolactone	Tissue engineering	Highly processable, Many commercial vendors available	Limited degradation
Polyurethanes	Prostheses Tissue engineering	Mechanically strong, Handle physical stresses well	Limited degradation, Require copolymerization with other polymers
Polylactide	Tissue engineering Drug delivery	Highly processable, Many commercial vendors available	Limited degradation, Highly acidic degradation products
Polycarbonates	Drug delivery Tissue engineering Fixators	Chemistry-dependent mechanical properties, Surface eroding	Limited degradation, Require copolymerization with other polymers
Polyamides	Drug delivery	Conjugatable side group, Highly biocompatible degradation products	Very limited degradation, Charge induced toxicity

1.2.2. Synthesis of PBAEs and PAAs

Poly(β-amino ester)s (PBAEs) and poly(amido amine)s (PAAs) are important classes of biodegradable synthetic polymers that have been investigated as transfection vectors, drug and protein delivery vehicles and tissue engineering scaffolds due to their cationic nature, pH sensitivities, nontoxic degradation products and high biocompatibilities [16]. PBAEs are synthesized via aza-Michael addition of primary amines or secondary diamines to diacrylates by step-growth polymerization. This reaction does not produce any side products. After removing unreacted starting materials by precipitation, the resultant polymers can be stored in cold conditions [17]. Furthermore, the synthesis can be carried out without adding solvents, catalysts or in the absence of sophisticated protecting group strategies. The solvent, if any, influences molecular weight and reaction time. To give an example, the usage of THF instead of DCM results in lower molecular weight [18]. Moreover, solvent-free procedures occur faster than the formulations using solvent since the higher monomer concentration allows an increase in temperature which decreases the viscosity and facilitates the reaction [19]. In the presence of water PBAEs are degradable to diols, bis(β-aminoacids), and poly(acrylic acid) chains under physiological conditions by cleavage of ester linkages due to hydrolysis. Hydrophilicity of the polymer accelerates the degradation rate of PBAE since swollen chains enable water diffusion [20].

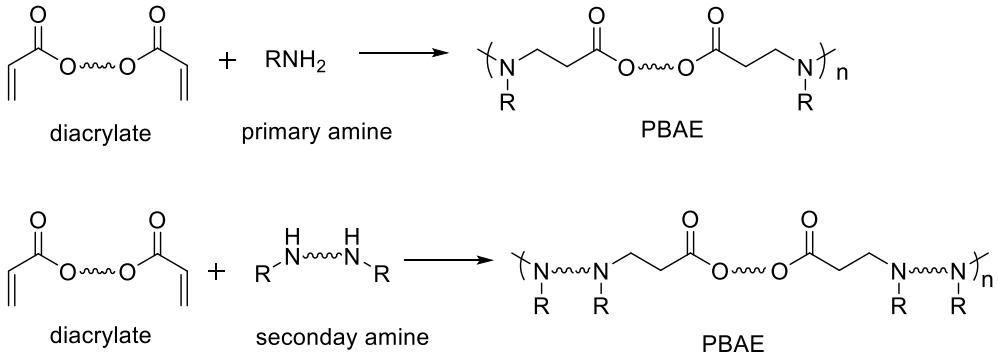

Figure 1.3. Synthesis of PBAEs.

PAAs are synthetic tert-amino polymers which are easily synthesized via aza-Michael type polyaddition of primary or bis-secondary amines to bisacrylamides. The reaction gives the highest molecular weight in protic solvents such as water or alcohols and it is mostly affected by the reactant concentration since the aza-Michael addition is an equilibrium reaction [21]. In aqueous medium, reaction temperature and time balance should be adjusted carefully to prevent the hydrolytic cleavage of amide bonds. Moreover, it is stated that $CaCl_2$ can be added as a catalyst to improve the incorporation of less reactive amines and it does not disturb the biological activity of PAA [22]. The polymers can be purified by dialysis and the resultant product is soluble in water and in organic solvents such as chloroform, dimethyl sulfoxide, and alcohols. On the other hand, amphoteric PAAs containing acid functions as side substituents which are carboxylic, sulfonic or phosphonic groups dissolve only in water. During the synthesis of amphoteric PAAs a base is required to activate the acid functionalized amines [21].

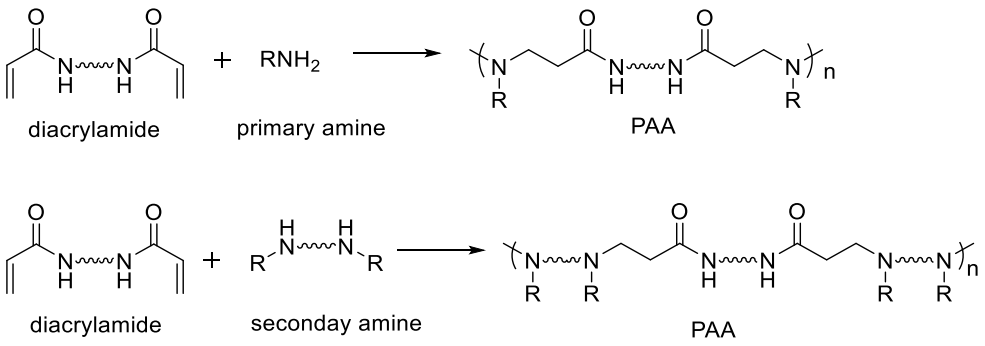

Figure 1.4. Synthesis of PAAs.

Since the synthesis procedure is tolerant to various types of amines and bisacrylates or bisacrylamides, PBAEs and PAAs have highly diversified functional groups. Biodegradability and biological properties of them can be arranged by changing the nature of starting materials, their hydrophobic/hydrophilic balance, and the amount of charged groups on them. In addition, further reactions to incorporate additional functionalities can be performed for specific purposes. To illustrate, in a recent work of our group, bisphosphonate was incorporated into side chains of PAA macromer to investigate the potential of its hydrogel in bone tissue engineering [23]. Furthermore, the chain end group

which has an impact on the final application can be tailored by changing the ratio of components. Acrylate terminated macromers which are easily prepared using acrylate-acrylamide/amine molar ratios > 1 can be crosslinked to be utilized in tissue engineering application whereas amine end capped polymers have potential for gene delivery applications [24, 25].

1.2.3. Tissue Engineering Applications of PBAEs and PAAs

Hydrogels which are 3D networks of hydrophilic polymers represent a valuable class of biomaterials. They are capable of holding large amounts of water, thus giving them physical properties comparable with biological tissues; this minimizes the tissue damage and inflammatory responses. Their interconnected porous structures make them good candidates for tissue engineering scaffolds [26]. Tissue engineering aims to develop artificial tissues and organs that can repair individual tissue defects. An ideal tissue engineering scaffold should mimic the extracellular matrix, support and direct cell growth, diffuse oxygen and nutrients and provide mechanical support. Scaffold degradation kinetics should match the requirements of the application [27].

Flexibility in PBAE and PAA chemistry make them preferable materials in hydrogel design. PBAE and PAA macromers can be easily crosslinked to obtain biodegradable networks by free radical polymerization (using photo [28–30]) or thermal [31, 32] initiator) thanks to their polymerizable end groups. The influence of starting materials' chemistry and their ratio on final network properties such as swelling capacity, mass loss profile, mechanical strength, degree of crystallinity, and cellular interaction were investigated to estimate their potential in tissue engineering [30, 33–38]. The first combinatorial library of 120 PBAE macromers was developed using twelve amines and ten diacrylates (diacrylate molar ratio of 1.2). After the photopolymerization of the macromers, degradation times (< 1 day to minimal mass loss in three months) and mechanical properties (∼4 to 350 MPa) of networks were collected to have a database for the rapid screening of properties for further studies [20]. Brey et al. selected three macromers from the library and synthesized them by altering the starting materials' ratio. It was found that increasing the diacrylate to amine ratio

decreases the molecular weight and the molecular weight affects the mechanical properties, degradation times and biological properties of final networks. Networks based on lower mass macromers have higher compressive and tensile moduli and slower degradation rates. Additionally, the attachment and spreading behaviour of Saos-2 cells on these materials is better than gels containing larger molecular weight macromers [39].

It is known that functionalization of a surface by bioactive groups such as tripeptide arginine-glycin-aspartic acid (RGD) improves the biological properties of synthetic materials [40]. Nonetheless, despite its good cell adhesion, peptide usage requires complex synthesis and causes high production expense. Utilization of biomimetic functional groups such as agmantine can overcome the insufficient cell adhesion and proliferation problems of synthetic hydrogels in a cost-efficient way [28, 29, 31, 41, 42]. To illustrate, biological studies of the hydrogels formed by agmatine containing PAA-Jeffamine-PAA triblock copolymers confirmed excellent cell adhesion compared to the glass control when the polymer concentration is increased at fixed molecular weight (JPJ-4) or remained constant by varying the molecular weights of polymers [29]. Martello et al. synthesized 2-hydroxyethylmethacrylate (HEMA) hydrogels cross-linked with RGD-mimicking PAA by changing monomer ratio and reaction time to investigate the effect of these parameters on final properties for tissue engineering. They observed 208 % higher cell proliferation onto the PAA based hydrogels and shorter chains showed better performance due to the stiffness of the surface. Interestingly, increment in the HEMA concentration did not affect biological properties despite the antifouling character of HEMA [43]. Likewise, it is shown that incorporation of phosphonate, bisphosphonate or their acidic forms into polymer structure can enhance cell adhesion and osteoblast differentiation [44].

Recently, phosphorous containing PBAEs and PAAs have been synthesized by our group to examine the effects of these functional groups on degradation rate, toxicity, and cell interaction of the final networks. For instance, PBAEs based on phosphonated amine and different diacrylates (HDDA, BDDA, HDEDA) provide a more favorable matrix for Saos-2 cell attachment than nonphosphonated ones as shown in Figure 1.5. It is also indicated that other than functionalization, hydrophobic hydrophilic-balance of structure and

stiffness are significant factors on biological properties [45]. Besides, inclusion of anionic groups in PBAE or PAA polymers through amino acid like structures is a strategy to obtain new pH sensitive zwitterionic polymers having promoted biodegradation properties compared to traditional ones. Glycine containing zwitterionic PBAE was synthesized to form hydrogels whose swelling, degradation and release behaviour can be controlled by pH [46].

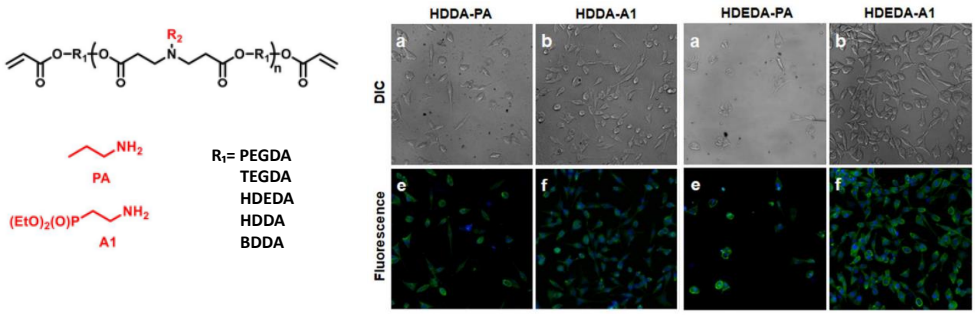

Figure 1.5. Cell attachment of Saos-2 cells on PBAE films. Reprinted from [45].

In-situ forming, injectable gels have gained importance in biomedical applications since the flowing form of solution allows to completely fill a cavity with minimal invasive procedures. Other than photocrosslinking, Michael type addition [47–50], ionic crosslinking [51], and pH/thermoresponsive behaviour [52–54] are common methods to prepare PBAE-PAA injectable hydrogels. In advanced applications of injectable hydrogels, drugs, proteins or growth factors can be encapsulated safely and released in a controlled manner to encourage the healing process [54, 55]. For instance, PAA polymeric nanoparticles were synthesized to encapsulate proteins by UV-induced crosslinking without involving of organic solvents, harsh mechanical stress or sonication which are harmful to biomolecules [56]. Trigger-responsive PBAE macromers with acid sensitive (containing ketal bonds) and reduction responsive (having disulfide bonds) diacrylates were photopolymerized to obtain protein encapsulated hydrogels providing control over the release of protein in response to external conditions [57].

1.2.4. Gene Delivery Applications of PBAEs and PAAs

Gene delivery shows great promise to treat genetic diseases, cancer and AIDS by transferring encoded genes into a patient for therapeutic protein production [58]. Development of safe and efficient gene delivery vectors is essential to achieve success in clinical applications. Viruses are viral vectors that have high transfection efficiency, but they are not safe in terms of toxic side effects, non-specific cell targeting and immune responses. Cationic polymers are promising alternatives to viral vectors due to having properties such as simple manufacturing, various chemical modifications, large cargo capacity, low immunogenicity and good stability. They can form self-assembly complexes (polyplexes) with negatively charged DNA thanks to electrostatic interactions. The overall positive charge of polyplexes facilitates their cellular uptake via endocytosis thanks to the interactions between complex and negatively charged cellular membrane. The cationic polymer mediated gene delivery is illustrated in Figure 1.6 [59].

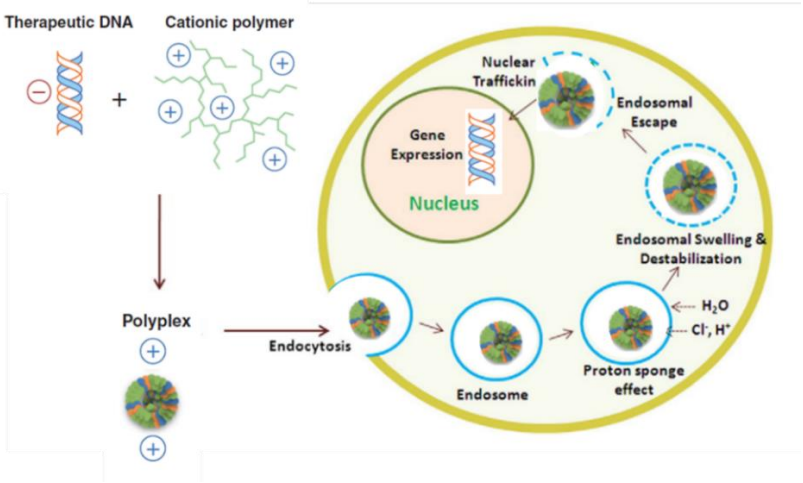

Figure 1.6. Cationic polymer mediated gene delivery. Reprinted from [59].

Buffering capacity, which is the capacity of polymer to bind protons when the pH in the endosomes decreases from pH 7.4 to 5.1, is an important property of polymeric vectors [60]. Polyethyleneimine (PEI) has been widely studied as non-viral gene delivery vector because its high pH-buffering capacity enables the endosomal escape which is a necessity to

transfer DNA successfully to the nucleus. Nevertheless, despite its high transfection efficiency, high molecular weight PEI is very toxic due to the lack of biodegradability [61]. Degradable PBAEs and PAAs containing tertiary amines for DNA binding are less toxic substitutes for PEI in gene delivery applications. As mentioned before, the structures of PBAE and PAA can easily have high diversity by using different primary amines. Thus, functional groups such as alcohol [58, 62–64] amine [60, 65] or positively charged agmatine [66, 67] or nicotinamide [68] can be incorporated to the structure to obtain multifunctional vectors. The structure-function relationships were examined by preparing polymer libraries to understand the influence of small changes in structure on DNA binding capability, colloidal stability, buffer capacity, and toxicity of polymer vectors [58, 62, 69, 70]. Zugates et al. showed that end modification of PBAEs is an efficient way to improve its efficiency. They used 5-amino-1-pentanol containing polymer whose success was demonstrated in a previous study [71] and best results were achieved with primary diamine end cappings. They noted that even a single carbon and functional group alterations in the terminal groups can have an important impact on the result [62]. Other than hydroxyl functionalized side chains and amine functionalized end groups, guanidinium conjugated polymers have shown enhanced transfection efficiency [72]. Therefore, PAA copolymers containing both agmatine and 4-aminobutanol [66] or ɣ-aminobutyric acid [67] were synthesized to find the optimal combination. Interestingly, in both studies the copolymer containing 80 % agmatine groups and 20 % alcohol or carboxyl groups showed the best transfection efficiency with the lowest cytotoxicity.

In recent years, incorporation of disulfide bonds to get reducible PBAEs and PAAs has gained attention because the formed polyplexes are stable in extracellular environment where the concentration of reducing enzyme such as glutathione is 100-1000 times lower than inside the cell. Thus, reducible disulfide bond can degrade and release the cargo only after reaching intracellular environment. To illustrate, Liu et al. designed disulfide containing PBAEs with folate and lactobionic acid to improve efficiency while reducing the side effects. The synthesized polymeric vectors have potential in targeted cancer gene therapy thanks to the synergistic effect of GSH triggered degradability improved cellular uptake as a result of ligand receptor interaction [73]. It was indicated that disulfide containing PBAEs have better transfection efficiency and lower cytotoxicity than

hydrolytically degradable ones [74]. On the other hand, the stability of disulfide needs to be investigated. Elzes et al. showed that the degradation and stability of PAAs can be controlled by varying the steric hinderance adjacent to disulfide bond [75].

Combining two widely used nonviral gene delivery agent families, PEI and PBAE or PAA, dramatically improves the gene transfection efficiency of the resultant polymeric vector though the low molecular weight PEI is used [76, 77]. Huang et al. mentioned that the star polymer composed of PEI (800 Da) and PBAE (5.2kDa) exhibited similar transfection but reduced toxicity compared with high molecular weight PEI (25kDa) [78]. In a recent study of our group, bone targeting transfection agents were synthesized from branched PEI (1.8 kDa) and PAA containing (bis)phosphonic acid and 5-amino 1-pentanol at various ratios. The polymers have selectivity in transfection for osteosarcoma cell lines because of (bis)phosphonic acid. Also, the best combination (0.7 alcohol: 0.3 alendronate) showed similar transfection efficiency as FuGENE with lower toxicity as shown in Figure 1.7 [79].

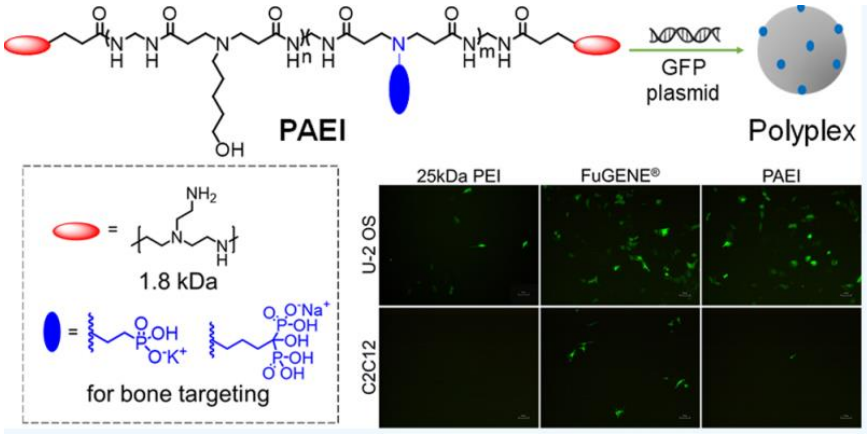

Figure 1.7. Structures of PEI-PAA containing gene delivery agents and fluorescence microscopy images of transfected cells. Reprinted from [79].

1.2.5. Drug Delivery Applications of PBAEs and PAAs

The usage of drugs in chemotherapy has some challenges such as low solubility and short half-life of drugs and nonspecific cell interactions causing toxicity. To solve this problem, drugs can be chemically attached to a water-soluble polymer through a cleavable linker or physically incorporated into a self-assembly system thanks to hydrophilic, hydrophobic, or electrostatic interactions [80]. Figure 1.8. a1-4 represents the common drug loading methods to hydrogels and a5 shows schematic illustration of polymeric micelle formation where the hydrophobic drug is carried in the hydrophobic core part and the hydrophilic block of amphiphilic polymer (outer shell-corona) determines micelle's solubility, stability and biocompatibility. The most common polymers used for the hydrophilic part are poly(ethylene glycol), poly(N-vinylpyrrolidone) and poly(2-hydroxyethyl methacrylate) while materials for the hydrophobic segment are poly(propylene oxide), poly(D,L-lactide), poly(lactide-*co*-glycolide), poly(ε-caprolactone), poly(β-amino ester) and poly(amido amine) [81]. The prolonged circulation time and nano-size structure of polymeric micelles facilitate the accumulation of drug in tumor tissue or inflammation site where vascular permeability is increased and lymphatic drainage is diminished which is defined as the enhanced permeability and retention (EPR) effect [82].

The EPR effect helps to concentrate the polymeric micelles in the tumor site but to get successful therapeutic responses drugs should be released efficiently [83]. Figure 1.9 highlights the prevalent release mechanism of drugs from hydrogels. To clarify, release rate depends on pore size when the drug is encapsulated physically. For example, while fast release is observed from the hydrogels having larger pores than the drug's size, drug release rate depends on degradation for the situations in identical pore and drug dimension. In addition, the swelling ratio determines the release kinetics in hydrogels possessing small mesh size. Osmotic pressure increases after large volume of water enters the hydrogel resulting in a boost of the diffused drug amount [84]. Direct degradation of the polymer and cleavable covalent linkages are other strategies preferred in the treatment of long-term diseases where a slow and controlled degradation profile is desired. The typical degradation mechanism of hydrogels involves hydrolysis and enzyme activity.

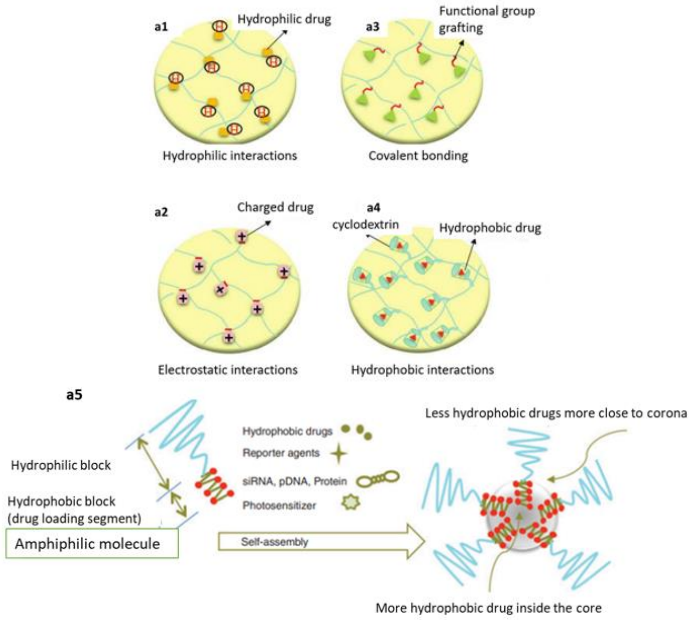

Figure 1.8. Common drug loading methods to hydrogel (a1-4) s and schematic illustration of polymeric micelle formation (a5) Reprinted from [81, 84].

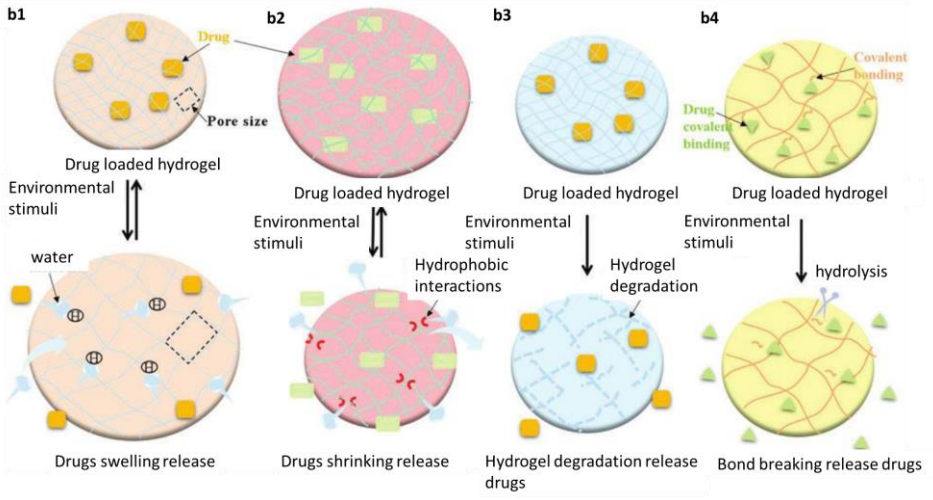

Figure 1.9. Release mechanism of drugs from hydrogels. Reprinted from [84].

Microstructural adjustment of polymeric micelles can be altered by external stimuli such as pH, temperature, ionic strength, light, or presence of an enzyme [85, 86]. Among these responses, pH responsiveness is the most utilized one because the pH of the extracellular matrix of tumor (pH= 6.5) and even intracellular compartments such as endosomes and lysosomes (pH= 4-6) are more acidic than blood and normal tissues (pH= 7.4). Therefore, the design of polymeric micelle systems based on PBAEs and PAAs which have a pK_b value around 6.5 is a rapidly growing area for therapeutic drug delivery applications [82, 87–91]. For example, a cytotoxic peptide combined PEG-PBAEs self-assembled into a micelle like structure where PBAE block as hydrophobic core and PEG as hydrophilic corona. This micelle can stabilize the conjugated peptide in core and prevent enzyme degradation besides chemotherapeutic drug DOX can be loaded into the micelles and released under acidic medium to kill cancer cells. The synergistic cancer treatment with DOX loaded peptide micelles could more efficiently restrain tumor growth than DOX loaded polymer micelles and peptide micelles [92]. An interesting esterase and pH sensitive study was done by combining mesoporous silica nanoparticles with PBAEs as shown in Figure 1.10. It was aimed that the low pH and high esterase concentrations in cancer cells assist the release process of cargos. The release efficiency which is around 20 % at pH 7.4 reaches to 80 % at pH 4 and 70 % in the presence of esterase enzyme [93].

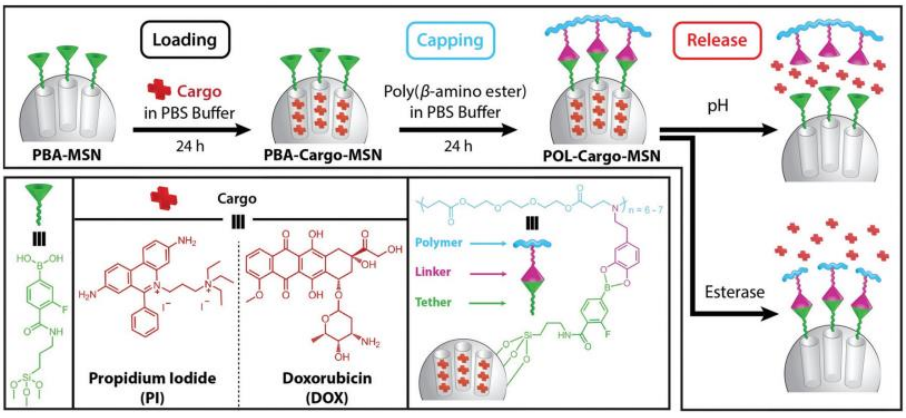

Figure 1.10. Schematic illustration of esterase and pH triggered release of drugs from PBAE-silica nanoparticle system. Reprinted from [93].

For the last few decades, many researchers have focused on disulfide containing polymeric micelle systems in which the disulfide bonds are damaged in intracellular matrix of tumor cells where the glutathione concentration is 100-1000 times higher than extracellular matrix [94–97]. The first study for DOX release from a pH and reduction dual responsive micelle was designed by the copolymerization of PEG and PBAE containing disulfide bonds in the main chain by Chen et al. As represented in Figure 1.11, self-assembled particles can demicellize at high reducing molecule (DTT) concentration and in acidic medium [98]. Moreover, pH and redox responsive PBAE or PAA hydrogels can also be fabricated for controlled drug delivery. By choosing a variety of starting materials with different hydrophobicity, swelling, degradation and release profiles can be tailored [99, 100]. In a recent study of our group, a simple one-step synthesis of PBAE hydrogels with no side products was studied. The therapeutic cargo was easily loaded in the hydrogel by adding the drug molecule into the precursor mixture. The cargo molecule was released in a controlled matter depending on external pH and redox triggers and the activity of released molecule was tested by photodynamic therapy [100].

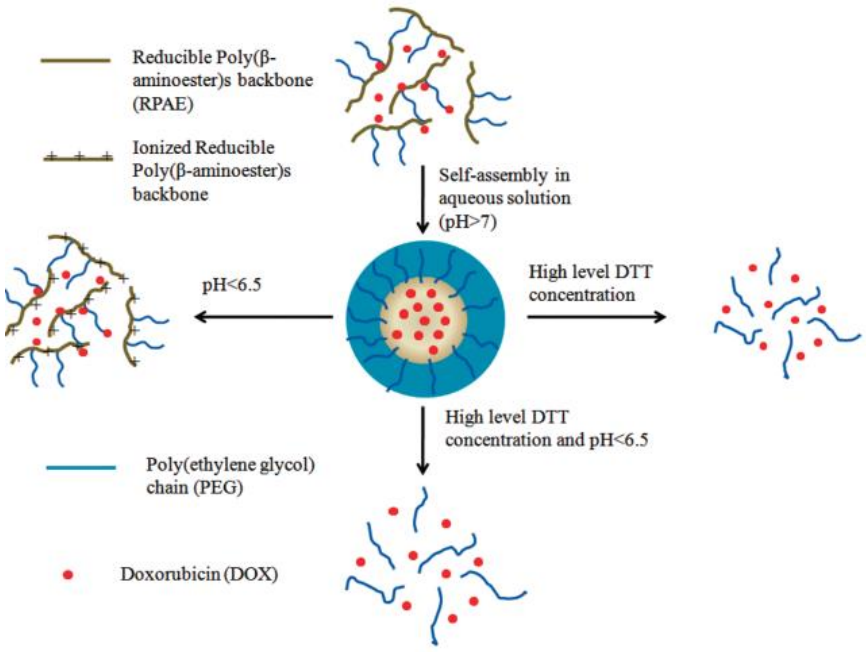

Figure 1.11. Micelle destabilization depending on medium conditions. Reprinted from [98].

1.3. (Bis)phosphonate Containing Biomaterials

Phosphorous-containing groups (PCG) such as phosphonates, phosphonic acids and bisphosphonates have been widely used in monomer modifications because their special properties extend the application areas of resultant polymers. Materials which involve PCG have been used in industry as corrosion and deposit inhibiting agents due to their strong binding ability to metal surfaces [101–103] Additionally, complex formation property of PCG makes them possible dispersants [104,105]. In recent years, they have also been considered as candidates for flame retardant materials due to the formation of a protective coating which prevents oxygen transport toward the burning area [106]. Although there are different applications of this kind, biomedical applications of PCG are explained in detail in this thesis. Biodegradability, hemocompatibility and protein adsorption resistance make them useful in various bioapplications [107, 108]. They are mostly preferred in bone targeting systems, bone tissue engineering scaffolds and dental materials due to the strong interactions with Ca^{2+} in hydroxyapatite [109–111].

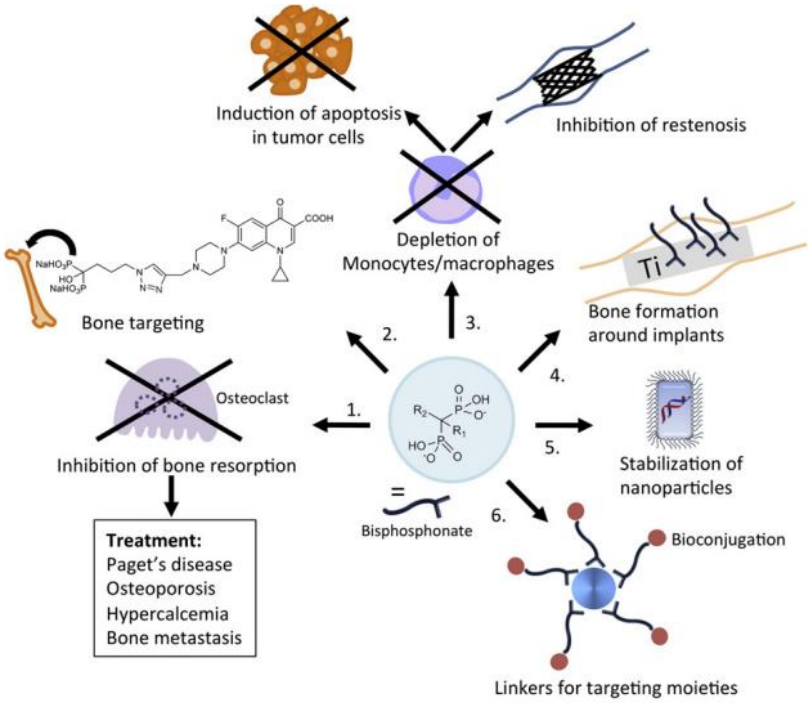

Figure 1.12. Bioapplications of phosphorous containing materials. Reprinted from [112].

1.3.1. Bone Targeting by Conjugation to (Bis)phosphonates

Phosphorus containing groups, especially bisphosphonates have high affinity to Ca^{2+} ions, in other words, they are remarkably selective to bone tissue rather than other tissues. They have effects on osteoblast and osteoclast cells which are responsible for the formation of new bone and breaking down of old bone. Therefore, they are widely used in the treatments of bone diseases such as osteoporosis, Paget's disease, and osteolytic tumors. There are commercially available bisphosphonate drugs in the market such as alendronate, clodronate, etidronate, ibandronate, pamidronate, risedronate, tiludronate and zoledronate [112]. Other than the management of osteoarticular disorders, bisphosphonates have been conjugated to drugs [113–117], proteins [118,119] and imagining agents [120,121] to target these molecules to bone tissue where specific targets are rare. The bisphosphonate drug conjugation is based on chemical modification and the linker between bisphosphonate and drug should be stable during systemic circulation and also be labile at the treatment site to release the drug. In addition, conjugation can change the pharmacological activity of conjugated drugs due to the modifications in reactive groups during linking but the drug needs to be released in its free form. Therefore, the efforts to develop new targeted conjugation systems to diminish drug's toxicity and to upgrade its bioavailability at the desired site continue. To illustrate, Xie et al. designed a differentially degradable dual conjugate prodrug as shown in Figure 1.13 [122]. EP4 is associated with bone forming and growth activity but the direct usage of EP4 agonist as a bone anabolic drug is impractical due to its side effects such as vasodilation and gastrointestinal disturbance [123]. In this study, EP4 agonist and alendronate are linked via a peptide linker which is cleaved by esterase to release EP4 agonist and alendronate can be liberated via the action of cathepsin K enzyme (Cat K) which is released by osteoclasts to cleave collagen matrix when they travel on the bone surface during bone resorption [124]. They observed that although 50 % of EP4 agonist was degraded before reaching bone, the adherent conjugate released both drugs at a maintained rate. They concluded by mentioning the necessity of further stabilization of the ester bond to enhance system's stability [122]. Furthermore, although other molecules such as D-aspartic acid octapeptide, polymalonic acid and tetracycline have affinity to bone, bisphosphonates' affinity can be adjusted by changing the other two substituents connected on geminal carbon. The hydroxyl or amine group (R^1) enhances

binding to bone whereas R^2 provides pharmacological properties. Bisphosphonates which are chemically bonded with a hydrazine functionalized linker with diverse spacer length and hydrophilicity were synthesized to investigate their binding affinity, drug conjugation and pH sensitive drug release capacity. It was observed that the cleavage of hydrazone bond formed after drug conjugation depends on pH. The release at lower pH environment such as bone resorption area and site of wound healing is much faster than release at physiological pH [125].

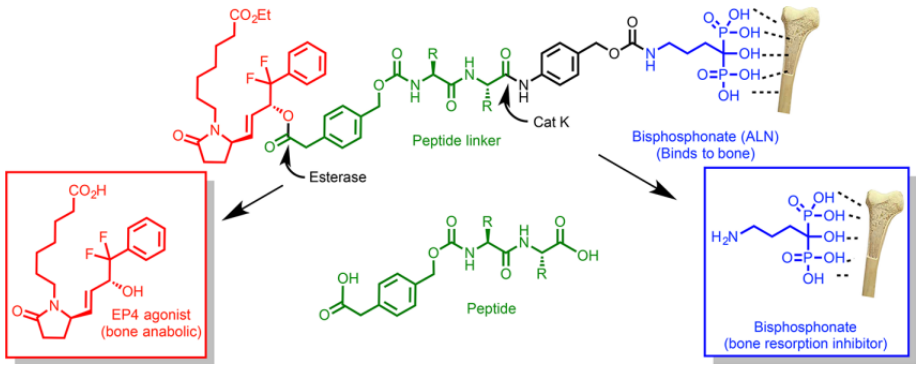

Figure 1.13. Structure of differentially degradable dual conjugate prodrug. Reprinted from [122].

Polymers offer the opportunity to combine different functionalities into a nanoscale material, thus (bis)phosphonate conjugated polymers are widely used to conjugate drugs, imaging agents or proteins to deal with the limitations of low molecular weight drugs [126–129]. Living/controlled polymer synthesis methods such as atom transfer radical polymerization (ATRP) and reversible addition-fragmentation chain transfer (RAFT) are the most common ways for the preparation of block copolymers with low polydispersity index. A wide range of functional monomers can be reacted, or reactive chain ends can be modified for versatile biomedical applications. For example, ATRP synthesis of polymers including bone tissue targeting alendronate and cell binding N-hydroxysuccinimide group was synthesized to evaluate the binding of cells to a target tissue. They remarked the designed polymer significantly increased cell attachment and enhance healing in bone injury site [130].

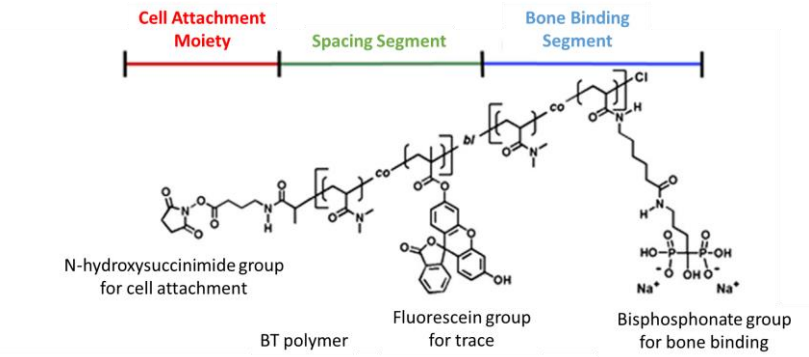

Figure 1.14. A multifunctional polymer containing bone targeting and cell binding groups. Reprinted from [130].

Also, the EPR effect provides passive targeting of polymers via the phosphorous group's targeting to skeleton which is the most common organ affected by metastatic cancer [131]. Moreover, noncovalent associations of macromolecular structures such as hydrophobic or electrostatic interactions facilitate the chance of carrying different molecules [132,133]. Self-assembly behaviour of well-defined phosphonic acid-based amphiphilic polymers synthesized from only one monomer was studied for potential hydrophobic drug loading and delivery applications [134]. Likewise, a zwitterionic poly(ammonium bisphosphonate (meth)acrylate)-g-PEO copolymer was produced after removal of ethyl groups on the phosphonates by using bromotrimethylsilane without cleavage of ester bonds. Zwitterionic copolymers assembled into aggregates in water because of electrostatic interchain interactions, the formed core-shell nanoparticles are candidates of bone targeting drug carriers [135]. A sophisticated bone targeting system based on alendronate modified polyethylene glycol was designed to anchor on the surface of methotrexate loaded calcium phosphate as illustrated in Figure 1.15. Bone targeting ability was verified by comparing the intensity of fluorescently labelled alendronate functionalized nanoparticles with carboxylic acid functionalized ones. Calcium phosphate is an acid sensitive material that dissolves and releases the loaded drug in acidic environment. Accordingly, the model drug was released much more in cancer metastasis site than in physiological conditions because cancer cells create acidic medium around themselves [136].

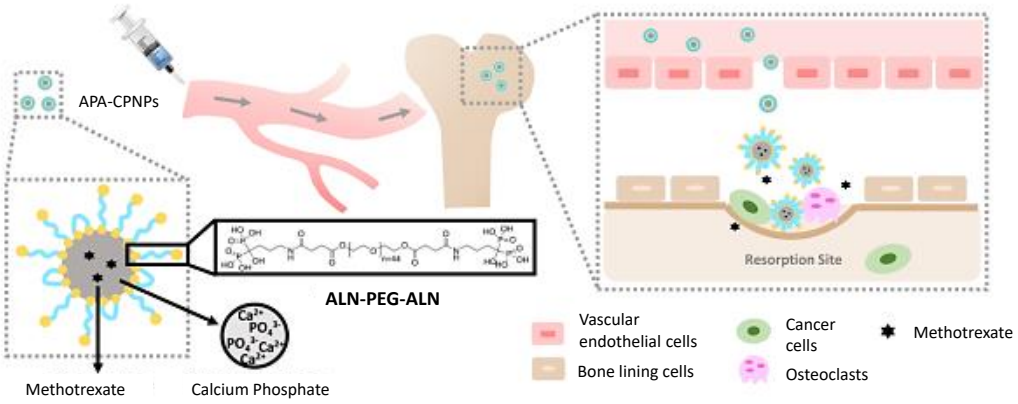

Figure 1.15. Schematic illustration of bone targeting of drug loaded calcium phosphate particles. Reprinted from [136].

1.3.2. Bone Tissue Engineering Applications

Bone tissue can regenerate itself but regeneration capacity of the bone is insufficient in cases of large defects or multiple fractures. There is a risk of rejection and infection in allograft (tissue graft from a donor of the same species) and xenograft (tissue graft or organ transplant from a donor of a different species) applications that can be used in such cases. Autografting, in which the patient's own tissue is used, is the gold standard for bone defect repair; however, it has disadvantages such as the difficulty in placing the transplanted bone in irregular damaged areas. Bone tissue engineering is a promising method that can solve these problems [137,138] Therefore, development of scaffolds which can mimic the properties of bone by accelerating the formation of hydroxyapatite and facilitating osteoblast attachment is very important.

Bone is a composite material consisting of an organic protein component collagen which is the scaffold for the inorganic mineral component, hydroxyapatite [$Ca_{10}(PO_4)_6(OH)_2$] [139]. Mineralization plays an essential role in bone growth [140]. The anionic amino acids such as glutamate, aspartate and phosphoserine in the extracellular matrix of bone serve as nucleation points for the binding of Ca^{2+} ion, induce mineralization

and promote the transformation of amorphous calcium phosphates into stable, crystalline, mature bone apatite as shown in Figure 1.16 [141–143].

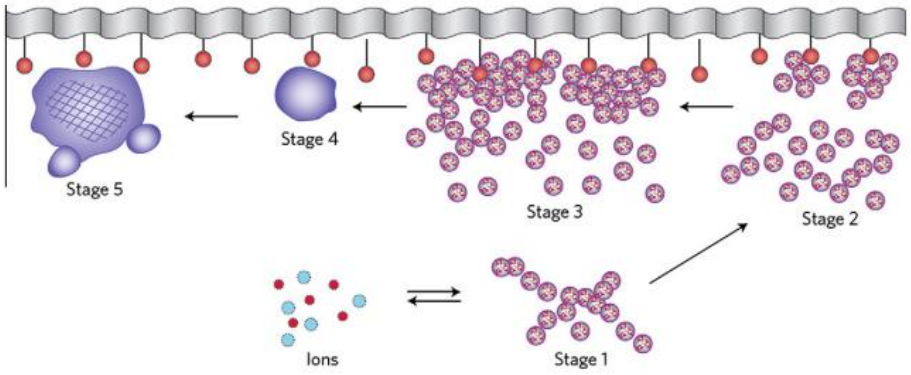

Figure 1.16. Representation of calcium phosphate nucleation and growth on anionic group functionalized surfaces. Reprinted from [144].

Inspired by the process the natural mineralization process of bone extracellular matrix, negatively charged functional groups such as carboxylate [145–149], sulfonic acid [150–153] and (bis)phosphonic acid [154–161] are incorporated into polymers and networks used in bone tissue engineering scaffolds to mimic nucleation of apatite-like phases. To illustrate, vinyl phosphonic acid, one kind of phosphoprotein-like small molecule was photocrosslinked with methyl acryl containing collagen to develop uniformly mineralized collagen hydrogels. Enhanced mechanical properties showed the successful binding between CaP minerals and network and simulate the stiffening process of bone formation [139]. Dey et al. synthesized poly(vinylphosphonic acid-*co*-acrylic acid) via free radical polymerization as a potential candidate to mimic binding ability of bisphosphonates to divalent metal ions and at the same time eliminating side effects associated with bisphosphonate drugs. The maximum calcium chelation capacity of copolymer was investigated with 30 mol% VPA content which offers the best structural mimic of bisphosphonate and promote mineralization [162]. In a recent work of our group, of bisphosphonic acid-functionalized dimethacrylates were used as crosslinkers in poly(2-hydroxyethyl methacrylate) (pHEMA) hydrogels to investigate the effect of functionalization on properties such as mineralization, swelling and mechanical properties. The influence of crosslinker structure on mineralization, improved

mechanical properties after mineralization and self-recoverability of hydrogels swelled in $CaCl_2$ solution imply that the designed crosslinkers have potential in bone tissue engineering scaffolds [163]. An injectable double network hydrogel for bone tissue engineering was designed using thermal sensitive carboxylic acid containing gellan gum and photopolymerizable crosslinkers, poly(ethyleneglycol) methyl ether methacrylate (PEGMA) and poly (ethyleneglycol) diacrylate (PEGDA) with the incorporation of 2-methacrylamidoethyl dihydrogen phosphate monomer to regulate the formation of hydroxyapatite. Although the mechanical properties of the network were decreased as the MDP concentration increased, mineralization capacity was observed to be enhanced [164].

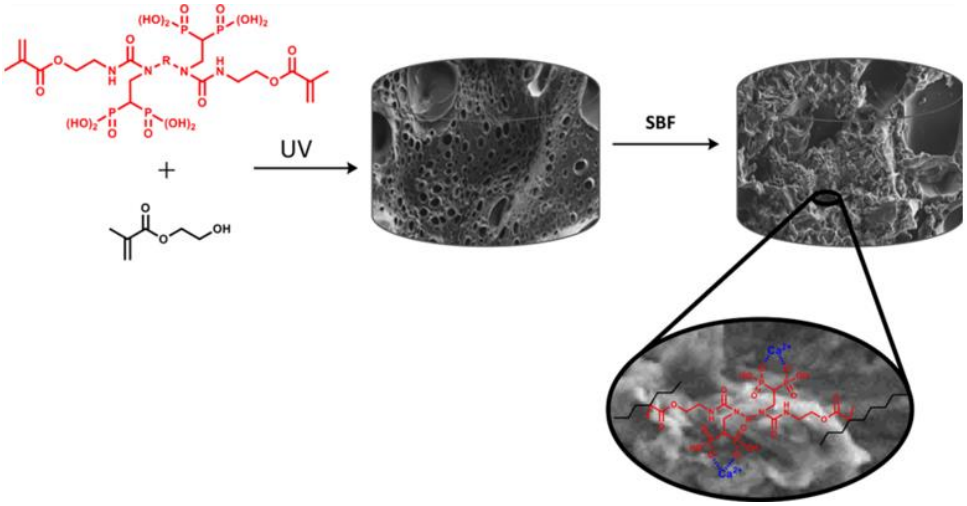

Figure 1.17. SEM images of bisphosphonic acid-functionalized dimethacrylate crosslinked HEMA hydrogels. Reprinted from [163]. (Further permission related to figure excerpted should be directed to ACS).

In vitro mineralization capacity of a polymer or network is investigated by immersing it in simulated body fluid (SBF) with similar ion concentrations to human plasma. However, it is a slow process, soaking in highly concentrated Ca^{2+} and subsequently HPO_4^{2-} solutions [165–167] can be a method to accelerate it. The process is usually characterized by FTIR, TGA, SEM and XRD. For example, the hydroxyapatite formation on PAA cryogels functionalized by 5-amino-1-pentanol and alendronate was carried out by following the increase in intensity of peaks corresponding to HAP phosphate which are at 1016 (ν_3 PO

mode), 559, 600 (ν_4 PO mode) and 964 cm^{-1} (ν_1 PO mode). It was noticed that the changes in IR spectrum became more visible with increase in alendronate concentration [23]. Mineralization of a phosphorylated star shaped block copolymer with the structure shown in Figure 1.18 was tested by incubating the hydrogel in SBF for 8 weeks. After observing formation of massive needle shaped hydroxyapatite crystals in SEM images, further in vivo mineralization studies were confirmed by alizarin red staining [168].

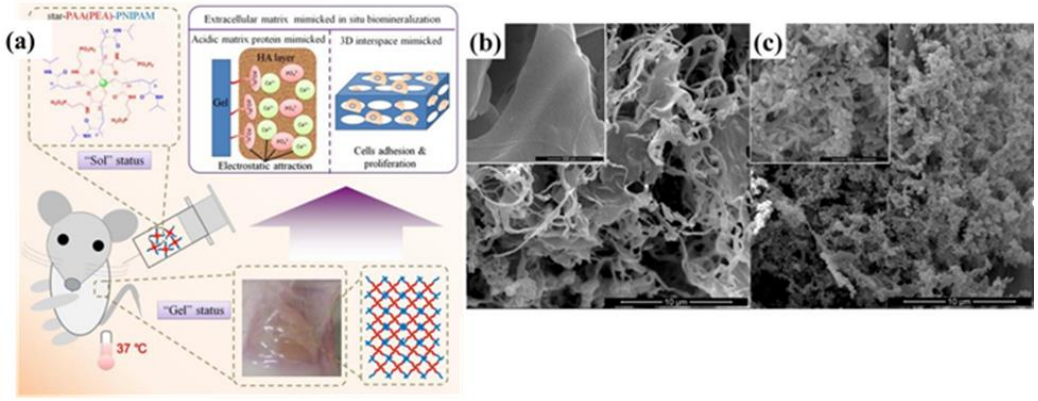

Figure 1.18. Schematic illustration of the system (a), before (b) and after (c) SEM images of phosphorylated injectable hydrogel incubated in SBF. Adapted from [168].

Other than chemical functionality, various parameters such as pH, temperature, salt and polymer concentration and polymer architecture have an influence on nucleation and growth of different calcium phosphate phases [144,149]. Griffin et al mentioned that the initial pH of hydrogels which was adjusted to either 7 or 11 has an important impact on formed calcium phosphate minerals on commercially available Pluronic 127 gels in terms of crystal phase, its size and morphology. Highly crystalline, millimeter-scale brushite ($CaHPO_4.2H_2O$) crystals grow on gels at pH 7 whereas nanoscale particles of calcium hydrogen phosphate hydrate ($Ca_8(HPO_4)_2(PO_4)_4(H_2O)_5$ like hydroxyapatite form in composites at pH 11 [169]. Also, the mineralization of an injectable hyaluronic acid hydrogel is promoted thanks to premineralization treatment done by soaking Ca^{2+} solution. The clusters of bisphosphonate and Ca^{2+} ions which is formed ex vivo act as a nucleation point and support mineralization as shown in Figure 1.19 [142].

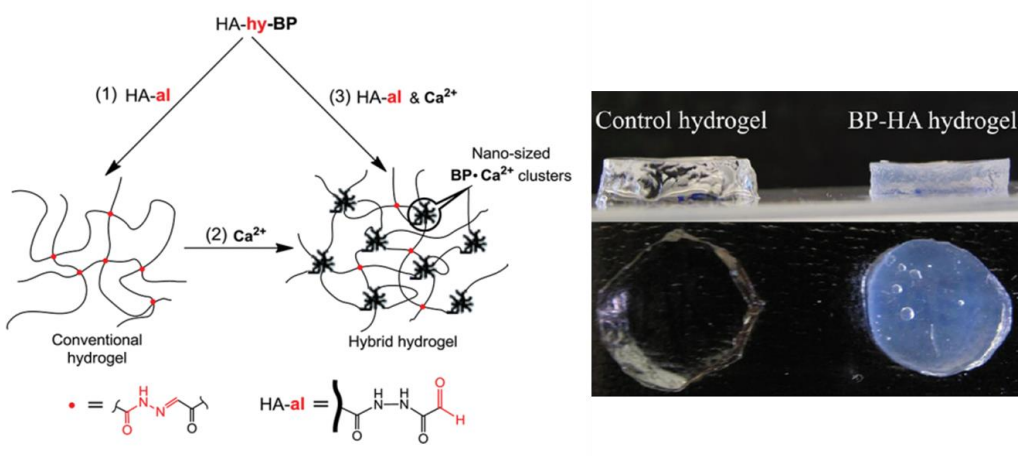

Figure 1.19. Preparation of networks and 7-day mineralization of hydrogels in PBS. Adapted from [142].

Another prerequisite of bone tissue engineering materials is promoting cell adhesion and osteogenic activities. It is known that osteoconductivity (ability to encourage and support new bone formation) and osteoinductivity (ability to induce differentiation to an osteoblast-like lineage) are improved on mineralized polymer scaffolds compared to unmineralized ones [141]. Addition of chemical functionalities such as (bis)phosphonate groups is also a strategy to enhance cell attachment and osteogenic potential of scaffolds [44, 45, 170–173]. To illustrate, although PEG based hydrogels are widely used in biomedical applications, their low cell attachment rate due to the formation of a hydrated layer discouraging the adsorption of adhesion proteins is a drawback. Dadsetan et al demonstrated that incorporation of phosphate moiety developed cell attachment, proliferation and differentiation of osteoblast precursor cells in a dose-dependent pattern. [174]. In a recent study, the HAP formation ability and osteogenic activity capacity of PEGDA hydrogels were enhanced by using a phosphonated siloxane macromere [175]. While phosphonate groups are known as hydrophilic, the carbon containing ethyl groups and the connection part to siloxane have an effect to increase hydrophobicity and adjust the required balance for mentioned bioapplications in this study.

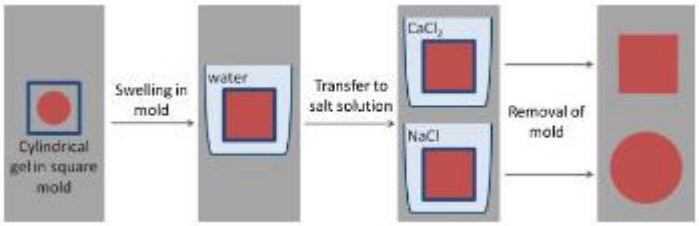

Figure 1.20. Swelling characteristics of bisphosphonate functionalized hydrogels in $CaCl_2$ and NaCl solutions. Reprinted from [176].

Over the past years, formation of supramolecular hydrogels by reversible bonds such as hydrogen bonds, metal ligand coordination, ionic, hydrophobic and host-guest interactions have intensified in the biomedical field in an effort to overcome the recovery problem of permanent networks after a damage. [108, 110, 177]. The reversible dynamic physical bonds enable the design of self-healing materials, in addition to providing a proper environment for cell encapsulation [178, 179]. The hydrogels formed by non-covalent ligand coordination between (bis)phosphonate groups and cation containing particles such as Mg^{2+}, Ca^{2+} and Fe^{3+} have also attracted increasing interest [180–184]. For example, alendronate functionalized poly (2-oxazoline)s was crosslinked with calcium using reversible physical bonds and self-healing properties of the robust networks were showed by rheology method. The amount of alendronate, the side chain's flexibility and polymer's polarity are the factors effecting gel formation [184]. As exhibited in Figure 1.20, bisphosphonate Ca^{2+} coordination bonds are quite strong. Bisphosphonate functionalized hydrogels can fix the mold's shape when swelled in calcium solution, however, samples soaked in sodium solutions swelled back to their original shape after rinsing with water [176].

The incorporation of inorganic materials such as calcium silicates or calcium phosphates is a way to improve mechanical properties and mimic the composite structure of bone [185]. For example, hydrogels formed bisphosphonated hyaluronan reinforced by the addition of bioglass content. Besides, they have self-healing ability as well as mineralization capacity in SBF [182]. As shown in Figure 1.21. the interaction between drug loaded magnesium silicate nanoparticles and bisphosphonated polysaccharide was used to design a self-healing and pH responsive hydrogel which can be injected in tumor specific

environment for local controlled drug delivery application. The kinetics of physically crosslinked hydrogel formation was studied by rheology. As seen in Figure 1.21 a and b, liquid to gel transition was observed in the presence of magnesium silicate nanoparticles (represented as blue balls) whereas the storage modulus did not become larger than the loss modulus with the control sample including silica nanoparticles (represented as black balls) [186].

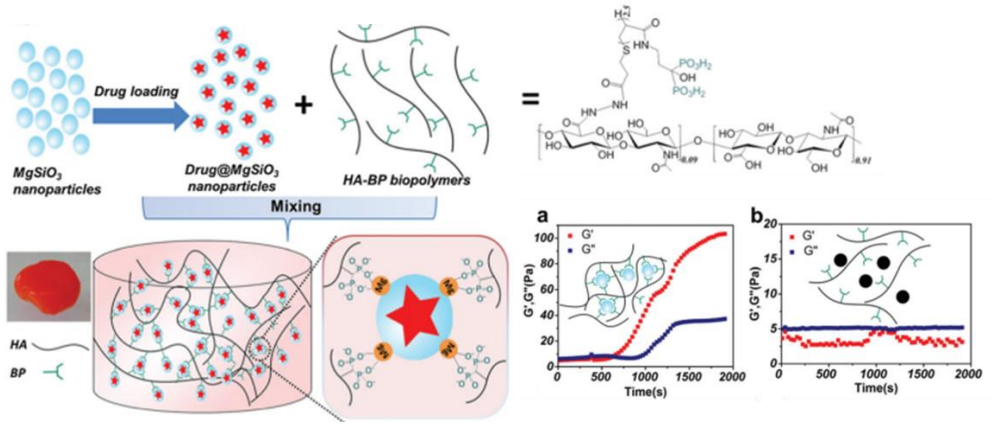

Figure 1.21. Rheology kinetic experiments of composite hydrogels formed by dynamic interaction between $MgSiO_3$ and bisphosphonate. Adapted from [186].

In last years, physically and covalently dual crosslinking has also been a method to obtain better mechanical properties compared to traditional chemically crosslinked networks and self-healing property like physically crosslinked networks as well as adhesiveness to mineral surfaces. Dual crosslinked hydrogels can be used in bone tissue engineering scaffolds and bone adhesive glues [187]. For instance, a method for the formation of in situ assembly self-healing hydrogel was developed based on the dynamic metal bisphosphonate coordination bonds between calcium phosphate coated silk fibroin and bisphosphonate linked polysaccharide [188]. This reversible character enabled injectability as seen in Figure 1.22. Also, the self-healing property of hydrogels were tested visually. They were cut into pieces and it observed that the pieces joined together in few minutes. Photocrosslinkable groups on polysaccharide were polymerized after the dynamic hydrogel structure to promote mechanical properties. They declared that the hydrogel formed by protein fibers, calcium

phosphate minerals and polysaccharide glue can be an effective scaffold without addition of extra growth factors.

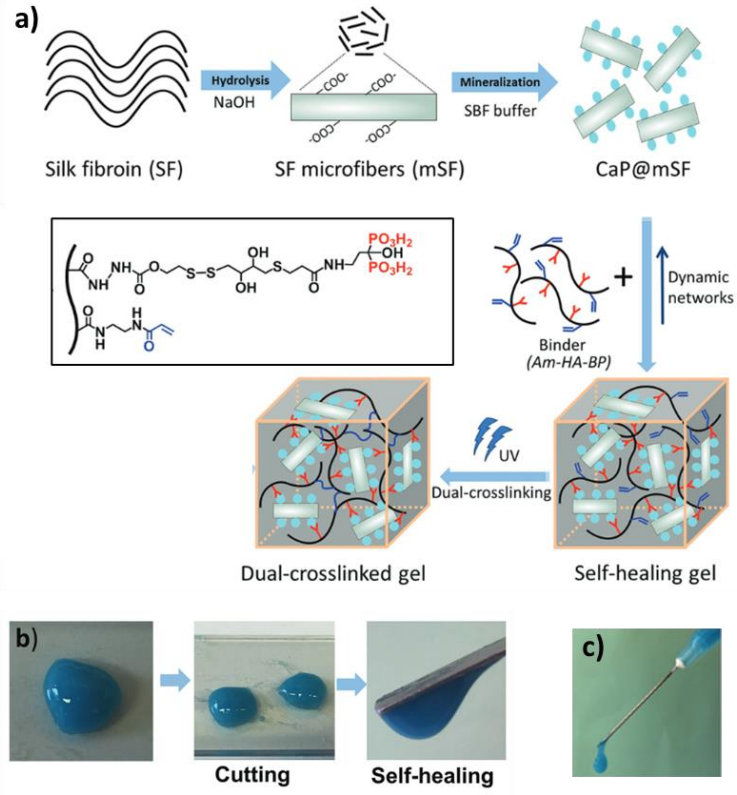

Figure 1.22. Formation of dual crosslinked hydrogels (a), their self-healing (b) and injectability (c) properties. Adapted from [188].

1.3.3. Dental Applications

Dental adhesives have been broadly used in dentistry to enhance the bonding quality between the composite resin restorations and dentin. Dental adhesive formulations consist of monofunctional comonomer, crosslinking monomers, cosolvent, initiator and additives. Total-etch and self-etch adhesives are the two types of materials currently available on the market. Total-etch systems require initially a phosphoric acid treatment, washing and air-drying steps whereas self-etch systems do not need a separate etching step [189]. The self-etch adhesive formulation involves acidic monomers functionalized with groups such as

phosphonic [190–192] and bisphosphonic [193, 194] acids which can dissociate in the presence of water, etch dental tissue, simultaneously improve the infiltration of the adhesive into demineralized surface as well as form a strong bond between dental tissue and the composite [189]. In other words, the acidic part of the monomer binds the tooth substance while polymerizable part forms an insoluble crosslinker network with other components which prevents bonding failure. The ‘Adhesion-decalcification’ concept explains the correlation between the bonding performance of the adhesives and the chemical stability of the monomer-Ca salts formed with the interaction of the acid monomer and HAP [195]. Therefore, small changes such as polarity, spacer length and hydrophilicity in the monomer structure can induce noteworthy differences in their adhesive performances [196, 197]. For example, the presence of sulfur atom in the structure enhances the solubility of monomers by increasing the chain flexibity which improves the adhesive properties of the formulation [198].

Desired properties of adhesive monomers are high rate of free radical polymerization, ability to form strong bonds with tooth tissue and sufficient stability in the mouth environment [193]. Methacrylates and methacrylamides have sufficient reactivity to obtain high-rate polymerization, nonetheless, methacrylates are not stable under aqueous conditions due to hydrolysis of ester groups. Furthermore, components bearing urea groups provides hydrogen bonding induced pre-organization that brings double bonds close to each other and increases rate of polymerization. Besides, urea derivatives can chelate metals and promote chemical bonding to dental tissue [199, 200]. Extensive research has focused on designing a new monomer which is highly reactive and stable as well as has strong affinity to HAP [201]. For instance, in a previous work of our group, the first bisphosphonate/bisphosphonic acid containing urea dimethacrylates were synthesized and their polymerization rates interactions with synthetic HAP were investigated [201]. A different approach for self-etching adhesives was studied by Salimando et al by synthesizing well-defined copolymers containing phosphonic acid and polymerizable groups as shown in Figure 1.23. Although acidic monomers are commonly used for adhesive applications, formulations with polymerizable acidic polymers are quite limited. The influences of well-controlled chemical structure and variety of functional groups on final properties were searched in detail [202]. Other than self-etching adhesive applications, phosphonic acid

functionalized copolymers can be utilized as antibiofouling coatings to inhibit bacterial adhesion. Phosphonic acid containing monomer ensures the immobilization on tooth enamel by binding HAP while the other PEG based monomer manages bacterial resistance [203].

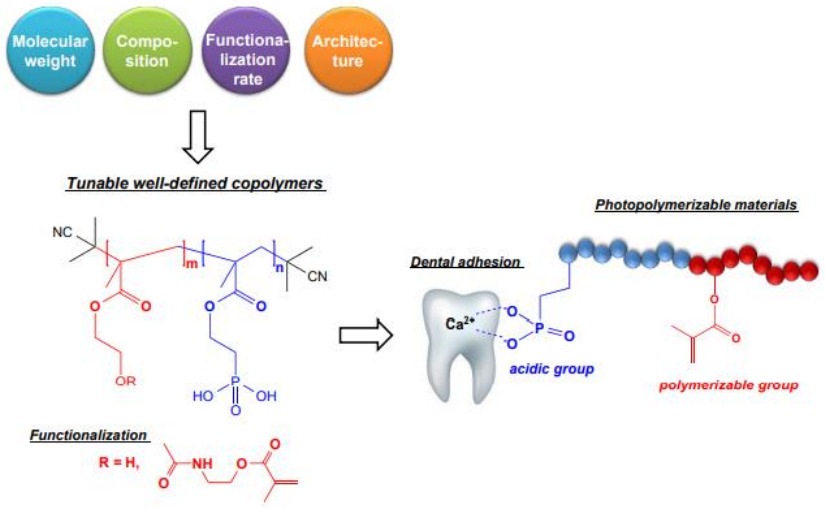

Figure 1.23. Polymerizable acidic polymers for self-etch adhesives. Reprinted from [202].

Tooth enamel is known as the hardest tissue in human body, consisting of 96% inorganic materials. Thus, shortage of living cells causes insufficient self-repair ability of tooth enamel. Dental caries is one of the most widespread diseases in the world [204]. It starts once demineralization caused by acid producing bacteria dominates in the dynamic demineralization-remineralization balance in the mouth. Before the cavitation forms, a subsurface lesion which can be remineralized is present. However, in most cases natural remineralization is inadequate [205]. Therefore, there is a great interest to design strategies to repair low level dental caries. Utilization of polymers which support biomineralization such as acid functionalized ones is a way to achieve it [206–209]. To illustrate, phosphonate terminated PAA dendrimer was synthesized which has a similar structure and self-assembly behaviour to amelogenin, the major enamel protein and plays a vital role in the biomineralization of tooth enamel. It encouraged in situ remineralization, also organized the size and shape of hydroxyapatite at the same time the functional groups provided strong dendrimer tooth binding capacity (Figure 1.24) [210]. Furthermore, alendronate functionalized polyacrylic acid was synthesized to mimic non-collagenous proteins and act

as a nucleation point for mineralization. Zinc ions were used as antibacterial agents to inhibit the cariogenic bacteria activity and are designed to be released in acidic caries medium. The positive effect of alendronate on mineralization in artificial saliva was demonstrated [211].

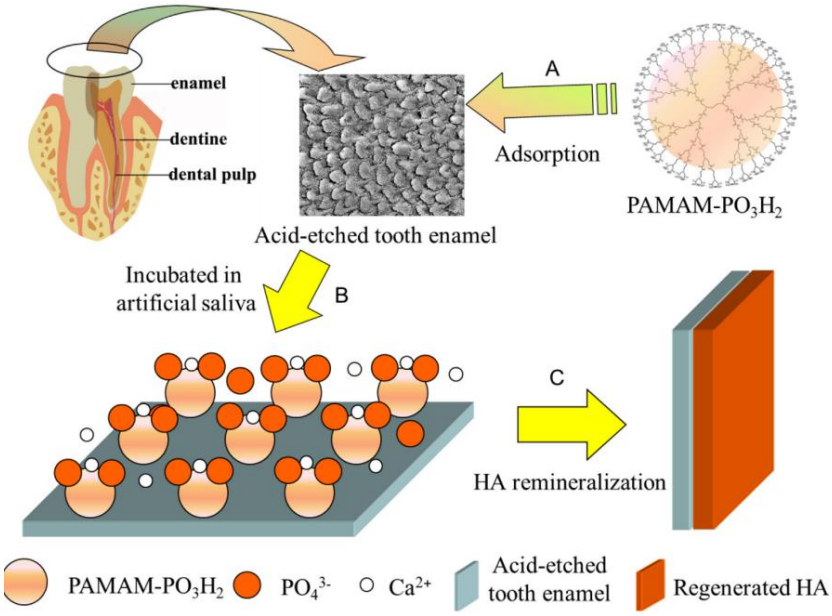

Figure 1.24. Schematic demonstration of the adsorption of PAMAM-PO_3H_2 on the surface of tooth enamel. Reprinted from [210].

2. OBJECTIVES AND SCOPE

The aim of this study is to synthesize novel monomers, polymers and crosslinked networks with (bis)phosphonate functionality and evaluate their properties for bone related biomedical applications such as tissue engineering and targeted drug delivery.

The first two chapters cover the studies about photopolymerizable, pH sensitive and degradable macromers. In the first project, phosphonate incorporated poly(β-aminoester) macromers with varied hydrophobicity were synthesized and homo- or copolymerized with PEGDA to prepare networks with different mechanical properties. In the second project, poly (amido amine) macromers containing adjustable amount of phosphonic acid were designed and their pH and ion sensitive hydrogels providing structure dependant hydroxyapatite nucleation were fabricated by homo- or copolymerization with 2-hydroxyethyl methacrylate. The following two chapters focus on polymers showing enhanced interaction with Ca^{2+} ion due to bisphosphonate groups. In the third project, bisphosphonate functionalized acrylamides were synthesized and used to produce block copolymers with N-isopropyl acrylamide via RAFT polymerization technique to investigate the effect of polymer structure on thermoresponsive behaviour. In the last project, alendronate was electrostatically or covalently incorporated into polymer via post polymerization modification and HAP affinity of resultant polymers were evaluated to explore their potential for dental materials and controlled release applications.

In summary, in this thesis the influences of phosphonate based functional groups and hydrophobicity on properties such as degradation rate, mineralization capacity, aqueous behaviour and HAP affinity were investigated to analyze their potential as biomaterials.

3. STRUCTURE-PROPERTY RELATIONSHIPS OF NOVEL PHOSPHONATE-FUNCTIONALIZED NETWORKS AND GELS OF POLY(β-AMINO ESTERS)

This chapter is published as: Altuncu, S., F. Demir Duman, U. Gulyuz, H. Yagci Acar, O. Okay and D. Avci, "Structure-property relationship of novel phosphonate-functionalized networks and gels of poly (β-amino esters)", *European Polymer Journal*, Vol. 113, No. April, pp.155-164, 2019.

3.1. Introduction

pH sensitivity, biodegradability and high biocompatibility make poly(β-amino esters) (PBAEs) important biomaterials with many potential applications including drug and gene delivery and tissue engineering, where their degradation should be tuned to match tissue regeneration rates. Although PEGDA hydrogels are one of the most widely studied biomaterials due to their biocompatibility and bioinertness, they have very slow degradation in vivo and hence are unsuitable for long-term implant applications. Therefore, it is desirable to adjust their degradation by functionalization to match tissue regeneration rates. In this part, we have synthesized novel phosphonate functionalized PBAE macromers through Michael addition of a new difunctional phosphonated secondary amine and three different diacrylates with various hydrophilic/hydrophobic properties. The macromers were then copolymerized with PEGDA, to form gels with tunable degradation and mechanical properties. We focus on the effect of the chemical structure of PBAE macromers on gel properties such as swelling and degradation. Moreover, for the first time in the literature, we have also studied the mechanical properties of the gels as a function of the type and the amount of the macromers.

3.2. Experimental

3.2.1. Materials and Methods

4,9-dioxa-1,12-dodecanediamine, diethyl vinylphosphonate, 1,6-hexanediol diacrylate (HDDA), poly(ethylene glycol) diacrylate (PEGDA, M_n = 575 Da), 1,6-hexanediol ethoxylate diacrylate (HDEDA), tris(trimethylsilyl) phosphite (TMSBr), 1,8-diazabicyclo[5.4.0]undec-7-ene (DBU) and 2,2-dimethoxy-2-phenylacetophenone (DMPA) were commercially available from Aldrich Chemical Co. and were used as received. Roswell Park Memorial Institute (RPMI) 1640 medium (with L-glutamine and 25 mM HEPES), penicillin/streptomycin (pen-strep) and trypsin-EDTA were purchased from Multicell, Wisent Inc. (Canada). Fetal bovine serum (FBS) was obtained from Capricorn Scientific GmbH (Germany). Thiazolyl blue tetrazolium bromide (MTT) and phosphate buffered saline (PBS) tablets were provided by Biomatik Corp. (Canada). The 96-well plates were purchased from Nest Biotechnology Co. Ltd. (China). NIH 3T3 mouse embryonic fibroblast cells were a kind gift of Dr. Halil Kavakli (Department of Molecular Biology and Genetics, Koc University, Istanbul, Turkey).

^{1}H, ^{13}C and ^{31}P NMR spectra were measured with a Varian Gemini 400 spectrometer using deuterated chloroform ($CDCl_3$) or methanol (MeOD) as solvent. Chemical shifts (δ) were reported as ppm downfield from tetramethylsilane (TMS) as an internal standard. Coupling constants (*J*) were given in hertz (Hz). IR spectra were obtained on a Thermo Scientific Nicolet 6700 FTIR spectrometer in the range of 4000–650 cm^{-1}. Potentiometric titrations were carried out using a WTW Inolab 720 pH meter and WTW SenTix 41 epoxy pH electrode at room temperature. Glass transition temperatures (T_g) of the macromers and gels were determined by using a differential scanning calorimeter (DSC, TA Instruments, Q100). The samples were analyzed at a heating rate of 10 °C/min and in a temperature range of -90–200 °C. Degradation studies were done using a VWR Incubating Mini Shaker operating at 37 °C and 200 rpm.

3.2.2. Synthesis of Phosphonate Functionalized Diamine (PA)

For the first method, 4,9-dioxa-1,12-dodecanediamine (0.5 g, 0.52 mL, 2.45 mmol) and diethyl vinylphosphonate (0.84 g, 0.79 mL, 5.15 mmol) were mixed at room temperature for two days. The mixture was washed with hexane to remove unreacted diethyl vinylphosphonate and the pure product was obtained as colorless liquid in 85% yield. For the second method, 4,9-dioxa-1,12-dodecanediamine (0.5 g, 0.52 mL, 2.45 mmol) and diethyl vinylphosphonate (0.80 g, 0.75 mL, 4.89 mmol) were mixed in water (1.5 mL) at 85 °C for 45 min. After removal of water, the mixture was washed with hexane to remove unreacted starting materials and the pure product was obtained as colorless liquid in 74% yield. ^{1}H-NMR (400 MHz, $CDCl_3$, δ): 1.31 (t, $^{3}J_{HH}$ = 8 Hz, 12H, CH_3), 1.60 (m, 4H, C*H*$_2$-CH_2-NH), 1.74 (quint, $^{3}J_{HH}$ = 8 Hz, 4H, CH_2), 1.94 (m, 4H, CH_2-P=O), 2.68 (t, $^{3}J_{HH}$ = 8 Hz, 4H, CH_2-NH) 2.88 (m, 4H, C*H*$_2$-CH_2-P=O), 3.40 (t, $^{3}J_{HH}$ = 8 Hz, 4H, CH_2-O), 3.45 (t, $^{3}J_{HH}$ = 4 Hz, 4H, CH_2-O), 4.09 (m, 8H, CH_2-O-P=O) ppm. ^{13}C-NMR (100 MHz, $CDCl_3$, δ): 16.35, 16.41 (d, CH_3), 25.68, 27.07 (d, CH_2-P=O), 26.30 (CH_2), 29.93 (*C*H_2-CH_2-NH), 43.23, 43.25 (d, NH-C*H*$_2$-CH_2-P=O), 46.86 (CH_2-NH), 61.51, 61.58 (d, CH_2-O-P=O), 69.09 (CH_2-O), 70.63 (CH_2-O) ppm. ^{31}P-NMR (162 MHz, $CDCl_3$, δ): 30.47 ppm. FTIR (ATR): 3503 (N-H), 2935 (C-H), 1236 (P=O), 1022, 954 (P-O) cm^{-1}.

3.2.3. Synthesis of PBAE Macromers

For the first method, the diacrylates (PEGDA, HDEDA or HDDA) and PA were mixed at a molar ratio of 1.1:1, 1.2:1 and 1.3:1 in 10 mL vials at room temperature for 4 days while stirring. If the stirring was stopped due to an increase in viscosity, a very small amount of dichloromethane (DCM) was added to the mixture and removed under reduced pressure after the reactions. The macromers were obtained as colorless viscous liquids in 78-85% yield after washing with petroleum ether (HDEDA and HDDA-based ones) or diethyl ether (PEGDA-based ones) to remove unreacted diacrylates, PA or monoaddition products; and dried under reduced pressure. For the second method, PA (0.5 g, 0.94 mmol) and DBU (0.14 g, 0.14 mL, 0.94 mmol) were mixed in MeOH (1 mL). Then PEGDA (0.65 g, 0.58 mL, 1.13

mmol) was added and the mixture was stirred at room temperature for 12 h. After removal of MeOH, the residue was washed with diethyl ether to remove unreacted diacrylates, PA or monoaddition products; and dried under reduced pressure to give the product in 32-35 %.

To obtain dealkylated macromers, TMSBr (3.6 mmol) was dropwisely added to a solution of macromers based on HDDA and PEGDA (corresponding to 0.6 mmol phosphonate) in dry DCM (1.2 mL) in an ice bath under nitrogen. The mixture was stirred for 10 h at 30 °C. The solvent and unreacted TMSBr were removed under reduced pressure. The residue was stirred with methanol (1.2 mL) for 15 min. The solution was concentrated under reduced pressure to give pure products. Dealkylated macromers M1-d and M3-d obtained as light-yellow solid in 67 % and 63 % yield respectively.

3.2.4. pK_b Measurements

The pK_b values of the macromers were determined by titration method. 50 mg of macromer was dissolved in deionized water to give a final concentration of 1.0 mg/mL. The pH of the macromer solutions was set to pH 2.0 using 2 M HCl and titrated to pH 11 with 0.1 M NaOH solution. The pH of solutions was measured after each addition using a pH meter (WTW Inolab pH 720) at room temperature. The pK_b value was determined from the inflection point of the titration curve which responds to the pH value where 50% of protonated amine groups are neutralized.

3.2.5. Synthesis of PBAE Networks

A 10 % (w/v) DMPA solution in DCM was added to a macromers M1, M2, M3 (HDDA, HDEDA, PEGDA based macromers respectively) and PEGDA mixture (80:20 or 50:50 w% PEGDA:macromer) to give a final concentration of 1 w% DMPA. After the removal of the solvent in a vacuum oven, the mixture was placed into a vial and polymerized

in a photoreactor containing 12 Philips TL 8W BLB lamps, exposing it to UV light (365 nm) for 30 min. For comparison, the macromers alone were also polymerized under the same conditions. The polymer samples thus formed were weighed and immersed in ethanol for approximately 12 h to remove unreacted components. After drying in a vacuum oven until constant weight, the samples were weighed again (final mass).

PEGDA and phosphonic acid functionalized PBAE macromer (M1-d and M3-d) mixtures with weight ratios of 50:50 and 80:20 were dissolved in water at total water concentration of 75 wt%. Irgacure 2959 (2 wt% of total monomer weight) was added as a photoinitiator and the mixtures were polymerized using the same procedure with PBAE gels. Unreacted species were removed by immersing ethanol and water, then the swollen samples were lyophilized. The gel fraction W_g, that is, the fraction of insoluble polymer, was calculated from the initial and final mass of the gel specimens.

3.2.6. Swelling Studies

Swelling studies were conducted by immersing dry gel samples (45±15 mg) into PBS (pH 7.4) solution at 37 °C. The samples were removed from the solution at pre-determined time intervals, blotted on filter paper and the swollen weight was measured. The increase in the weight of the samples was recorded as a function of time until equilibrium was reached. The degree of swelling (Q) was calculated using the equation:

$$Q = \frac{Ws - Wd}{Wd}\ x\ 100 \qquad (3.1)$$

where W_s and W_d refer to the weight of swollen and dry samples respectively. The average data obtained from triplicate measurements were reported. The standard deviations were less than 5.2%.

3.2.7. Degradation Studies

In vitro degradation of the gel samples as prepared above (45±15 mg, initial mass) were carried out in PBS (pH 7.4) solution at 37 °C on a temperature-controlled orbital shaker constantly agitated at 200 rpm. At various time (2 days, 1, 2 and 4 weeks) points, three samples were removed, lyophilize and weighed (final mass). The mass loss was calculated from the initial and final mass values.

3.2.8. Mechanical Analysis

Mechanical properties of PBAE gels in equilibrium with PBS solution were determined through uniaxial compression measurements on a Zwick Roell test machine using a 500 N load cell in a thermostated room at 23 ± 2 °C. The cylindrical gel samples were cut into cubic samples with dimensions 3x4x4 mm. Before the tests, a complete contact between the gel specimen and the metal plate was provided by applying an initial compressive force of 0.01 N. The tests were carried out at a constant cross-head speed of 1 $mm.min^{-1}$. Compressive stress is presented by its nominal value σ_{nom}, which is the force per cross-sectional area of the undeformed gel specimen, while strain is given by ε which is the change in the specimen length with respect to its initial length. Young's modulus E of the hydrogels was calculated from the slope of stress-strain curves between 10 and 15% compressions. For reproducibility, at least three samples were measured for each gel and the results were averaged.

3.2.9. *In vitro* Cytotoxicity Assay

NIH 3T3 cells were used to evaluate the cytotoxicity of the degradation products of the prepared gels. The cells were cultured in RPMI 1640 complete medium supplemented

with 10% (v/v) FBS and 1% (v/v) pen-strep in 5% CO_2-humidified incubator at 37 ºC and passaged every 2-3 days. For the cytotoxicity assay, the cells were seeded at a density of 10^4 cells/well in RPMI 1640 complete medium into 96-well plates and incubated at 37 ºC in 5% CO_2 atmosphere until 60-80% confluency. Then, the degradation products of the hydrogels in different concentrations ranging between 10-200 µg/mL were introduced into the wells. After 24 h further incubation, the cell viability was assessed using MTT colorimetric assay by the addition of 50 µL of MTT solution (5 mg/mL in PBS) into each well with 150 µL of culture medium and incubated for 4 more hours. The purple formazan crystals formed as a result of mitochondrial activity in viable cells were dissolved with ethanol:DMSO (1:1 v/v) mixture. Each sample's absorbance at 600 nm with a reference reading at 630 nm was recorded using a BioTek ELX800 microplate reader (BioTek Instruments Inc., Winooski, VT, USA). Cells which were not exposed to degradation products of gels were used as controls. 100% viability was assumed for the control cells; hence the relative cell viability was calculated from equation (2):

$$Cell\ viability\ (\%) = \frac{Absorbance_{sample}}{Absorbance_{control}} \text{x } 100 \qquad (n = 4) \qquad (3.2)$$

3.2.10. Statistical Analysis

Statistical analysis of the degradation products was conducted by using nonparametric Kruskall–Wallis one-way analysis of variance followed by multiple Dunn's comparison test of GraphPad Prism 6 software package (GraphPad Software, Inc., USA). All measurements were expressed as mean values ± standard deviation (SD). $p < 0.05$ was accepted as statistically significant difference ($n=5$).

3.3. Results and Discussion

3.3.1. Synthesis and Characterization of Phosphonate Functionalized Diamine and PBAE Macromers

A novel phosphonate-functionalized secondary diamine (PA) was synthesized via solvent-free aza-Michael reaction between 4,9-dioxa-1,12-dodecane diamine and diethyl vinylphosphonate (Figure 3.1). The molar ratio of the diamine to diethyl vinylphosphonate was fixed at 1:2.1 to fully end-modify the amine and reaction was conducted at room temperature for two days (method 1). The product was obtained as a colorless viscous liquid in high yields (85 %). However, shortening the reaction to 45 minutes at 85 ºC using water as solvent also produced good results (method 2), similar to refs. [212–214]. It was reported that water activates the aza-Michael addition between amines and diethyl vinylphosphonates by both hydrogen bonding between water and phosphonate group and water and the amine [212]. PA is highly soluble in polar (water, ethanol) and weakly polar solvents (chloroform, diethyl ether), but insoluble in non-polar organic solvents (hexane) (Table 3.1).

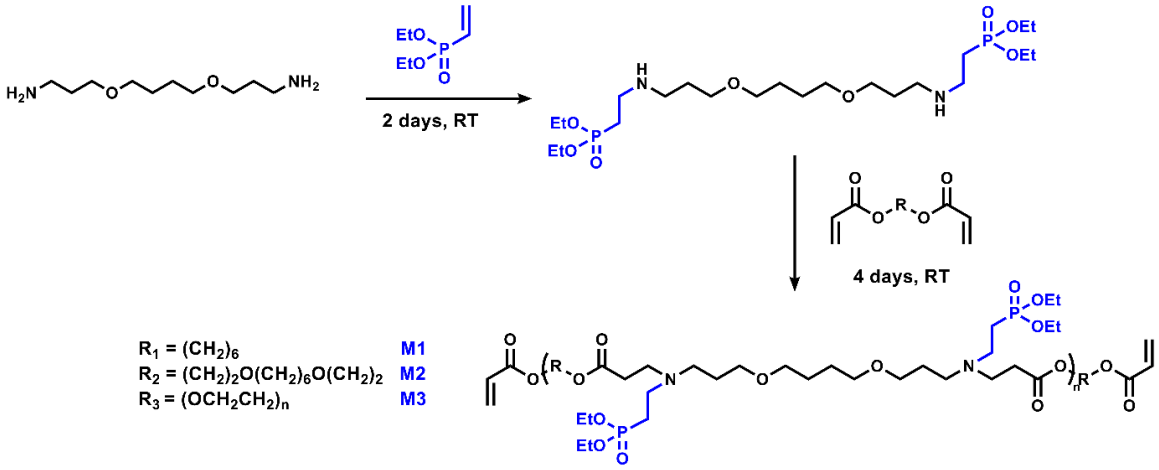

Figure 3.1. Synthesis of PA and PBAE macromers M1, M2, and, M3 derived from HDDA, HDEDA, and PEGDA, respectively.

Table 3.1. Solubilities of PA and the synthesized macromers.

Amine/Macromer	$CHCl_3$	H_2O	Petroleum ether	Diethyl Ether	Hexane	Ethanol
PA	+	+	+	+	-	+
M1	+	-	-	-	-	+
M2	+	+/-	-	-	-	+
M3	+	+	-	-	-	+

The structure of PA was confirmed by ^{1}H-, ^{13}C- and ^{31}P-NMR and FTIR spectroscopy. For example, ^{1}H NMR spectrum of the amine shows the characteristic peaks of methyl protons at 1.31 ppm, methylene protons adjacent to phosphorus at 1.94 ppm and methylene protons adjacent to nitrogen at 2.68 and 2.88 ppm (Figure 3.2). The small shoulders of peaks at 1.94 and 2.88 ppm are probably due to the small amount of diadduct (6 %) formation resulting from a slight excess of diethyl vinylphosphonate (2.1 mol) used compared to 4,9-dioxa-1,12-dodecane diamine (1 mol). This side product, which is a tertiary amine, was not isolated since it will not undergo reaction with diacrylates used for PBAE synthesis. The ^{13}C NMR spectrum of PA showed a doublet at 25.68, 27.07 ppm due to the carbon attached to phosphorus (Figure A.1). The FTIR spectra of PA showed absorption peaks of NH, P=O and P-O at 3503, 1236, 1022 and 954 cm^{-1} (Figure A.3)

Three PBAE macromers with different backbone structures were synthesized (Method 1 in experimental section; later method 2 [215] was applied to shorten the reaction time, but results from here on refer to macromers produced using method 1) from the step-growth polymerization of three diacrylates (HDDA, HDEDA and PEGDA) and PA to evaluate how chemical alterations affect final properties of the resultant networks (Figure 3.1). The diacrylate: PA molar ratios were used as 1.1:1, 1.2:1 and 1.3:1 in order the obtain macromers with different molecular weights (Table 3.2). In the following, the macromers derived from HDDA, HDEDA and PEGDA are abbreviated as M1, M2, and M3, respectively. The hydrophilicity of the macromers increases in the order of M1 < M2 < M3. Their water-

solubilities are highly dependent on the diacrylate they were synthesized from, e.g., M3 is soluble, M1 is not soluble, and M2 is slightly soluble, as expected from the order of their hydrophilicities (Table 3.1).

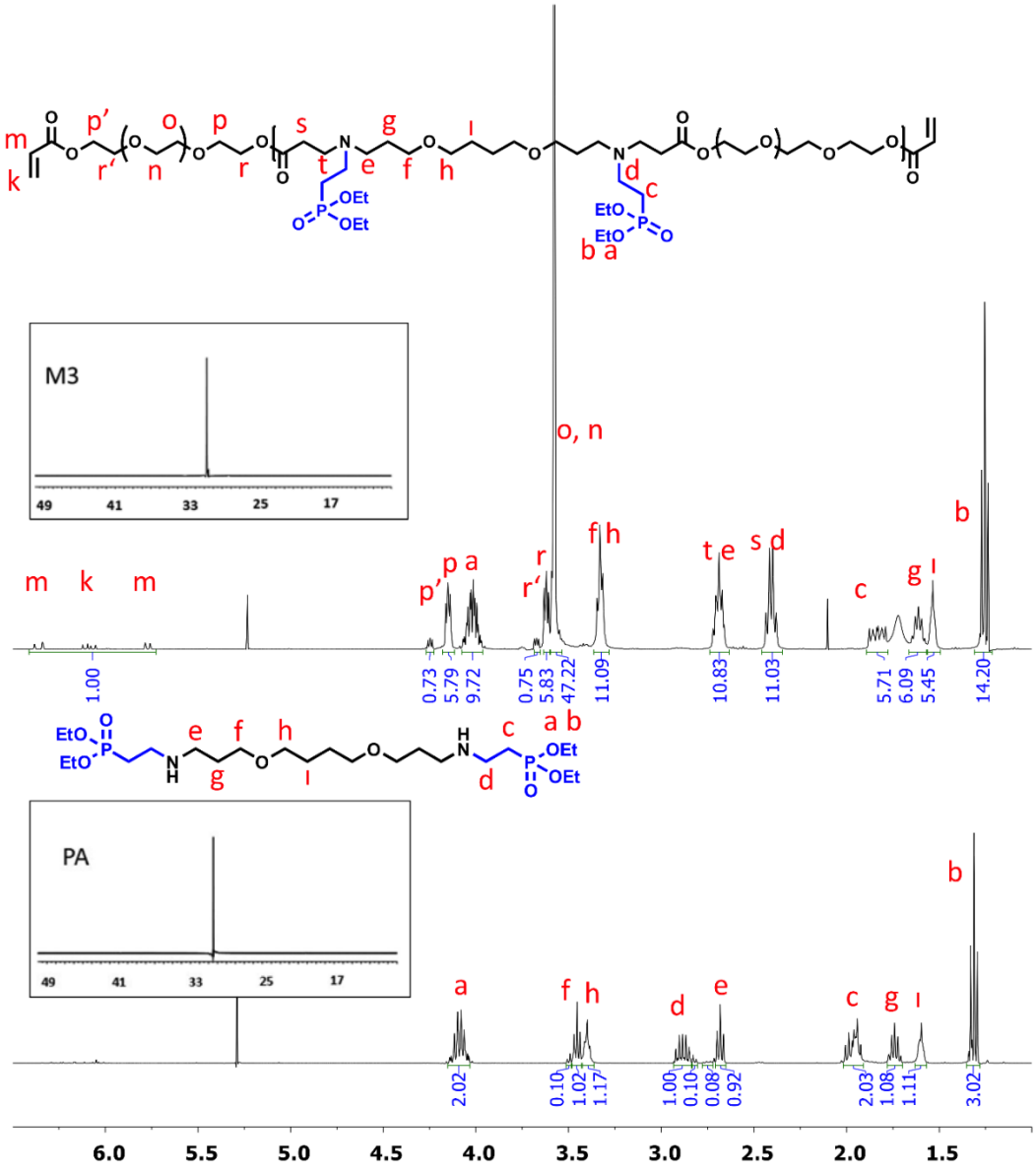

Figure 3.2. ^{1}H NMR spectra of PA and M3 (PEGDA:PA mol ratio of 1.1:1).

The structures of PBAE macromers were confirmed using ^{1}H NMR spectroscopy (Figure 3.2). The peaks at 5.8-6.5 demonstrate the maintenance of the acrylate terminal

groups, and the average number of repeat units (n) of the macromers was calculated via comparison of the areas of the acrylate protons (labeled as k and m at 5.8-6.5 ppm) to phosphonate ester (labeled as b at 1.3 ppm or f, h at 3.4 ppm) protons, and was found as 5.0 (M_n ~ 6300), 8.5 (M_n ~ 7000) and 4.6 (M_n ~ 4400) for M3, M1 and M2 macromers respectively, prepared at 1.2:1 diacrylate: PA ratio. These molecular weights were higher than those obtained for their bisphosphonated analogues because of lower steric hindrance of the PA [216]. FTIR spectra of the macromers show peaks at around 1020 and 950 cm^{-1} corresponding to the P-O stretching vibrations of phosphonate groups (Figure 3.3).

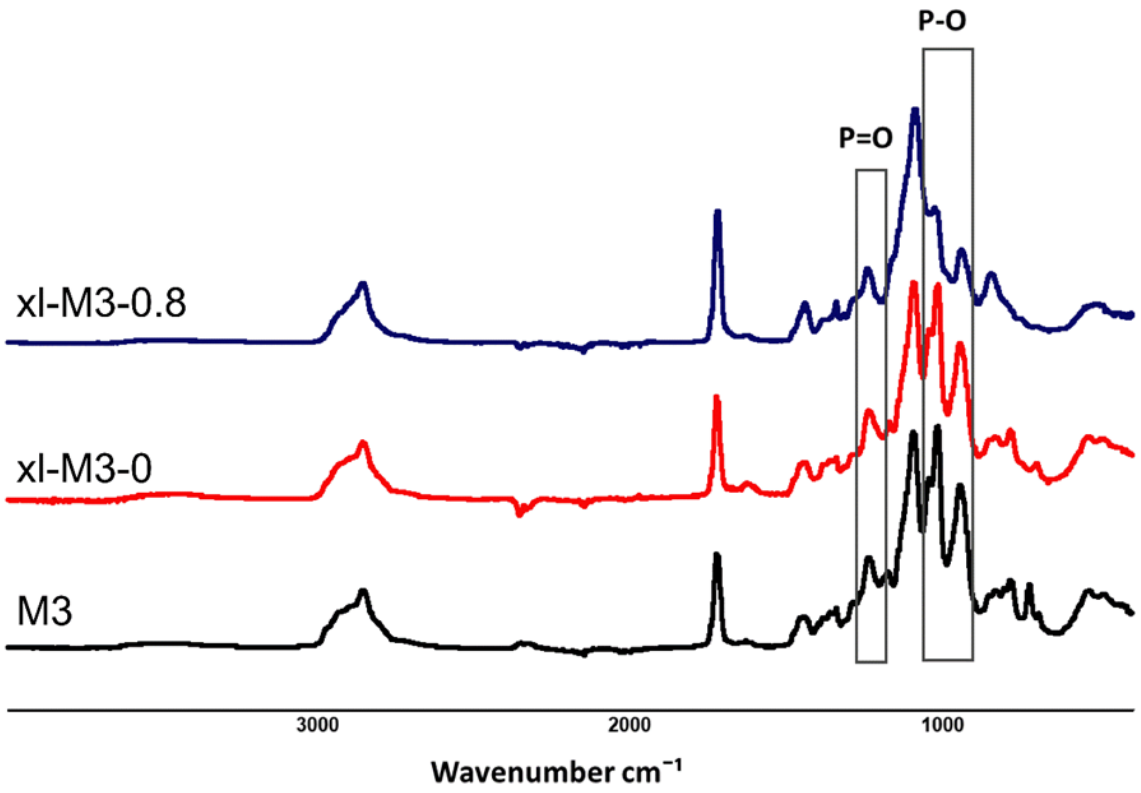

Figure 3.3. FTIR spectra of M3, xl-M3-0 and xl-M3-0.8.

Two phosphonic acid functionalized macromers (M1-d and M3-d) with different hydrophobicity were synthesized by the dealkylation of the phosphonate groups by trimethylsilyl bromide (TMSBr). The molar ratio of the phosphonate to TMSBr was fixed at 6:1 and reaction was conducted at 30 °C for 10 h to achieve full deprotection. The acidic

macromers were obtained as water soluble solids in 63-67 % yields. The structure of the dealkylated macromers were confirmed by ^{1}H NMR and FTIR spectroscopy as shown in Figure 3.4. The complete disappearance of ethyl peaks of the phosphonate groups supports the dealkylation process. Also, the methylene protons adjacent to nitrogen shifted downfield due to formation of quaternary ammonium salts. The FTIR spectra of TMSBr treated macromers show broad peaks in the region of 3200-2600 cm^{-1} because of the OH stretching (Figure A.4).

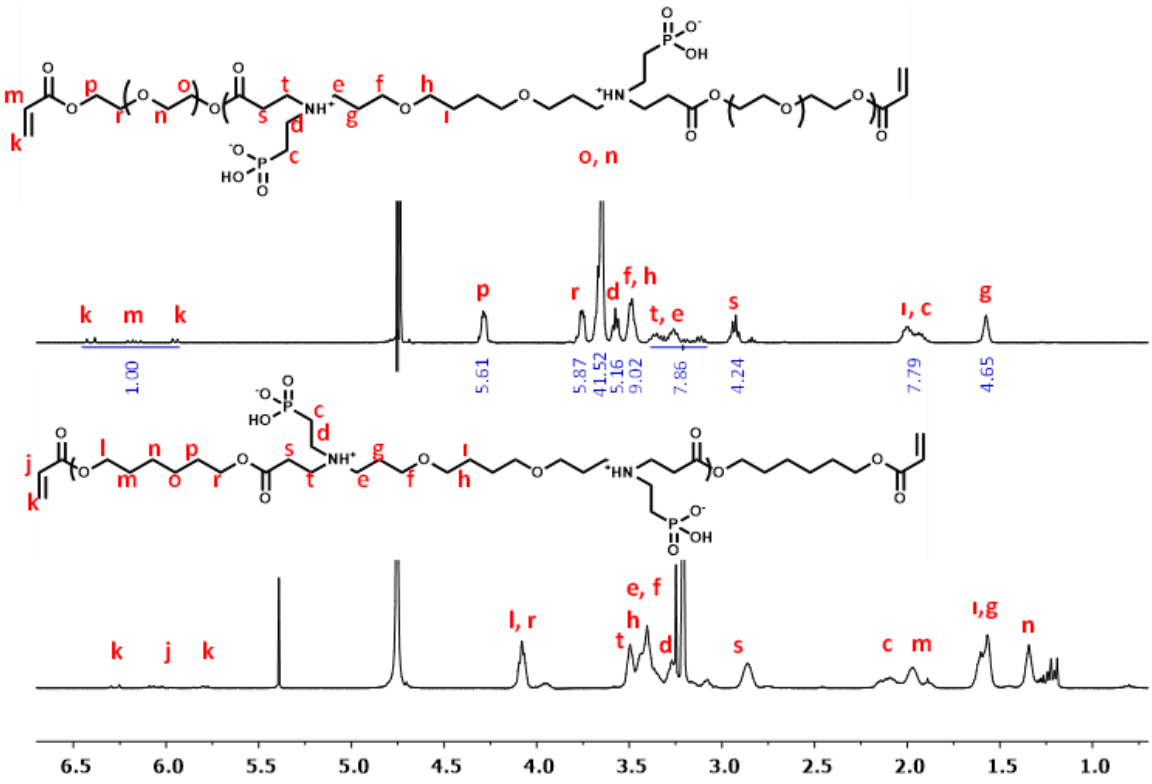

Figure 3.4. ^{1}H NMR spectra of M1-d and M3-d.

The solubility of PBAEs depends on solution pH due to tertiary amines in their structures. The abundance of these amine groups also gives PBAEs high buffer capacity. Therefore, PBAEs can be used as pH-responsive biodegradable polymers with tunable pH transition point for drug and gene delivery carriers. Their pH sensitivity can be modified by changing the diacrylates and the amines [217, 218]. In order to investigate the effect of PBAEs' structure on their pH sensitivities acid-base titration method was used (Figure 3.5).

All the studied polymers exhibited pH buffering capacities with slightly different buffering regions. The pK_b values of M1, M2 and M3 macromers with the lowest, medium, and highest hydrophilicity, respectively, were found to be 5.5, 5.7 and 6.1, indicating effect of hydrophilicity on the pK_b values. The electron donating alkyl groups lead to high electron density on the nitrogen atom and hence decrease pK_b, however oxygen atoms on HDEDA and PEGDA-based macromers are electron withdrawing, hence partially cancel the effect of alkyl groups. Similar behavior was observed by Song et al. [218]. As shown in Figure 3.5b, the plateaus indicating the buffering capacity are influenced by the dealkylation process. The phosphonic acid containing macromers, especially M3-d, do not show a distinct plateau region due to the increased hydrophilicity [218]. Continuous deprotonation of phosphonic acid groups with an increase in pH might be another reason of not observing wider plateau.

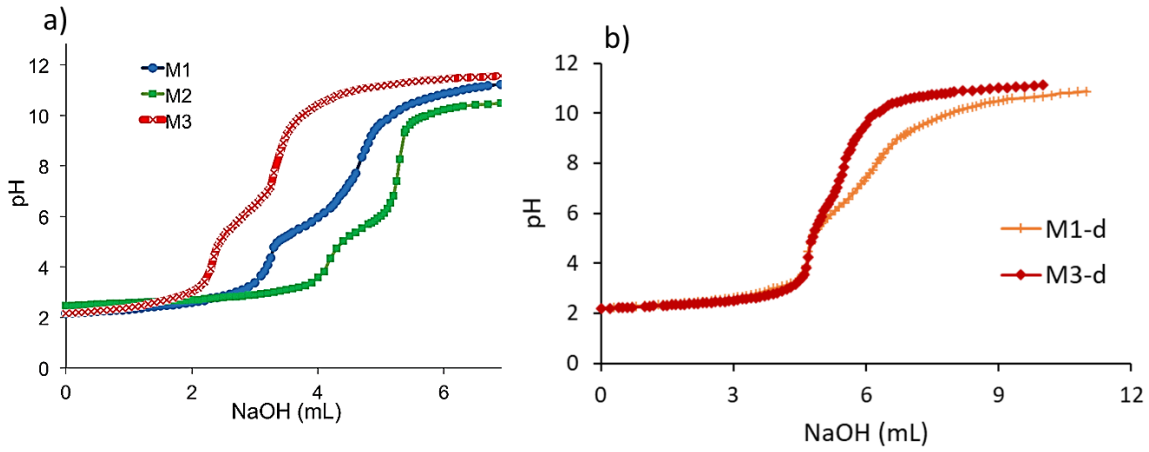

Figure 3.5. Titration curves of macromers.

PBAEs have low (sub-ambient) T_g due to their highly flexible structures resulting from the long ethylene glycol or alkyl chains in their backbones and lack of rigid side groups [219]. The T_g's of macromers were found to be -56, -59 and -60 ºC for M3, M2 and M1 macromers (Table 3.2).

Table 3.2. PA: diacrylate ratios, number of repeat units (n), number average molecular weights (M_n) and T_g of the macromers.

Macromer	**PA:diacrylate ratio**	**n [a]**	**M_n [a]**	**T_g (°C)**
M1	1:1.1	9.2	7500	-
M1	1:1.2	8.5	6960	-60
M2	1:1.2	4.6	4360	-59
M3	1:1.1	7.1	8700	-
M3	1:1.2	5.0	6280	-56
M3	1:1.3	4.1	5250	-

[a)]calculated from ^{1}H NMR spectra

3.3.2. Synthesis and Characterization of PBAE Networks

The mechanical properties of biodegradable polymers usually deteriorate in parallel with the biodegradation after the polymer is implanted in the body; hence their use in load-bearing applications is problematic. To address this problem, novel biodegradable polymer designs are investigated where the degradation rate can be tuned by minor modifications of structure. For example, Safranski et al. investigated thermo-mechanical properties of semi-degradable poly(β-amino ester)-*co*-methyl methacrylate networks under simulated physiological conditions [219]. These networks showed improved mechanical properties during degradation.

The PBAE macromers synthesized in this work can be used to prepare gels with different hydrophilicities and hence, different degradation and loss profiles affecting their mechanical properties. These macromers can also control the hydrophilic/hydrophobic

properties of gels they are incorporated into. To investigate these features, copolymers of the synthesized PBAE macromers with PEGDA were prepared by free radical polymerization under UV light using DMPA as photoinitiator. For comparison, the reactions were also conducted in the absence of the PEGDA cross-linker. In the following, the gel compositions were designated as xl-Mi-w, where Mi denotes type of the macromer (i = 1, 2, or 3 for HDDA, HDEDA, and PEGDA, respectively), w is the weight fraction of PEGDA in the comonomer feed (Table 3.3). For instance, xl-M1-0.80 presents the gel formed from HDDA macromer in the presence of 80 w% PEGDA, while xl-M1-0 denotes the gel obtained by homopolymerization of HDDA macromer (M1). After removal of unreacted macromers in ethanol, the gel fractions W_g were obtained as 53-98%. To understand the effect of anionic character on the final properties of hydrogels, copolymers of the dealkylated PBAE macromers with PEGDA were fabricated. The hydrogels based on phosphonic acid functionalized macromers were obtained with a gel fraction W_g between 81 and 92%.

FTIR analysis of the gel networks confirmed the presence of P=O and P-O peaks at 1244, 1024 and 952 cm^{-1} (Figure 3.3). Glass transition temperatures T_g of PBAE networks with $w \leq 0.50$ were around -50 °C, similar to those of the macromers they were synthesized from (Table 3.3). The networks with a higher PEGDA content, i.e., at w = 0.80 showed increased T_g (ca. -20 °C) due to higher crosslink density resulting from the lower molecular weight of PEGDA (M_n = 570 Da). However, the networks with 50% PEGDA showed two T_g values (-28 and -52 °C for xl-M1-0.50; -50 and -40 °C for xl-M3-0.50) (Table 3.3). This behavior is interpreted as due to block copolymer structure and the two T_g values correspond to the respective ones of PBAE and PEGDA, showing the heterogeneity of the components.

Table 3.3. Gel compositions, gel fraction W_g, degree of swelling Q, and T_g values.

Network	**W_g (%)**	***Q* (%)**	**T_g (°C)**
xl-M1-0	64.5±2.6	-	-53
xl-M1-0 *	53±4.2	-	-
xl-M1-0.50	93.2±0.1	38.8±3.3	-52, -28
xl-M1-0.80	91±2.2	31.3±4.0	-21
xl-M2-0	65.9±3.1	-	-
xl-M2-0 *	79.8±2.4	-	-
xl-M2-0.50	66.8±2.5	34.5±2.0	-
xl-M2-0.80	86.2±1.1	28.6±2.1	-24
xl-M3-0	81.3±4.8	-	-51
xl-M3-0 *	95.6±1.3	-	-
xl-M3-0.50	91.0±1.0	51.6±3.0	-50, -40
xl-M3-0.80	97.8±0.3	31.4±0.6	-20

*In the synthesis of macromers, diacrylate:amine molar ratio was used as 1.1:1.

3.3.3. Swelling of Networks

The gel networks (xl-Mi-w) were swollen in PBS (pH 7.4) to observe the influence of macromer molecular weight, amount and hydrophilicity of the macromer on their swelling behavior before and after degradation (Figure 3.6). Before degradation, swelling degrees were low (28.6-51.6%) because both the macromer and PEGDA components of the networks are crosslinkers. Moreover, the amount of the macromer does not influence the swelling

percentages except xl-M3-0.50. The presence of HDEDA vs. HDDA in the backbone of the PBAE macromer was found to not make an important difference in swelling; indicating that the hydrophilicities of the phosphonate-functionalities and PEGDA determine the swelling. However, when PEGDA-based PBAE macromer is used, the increased amount of PEGDA does make a difference, leading to the exception of xl-M3-0.50. This assertion is confirmed by the data of networks with 20 w% PBAE macromers (w = 0.80), where the swelling percentages were found to be similar to those of the 50% (w = 0.5) samples, the M3 sample showing only slightly higher swelling, since it aquires slightly higher amount of PEGDA with respect to M1 and M2 samples.

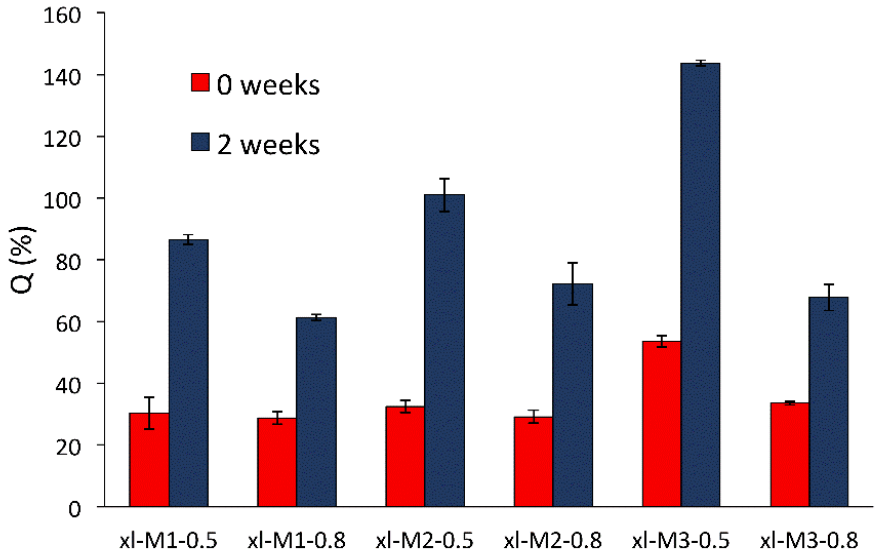

Figure 3.6. Swelling percentages (Q) of the gels before and after degradation for 2 weeks.

The degradation of the gels (xl-Mi-w) over time have been monitored by the time-dependent swelling measurements. After degradation in PBS for 2 weeks, the swelling degree of degraded gels increased compared to those of non-degraded ones with the same composition (Figure 3.6). While xl-M3-0.50 gel swelled 51.6% initially, after 2 weeks of degradation its swelling percentage was found to be about 143.7%. The swelling of the degraded gels increases with an increase in both PBAE content and its hydrophilicity, which also determines degradation rate of the gels. An explanation is that degradation destroys the

integrity of the hydrogel and enhances the penetration of water into the gel. This explanation was checked using mechanical tests conducted on virgin and degraded gels, as will be discussed later.

3.3.4. Degradation of Networks

Tissue-engineering scaffolds should both guide the proliferating cells to form new tissue and disappear when their job is completed. Therefore, the degradation rate of the scaffold should be tuned such that it turns slowly into a porous matrix into which molecules can diffuse, cells enter, adhere, proliferate and interconnect; and breaks apart at the appropriate time. Hence it is important to investigate degradation behavior of any new candidates for tissue-scaffold materials.

Figure 3.7 shows degradation of the PBAE gels (xl-Mi-w) in PBS (pH 7.4) at 37 °C. The dependence of degradation rate on PBAE structure is clearly evident. The gels formed from more hydrophobic PBAE macromer degrade slower; degradation rates were found to increase in the following order: xl-M1 < xl-M2 < xl-M3, in accord with the order of the increase of hydrophilicity. For example, xl-M3 and xl-M1 gels degraded 80% and 15%, respectively, within 2 days. The degradation of xl-M2 gels was completed in 6 days, and xl-M3 gels in 3 days. The more hydrophobic xl-M1 network has lower water uptake and undergoes slower cleavage of ester linkages compared to the other gels. Therefore, this trend was also consistent with the swelling behavior (after 2 weeks), which is an indirect method for measurement of degradation. It was also observed that the gels formed using low molecular weight PBAE macromers of the corresponding chemical structure have significantly lower degradation rate, e.g., the lower molecular weight xl-M3 gel prepared at a PA: diacrylate ratio of 1:1.2 had less degradation (80.4%) than the higher molecular weight one, 96.7%, formed at a ratio of 1:1.1. This behavior is due to more hydrolyzable linkages in the macromer and low crosslinking density.

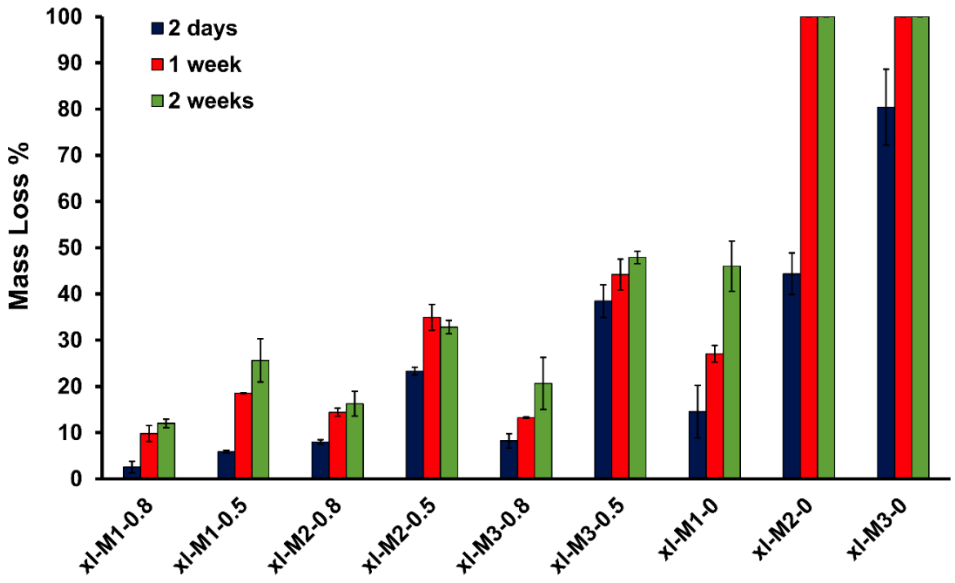

Figure 3.7. The mass loss of PBAE gels and PEGDA-PBAE copolymers in 2 days, 1 week and 2 weeks in PBS.

In order to tune degradation properties of PEGDA gels, PBAE macromers were copolymerized with PEGDA at different ratios. By changing the structure (hydrophilic/hydrophobic properties and molecular weight) of the macromers, gels with mass losses ranging from 12.0 % to 47.9 % in 2 weeks were obtained (Figure 3.7). The mass losses of gels obtained from M1 macromer with the highest hydrophobicity showed significant acceleration after 2 days. We conjecture that the water uptake for these was initially slow due to their hydrophobicity but became faster with increased diffusion of water due to formation of the first pores, which in turn accelerated the degradation. However, the hydrophilic character of oxygen containing macromers M2 and M3 enhances their water uptake resulting in fast degradation from the beginning. For example, the mass loss of xl-M1-08 reached 26% starting from 2.5% and xl-M3-0.8 reached 32% starting from 8%; in 4 weeks.

The degradation of PEGDA hydrogels crosslinked with dealkylated macromers (xl-Mi-w-d) were investigated in water and in 0.2 M $CaCl_2$ solution for 2 days as shown in

Figure 3.8a. The mass loss of xl-M3-0.8 control hydrogel (fabricated in the presence of water) is 16.6% which is two times higher than the degradation of bulk network prepared with the same composition (degradation profile is shown in Figure 3.7). Addition of water during hydrogel formation causes larger pores that may increase water diffusion and accelerate mass loss. However, phosphonic acid presence did not lead to an increase in degradation. The zwitterionic nature caused by the positive charge of tertiary amines in the backbone and negative charge on phosphonic acid may cause this outcome. On the other hand, the effects of larger pores as well as dealkylation on swelling percentages of 20 w% macromer containing hydrogels were clearly observed as shown in Figure 3.8b. Nevertheless, a noticeable shrinkage in $CaCl_2$ was not examined. It was expected that the interaction between phosphonic acid groups and Ca^{2+} ions form physical crosslinking which induces shrinkage but the formed zwitterionic group overcomes the anionic nature of phosphonic acid group. In addition, when the phosphonate amount reached to a certain level we could observe a noticeable change. The mass losses of xl-M3-50 hydrogels (for control and xl-Mi-w-d) are lower in $CaCl_2$ solution than in water, but this effect was not observed for xl-M3-0.8 hydrogels. Degradation slows down in the presence of divalent metal ion because the interaction between unpaired electrons of oxygen in the backbone of PBAE and Ca^{2+} increases crosslink density.

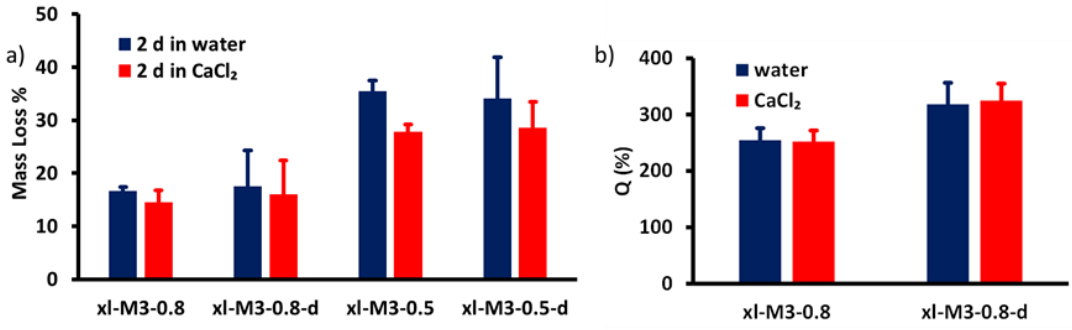

Figure 3.8. (a) The mass loss and (b) swelling of dealkylated PBAE hydrogels in water and 0.2 M $CaCl_2$ solution.

The surface morphologies of the networks (xl-Mi-w) were examined at various degradation percentages by SEM (Figure 3.9). The SEM images showed a smooth surface before degradation, which became porous and rough after degradation. The xl-M3-0 network prepared without PEGDA comonomer after 80% degradation showed a sponge-like appearance with interconnected pores. However, the copolymer network xl-M3-0.80 with 15% degradation showed smaller pore size. These observations demonstrate that porosity of the networks upon degradation can be controlled by changing the PBAE content and structure.

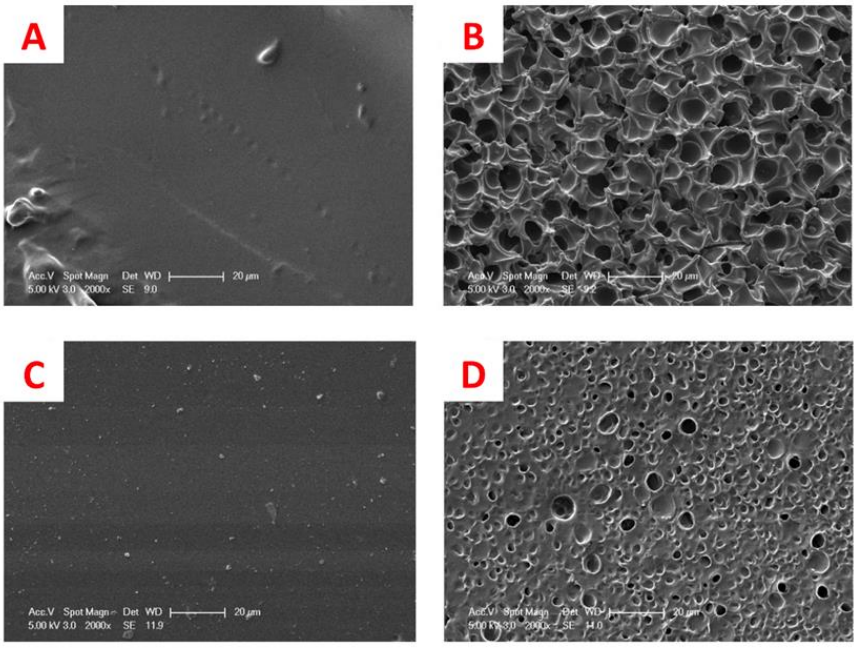

Figure 3.9. SEM images of networks: xl-M3-0 before (a) and after 80% degradation (b); xl-M3-0.80 before (c) and after 15% degradation (d).

In order to determine degradation mechanism of the networks xl-Mi-w, NMR and FTIR spectra of the degradation products of two of the PBAE networks, xl-M3-0 and xl-M2-0, were investigated after full degradation in water. FTIR spectrum of the degradation products of xl-M3-0 showed i) formation of a peak at 3481 cm^{-1} (due to OH groups), ii) broadening and decreasing intensity of C=O peak and formation of a new broad peak at 1594

cm^{-1} (Figure 3.10). ^{1}H NMR spectrum of the same sample indicated that the integral of the peak at 4.25 ppm due to the methylene protons adjacent to the ester ($COOCH_2$) is decreasing and a new peak at 3.6 ppm, due to the methylene adjacent to hydroxyl group ($HOCH_2$) is increasing. According to these results, we can say that networks degrade via hydrolysis of the multiple ester groups on the backbone into small molecule diols, bis(b-amino acids) and poly(acrylic acid) kinetic chains as reported in the literature [20, 37, 220].

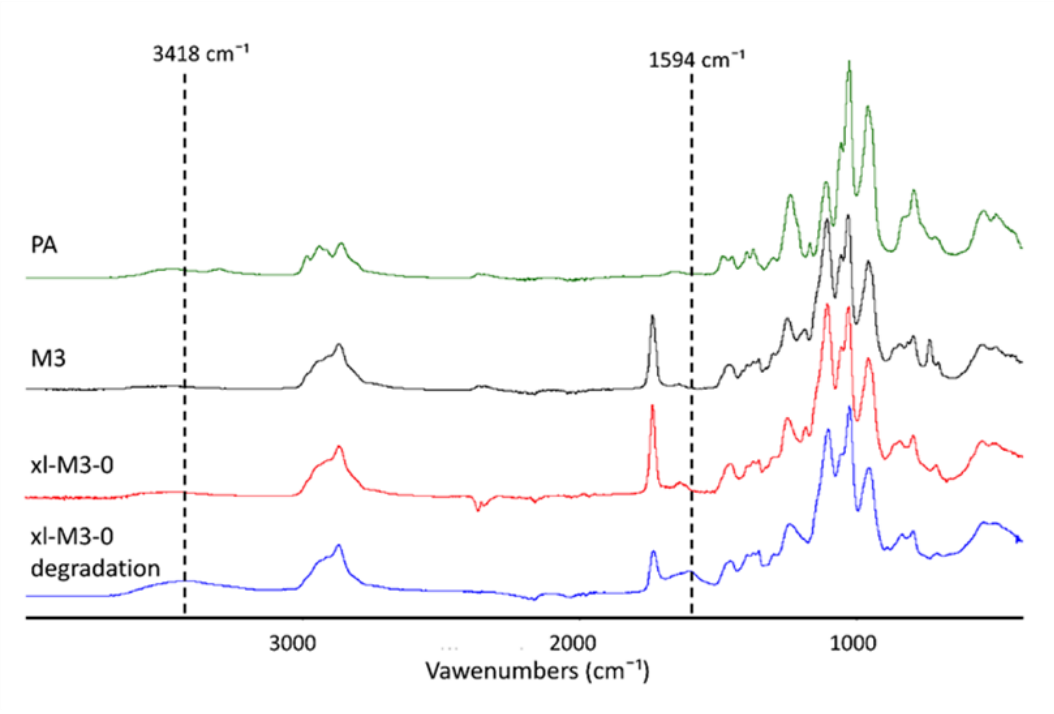

Figure 3.10. FTIR spectra of PA, M3, xl-M3-0 (before degradation) and xl-M3-0 (after 2 days of degradation in water).

3.3.5. Mechanical Properties of PBAE Networks

Mechanical properties of the gels (xl-Mi-w) in their equilibrium swollen states were investigated by uniaxial compression tests. Figure 3.11a shows stress-strain curves of the gels prepared at PEGDA weight fractions *w* of 0.80 (solid curves) and 0.50 (dashed curves). At w = 0.80, the gels sustain 25±2% compressions under around 6 MPa stresses, with a

maximum fracture stress of 7.4±0.8 MPa observed for xl-M2 gel. Decreasing the weight fraction *w* from 0.80 to 0.50 slightly increases the fracture strain while fracture stress decreases to 4±1 MPa indicating that incorporation of a larger amount of macromer into the gel network deteriorates their ultimate mechanical properties. Figure 3.11b presenting Young's moduli *E* of the gels reveals that, at *w* = 0.80, *E* is independent of the type of the macromer and remains at 27 MPa. The moduli of the hydrogels 2- to 3-fold decrease upon increasing the amount of macromer and the largest decrease was observed in xl-M2 gels.

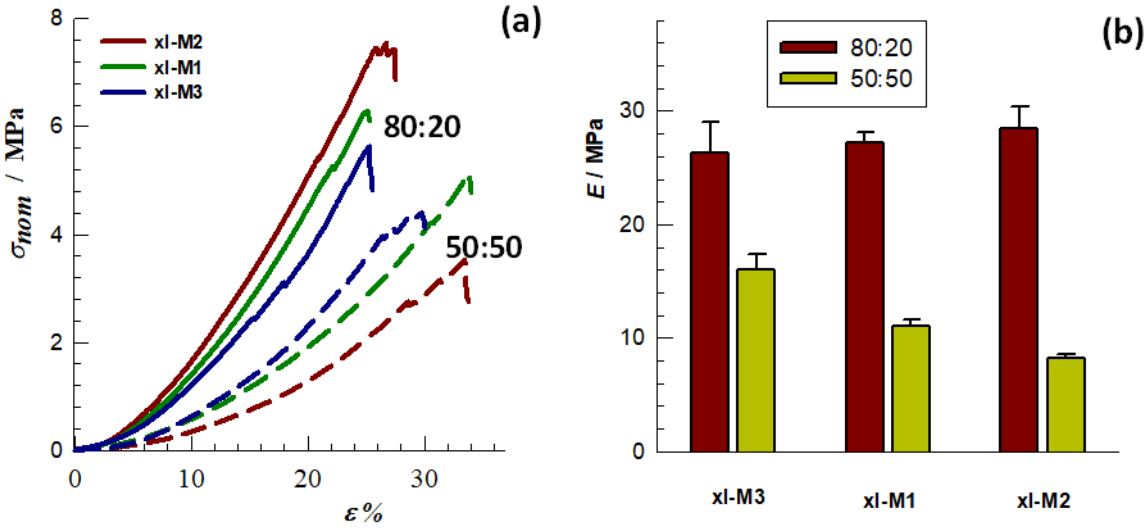

Figure 3.11. (a) Stress-strain curves of the gels at w = 0.80 (solid curves) and 0.50 (dashed curves). (b) Young's moduli E of the gels formed at w = 0.80 (dark red) and 0.50 (dark yellow).

Mechanical tests were also conducted on the gel specimens subjected to various degradation times up to 4 weeks. Typical stress-strain curves of virgin and 2 weeks-degraded xl-M3 and xl-M1 gels at w = 0.50 are shown in Figure 3.12a while Figure 3.12b compares their moduli at various degradation times. The tests revealed that the strain at break remains almost unchanged during the course of degradation up to 2 weeks while both the fracture stress and the modulus decrease. This decrease was significant at w = 0.50 indicating that increasing amount of macromer also increases the degradation rate of the gels. Moreover,

the more hydrophobic xl-M1 gel degraded slightly slower than the less hydrophobic xl-M3 gel which is in accord with the previous results.

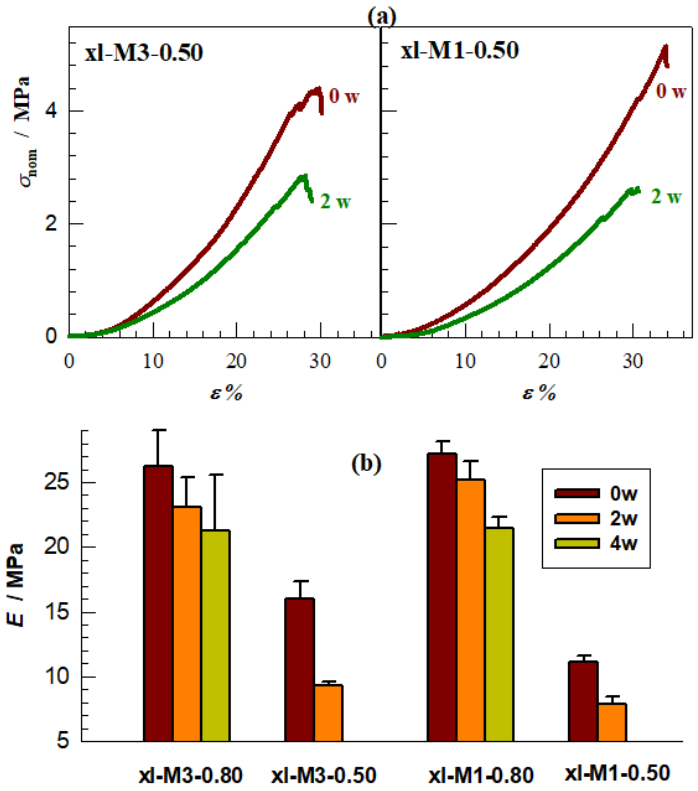

Figure 3.12. (a) Typical stress-strain curves of virgin and 2 weeks-degraded xl-M3 and xl-M1 gels formed from PEGDA and HDDA, respectively. w = 0.50. (b) The modulus E of gels at various degradation times.

Because both the degree of swelling Q of the hydrogels and their moduli E change during degradation, direct evidence of the change in the network structure can be obtained from their effective cross-link densities ν_e. According to the theory of rubber elasticity, Young's modulus E of an affine network is related to its cross-link density ν_e by refs [293, 294]. The relationship between Young's modulus and cross-linked density can be found from the formula:

$$E = 3\nu_e RT\left(\nu_2\right)^{1/3}\left(\nu_2^0\right)^{2/3} \tag{3.3}$$

where ν_2^0 and ν_2 are the volume fractions of cross-linked polymer just after the gel preparation and at the state of the measurements, respectively, *R* and *T* are in their usual meanings. Although the gels were prepared under solvent-free condition, the presence of unreacted macromers after gelation acting as a diluent leads to a decrease of ν_2^0 below unity. For the following calculations, we estimated ν_2^0 as equal to the gel fraction W_g. Moreover, ν_2 was calculated from the degree of swelling *Q* as:

$$\nu_2 = \left(1 + Q\, d_2 / d_1\right)^{-1} \tag{3.4}$$

where d_1 is the density of water (1 g mL^{-1}) and d_2 is the polymer density measured as 0.82 g mL^{-1}. By substituting *Q* and *E* values into eqs 3.3 and 3.4, we estimated the cross-link density ν_e of the gels at various times. Figure 3.13a shows the variation of ν_e of xl-M1 and xl-M3 gels with the degradation time. The fraction of degraded network chains calculated as 1- $\nu_\varepsilon / \nu_{e,o}$, where $\nu_{e,o}$ is the initial cross-link density at time = 0, is shown in Figure 3.13b. During the first two weeks, the crosslink density of the gels with w = 0.80 does not change much (filled symbols), and even remains unchanged for the M1 gel with the highest hydrophobicity. In contrast, ν_e of the gels with w = 0.50 rapidly decreases while the fraction of degraded network chain increases. After 2 weeks, around 20 and 30% of the network chains contributing to the gel elasticity are lost in xl-M1 and xl-M3 gels, respectively. These results show the significant effect of both the type and the amount of the macromers on the degradability of the gels.

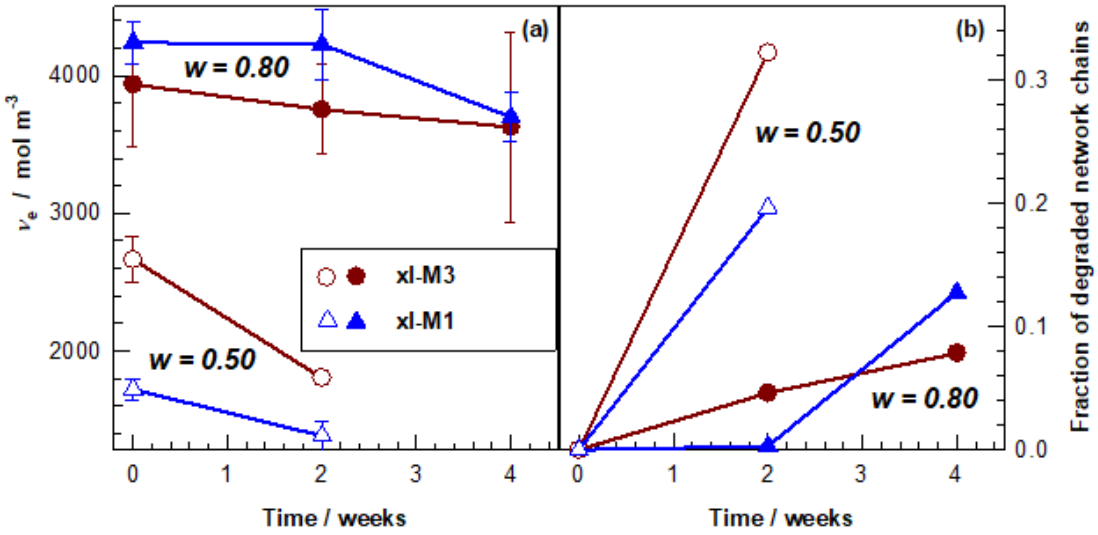

Figure 3.13. The cross-link density ν_e of the hydrogels (a) and the fraction of degraded network chains, 1- $\nu_e / \nu_{e,o}$, (b) both plotted against the degradation time. Empty symbols: w = 0.5, filled symbols: w = 0.8.

3.3.6. *In Vitro* Cytotoxicity of Polymer Degradation Products

The cytotoxicity measurement is an important step to determine the biocompatibility of a material for biomedical applications. The cytotoxicity of the degradation products of PBAE gels was investigated on NIH 3T3 cells using MTT cell metabolic activity assay (Figure 3.14). Following ISO standard 10993–5 [295], the cells in RPMI-1640 culturing medium was used to evaluate if there is a cytotoxic response to degradation products. Cells cultured under normal conditions without any material were used as a control. There was no significant difference between toxicities (cell viability > 80%) of PBAE degradation products at any concentrations against NIH 3T3. These values were also found not to be significantly different than those of control, indicating the synthesized PBAE gels as non-toxic materials.

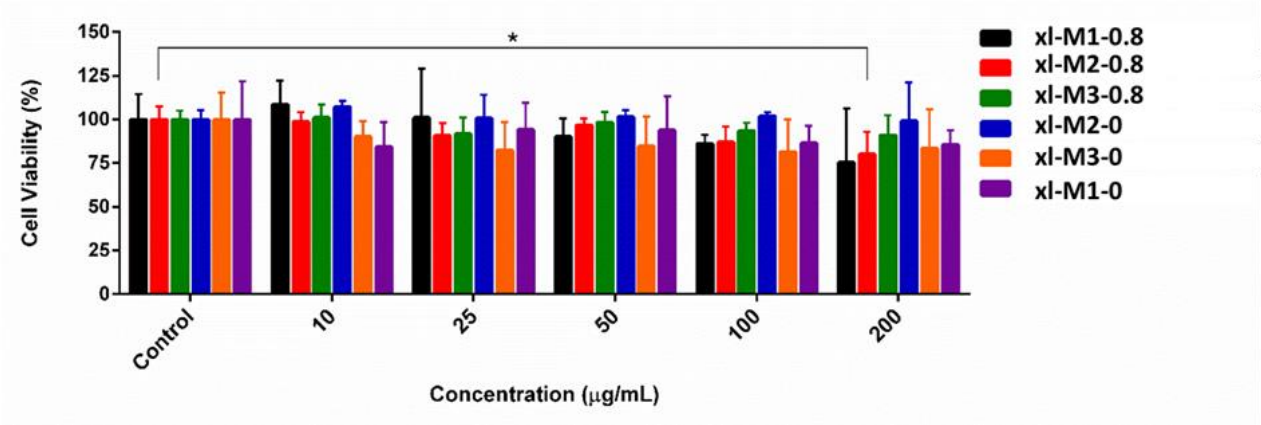

Figure 3.14. The effect of degradation products on cell viability of NIH 3T3 mouse embryonic fibroblast cells. Cells were treated with different concentrations of the products for 24 h. The cell viability test was performed by MTT assay (±SD; n = 5; $p < 0.05$ compared with all concentrations).

3.4. Conclusions

We demonstrated that novel phosphonate-functionalized secondary diamines with different spacers can be easily synthesized by Michael addition reaction and can be used for the synthesis of novel phosphonate-functionalized PBAEs. The phosphonic acid functionality can be achieved via selective cleavage of phosphonate groups by TMSBr and macromers with zwitterionic nature can be obtained. It was observed that by changing the PBAE structure it is possible to obtain homo- and copolymeric gels of different swelling, degradation and mechanical properties. Swelling percentages of PEGDA gels before degradation were independent of the PBAE crosslinker identity but after degradation increased with an increase in PBAE crosslinker content and was dependent on the type of crosslinker. The degradation rates of PBAE gels were controlled by the hydrophilicity (M1 < M2 < M3) and molecular weight of the PBAE macromer. Their degradabilities are about two to ten times higher than that of PEGDA gels containing 20 and 50 w % of PBAEs in two days. Mechanical tests reveal that PBAE gels prepared at a PEGDA weight fraction of 0.80 sustain 25±2% compressions under around 6 MPa stresses. Decreasing PEGDA weight fraction slightly increases the fracture strain while fracture stress decreases to 4±1 MPa

indicating that incorporation of a larger amount of macromer into the gel network deteriorates their ultimate mechanical properties. The results also show that the extent of decrease of the gel cross-link density during degradation correlates strongly and positively with increasing amount and hydrophilicity of the PBAE macromers. The cytotoxicity study of the degradation products on NIH 3T3 mouse embryonic fibroblast cells supports the biocompatibility of these materials for biomedical applications. Overall, these three PBAE macromers and their homo- and copolymers show promise to be used as scaffolds for tissue engineering applications.

4. PHOSPHONIC ACID-FUNCTIONALIZED POLY(AMIDO AMINE) MACROMERS FOR BIOMEDICAL APPLICATIONS

This chapter is published as: Altuncu, S., E. Akyol, M. N., Guven, G. Demirci, H. Yagci Acar and D. Avci, "Phosphonic acid-functionalized poly (amido amine) macromers for biomedical applications", *Journal of Biomedical Materials Research-Part A*, Vol. 108, No. 10, pp.2100-2110, 2020.

4.1. Introduction

Hydrogels, which are 3D networks of hydrophilic polymers capable of holding large amounts of water or biological fluids, hence resembling in some respects biological tissue, have great potential for biomedical applications in fields such as drug delivery systems, biosensors, self-healing materials and tissue engineering. Synthesis of biodegradable hydrogels with tunable properties such as nanopore size, mechanical properties and degradation times are important. Poly(amido amine)s **(**PAAs) are a promising class of synthetic biocompatible and biodegradable polymers used for hydrogel synthesis. The use of various types of amines and bisacrylamides with different substitutent groups during PAA synthesis enables incorporation of additional functionalities; the biodegradability of the PAAs can be arranged by changing the nature of starting materials, their hydrophobic/hydrophilic balance and the amount of charged groups on them. These properties can carry over to their hydrogels, too. Therefore, in this part, novel phosphonic acid-functionalized poly(amido amine) (PAA) macromers are synthesized through aza-Michael addition of 2-aminoethyl phosphonic acid or its mixture with 5-amino-1-pentanol at different ratios onto N,N′-methylene bis(acrylamide) to control the amount of phosphonic acid functionality. The macromers were homo- and copolymerized with 2-hydroxyethyl methacrylate at different ratios to obtain hydrogels with various hydrophilicities. We expect

to combine advantageous properties of phosphonic acid group such as mineralization, mechanical and cell adhesion with biodegradability and biocompatibity of PAAs to obtain degradable hydrogels. The effect of the macromer structure on hydrogels' swelling, biodegradation and mineralization properties were evaluated.

4.2. Experimental

4.2.1. Materials and Methods

N,N′-methylene bis(acrylamide) (MBA), 5-amino-1-pentanol (AP), 2-aminoethyl phosphonic acid (AEPA), 2-hydroxyethyl methacrylate (HEMA), 2-hydroxy-4′-(2-hydroxyethoxy)-2-methylpropiophenone (Irgacure 2959) and all solvents were purchased from Aldrich Chemical Co. and used as received. Dulbecco's Modified Eagle Medium (DMEM) (with l-glutamine and high glucose (4.5g/l)), penicillin/streptomycin (pen-strep), fetal bovine serum (FBS) and trypsin-EDTA were purchased from Diagnovum, Ebsdorfergrund (Germany). Thiazolyl blue tetrazolium bromide (MTT) was provided by Gold Biotechnology (USA). Phosphate buffered saline (PBS) tablets were provided by BBI Life Sciences (China). 96-well plates were purchased from Nest Biotechnology (China). NIH 3T3 mouse embryonic fibroblast cells and Saos-2 human osteosarcoma cells were a kind gift of Dr. Halil Kavakli (Department of Molecular Biology and Genetics, Koc University, Istanbul, Turkey). U-2 OS human bone osteosarcoma epithelial cells were a kind gift of Prof. Devrim Gozuaçik (Department of Molecular Biology, Genetics and Bioengineering, Sabanci University, Istanbul, Turkey).

^{1}H NMR spectra were recorded with a Varian Gemini 400 MHz spectrometer at ambient temperature in deuterated solvents. FT-IR spectra were obtained with a Nicolet 380 FT-IR spectrometer (Thermo Scientific) equipped with an attenuated total reflection (ATR) element. Potentiometric titrations were carried out using a WTW Inolab 720 pH meter and WTW SenTix 41 epoxy pH electrode at room temperature. The thermal transitions were

verified by differential scanning calorimetry (DSC) with the DSC Q100 apparatus (TA Instruments) using heating rate of 10 °C min^{-1} under nitrogen. Degradation studies of the hydrogel samples were performed using an incubator shaker (VWR) operating at 37 °C and 200 rpm. The morphologies of the hydrogel samples were examined using scanning electron microscopy (SEM) (FEI-Philips XL30) under an accelerating voltage of 7.0 kV after sputter coating of the lyophilized samples with a gold layer. The EDX analysis was used to identify the elemental composition of materials. Thermogravimetric analysis (TGA) studies were performed under nitrogen with a TGA STA 6000 (Perkin Elmer) using a heating rate of 10 °C min^{-1}.

4.2.2. Synthesis of PAA Macromers

Three PAA macromers were prepared by combining MBA with AP and/or AEPA at mol ratios MBA:AP:AEPA of 1.1:1.0:0, 1.1:0.7:0.3 and 1.1:0:1.0; and were denoted as PAA0, PAA30 and PAA100, respectively. The synthesis was carried out using a total concentration of 1.5 M in water/methanol mixture (v/v= 1/3) for the two/three starting compounds; at 50 °C for 3 days. For example, for the synthesis of PAA30, first AEPA was neutralized with potassium hydroxide by stirring a mixture of AEPA (265.1 mg, 2.12 mmol) and potassium hydroxide solution (0.13 g, 2.33 mmol in 2.5 mL water) at room temperature for one hour. Then, AP (0.51 g, 4.95 mmol) and MBA (1.2 g, 7.78 mmol) dissolved in 7.5 mL methanol were added to the solution under nitrogen atmosphere. The solution was stirred at 50 °C for 3 days and then methanol was removed under reduced pressure. The solution was then diluted with water and dialyzed using a membrane with a molecular weight cut-off of 1000 in distilled water to remove the unreacted components. The macromer was obtained as a white solid in 47 % yield after lyophilization. The synthesis of PAA0 and PAA100 follow the same procedure, without AEPA or AP. The yields of the products were 52 and 44 %, for PAA0 and PAA100, respectively.

4.2.3. pH-sensitivity of PAA Macromers

PAA macromers (50 mg) were dissolved in deionized water at a concentration of 1.0 mg/mL and the pH of the solution was adjusted to around 2.0 using 2.0 mol/L of HCl solution. Then the solution was titrated with 0.1 mol/L NaOH solution at increments of 0.5 mL until pH 11.0. The pH values of the solution were monitored by a pH meter (WTW Inolab pH 720) at room temperature.

4.2.4. Synthesis of PAA and PAA-crosslinked HEMA Hydrogels

HEMA and PAA macromer mixtures with weight ratios between 72:28 to 0:100 (HEMA: PAA) were dissolved in water at total monomer concentration of 25 w %. Irgacure 2959 (1 w % of total monomer weight) was added as a photoinitiator and the mixture was polymerized in a syringe by exposure to UV light (365 nm) for 30 min in a cylindrical photoreactor (inner radius 15 cm, height 30 cm) containing 12 Philips TL 8W BLB lamps on the perimeter. The hydrogel samples (diameter: 4mm, length: 7mm) were dried in lyophilizer and weighed (W_1). The samples were then immersed in ethanol (12 h) and in ultrapure water (24 h) to remove unreacted components. The samples were lyophilized and weighed again (W_2). The gelation percentage (GP) was calculated as

$$\mathrm{GP} = \frac{W_2}{W_1} \times 100. \tag{4.1}$$

4.2.5. Degradation of Hydrogels

Each lyophilized hydrogel was weighed as W_i and then immersed in PBS (pH 7.4) or 0.5 M $CaCl_2$ solution at 37 °C. After the incubation at 37 °C for 1, 2 and 4 weeks, the samples

were removed, rinsed with water, freeze-dried and re-weighed as W_f. The degradation % was calculated according to

$$Degradation\ (\%) = \frac{W_i - W_f}{W_i} \times 100. \quad (4.2)$$

4.2.6. Swelling of Hydrogels

The dry hydrogel samples were weighed (W_i) and immersed in PBS (pH 5) or 0.5 M $CaCl_2$ solution at 37 °C. The samples were removed from the swelling medium after 24 h, blotted on filter paper and weighed (W_s). The swelling % was calculated using the following equation

$$Swelling\ (\%) = \frac{W_s - W_i}{W_i} \times 100. \quad (4.3)$$

4.2.7. Mineralization of Hydrogels

The hydrogels were mineralized using two different methods. In the first method, the samples were immersed in simulated body fluid (SBF) [221] for a period of four weeks, replacing the solution with a fresh one in every two days, rinsed with ultrapure water and lyophilized. In the second method, the samples were immersed in a 5xSBF solution prepared as described in literature [222] for 2 days, replacing the solution with a fresh one after one day. The samples were then immersed in ultrapure water for 24 h by refreshing the water in 6 h and lyophilized.

4.2.8. *In vitro* Cytotoxicity Assay

NIH 3T3, U-2 OS and Saos-2 cells were used to evaluate the cytotoxicity of the degradation products of the prepared gels. The cells were cultured in DMEM complete medium supplemented with 10% (v/v) FBS and 1% (v/v) pen-strep in 5% CO_2-humidified incubator at 37 °C and passaged every 2-3 days. For the cytotoxicity assay, the degradation products of the hydrogels in different concentrations ranging from 12.5-200 µg/mL by serial dilution in 100 µl were introduced into 96-well plates. Then, the cells were seeded at a density of $15x10^3$ cells/well in 100 µl DMEM complete medium and incubated at 37 °C in 5% CO_2 atmosphere. After 48 h further incubation, the cell viability was assessed using MTT colorimetric assay by the addition of 50 µl of MTT solution (5 mg/mL in PBS) into each well with 150 µL of culture medium and incubated for 4 h. The purple formazan crystals formed as a result of mitochondrial activity in viable cells were dissolved with ethanol: DMSO (1:1 v/v) mixture. Each sample's absorbance at 600 nm with a reference reading at 630 nm was recorded using a Synergy – H1 microplate reader (BioTek Instruments Inc., Winooski, VT, USA). Cells which were not exposed to degradation products of gels were used as controls. 100% viability is assumed for the control cells. The relative cell viability was calculated from equation (4.4).

$$Cell\ viability\ (\%) = \frac{Absorbance_{sample}}{Absorbance_{control}} \text{x } 100 \qquad (n = 4) \tag{4.4}$$

4.2.9. Statistical Analysis

Statistical analyses of the degradation products were conducted by using ordinary one-way ANOVA analysis of variance followed by multiple Dunnett's comparison test of GraphPad Prism 8.3.0 software package (GraphPad Software, Inc., USA). All measurements were expressed as mean values ± standard deviation (SD) based on 4 replicas. $p < 0.05$ was accepted as statistically significant difference.

4.3. Results and Discussion

4.3.1. Synthesis and Characterization of the PAA Macromers

Three biodegradable PAA macromers were synthesized by aza-Michael addition of primary amines (AEPA and/or AP) and MBA as shown in Figure 4. 1. Herein we selected AEPA and AP alone and both together to react with MBA to investigate effect of phosphonic acid functionality on material properties. The molar ratio of the MBA to amines was fixed at 1.1:1 to obtain acrylamide terminated products which can be used as crosslinkers. AEPA was first activated towards aza-Michael addition by neutralization with potassium hydroxide. The solvent was selected as methanol: water (3:1 v/v) because potasium salt of AEPA being soluble only in water and methyl bisacrylamide highly soluble in methanol, all three macromers are soluble in the mixture. Also, it is known that the presence of water facilitates efficiency of the aza-Michael reaction by activating both the amine and the acrylamide through hydrogen bonding [223].

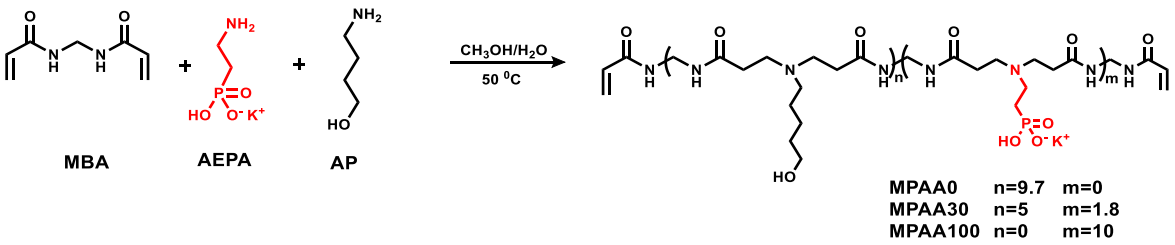

Figure 4.1. Synthesis of PAA macromers.

Table 4. 1. Compositions, number average molecular weights (M_n), yield and and T_g of the macromers

Macromer	AEPA:AP in feed (mol)	AEPA:AP in macromer (mol)	M_n[a] (g/mol)	Yield (%)	AEPA (w %)	T_g (°C)
PAA0	0:1.0	0:1.0	2650	52	0	1
PAA30	3.0:7.0	2.6:7.4	1943	47	11	15
PAA100	1.0:0	1.0:0	2946	44	42	64

[a]Calculated from ^{1}H NMR spectra

The composition and properties of the macromers are given in Table 4.1. The macromers were designated as PAAw, where w is the mol fraction of AEPA in the feed. The macromers were obtained as white solids in 44-52 % yields. They are highly soluble in polar (water, ethanol) solvents. Their structures were confirmed by ^{1}H-NMR and FTIR spectroscopy. For example, as seen in Figure 4.2, ^{1}H NMR spectra of all macromers show the characteristic peaks of acrylamide double bond protons at 5.65 (b) and 6.10 (a) ppm. The peak at 1.88 (g) ppm (in the spectrum of PAA100) belongs to methylene protons adjacent to phosphorous. This peak shifted from 1.88 to 1.56 (g) ppm in the spectrum of PAA30, indicating that PAA100 has zwitterionic structure. The peaks at 1.14 (j), 1.31 (k) and 1.37 (i) ppm (in the spectrum of PAA0) are ascribed to the methylene protons of AP. The peaks at 4.44 and 4.51 (c and n) ppm are the characteristic methylene (at the end and middle of the macromer) peaks of the MBA. The AEPA: AP mol ratio in the macromer (2.6:7.4) was found to be similar to the AEPA:AP mol ratio (3.0:7.0) in the feed (PAA30). The molecular weights and average number of repeating units of PAA macromers were calculated using ^{1}H-NMR by integrating acrylamide double bond protons at 5.65 and 6.10 ppm with respect to AP peaks at 1.14-1.37 ppm and/or AEPA peak at 1.56 ppm (Table 4.1). The FTIR spectra of the macromers (Figure 4.3) show strong peaks at around 1631 and 1528 cm^{-1} due to C=O and NH stretching. Also, the peaks at 1043 and 963 cm^{-1} corresponding to the symmetric and asymmetric vibrations of P-O are present in the spectra of PAA30 and PAA100.

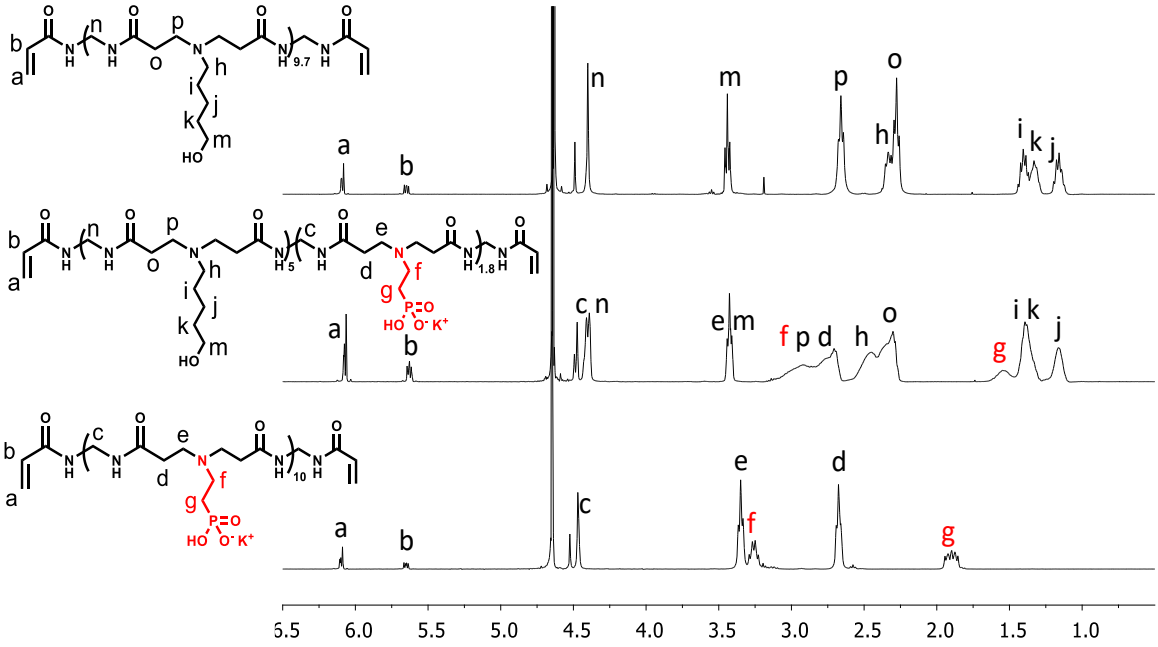

Figure 4.2. ^{1}H-NMR spectra of PAA0, PAA30 and PAA100.

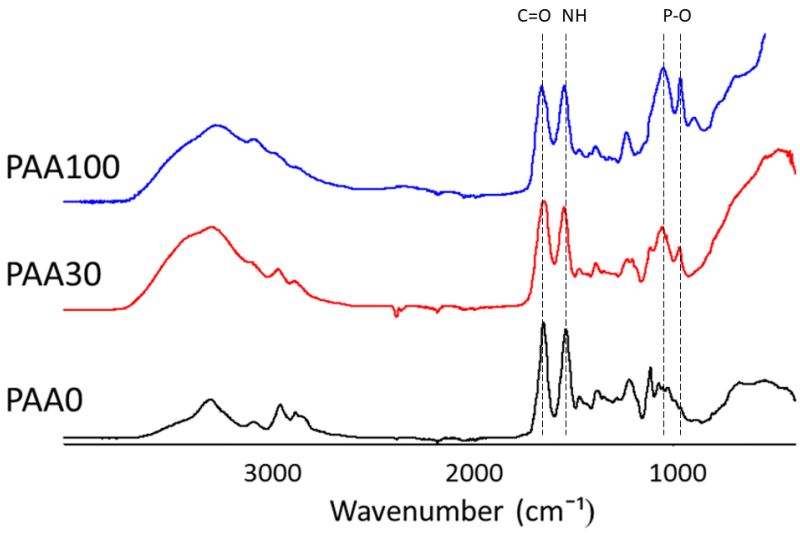

Figure 4.3. FTIR spectra of PAA0, PAA30 and PAA100.

The thermal properties of the macromers have been investigated using DSC, and their T_g's have been determined as 1, 15 and 64°C for PAA0, PAA30 and PAA100, respectively (Figure 4.4). We observed that incorporation of AEPA on the macromer structure increases

T_g. This increase can be explained by a decrease in the mobility of the macromer chains significantly due to electrostatic interactions of AEPA side groups.

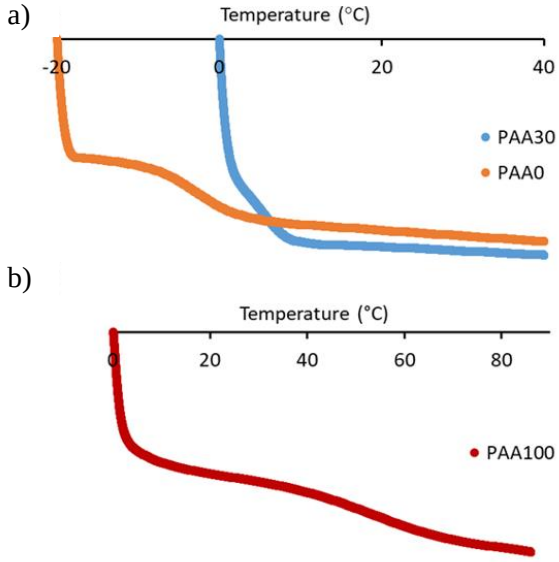

Figure 4.4. DSC curves of PAA macromers (a) PAA30 and PAA0 and (b) PAA100.

The pH sensitivity of PAA macromers was evaluated by the acid-base titration, as shown in Figure 4.5. The pH value increased gradually with the addition of NaOH solution, reaching a plateau in the pH range of about 5.8-7.8 for PAA0 and PAA30, which is characteristic for poly(amido amine)s as seen in the literature [224, 225]. The plateaus in the titration curves (Figure 4.5) indicate the buffering capacities of PAA0 and PAA30 in the physiologically relevant range of pH 6-7.4. When the pH is below the pK_b of the macromer the protonation of the tertiary amine groups occurs, whereas the same deprotonates when the pH is above the pK_b. It is also shown that the pH-responsiveness plateau is influenced by the composition or hydrophilicity of the macromers. The wider plateau of PAA0 indicates its better pH-responsive performance, whereas PAA100 with higher hydrophilicity does not show a distinct plateau region.

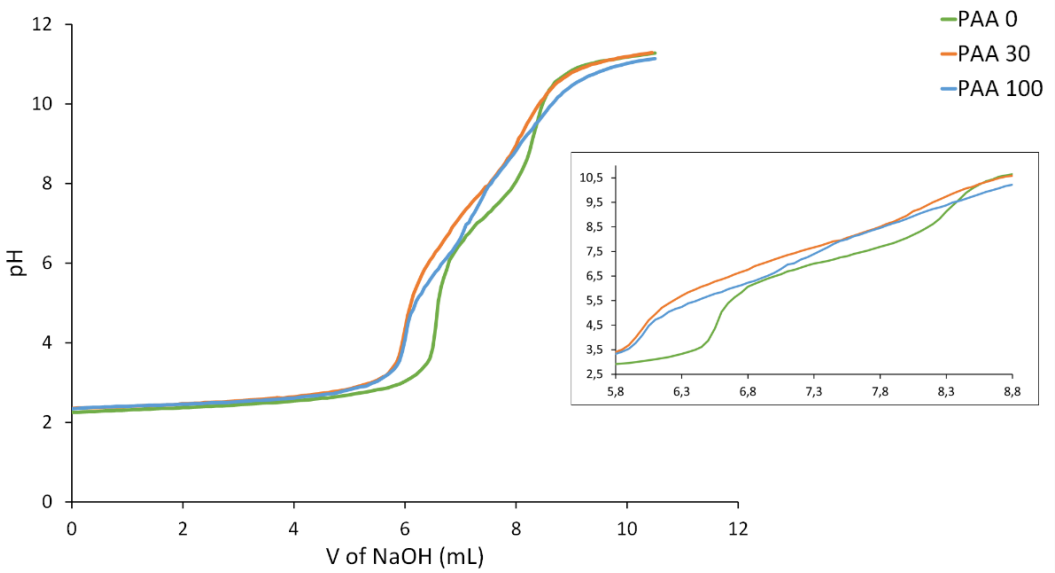

Figure 4.5. Acid–base titration curves of the 1 mg/mL aqueous solutions of PAA0, PAA30, and PAA100.

4.3.2. Synthesis of PAA and PAA-crosslinked HEMA Hydrogels

PAA macromers were used as crosslinkers in different amounts for the preparation of HEMA hydrogels as potential biomaterials and to investigate the effect of phosphonic acid functionalization on the final properties of the materials. Table 4.2 summarizes initial compositions and gelation percentages of the synthesized hydrogels. The samples are named as H-PAAx-y% where “H” stands for hydrogel, PAAx indicates crosslinker, x is the mol% of AEPA in PAA (in the feed) and y stands for weight% of PAAx. The syntheses were carried out successfully and the gelation percentage (GP) values of the hydrogels steadily decreased from 87% to about 72% when the phosphonic acid functionalized component was increased to 50% but did not decrease further when the ratio was increased towards 100%.

Table 4.2. Composition of PAA networks.

Hydrogels	HEMA:PAA (w %)	HEMA:AP:AEPA (w %)	Gelation (%)
H-PAA0-50%	50 : 50	50 : 18.8 : 0	87
H-PAA30-50%	50 : 50	50 : 13 : 5.8	72
H-PAA30-75%	25 : 75	25 : 20 : 8.7	75
H-PAA30-100%	0 : 100	0 : 26.5 : 11.6	72
H-PAA100-28%	72 : 28	72 : 0 : 11.6	80
H-PAA100-50%	50 : 50	50 : 0 : 21.2	74

4.3.3. Swelling and Degradation Studies of Hydrogels

Mass swelling percentages of the synthesized hydrogels were studied in 0.5 M $CaCl_2$ and two different buffers with pH 5 and pH 7.4. Swelling percentages of hydrogels after 24h are shown in Figure 4.6; they range from about 400% to about 950%. The hydrogels reached equilibrium very fast, in a period of the order of 15 minutes. In general, both molecular structure and molecular weight of the macromers are expected to affect the swelling properties of gels obtained from them. For example, the hydrogel with 50 w % of PAA30 (M_n = 1943) is observed to show slightly higher water uptake than the corresponding PAA0 (M_n = 2650)-crosslinked hydrogel at pH 7.4, indicating that the anionic character of the crosslinker dominates over the crosslink density. The incorporation of PAA30 into the hydrogel was increased to investigate the effect of the concentration of the phosphonic acid functionality. As seen from Figure 4.6, the equilibrium swelling percentages are almost same for all compositions probably due to relatively insignificant amount of phosphonic acid

functionality (5.8, 8.7 and 11.6 w %). The hydrogel prepared from PAA100 showed the highest swelling at pH 7.4 because of the highest charge or hydrophilic property. In this figure, the clearest trend is the higher swelling values in the more acidic medium (pH 5) at lower AEPA concentrations and its steady decrease with increase of the same. The high swelling comes from the increase in total charge due to the protonation of the amine groups, whose effect is increasingly ameliorated by the zwitterionic nature of the AEPA functionality attracting the chains together electrostatically. For example, the hydrogel with 50 w % of PAA100 is observed to show the lowest water uptake among all the hydrogels. When the hydrogels were immersed in 0.5 M $CaCl_2$ solution, exchange of potassium ions with calcium is expected. The interaction between phosphonic acid groups and Ca^{2+} ions may form physical crosslinking [162, 163]. However, it was observed that phosphonic acid content in the hydrogel needs to reach a certain level to observe a noticable shrinkage. The hydrogel (H-PAA100-50%) containing the highest AEPA (21.2 w %) swelled 45.8 % less in $CaCl_2$ solution compared to PBS.

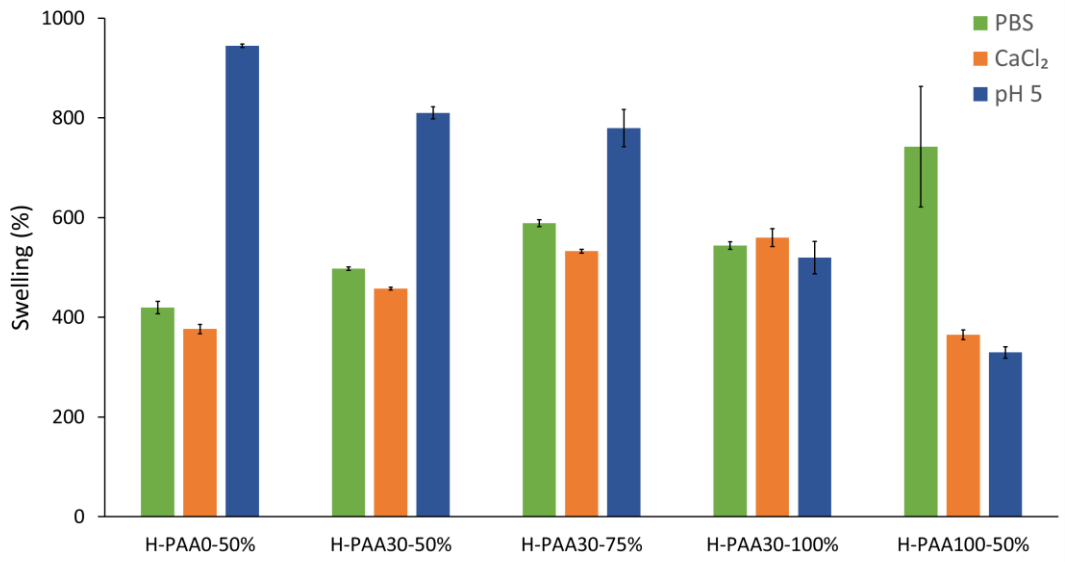

Figure 4.6. Swelling percentages of PAA hydrogels after 24 h. All the experiments were carried out in triplicates (n=3) and mean average values with standard error (±SD) were represented in the error bars.

The degradation of the hydrogels with 50 w % of PAA0 and PAA30 crosslinkers were investigated in PBS (pH 7.4) for 4 weeks, including the case with pre-treatment by immersion in 0.5 M $CaCl_2$ solution (Figure 4.7) It is seen that the degradations for both hydrogels are similar and around 20 % after 4 weeks if not pre-treated with the $CaCl_2$ solution. PAA degradation occurs by hydrolytic cleavage of amide bonds [17]. Therefore, the control hydrogels synthesized from the higher molecular weight macromer (PAA0) are expected to degrade faster because of the higher amount of amide linkages between the crosslinks. However, the hydrophilic character of the anionic group in the hydrogels synthesized from PAA30 macromer compensates this effect, explaining the similar degradations for the two hydrogels as seen in Figure 4.7a. For the pre-treated samples, one might expect similar degradation since their swelling was the same, and the water content would determine the effect of hydrolysis. Less degradation of the acid containing hydrogels than the control one shows that H-PAA30-50% forms chelates with Ca^{2+} ions whereas the control hydrogel does not. The Ca^{2+}-phosphonic acid complex acts as a second crosslinked network and slows down the mass loss [142].

Figure 4.7b shows the SEM micrographs of the PAA30 hydrogel before and after degradation. The SEM micrograph of degraded H-PAA30-50% shows that the hydrogel seems to have degraded choosing an orientation somehow. The oriented pattern of degradation may prove its homogeneity.

4.3.4. Mineralization of Hydrogels

The mineralization abilities of the synthesized hydrogels were evaluated in two ways: (a) immersion in SBF for 4 weeks, (b) immersion in 5xSBF for 2 days. SBF was chosen because it closely mimics the ionic concentrations and pH typically observed in plasma [149]. Hence, formation of apatite like structure on a scaffold in SBF indicates its capacity for bone tissue engineering applications. However, the mineralization was slow under SBF conditions. Therefore, 5xSBF with higher concentrations of Ca^{2+} and HPO_4^{2-} was used to

increase rate of mineralization. Before soaking in the mineralization solutions, some of the hydrogels were immersed in 0.2 M $CaCl_2$ solution to exchange potassium ions bound to phosphonic acid groups with calcium, expecting acceleration of mineralization because of increase in Ca^{2+} release from the polymer [296]. Mineralization of the hydrogels was studied by using SEM, FTIR and TGA.

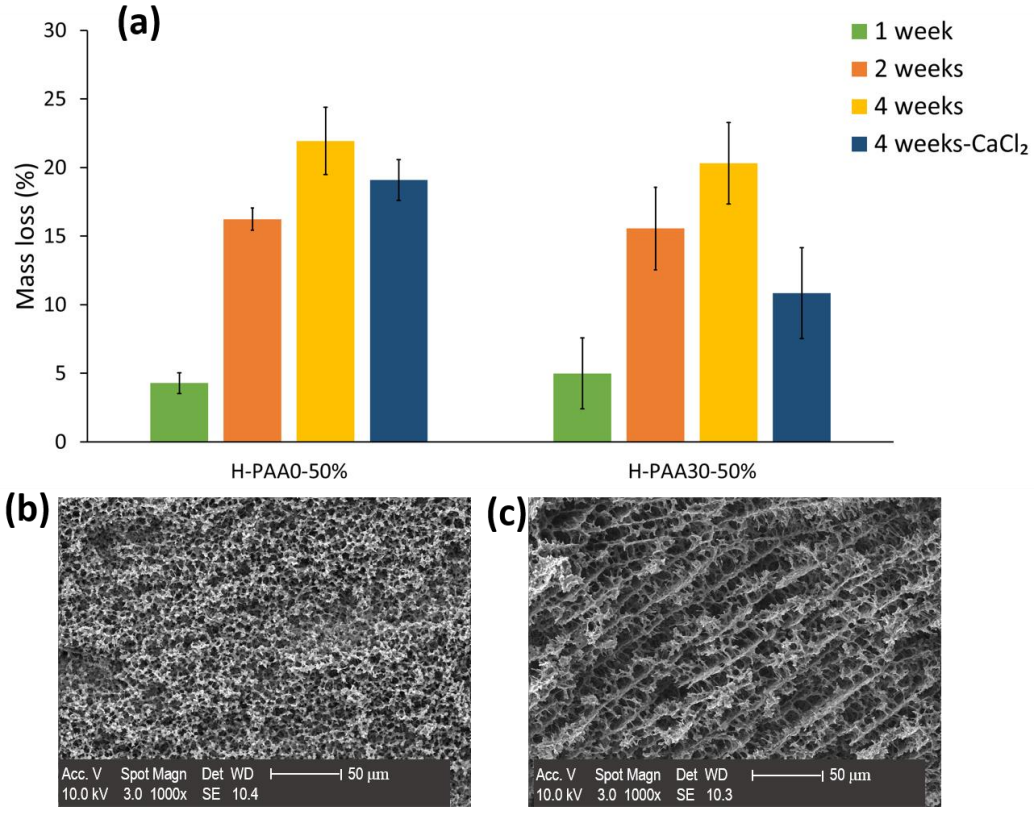

Figure 4.7. (a) The degradation of H-PAA0-50% and H-PAA30-50% hydrogels in pH 7.4; (b) SEM micrographs of H-PAA30-50%, (b) before and (c) after 4 weeks degradation.

SEM micrographs of H-PAA0-50% (control) and H-PAA30-50% after soaking in SBF for 4 weeks are presented in Figure 4.8, together with the associated FTIR spectra. Suprisingly, the control hydrogel containing only AP groups showed mineral layers (Figure 4.8b) and its FTIR spectrum showed strong peaks at 1002 and 548 cm^{-1} corresponding to P-O bond, similar to HAP. The control hydrogel's (H-PAA0-50%) better mineralization

performance might be explained with the observation in the literature that not only polyanions, but also polycations such as linear PEI have a strong influence on CaP mineralization [226]. LPEI accelerates the transformation brushite ($CaHPO_4,2H_2O$) (DCPD) to HAP by acting as a proton acceptor, which takes up the protons released from either the calcium phosphate precipitate during the phase transformation or from ions present in solution during a presumed, but so far not directly observed, dissolution–reprecipitation process [227]. For H-PAA30-50 % hydrogels, we could not observe any CaP formation unless we immerse the hydrogels in $CaCl_2$ solution before mineralization (Figure 4.8c and 4.8d). The premineralization treatment making CaP formation possible for H-PAA30-50 % hydrogels probably formed limited nucleation points on phosphonic acid groups which support mineralization [142, 147]. EDX was used to determine the elemental composition of the inorganic complex shown in Figure 4.8e. The stoichiometric ratio of Ca/P was calculated as 1.67 which is same with theoretical value of HAP. Additionally SEM mapping analysis demonstrates the deposition of Ca, P and O atoms on this part.

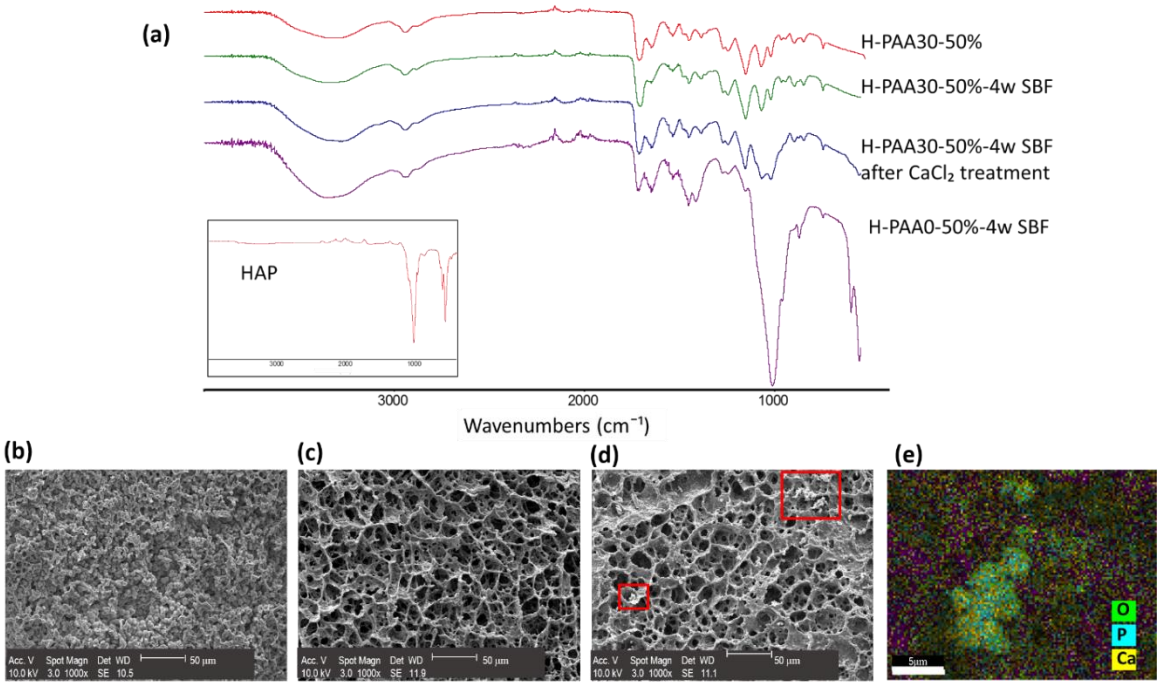

Figure 4.8. (a) FTIR spectra of H-PAA30-50% before (top); and H-PAA30-50% and H-PAA0-50%, treated as labeled, with HAP inset, (b–d) SEM micrographs of the top three cases listed in (a), in order, (e) ×8000 and mapped image of (d).

Studies in 5xSBF did give results in 2 days, confirming the importance of the ion concentration in SBF. For studies in 5xSBF, hydrogels with three different compositions of PAA30 (50%, 75% and 100%) were used. This way we also evaluated the effect of matrix structure (concentration of phosphonic acid and AP) on formation of apatite-like phases on a hydrogel. These hydrogels have increasing concentration of both AEPA and AP (5.8, 8.7 and 11.6 w % AEPA and 13, 20 and 26.5 w % AP). The mineralized samples were characterized by FTIR analysis (Fig 4.9a). The FTIR spectra of the PAA30-100% hydrogels contained two broad peaks at around 1015 and 556 (P-O) cm^{-1} which is related with HAP. The TGA thermograms of HPAA30-100% before and after mineralization show the initial weight loss around 100 °C due to removal of water, the main weight loss between 200 and 400 °C because of main chain degradation and char yield at 600 °C (Figure 4.9b). The char yield of the hydrogels after mineralization were higher (27%) than those (19%) of before mineralization, confirming mineral deposition. SEM images of these hydrogels showed mineral layers (Figure 4.9d and e). FTIR spectrum of the hydrogel samples synthesized with PAA30-75% also showed an apatite-like mineral (Figure 4.9a). However, the hydrogel samples prepared from PAA30-50% showed no noticable mineralization, with no change in FTIR spectrum after mineralization (Fig 4.9a). Surprisingly, the hydrogels (H-PAA100-50%) containing only AEPA showed no mineralization, either.

From the results given above, it can be concluded that macromer concentration and its composition is very important for mineralization. The AEPA:AP ratio in H-PAA30-100% homogel is the most proper one due to hydrophilicity and architecture for mineralization.

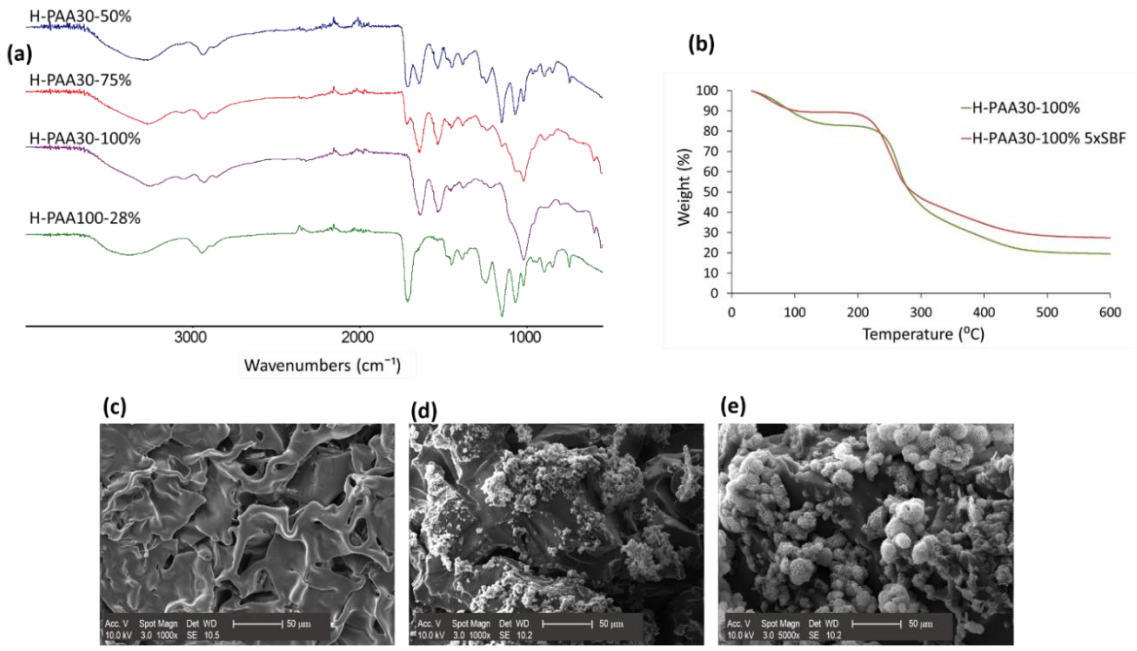

Figure 4.9. (a) FTIR spectra of samples as labeled, after 2 days treatment in 5xSBF, (b) TGA thermograms of H-PAA30-100% before and after the same treatment, (c and d) SEM micrographs of the same, before and after treatment, (e) ×5000 image of (d).

4.3.5. Cytotoxicity of PAA Hydrogels

To evaluate cytotoxicity of the degradation products a dose dependent study was performed on NIH 3T3, U-2 OS and Saos-2 cells using the standard MTT assay (Figure 4.10). Based on ISO 10993-5, the cell viability above 80% is defined as noncytotoxic and between 80 and 60 as weakly cytotoxic [295]. Viability of all type of cells treated with degradation products were above 75%, indicating that degradation products showed no significant toxicity on NIH 3T3, U-2 OS and Saos-2 cells.

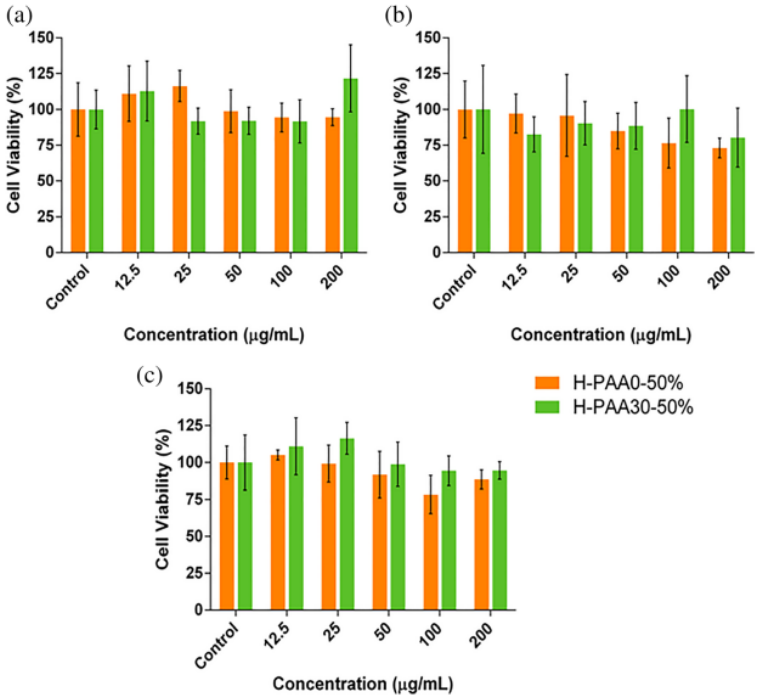

Figure 4.10. The effect of degradation products on cell viability of (a) U-2 OS, (b) Saos-2 human osteosarcoma cells, (c) NIH 3T3 mouse embryonic fibroblast cells. Cells were treated with different concentrations of the products for 24 hr. The cell viability test was performed by MTT assay (±SD; n = 5; $p < .05$ compared with all concentrations).

4.4. Conclusions

It was shown that phosphonic acid functionalized primary amines can be used for the synthesis of novel phosphonic acid-functional PAA macromers and these macromers can be incorporated into hydrogels by homo- or copolymerization with HEMA at different ratios to control the phosphonic acid concentration, thus hydrophilicity. The T_g of the PAA macromers increased with incorporation of phosphonic acid on the macromer structure. Swelling of the hydrogels is mostly governed by the amount of phosphonic acid in their structures, pH of the medium and $CaCl_2$-pre-treatment. The degradability of hydrogels decreases when they are pre-treated with $CaCl_2$, due to the presence of Ca^{2+}-phosphonic acid complex, parallel to their swelling behaviour. It was observed that small changes in composition of the hydrogels can influence the generation of hydroxyapatite-like mineral

phases. While hydrogels prepared from only AP functionalized macromers promote mineralization, the hydrogels obtained from only AEPA functionalized ones have no apatite nucleation ability. The hydrogels which have both AP and AEPA in their structures showed different mineralization abilities depending on their ratios, probably due to hydrophilicity. The pre-treatment of hydrogels with $CaCl_2$ increases the capacity of the hydrogels for mineralization. The degradation products of these new materials showed no toxicity on cells and therefore they can be considered as potential candidates in various biomedical applications.

5. BISPHOSPHONATE FUNCTIONALIZED MONOMERS AND THEIR CONTROLLED POLYMERS

5.1. Introduction

Polymers obtained through free radical polymerization (FRP) are produced with a broad mass distribution. Living/controlled radical polymerization (LRP) techniques allow synthesis with greater control over molar mass and polydispersity providing well defined end groups and architectures such as block and star polymers [228]. The ability to produce well-defined polymers thanks to LRP can improve the understanding of the relationship between the structure and property which is important to obtain more efficient sophisticated materials. The technique used in this chapter is reversible addition-fragmentation chain transfer (RAFT) polymerization. It has an advantage over the other LRP techniques due to its tolerance of many functionalities in monomer like -OH, -AHA, $-NR_2$ and $-SO_3H$. RAFT provides reversible deactivation of propagating radicals via degenerative chain transfer [229]. The general mechanism is illustrated in Figure 5.1. Thiocarbonylthio compounds which are known as chain transfer agents (CTA) are used to control radical polymerization. RAFT process starts like conventional FRP where a radical is created from an initiator (Step 1). Oligomeric radicals react with the highly reactive C=S bond of CTA and the radical intermediate can fragment to form a reinitiating R radical (Step 2). The initial concentration of the initiator should be low to initiate most of the reinitiating R radicals (Step 3). This radical reacts with monomers and polymer chains (P radical) grow and reversibly add to another thiocarbonylthio group. The main step of RAFT (main equilibria) is established between the propagating polymeric radical and dormant macroCTA (Step 4) and the intermediate radical 4 can fragment in either direction [228, 230]. In a well-designed RAFT process, the rate of chain equilibration is faster than propagation, so the degree of polymerization for each side (n and m) are almost similar [231]. As a result, uniform chain growth and narrow polydispersity can be obtained. The possibility of termination reactions is limited because of the low concentration of propagating radical chain thanks to rapid interchange in the chain transfer step. However, it can still occur via coupling or

disproportionation when monomer conversion is high (Step 5). Therefore, the thiocarbonylthio chain end can be preserved by ending the polymerization at moderate conversion and the living chain end can be reacted with another monomer to form block copolymers [230].

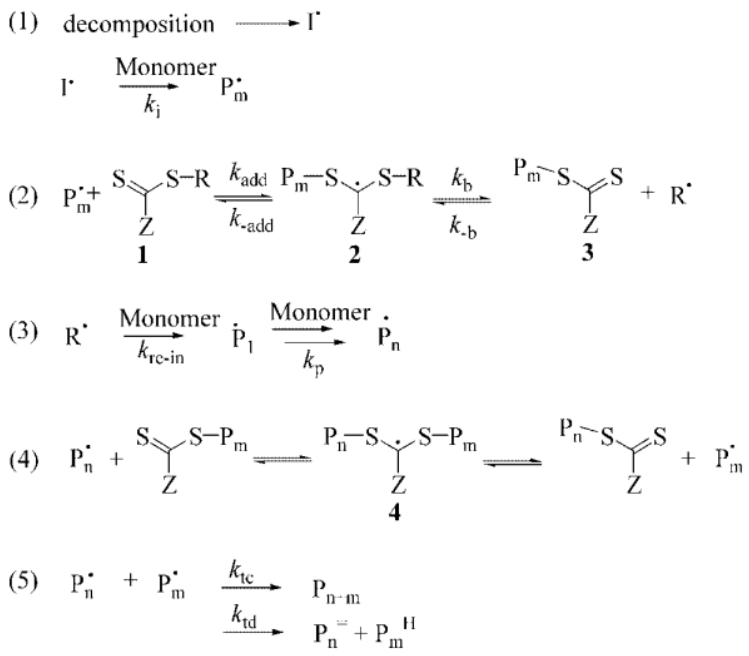

Figure 5.1. General mechanism of RAFT polymerization. Reprinted from [228].

The efficiency of a CTA depends on the structures of R and Z groups (Figure 5.2). The R group must be a good leaving group and be an effective reinitiating species. Steric factors, radical stability and polar effects have an influence on the leaving/reinitiating capacity of an R group. For example, increased radical stability enables the R group to be a good leaving group, but they may have negative effects on the reinitiating capacity. The Z group modifies the addition and the fragmentation rates. It should activate the C=S bond during the radical addition and give minimal stability to formed radical to facilitate fragmentation. For instance, the most reactive CTAs such as dithioesters (Z= alkyl or aryl) and trithiocarbonates (Z= SR) allow the preparation of low dispersity polymers from more activated monomers (MAM) where the double bond is conjugated to an aromatic ring, a

carbonyl group or a nitrile. The radicals of MAM which are less reactive in radical addition do not add efficiently to less reactive CTAs (where Z= OR, NRR). Low rates of the addition of a monomer to the CTA and high rates of fragmentation of adduct radical increase the radical concentration in the system and polymerization occurs like a conventional FRP [228], [231]. Therefore, R and Z groups should be selected by taking into consideration of the reactivity of the monomer being polymerized. Guidelines for selection of CTAs is given in Figure 5.2.

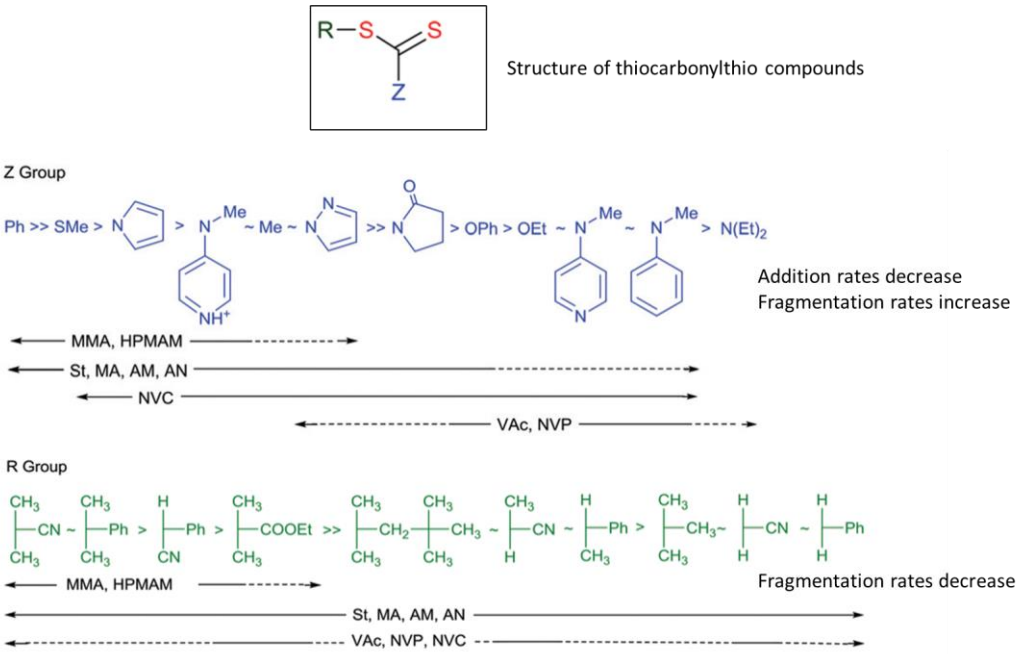

Figure 5.2. General structure and guidelines for selection of CTAs. Dashed line shows partial control. Adapted from reviews [232, 297].

As mentioned in the introduction part, phosphorous containing polymers have found various applications in different fields. Phosphorous incorporated polymers can be synthesized by direct (co)polymerization of phosphorous based monomers or by post modification of polymers using a phosphorous based moiety. In order to obtain the polymers with controlled architecture and molecular weight as well as well-defined and functionalizable end groups, different LRP techniques were used in the polymerization of

phosphorous containing monomers [106, 134, 233, 234]. A mini review giving the examples of nitroxide-mediated polymerization (NMP), atom transfer radical polymerization (ATRP) and RAFT polymerization of phosphorous containing monomers was written by Xu et al. [235]. David et al. showed the inhibiting effect of the phosphorous atom in the ATRP process due to the complex between phosphorous and copper ions, which causes poor monomer conversion [298]. A large variety of monomers including methacrylate (functionalized with phosphonate [234,236,237] α-hydroxy phosphonate [238], difluorophosphonylated group [239], amino bisphosphonate [240], phenylphosphonic acid [241]), methacrylamide (bearing a long alkyl chain and phosphonate [134], alendronate [242]) and acrylamide (containing phosphonate [243] and tetraethyl aminomethylbisphosphonate [244]) were (co)polymerized via RAFT polymerization since this technique is tolerant of a wide variety of functionalities. However, addition of phosphonated moiety into copolymer structure can be limited because of the lower reactivity of phosphonated monomers than commonly used monomers [299]. The RAFT polymerization method allows polymerizations to be carried out in different reaction conditions; therefore, polymerization kinetics-condition relationship can be considered in detail. For example, the effect of solvent polarity on RAFT polymerization kinetics of an aminobisphosphonated methacrylate was investigated. Polymerization with low dispersity and high rate was observed when using polar solvents and conversion decreased in less polar solvents [240].

Vinylphosphonic acid (VPA) was the first example of a monomer containing unprotected phosphonic acid to be prepared by RAFT/MADIX (when the CTA is xanthate) polymerization [245]. Block copolymers of PVPA with low molecular weights were polymerized but a large amount of VPA remained at the end of the reaction [246]. Addition of 0.5 equivalents of NaOH increased the polymerization rates and the final conversion, yet in the presence of 1 equivalent of NaOH polymerization was retarded [247]. It is also possible to produce phosphonic acid versions of these polymers by hydrolysis of phosphonate esters [134, 236, 240, 243, 248]. Introduction of phosphorous based groups after LRP polymerization of a convenient monomer is another strategy to achieve phosphorous containing polymers [130, 249]. For example, aminobisphosphonate moieties were incorporated into polymers obtained by RAFT polymerization of protected amine monomers via Kabachnik-Fields and Moedritzer-Irani reactions [250]. On the other hand,

phosphonate and bisphosphonate functionalized CTAs or ATRP initiators can be used to polymerize appropriate monomers [251, 252]. Dufils et al. showed that rate of vinyl acetate polymerization is not affected by the phosphonate moieties in CTA even polydispersity index values were lower than 1.4 [253].

Thermoresponsive polymers which undergo volume-phase transitions in solution triggered by changes of temperature have been extensively investigated for biomedical applications such as sensors, drug delivery and tissue engineering [254–256]. Polymers showing lower critical solution temperature (LCST) alter their hydrophilicity and undergo a soluble to insoluble transition above the critical temperature. Below LCST polymer chains form hydrogen bonds with water, which enables solubilization of polymer. Above LCST hydrogen bonding between polymer chains is favored, as a result polymer chains become hydrophobic and collapse. LCST is an entropically driven action [257]. The change of physical state can be observed with the bare eye. Thus, the temperature at which the polymer solution becomes cloudy is called the cloud point. Poly(N-isopropylacrylamide) (PNIPAM) is one of the most widely studied thermoresponsive polymer because its LCST is around 32 °C, being close to human body temperature [258]. Salt ion concentration, pH of the solution, molecular weight and composition of polymer are the factors that can affect the LCST of polymers [257].

Adjustment of the LCST of a polymer can be accomplished by copolymerizing with different monomers altering the overall hydrophilicity of the polymer. Addition of hydrophilic groups into a thermoresponsive polymer increases the LCST due to the stronger interaction with water compared to the original homopolymer, whereas, hydrophobic ones decrease the LCST [259]. In addition, pH or ion sensitive components can be combined with thermoresponsive polymers to enrich polymer properties. For example, thermosensitive polymers based on poly(N-n-propylacrylamide), P(NnPAAm), bearing phosphonated groups were synthesized and phosphonated ester groups were hydrolyzed. The LCST of polymers increased from 22 °C to 25.6 °C with the addition of phosphonic acid content. Also, the influences of temperature and pH were investigated to understand complexing properties of polymers for nickel cations. It was observed that the best sorption capacities

were achieved at temperatures around LCST where polymer-polymer interaction is boosted and composes a core, but the phosphonate rich segment remains soluble because of its higher hydrophilicity and becomes more accessible for metallic cations [260]. The effect of architecture on sorption properties of this polymer was also studied and no significant differences were observed [261]. Furthermore, well-defined NIPAM based diblock copolymers containing carboxylic azo groups were synthesized by Ren et al. The LCST of the polymer was measured as 32 °C (pH=7), 31 °C (acidic medium) and 34 °C (basic medium) because of the solubility of carboxylic azo block. Surprisingly, the cloud point of carboxylic acid terminated polymer disappeared under basic conditions because of the electrostatic repulsion of the end groups. Addition of calcium ion induced chain entanglement of polymeric micelles because of the complex formation between Ca^{2+} and COO^- and macroscopic phase separation occurred [262].

Amphiphilic block copolymers containing a permanently water-soluble hydrophilic block and a thermoresponsive block are frequently used in injectable systems for biomedical applications thanks to their liquid-gel phase transitions. At the temperatures lower than LCST, the polymer is dissolved in water, whereas at higher temperatures the termoresponsive block becomes water insoluble that trigger micelle formation [256, 263, 264]. Copolymer composition, block length and architecture are the main determinants of the micellization process [265, 266]. Therefore, development of well-defined polymers produced by CRP is important to evaluate the structure property relationship. The free-standing micelle structures can form physical micellar gels when the polymer concentration is sufficiently high [267–270]. The repulsive interactions between the soluble polymer chains of diblock amphiphilic copolymers can cause gelation [271]. However, the critical gelation concentration of symmetrical triblock copolymers (hydrophobic outer block) is much lower than the concentration of the diblock copolymers (around 30 w% polymer [272]) because in the first case, hydrophobic outer blocks can be placed in different micelle cores besides the interaction of hydrophilic part [270]. For example, triblock copolymers were synthesized via ATRP using thermoresponsive PNIPAM as hydrophobic outer blocks and O-phosphorylethanolamine containing poly (acrylic acid) as a water-soluble inner block. The rheological measurements indicate that physical gels can form at temperatures between 32-45 °C at polymer concentrations lower than 2 w% depending on PNIPAM block length,

substitution degree of phosphonic acid group and polymer concentration [143]. Mineralization capacity of phosphonic acid containing PNIPAM based injectable polymers were investigated to evaluate their potential for bone tissue engineering [143, 273, 300]. Calcium phosphate particles such as HAP and β-tricalcium phosphate have been combined with in-situ gelling hydrogel systems to provide better osteoconduction and promote mineralization [274, 275].

The aim of this chapter is synthesizing new thermoresponsive polymers with bisphosphonate and bisphosphonic acid functionality as alternative to synthetic polymers used in bone tissue engineering. For this reason, we have synthesized new acrylamide monomers with different hydrophilicities (propyl, octyl and octadecyl groups) and bisphosphonate groups. They were copolymerized with NIPAM via FRP and RAFT polymerization. Also, a carboxylic acid containing NIPAM copolymer was functionalized with alendronate to obtain bisphosphonic acid groups in polymer structure. We focus on the relationship between the structure of polymers and their aqueous behaviour. The hydrophilicity of incorporated functionality as well as Ca^{2+}-bisphosphonic acid interaction can have influence on LCST and potential mineralization properties of polymers.

5.2. Experimental

5.2.1. Materials and Methods

Tetraethyl ethenylidenebis(phosphonate) was prepared according to the literature procedure described by Degenhardt and Burdsall [276]. 6-acrylamidohexanoic acid (AHA) was synthesized as described in the literature [277]. 4-((((4-carboxybenzyl) thio)carbonothioyl)thio)butan-1-ylium (chain transfer agent-CTA) was synthesized previously [301] and purified by column chromatography on silica gel using petroleum ether- ethyl acetate (50:50 v/v) as eluent for this work. NIPAM and 2,2′-azobis(isobutyronitrile) (AIBN) were crystallized from hexane before use. Dichloromethane

(DCM) (Merck) was dried over molecular sieves. Tetraethyl methyl bisphosphonate, propyl, octyl and octadeyl amine, acryloyl and methacryloyl chloride, trimethylsilyl bromide, triethyl amine, tris(trimethylsilyl)phosphite (TMSP), N-(3-Dimethylaminopropyl)-N′-ethylcarbodiimide hydrochloride (EDC-HCl), N-hydroxysulfosuccinimide sodium salt (Sulfo NHS) and all other reagents and solvents were obtained from Aldrich and used as received without further purification.

The chemical structures of monomer and polymers were confirmed by nuclear magnetic resonance (^{1}H, ^{13}C, ^{31}P NMR) and FTIR spectroscopies. NMR spectra were recorded on a Varian Gemini (400MHz). FTIR spectra were collected by Thermo Scientific Nicolet 380 spectrometer in the range of 4000-400 cm^{-1}. Polymers were analyzed by size exclusion chromatography (SEC) at room temperature in NMP as an eluent, with a setup consisting of UV and refractive index detector (Shimadzu Corporation, Kyoto, Japan) and PSS GRAM column as stationary phase. Narrowly distributed polystyrene standards (PSS, Mainz, Germany) were used to calibrate SEC. UV−vis absorption spectra were recorded on a Perkin Elmer Lambda UV/vis Spectrometer. Quartz cuvettes with path length of 1 cm were used. Number average molar masses were calculated by end group analysis in acetonitrile by using the equation

$$M_n^{UV} = \varepsilon.c.d.E^{-1} \quad (5.1)$$

where E is the extinction of trithiocarbonate chromophore group. The molar extinction coefficient ε is 16500 L/mol cm at 307 nm in acetonitrile. Cloud points of polymers were determined using a Cary 50 UV-Vis spectrometer equipped with a single cell Peltier thermostat. Turbidimetry measurements were carried out on 3 and 10 g/L polymer solutions prepared in D_2O at a wavelength of 600 nm during heating and cooling from 20 to 50 °C with 0.5 °C /min rate. Differential scanning calorimetry (DSC) was used to determine the glass transition temperatures (T_g) of the polymers. Samples (5–10 mg) were sealed in aluminium pans and heated under nitrogen atmosphere from 20 to 120 °C with a scanning rate of 10 °C min^{-1}.

5.2.2. Synthesis of Bisphosphonate Functionalized Amines (A1, A2, A3)

The relevant amine (propyl, octyl or octadecyl amine, 1 mmol) and tetraethyl vinylidene bisphosphonate (1.1 mmol) were mixed at room temperature for one day. Octadecyl amine reaction was done in dry DCM due to solubility reasons.

A1: ^{1}H NMR (400 MHz, $CDCl_3$): 0.89 (t, $^{3}J_{HH}$ = 7.2 Hz, 3H, C*H*$_3$-CH$_2$), 1.32 (t, $^{3}J_{HH}$ = 7.2 Hz, 12H, C*H*$_3$-CH$_2$-O), 1.48 (m, 2H, C*H*$_2$-CH$_3$), 2.54 (t, $^{3}J_{HH}$ = 7.2 Hz, 2H, C*H*$_2$-N), 2.53 (m, 1H, CH-P=O), 3.11 (m, 2H, C*H*$_2$-CH-(P=O)$_2$), 4.17 (m, 8H, CH$_2$-O-P=O) ppm. A3: ^{1}H NMR (400 MHz, $CDCl_3$): 0.86 (t, $^{3}J_{HH}$ = 6.8 Hz, 3H, C*H*$_3$-CH$_2$), 1.24 (s, 32H, C*H*$_2$-) 1.33 (m, 12H, C*H*$_3$-CH$_2$-O), 2.56 (t, $^{3}J_{HH}$ = 7.2 Hz, 2H, C*H*$_2$-N), 2.63 (m, 1H, CH-P=O), 3.12 (m, 2H, C*H*$_2$-CH-(P=O)$_2$), 4.17 (m, 8H, CH$_2$-O-P=O) ppm.

5.2.3. Synthesis of Bisphosphonate Functionalized Acrylamides (M1, M2, M3)

To a mixture of functionalized amine (3.02 mmol) and triethylamine (0.57 mL, 4.08 mmol) in anhydrous DCM (8 mL) under nitrogen, acryloyl chloride (0.47 mL, 4.83 mmol) or methacryloyl chloride (0.39 mL, 4.83 mmol) was added dropwise in an ice bath. The final mixture was stirred at room temperature for 2 h. After addition of water (2 mL) to terminate the reaction, chloroform (20 mL) was added and the organic phase was extracted with water (3x5 mL), HCl (3x5 mL) and $NaHCO_3$ (3x5 mL). The organic phase was dried over anhydrous Na_2SO_4, filtered and evaporated. The crude product was purified by reverse phase flash chromatography on C18 using MeOH-water as eluent.

M1 (50:50 MeOH-water, 54%): ^{1}H NMR (400 MHz, $CDCl_3$): 0.88 (t, $^{3}J_{HH}$ = 8 Hz, 3H, C*H*$_3$-CH$_2$), 1.32 (m, 12H, C*H*$_3$-CH$_2$-O), 1.55 (m, 2H, C*H*$_2$-CH$_3$), 3.47 (m, 3H, C*H*$_2$-N, CH-P=O), 3.81 (m, 2H, C*H*$_2$-CH-(P=O)$_2$), 4.16 (m, 8H, CH$_2$-O-P=O), 5.65 (d, $^{3}J_{HH}$ = 12 Hz, 1H, C*H*$_1$H$_2$=CH), 6.32 (d, $^{3}J_{HH}$ = 16 Hz 1H, CH$_2$=C*H*), 6.52 (q, $^{3}J_{HH}$ = 8 Hz, 1H, CH$_1$*H*$_2$=CH)

ppm. ^{31}P NMR: 19.5, 20.61 (main peak), 21.25 ppm. FTIR (ATR): 2987 (C-H), 1649 (C=O), 1613 (C=C), 1496 (NH), 1246 (P=O), 1014, 950 (P-O) cm^{-1}. M2 (60:40 MeOH-water, 53%): ^{1}H NMR (400 MHz, $CDCl_3$): 0.87 (t, $^{3}J_{HH}$ = 6.4 Hz, 3H, C*H*$_3$-CH$_2$), 1.26 (s, 10H, C*H*$_2$-CH$_3$), 1.33 (m, 12H, C*H*$_3$-CH$_2$-O), 1.54 (m, 2H, C*H*$_2$-CH$_3$), 3.48 (m, 3H, C*H*$_2$-N, CH-P=O), 3.81 (m, 2H, C*H*$_2$-CH-(P=O)$_2$), 4.17 (m, 8H, CH$_2$-O-P=O), 5.67 (d, $^{3}J_{HH}$ = 8 Hz, 1H, C*H*$_1$H$_2$=CH), 6.34 (d, $^{3}J_{HH}$ = 16 Hz 1H, CH$_2$=C*H*), 6.53 (q, $^{3}J_{HH}$ = 12 Hz, 1H, CH$_1$*H*$_2$=CH) ppm. ^{31}P NMR: 18.01, 18.77 (main peak) ppm. FTIR (ATR): 2921, 2852 (C-H), 1651 (C=O), 1614 (C=C), 1544 (NH), 1250 (P=O), 1020, 967 (P-O) cm^{-1}. M3 (100:0 MeOH-water, 47%): ^{1}H NMR (400 MHz, $CDCl_3$): 0.87 (t, $^{3}J_{HH}$ = 6.8 Hz, 3H, C*H*$_3$-CH$_2$), 1.25 (s, 30H, C*H*$_2$-CH$_3$), 1.33 (m, 12H, C*H*$_3$-CH$_2$-O), 1.52 (m, 2H, C*H*$_2$-CH$_3$), 3.49 (m, 3H, C*H*$_2$-N, CH-P=O), 3.80 (m, 2H, C*H*$_2$-CH-(P=O)$_2$), 4.17 (m, 8H, CH$_2$-O-P=O), 5.67 (d, $^{3}J_{HH}$ = 7.6 Hz, 1H, C*H*$_1$H$_2$=CH), 6.34 (d, $^{3}J_{HH}$ = 14.4 Hz 1H, CH$_2$=C*H*), 6.53 (q, $^{3}J_{HH}$ = 8 Hz, 1H, CH$_1$*H*$_2$=CH) ppm. ^{31}P NMR: 20.96, 21.51 (main peak), 22 ppm.

5.2.4. Synthesis of Copolymers of NIPAM and M1/M2/M3

Random and block copolymers of NIPAM and bisphosphonated acrylamides (M1, M2 and M3) were synthesized using FRP and RAFT polymerization as described below.

5.2.4.1. Synthesis of random copolymers of NIPAM and M1/M2/M3, P(NIPAM-*co*-Mx). NIPAM and M1/M2/M3 were dissolved in dioxane at different mol ratios ([NIPAM]/[monomer] = 95:5, 90:10 and 70:30) by adjusting the concentration as 2M. The reactions were carried out at 65 °C with 2 mol % AIBN after freeze-pump-thaw cycles. The obtained polymers were purified by precipitation into diethyl ether. Yields were calculated as 39, 28, 9% respectively at 5, 10, 30 % of phosphonated monomer concentration.

5.2.4.2. Synthesis of homopolymers of NIPAM by RAFT polymerization, PNIPAM (macroCTA). The mixture of NIPAM (200 or 100 eq), CTA (1 eq) and AIBN (0.1 eq, added from 1 g mL^{-1} stock solution) was dissolved in benzene adjusting 30 w% concentration. The

solution was deoxygenized by 3 freeze-pump-thaw cycles and placed into a preheated oil bath at 65 °C. The polymerization was conducted for 3 hours and quenched by opening the tube to the air. The polymer was purified by precipitation into diethyl ether. After drying in vacuum oven, it was dissolved in water and lyophilized. The yield was calculated to be 74%.

5.2.4.3. Synthesis of block copolymers of PNIPAM and Mx by RAFT polymerization, PNIPAM-b-PMx and PNIPAM-b-P(NIPAM-*co*-Mx). Block copolymer synthesis was carried out with two different procedures. In the first procedure, functionalized monomer (50 eq) and macroCTA, (PNIPAM), (1eq) were dissolved in trifluoroethanol. AIBN (0.2 eq) was added from a stock solution in trifluoroethanol (1 g mL^{-1}). After 5 freeze-pump-thaw cycles, solution was stirred at 70 °C for 25 h. In the second procedure, the second block was designed as a copolymer. Thus, the mixture of functionalized monomer and NIPAM ([NIPAM]/[monomer] = 90:10, 70:30 and 50:50, 50 eq. in total) was dissolved in trifluoroethanol containing macroCTA (1 eq) and AIBN (0.4 eq). After 5 freeze-pump-thaw cycles, solution was stirred at 68 °C for 22 h. The polymers were purified by precipitation into diethyl ether. After drying in vacuum oven, they were dissolved in water and lyophilized. Yields were calculated as 17 % for the first procedure and 21, 37 and 17 % for the second procedure ([NIPAM]/[monomer] = 90:10, 70:30 and 50:50 respectively).

5.2.5. Dealkylation of Bisphosphonate Functionalized Monomers and Polymers

TMSBr (0.37 mL, 2.8 mmol) was added dropwise to an ice-cold solution of monomer or polymer (corresponding to 0.7 mmol phosphonate group) in dry DCM (2 mL) under nitrogen. After stirring 5 h at 30 °C, excess TMSBr was removed under reduced pressure. Methanol (3 mL) was added and the mixture was stirred for 30 min. The solvent was evaporated and the crude product was analyzed without any purification.

5.2.6. Synthesis of 6-acrylamidohexanoic acid (AHA)

Acryloyl chloride was added dropwise to a mixture of 6-aminohexanoic acid and sodium hydroxide in water at 0 °C. After stirring 1 h in an ice bath and 2 h at room temperature, the mixture was acidified to pH 1. The precipitated white solid in water was dissolved in ethyl acetate and the aqueous phase was extracted with ethyl acetate. After evaporation of the total organic phase, 6-acrylamidohexanoic acid (AHA) was purified by recrystallization from ethyl acetate and the yield of AHA monomer was calculated as 42 %.

5.2.7. Synthesis of Copolymers of NIPAM and AHA

Copolymerization of 6-acrylamidohexanoic acid (AHA) and NIPAM were carried out using standart freeze-pump-thaw method via free radical polymerization. Monomers were dissolved in EtOH at [NIPAM]/[AHA] to 60:40 ratio by adjusting the concentration as 40 w%. The solution was stirred at 65 °C for 4h. After precipitating in warm water, yield of P(NIPAM-*co*-AHA) was calculated as 84 %.

To prepare the block copolymer, 6-acrylamidohexanoic acid (AHA) (100 eq), macroCTA (PNIPAM) (1 eq) and AIBN ($[CTA]_0/[AIBN]_0$ = 5) were dissolved in trifluoroethanol adjusting 40 w% concentration. After 5 freeze-pump-thaw cycles, the solution was stirred at 70 °C for 8 hours. The polymer was precipitated into warm water. The yield of PNIPAM-b-PAHA was calculated to be 56 %.

5.2.8. Functionalization of P(NIPAM-*co*-AHA) with Bisphosphonic Acid

Bisphosphonic acid functionality was added to polymers using two different synthetic ways. In the first method, oxalyl chloride (0.29 g, 0.19 mL, 2.27 mmol) in dry DCM (1.5 mL) was added dropwise to carboxylic acid containing copolymer solution (60 mg corresponding to 0.32 mmol COOH) in an ice bath under nitrogen. 10 drops of DMF solution (0.1 mL DMF in 0.5 mL dry DCM) was added as catalyst to the cold mixture and the mixture

was stirred for 5 h. The solvent was evaporated and tris(trimethylsilyl)phosphite (0.39 g, 0.433 mL, 1.30 mmol) was added onto the formed acid chloride in dry THF (0.3 mL). The mixture was stirred at room temperature for 2 h. After removal of THF, the residue was stirred in MeOH (1.5 mL) for 2 h. The product was purified by dialysis against water.

The second method is based on carbodiimide chemistry approach. carboxylic acid containing copolymer (40.7 mg corresponding to 0.12 mmol COOH), EDC.HCl (29.1 mg, 0.15 mmol) and NHS-Sulfo (32.9 mg, 0.15 mmol) were stirred in water (0.6 mL) under nitrogen for 30 min in an ice bath and extra 3h at room temperature. A few drops of DMF (0.1 mL) were added to increase the copolymer's solubility. Then, alendronate (ALN) (82.3 g, 0.25 mmol) was dissolved in water by adjusting the pH to 8-9 and added dropwise in two aliquots to ice-cold activated copolymer solution. The pH of the mixture was maintained at 8-9 and the reaction was stirred for 1 h in an ice bath and overnight at room temperature. The product was purified by dialysis against water.

5.3. Results and Discussion

5.3.1. Synthesis and Characterization of Bisphosphonate Functionalized Acrylamides

Three new bisphosphonate-functionalized secondary amines with different hydrophilicities were synthesized to be used in monomer synthesis as shown in Figure 5.3. These amines (A1, A2 and A3) were prepared using tetraethyl vinylidene bisphosphonate as a Michael acceptor which was reacted with propyl, octyl or octadecyl amine by aza-Michael addition at room temperature. Amines having different length of alkyl chains were chosen to investigate the hydrophobicity effect on both LCST and potential mineralization capacity of the resulting structures. Tetraethyl vinylidene bisphosphonate was used in 1.1 times excess amount to ensure full functionalization. The structures were confirmed using ^{1}H NMR spectroscopy. It was observed that the peaks have a complex structure due to the

phosphorus-hydrogen coupling. For example, the methine proton formed after the reaction in the A1 structure is seen as a triplet of triplet at 2.6 ppm, and the methylene proton attached to nitrogen is seen as a triplet of doublet at 3.15 ppm (Figure 5.4). The synthesized amines were used without any further purification since the extra tetraethyl vinylidene bisphosphonate does not give any side reaction during monomer synthesis.

In the next step, each of these three amines were reacted with acryloyl chloride in the presence of triethyl amine (TEA) in dry DCM to form acrylamides M1, M2 and M3 which were purified by reverse flash chromatography on C18 column using MeOH-H_2O as eluent. The monomers (M1, M2 and M3) were obtained as light-yellow liquids in 45-55 % yields. They are well soluble in MeOH, THF, ether, DCM, hexane but solubility in water changes depending on the alkyl chain. For example, M1 is soluble in water but M3 is insoluble.

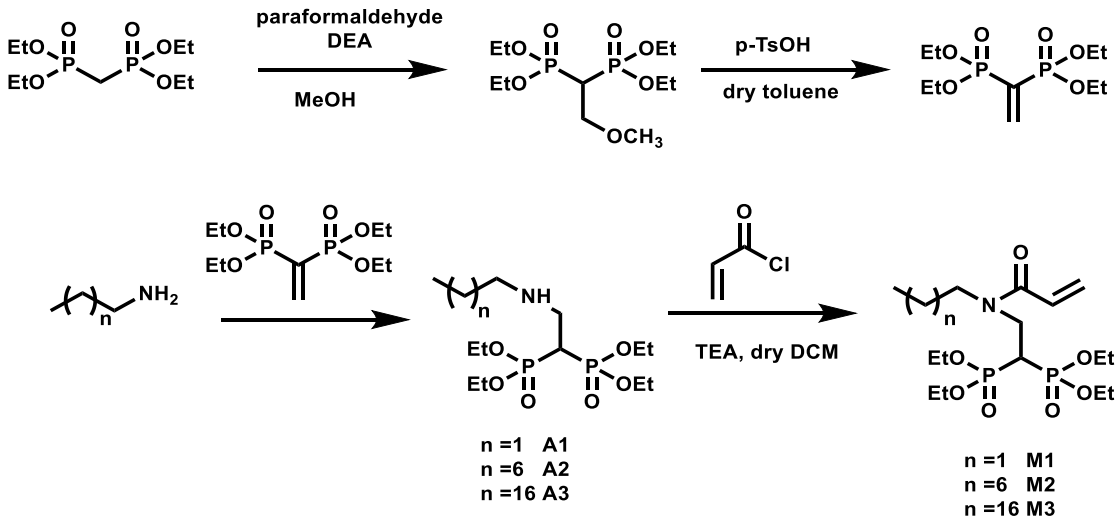

Figure 5.3. Synthesis of bisphosphonate functionalized amines (Ax) and acrylamides (Mx).

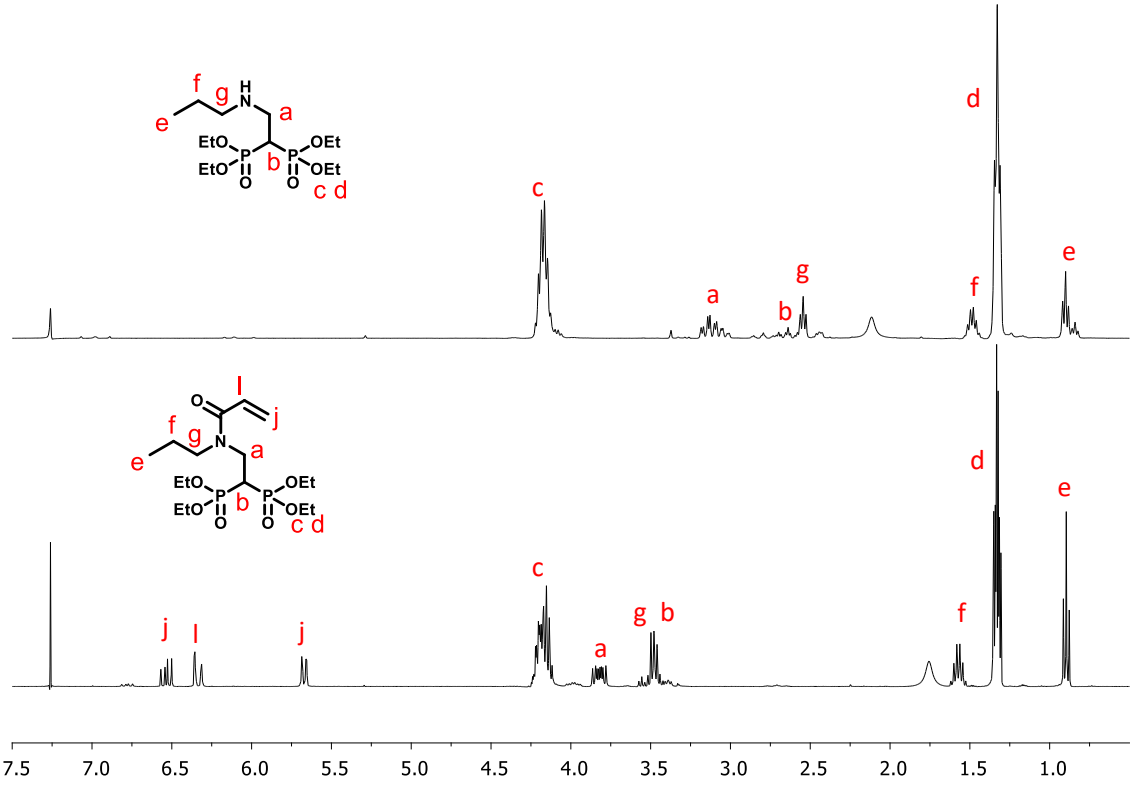

Figure 5.4. ^{1}H NMR of A1 and M1.

The spectral data are in agreement with the expected structure of the monomers. For example, the olefinic protons of M1 are between 5.67 and 6.53 ppm in ^{1}H NMR (Figure 5.4). The single bisphosphonate proton is a broad triplet of triplet, however these peaks overlap with the peaks due to methylene protons adjacent to nitrogen. ^{13}C and ^{31}P NMR spectra of monomers are shown in Figure 5.5. The methine proton is observed as a triplet at 32 ppm. The peak corresponding to phosphorus is seen at 18.8 ppm in ^{31}P NMR of M1. The FTIR spectra of each monomer show expected peaks both from bisphosphonate and acrylamide groups. The intensity of peaks between 2850 and 2950 cm^{-1} corresponding C-H vibration also increases for longer alkyl chains (Figure A.6). Methacrylamides of functionalized amines were also synthesized using the same procedure but purification of the monomers was not successful. Therefore, polymerization reactions of only acrylamides were carried out.

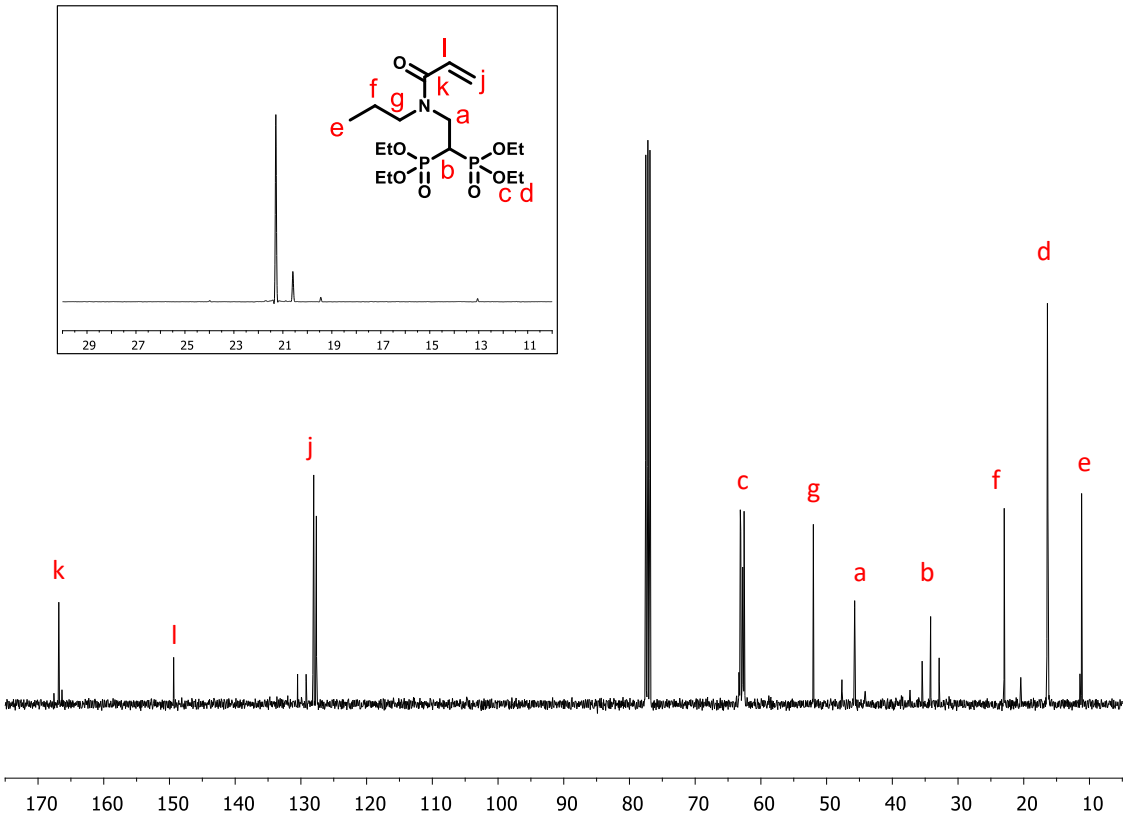

Figure 5.5. ^{13}C and ^{31}P NMR of M1.

It is known that bisphosphonic acid has high affinity to Ca^{2+} ions and dynamic coordination bonds can be formed between them. Therefore, the monomers were then silylated by trimethylsilyl bromide (TMSBr), and then the silyl ester groups were removed by methanolysis to obtain bisphosphonic acid-functionalized monomers. However, a decrease of both bisphosphonate ester and olefinic protons was observed in NMR characterization (Figure A.7). Fully dealkylation of similar monomer structures obtained by Michaelis-Arbuzov reaction was reported in literature [302]. However, Galaka et. al have also experienced a similar problem during some monomer dealkylation and claimed a new method needs to be developed for this transformation [278]. Therefore, we decided to carry out dealkylation reaction using TMSBr on polymers to protect polymerizable double bonds.

5.3.2. Synthesis and Characterization of Polymers

Novel thermoresponsive copolymers of bisphosphonate functionalized acrylamides and NIPAM were synthesized to investigate the relationship between structure and thermoresponsive behaviour. In addition to FRP technique, RAFT polymerization was also used to obtain narrow mass distribution.

5.3.2.1. Copolymers of NIPAM and M1/M2/M3 by FRP, P(NIPAM-*co*-Mx). Copolymers of NIPAM and bisphosphonated acrylamides were synthesized by free radical polymerization using AIBN as the initiator. Polymerization reactions were carried out in different solvents such as MeOH and dioxane and monomer concentrations (1, 2, 4 and 6 M). At high concentrations, reactions are in tendency to crosslink in a short time. Therefore, concentration is adjusted to 2 M and AIBN amount is determined as 2 mol %. The reaction temperature was raised from 60 to 70 °C to increase the reactivity of the monomers, thus, dioxane was used as solvent due to the low boiling point of MeOH. However, high conversions could not be achieved in 23 h (conversion were calculated as 22%). The copolymer ratio was calculated by integrating the methylene protons of phosphonate ester groups at 4.21 ppm with respect to methine proton of NIPAM at 3.96 ppm. For example, the ratio was calculated as 3 and 8 mol % for the copolymers with 5 and 10 mol % M1 in feed. It was observed that precipitated particles become dust like rather than solid when the amount of bisphosphonated acrylamide is higher, however the calculated ratio is comparable with the feed ratio. In the FTIR spectra of the copolymer (Figure 5.7) peaks at 975 and 1029 cm^{-1} correspond to the symmetric and asymmetric vibration of P−O.

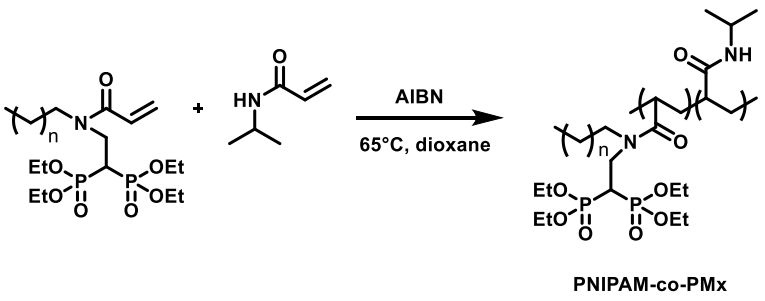

Figure 5.6. Synthesis of P(NIPAM-*co*-Mx) by FRP.

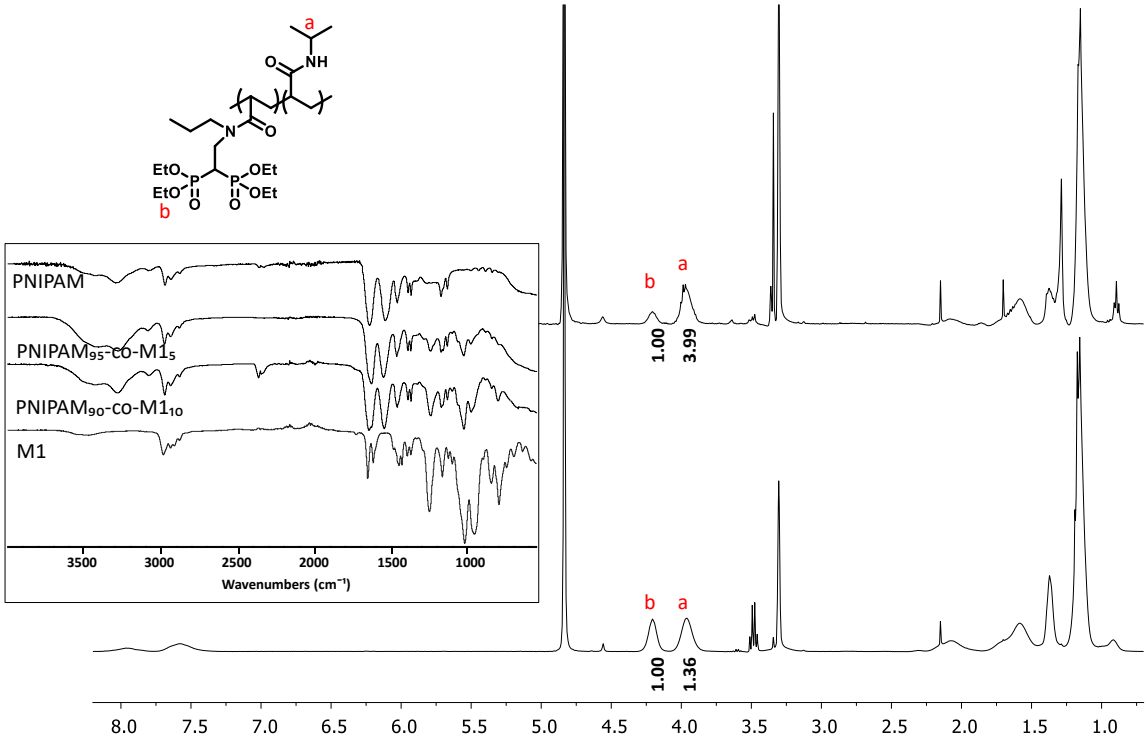

Figure 5.7. ^{1}H NMR spectra of P(NIPAM$_{90}$-*co*-M1$_{10}$) and P(NIPAM$_{95}$-*co*-M1$_{5}$). FTIR spectra of copolymers and M1.

5.3.2.2. Block copolymers of PNIPAM and M1/M2/M3 by RAFT. RAFT radical polymerization method was chosen to control the molar masses and polydispersity index values. First homopolymers of NIPAM was prepared by RAFT polymerization and used as macroCTA for the second block. 4-((((4-carboxybenzyl)thio)carbonothioyl)thio)butan-1-ylium was used as a chain transfer agent (CTA) which enables the end group analysis in molar mass determination. The NIPAM to CTA and AIBN ratio was varied to obtain polymers with controlled molecular weights. ($[CTA]_0/[AIBN]_0$ = 10, $[NIPAM]_0/[CTA]_0$ = 100 and 200). PNIPAM is soluble in cold water, chloroform, acetone and various alcohols such as methanol and trifluoroethanol. The resulting polymer was characterized by ^{1}H NMR (Figure 5.9).

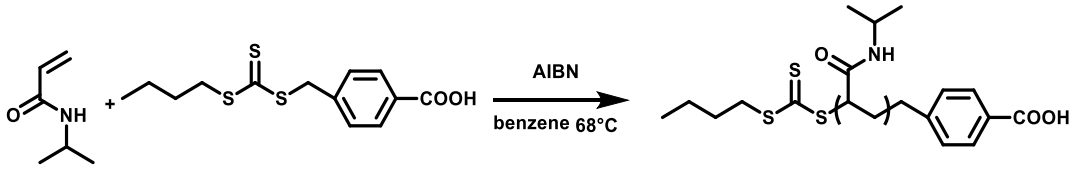

Figure 5.8. Synthesis of PNIPAM by RAFT polymerization.

The number average molar masses were determined by ^{1}H NMR, UV-vis spectroscopy and SEC. As seen in the ^{1}H NMR spectrum, CTA has characteristic signals for both end groups (aryl protons for R group, methyl protons for Z group). The number average molar mass (M_n) can be calculated by integrating these characteristic end group protons with respect to methine proton of NIPAM at 3.99 ppm. However, it was only possible to calculate M_n^{NMR-R} (with respect to R group of CTA, at 7.96 ppm) because the methyl proton of the Z group overlapped with methyl protons of NIPAM. The number average degree of polymerization (DP) values were found to be 171 and 98, close to the targeted values. The thiocarbonyl group of the Z group is a strong UV-chromophore showing maximum absorbance at 307 nm and an extinction coefficient ε in the order of 16500 L.mol^{-1} cm^{-1} in acetonitrile. Number average molar mass M_n^{UV} was calculated as shown in Table 5.1 by using the equation $M_n^{UV}= \varepsilon.c.d.E^{-1}$, where E is the extinction of trithiocarbonate chromophore group. It is assumed that the extinction coefficient of the chromophore is the same in CTA and the polymer. The molar masses and poly dispersity index values (PDI) for PNIPAM blocks were determined by SEC using NMP as eluent (Table 5.1). Low PDI values (1.2) indicated well-controlled chain growth. In addition, close molar mass estimations calculated by NMR and UV-vis spectroscopies show that the Z group of CTA is active which is important for further polymerization reactions.

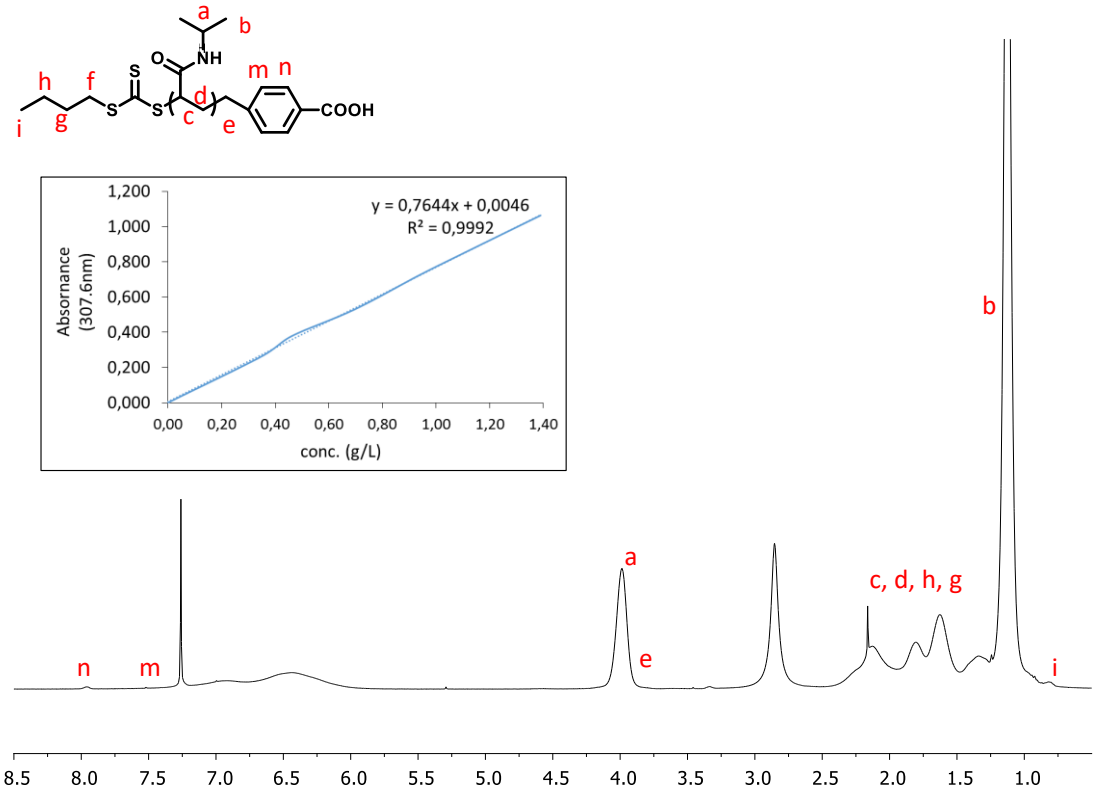

Figure 5.9. ^{1}H NMR spectrum and UV-vis measurements of PNIPAM.

Table 5.1. Characterization of PNIPAM polymers.

	M_n^{NMR-R} (kg/mol)	DP_n^{NMR}	M_n^{UV} (kg/mol)	M_n^{SEC} (kg/mol)	PDI	$[CTA]_0/[AIBN]_0$
$PNIPAM_{200}$	20	171	22	24	1.2	10
$PNIPAM_{100}$	11	98	16	11	1.2	10

For the synthesis of second block, firstly M1 was polymerized alone in the presence of macroCTA (PNIPAM) and AIBN by adjusting the ratio as $[CTA]_0/[AIBN]_0$ = 5 and $[M1]_0/[CTA]_0$ =50. After purification the yield was calculated as 17 %. The resultant polymer was characterized by ^{1}H NMR (Figure 5.11) and the degree of polymerization for the second block was calculated by integrating the methylene protons of phosphonate ester

groups at 4.17 ppm with respect to methine proton of NIPAM and aryl protons of CTA`s R group. DP was found as 2 which is 25 times less than targeted.

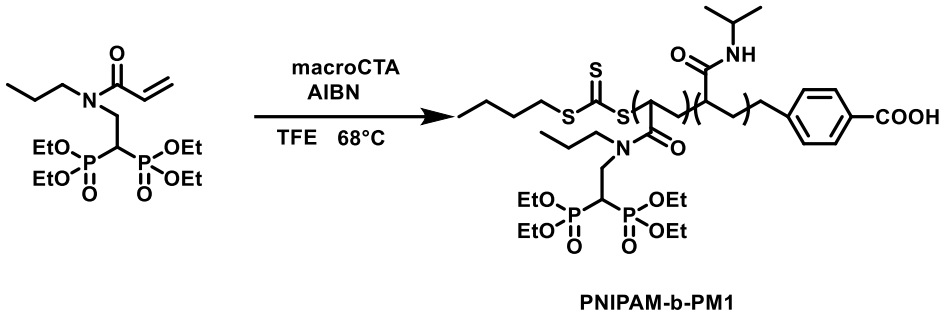

Figure 5.10. Synthesis of diblock copolymer of NIPAM and M1.

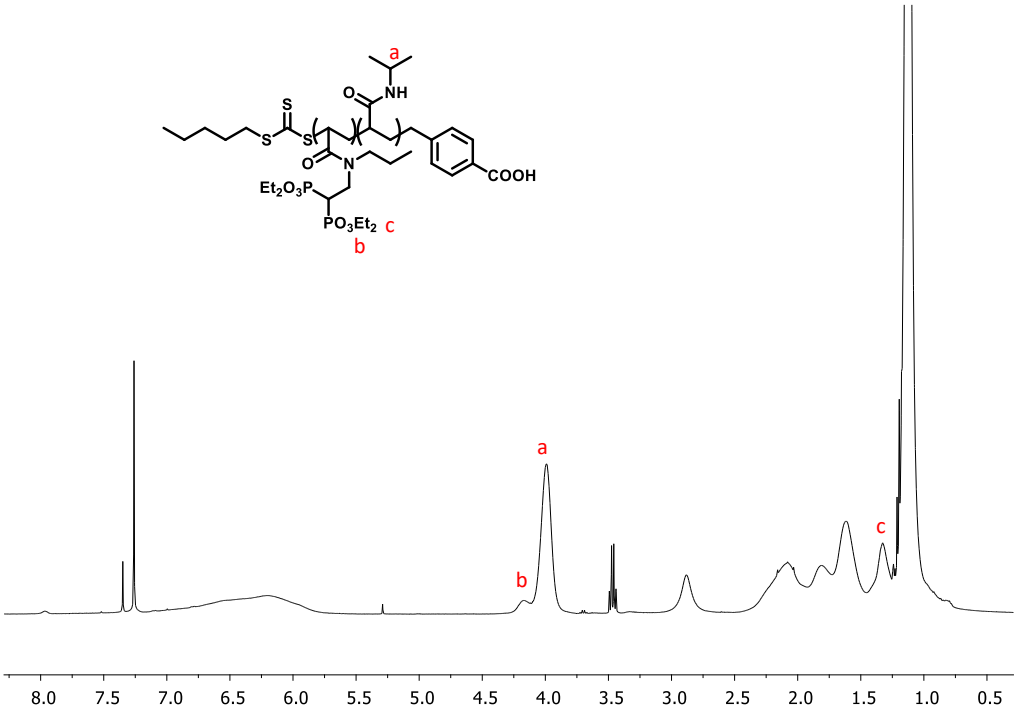

Figure 5.11. ^{1}H NMR spectrum of PNIPAM-b-PM1.

The low reactivity of the monomer can be explained by the labile methine proton. Wang et. al have found that N-acryl pamidronate monomer forms only oligomers when the amount of initiator is less than 5 mol %. Moreover, they mentioned the possibility of

termination of free radicals by the bisphosphonate group [273]. In addition to this, the sterically hindered polymerizable double bond in its structure might cause the second block to be very short. The polymerization of less hindered acrylamides containing phosphonate was also reported in different conditions [244, 279]. Therefore, as a second method, it was decided to synthesize the second block as a copolymer of NIPAM and synthesized monomers as shown in Figure 5.12. $PNIPAM_z$-b-P($NIPAM_y$-*co*-M_x) notation is used for the polymers where z, y and x show theoretical mol percentages of monomers used in the synthesis. Monomer based on octadecyl amine was not used in further reactions due to the low reactivity and solubility in water caused by the long alkyl chain. Degree of polymerization for the functionalized monomer was calculated by integrating the methylene protons of the phosphonate ester groups at 4.17 ppm with respect aryl protons of the R group. The percentage of bisphosphonate-functionalized monomer in the copolymer was calculated by comparing the integrals of c and b peaks shown in Figure 5.13. As seen from the ^{1}H NMR spectra, the intensity of the peak at 4.17 ppm corresponding to the monomer increases with an increase in M2 incorporation into the polymer. Nevertheless, M2 incorporation into the copolymer is around 50 % of the targeted amount. It can be concluded that bisphosphonate groups probably terminate the free radicals during reaction and result in low conversions.

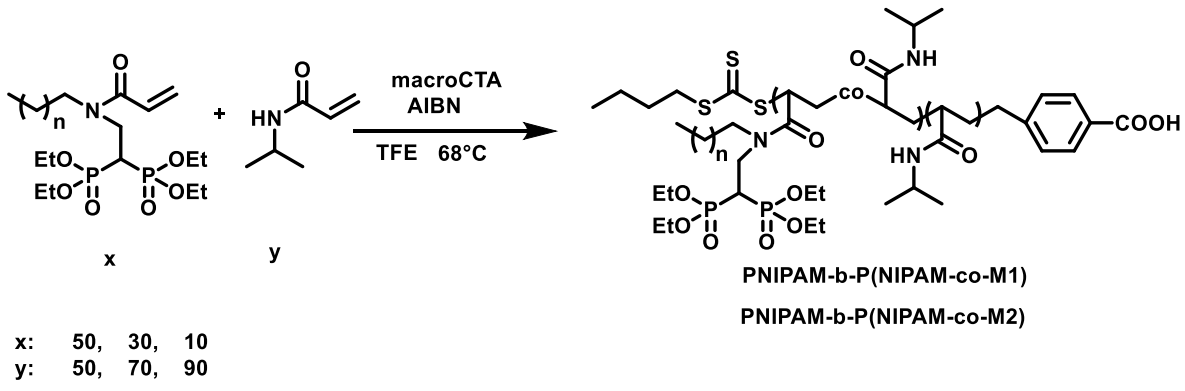

Figure 5.12. Synthesis of block copolymers (PNIPAM-b-P(NIPAM-*co*-Mx).

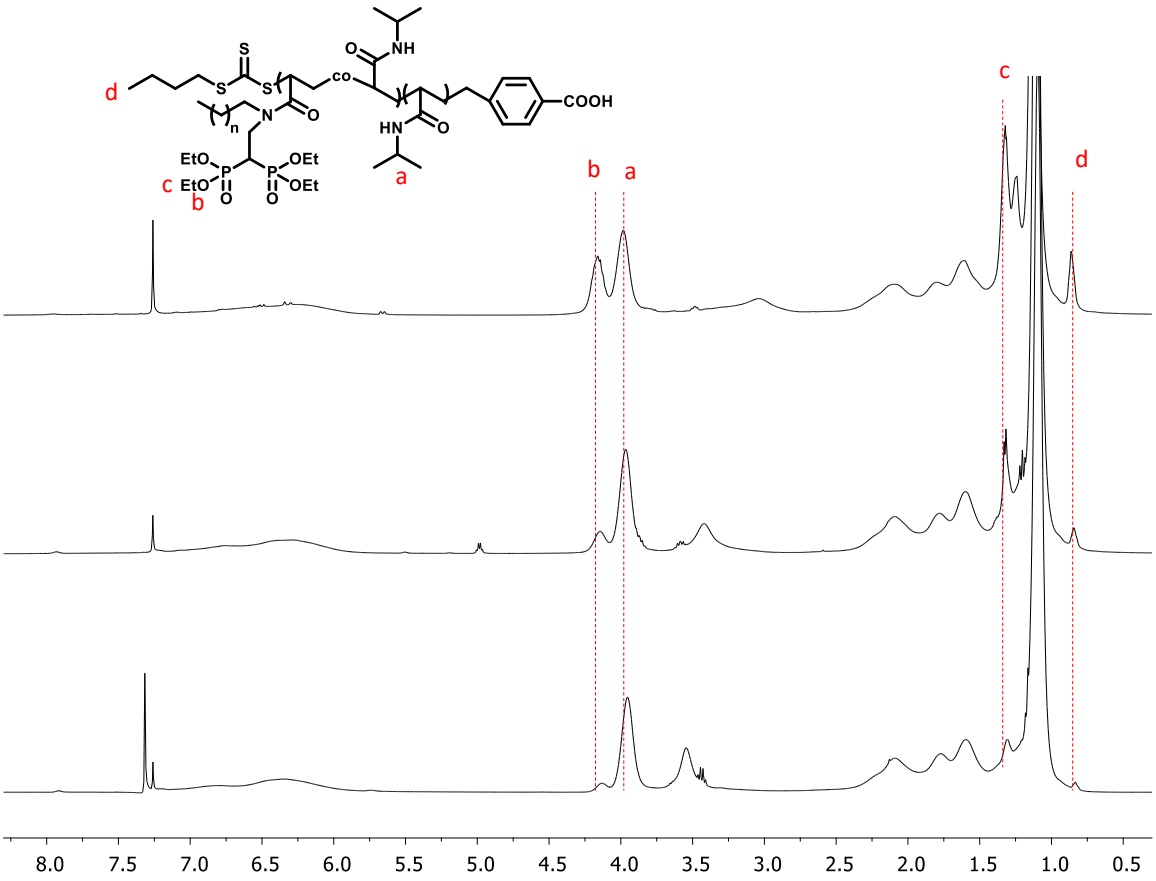

Figure 5.13. ^{1}H NMR spectra of the copolymers PNIPAM$_{200}$-b-(NIPAM$_y$-*co*-M2$_x$) y:x 45:5, 35:15, 50:50 respectively from bottom to top.

The number average molar masses of the polymers were determined by the same methods described above and the results are shown in Table 5.2. According to ^{1}H NMR, NIPAM incorporation for each polymer was different and calculated repeating unit of NIPAM could give inconsistent results than feed ratio when bisphosphonate functionalized monomer ratio was high. This problem causes lower M_n^{NMR-R} values than expected. M_n^{UV} values are calculated as the highest number average molar masses which show that some of the Z end groups of CTA were lost as a result low $[CTA]_0/[initiator]_0$ ratio. The CTA to AIBN mol ratio was determined as 2.5 for successful polymerizations. Lower ratios were not preferred since this causes high dispersivity. Polydispersity index values determined by SEC are also shown in Table 5.2. When this value is higher than 1.3, it indicates that polymerization is not carried out in a controlled way.

Table 5.2. Characterization of block copolymers (PNIPAM-b-P(NIPAM-*co*-Mx).

	M_n^{NMR-R} (kg/mol)	M_n^{UV} (kg/mol)	M_n^{SEC} (kg/mol)	PDI	$[CTA]_0/[AIBN]_0$
$PNIPAM_{200}$-b-$M1_{50}$	19	42	27	1.2	5
$PNIPAM_{200}$-b-($NIPAM_{45}$-*co*-$M2_5$)	32	46	31	1.2	2.5
$PNIPAM_{200}$-b-($NIPAM_{35}$-*co*-$M2_{15}$)	22	47	32	1.3	2.5
$PNIPAM_{200}$-b-($NIPAM_{50}$-*co*-$M2_{50}$)	20	not measured	31	1.4	1.25
$PNIPAM_{100}$-b-($NIPAM_{35}$-*co*-$M1_{15}$)	15	33	13	1.3	2.5

5.3.3. Dealkylation of Bisphosphonate Functionalized Polymers by TMSBr

The bisphosphonate functionality can be converted to bisphosphonic acid groups by using TMSBr which is a selective method for phosphonate esters and ensures that the ester or amide bonds in the molecule are not damaged. Therefore, synthesized polymers were subjected to a deprotection process by using excess TMSBr which was followed by methanolysis to make a correlation between hydrophilicity of functional group and LCST. ^{1}H NMR examination of the product showed the disappearance of phosphonate ester protons. However, ^{31}P NMR spectrum of this product did not show a phosphorus peak (Figure 5.15). A retro Michael reaction might be the reason for this unexpected result [280]. A stability problem of the acrylamide bond can also be the reason because the same reaction was successfully done for urea dimethacrylates by our group.

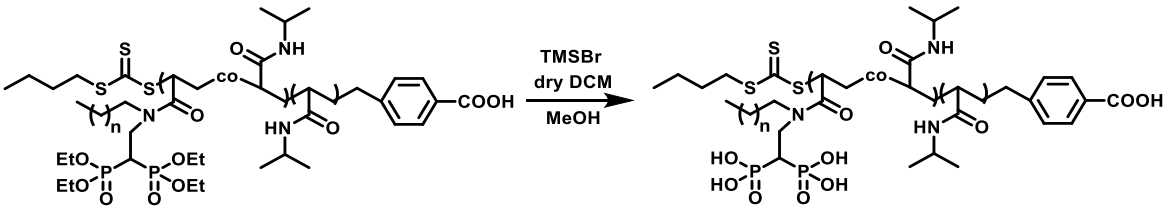

Figure 5.14. TMSBr dealkylation of block copolymers.

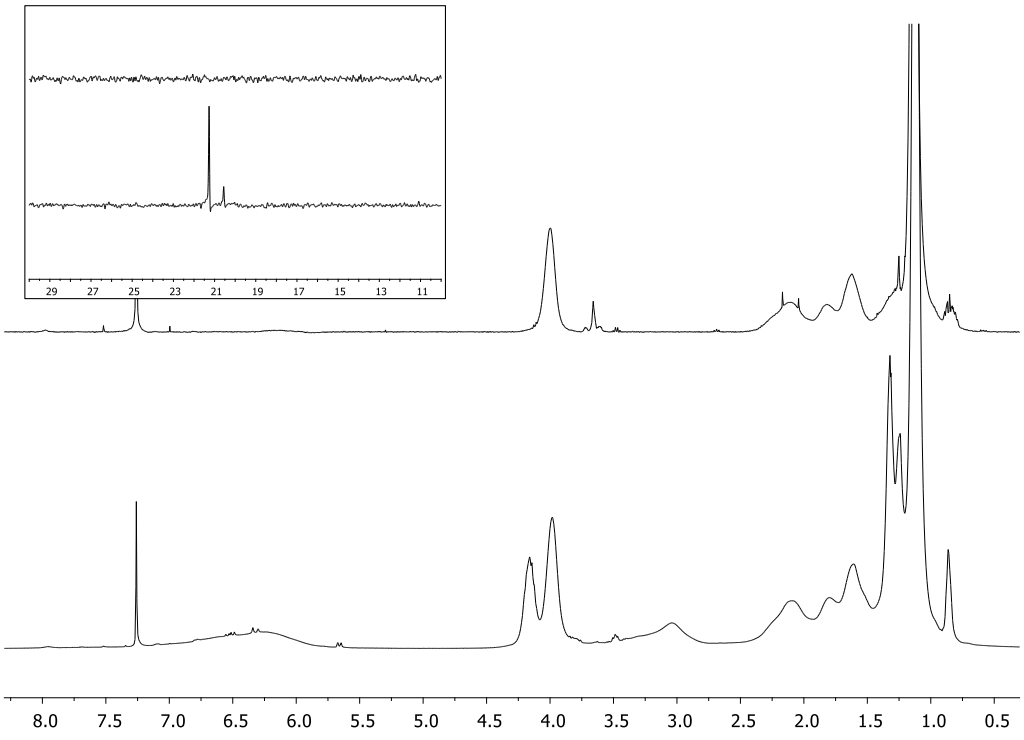

Figure 5.15. ^{1}H NMR and ^{31}P NMR spectra of the polymer before (below) and after (above) dealkylation.

5.3.4. Synthesis and Characterization of Copolymers of NIPAM and AHA

Since the hydrolysis of the bisphosphonate groups could not be achieved via the TMSBr reaction, incorporation of bisphosphonic acid groups by post-polymerization

modifications was decided as an alternative method. For this purpose, firstly a carboxylic acid-functionalized acrylamide (6-acrylamidohexanoic acid, AHA) was synthesized from the reaction of 6-aminohexanoic acid and acryloyl chloride in the presence of NaOH in water as shown in Figure 5.16. The monomer was purified by recrystallization from ethyl acetate and it was obtained as white solid in 42 % yield. AHA is soluble in highly polar (MeOH, DMF) and not soluble in slightly polar (DCM) solvents. The structure was confirmed by ^{1}H NMR and FTIR spectroscopies. The olefinic protons are seen at 5.7 and 6.2 ppm in ^{1}H NMR (Figure 5.17). FTIR spectrum of the monomer shows strong peaks at 1695 and 1542 cm^{-1} due to C=O and NH stretching (Figure 6.9).

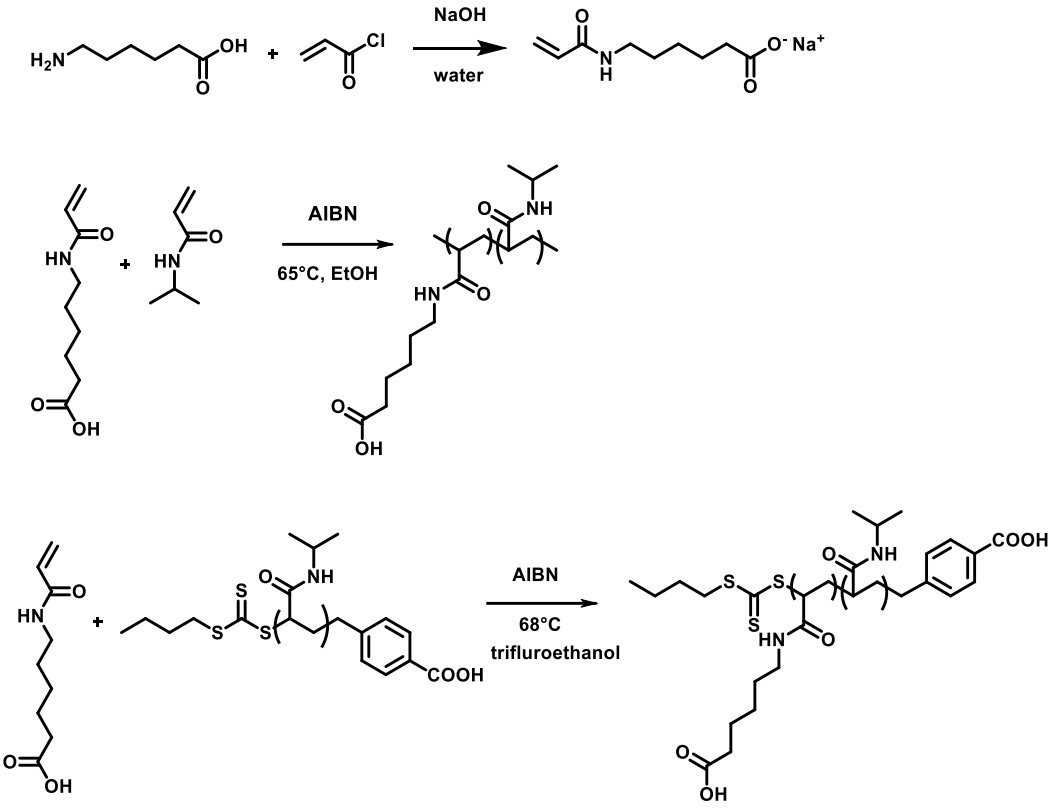

Figure 5.16. Synthesis of AHA monomer and its polymerization with NIPAM via FRP and RAFT polymerization.

The random copolymer of NIPAM and AHA was synthesized using 1 w% AIBN as the initiator in EtOH adjusting the concentration 40 w %. For block copolymers, the CTA to

AIBN mol ratio was determined as 5. The polymerization rate was quite fast, the yield was calculated as 84 % in 4 h for free radical polymerization and 56 % in 8 h for RAFT polymerization after purification by precipitating into water in which AHA is soluble. The polymers are MeOH and DMF soluble, but water insoluble eventhough monomers are water soluble. For example, 3 g/L polymer solution needs to be shaken for one day to become soluble. The resulting polymer was characterized by ^{1}H NMR (Figure 5.17) and FTIR. The peak at 2.3 ppm corresponding to methylene protons next to carboxylate group is relatively sharper than other peaks as it is far from the backbone. The degree of polymerization of the AHA monomer on block copolymers was calculated by integrating the methylene protons adjacent to amide nitrogen at 3.15 ppm with respect to methine proton of NIPAM. The polymer has good agreement between targeted and the NMR and GPC calculated molecular weights with low polydispersity of 1.1, indicating well-controlled polymerization. The FTIR spectrum of polymer showed peaks at 1710 and 1634 cm^{-1} due to carbonyl stretching of carboxylic acid and amide groups. Also, the peaks corresponding to NH and C-O stretching are present at 1539 and 1242 cm^{-1} (Figure 5.20a).

Table 5.3. Characterization of PNIPAM-b-PAHA.

	M_n^{NMR-R} (kg/mol)	**M_n^{SEC} (kg/mol)**	**PDI**	**$[CTA]_0/[AIBN]_0$**
$PNIPAM_{100}$-b-$PAHA_{50}$	20	18	1.1	5

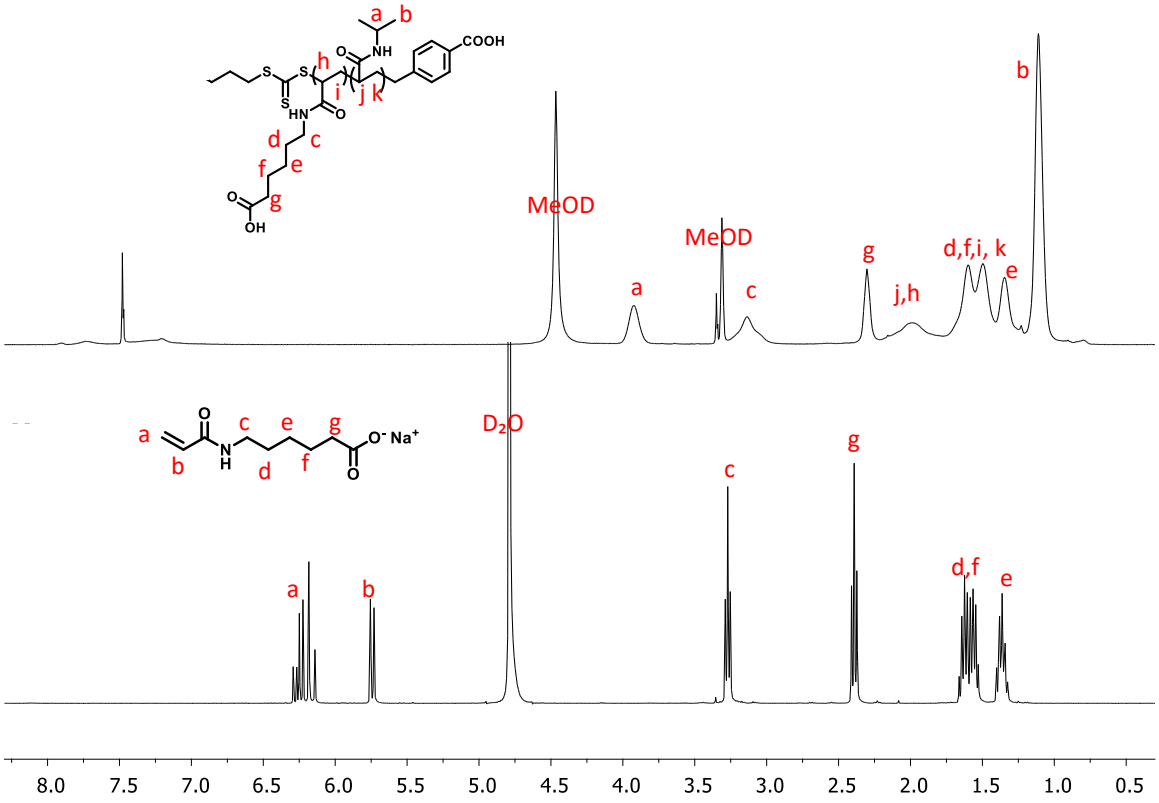

Figure 5.17. ^{1}H NMR spectra of AHA monomer and PNIPAM-b-PAHA.

5.3.5. Bisphosphonic Acid Incorporation to P(NIPAM-*co*-AHA)

The bisphosphonic acid incorporation to copolymer structure was studied using two different methods (Figure 5.18). In the first method, the bisphosphonic acid functionalized polymer, tmsp-P(NIPAM-*co*-AHA), was prepared in two steps: i) synthesis of the acid chloride derivative by reaction of the polymer and oxalyl chloride and ii) reaction of the acid chloride derivative with TMSP. The product was purified by dialysis to remove H_3PO_3. The polymer became water soluble after treatment. In the second method, bisphosphonic acid functionalized polymer, ale-P(NIPAM-*co*-AHA), was also prepared in two steps: i) reaction of copolymer with Sulfo NHS in the presence of EDC-HCl to form unstable reactive o-acylisourea ester intermediate and ii) reaction of the intermediate with sodium alendronate. The product was dialysed to remove unreacted starting materials.

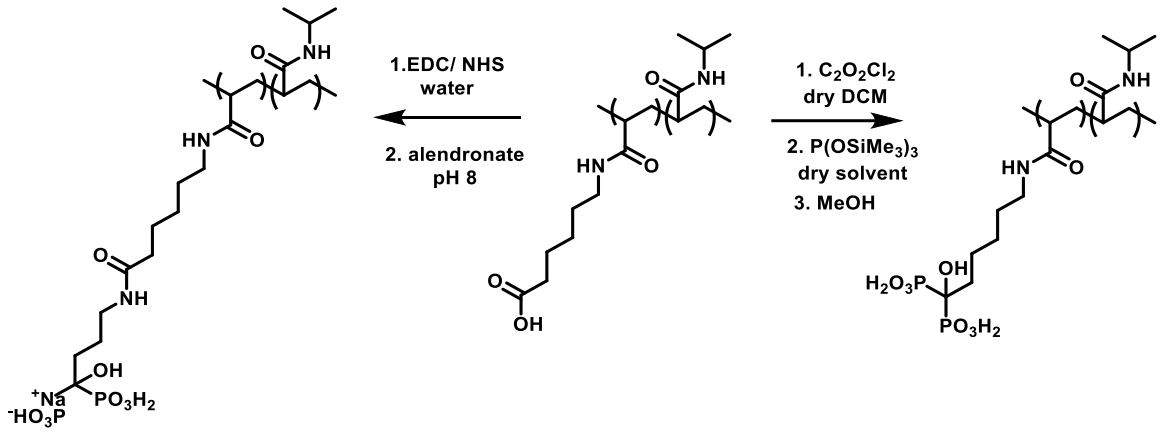

Figure 5.18. Synthesis of tmsp-P(NIPAM-*co*-AHA) and ale-P(NIPAM-*co*-AHA).

The resultant polymers were characterized by ^{1}H NMR as shown in Figure 5.19 and FTIR spectroscopy (Figure 5.20a and A.8). The formation of peaks at 2.02 and 3.44 ppm indicates alendronate incorporation when the method based on carbodiimide chemistry used. In addition, the peak corresponding to methylene protons adjacent to amide carbonyl showed a downfield shift after modification. The intensity of the band representing AHA carbonyl stretching diminished noticeably; furthermore, the intensity of the NH peak increased relatively to the amide carbonyl band. Also, thermal properties of copolymers were investigated using DSC. T_g of the copolymer was determined as 110 °C but after ALN addition no T_g could be found until 140 °C. Surprisingly, NIPAM's methine and methyl protons as well as methylene protons next to amide of AHA disappeared in the ^{1}H NMR spectrum of the product obtained by the other method (tmsp-P(NIPAM-*co*-AHA)). Amides are stable groups but the acidity of bisphosphonic acid might catalyze amide hydrolysis during dialysis. Therefore, FTIR spectrum of the product was also considered before purification and did not show any peak at 1539 cm^{-1} corresponding to amide NH (Figure A.8). As a result, we deduced that TMSP modification is not a proper method for the amide included structures, hence the second method (using EDC/NHS) was studied for block copolymers.

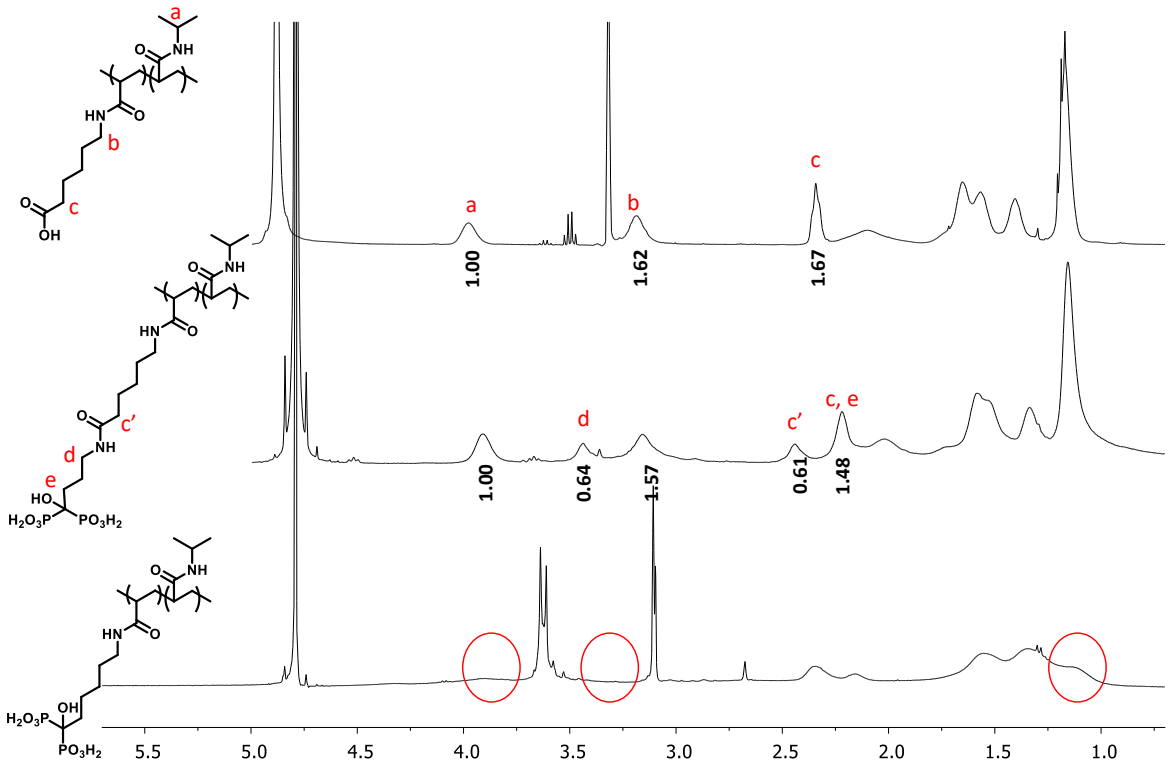

Figure 5.19. ^{1}H NMR spectra of P(NIPAM-*co*-AHA) after bisphosphonic acid modification.

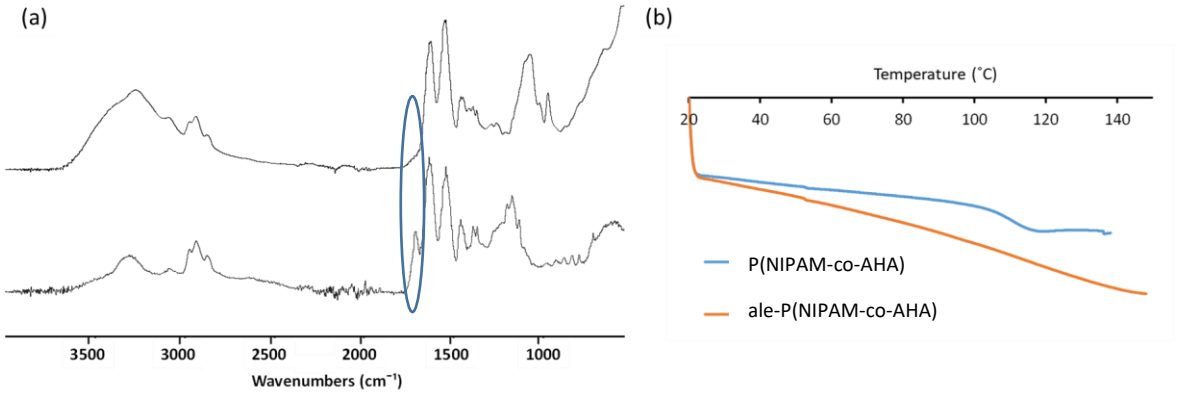

Figure 5.20. (a) FTIR spectra of ale-P(NIPAM-*co*-AHA) (above) and P(NIPAM-*co*-AHA) (below) (b) DSC curves of copolymers.

5.3.6. Aqueous Solution Properties of Polymers

5.3.6.1. Aqueous solution behaviours of PNIPAM homopolymers. Aqueous solution behaviours were studied to investigate the effect of polymer structure on LCST values. Cloud points of the synthesized polymers were determined using a Cary 50 UV-Vis spectrometer equipped with a single cell Peltier thermostat. Although heating and cooling curve repetitions give consistent results, the cooling curve shifts almost 2 °C compared to the heating curve. 1 °C hysteresis, which occurs in the inter-chain association and dissociation process due to additional hydrogen bonds formed in the collapsed state, can be seen also in PNIPAM [258]. The reason of the high shift could not be understood for this system and cloud points are given in terms of heating curves. The cloud point values of $PNIPAM_{200}$ and $PNIPAM_{100}$ solutions (10 g/L) were measured as 27.2 and 24.5 °C which are lower than the generally known value for PNIPAM (32 °C) due to the concentration of polymer solution and hydrophobic end groups of CTA. When the polymer chain is shorter the hydrophobic end group effect becomes very strong. The cloud points for PNIPAM increased to 30.6 °C and 28.1 °C in dilute solutions (3 g/L).

Table 5.4. Cloud points of block copolymers of NIPAM and Mx (10 g/L concentration).

Polymer	**BP (mole %)**	**Cloud point (°C)**
$PNIPAM_{200}$	-	27.2
$PNIPAM_{200}$-b-P($NIPAM_{45}$-*co*-$M2_5$)	1.0	29.1
$PNIPAM_{200}$-b-P($NIPAM_{35}$-*co*-$M2_{15}$)	2.5	28.6
$PNIPAM_{200}$-b-P($NIPAM_{50}$-*co*-$M2_{50}$)	8.0	27.8
$PNIPAM_{200}$-b-$M1_{50}$	1.2	27.9
$PNIPAM_{200}$-b-P($NIPAM_{35}$-*co*-$M1_{15}$)	0.7	27.8

5.3.6.2. Aqueous solution behaviours of PNIPAM-b-P(NIPAM-*co*-Mx) polymers. As seen in Table 5.4, cloud points were measured between 27.8 and 29.1 °C after incorporation of second block that induces 0.6 and 1.9 °C increase in cloud points. The ethyl groups in bisphosphonate structure and alkyl chains in monomer structure cause hydrophobicity while the presence of oxygen increases hydrophilicity. Cloud point of PNIPAM showed a small increase with the incorporation of 1.2 % bisphosphonate functionalized monomer ($PNIPAM_{200}$-b-$M1_{50}$). However, the addition of NIPAM during the formation of second block is different for other polymers which makes the comparison between bisphosphonate ratio and cloud points not possible that can be the reason of lack of order. According to ^{1}H NMR integrals of $PNIPAM_{200}$-b-P($NIPAM_{35}$-*co*-$M2_{15}$), during the second block formation incorporated NIPAM amount is very small. Therefore we can compare $PNIPAM_{200}$-b-$M1_{50}$ and $PNIPAM_{200}$-b-P($NIPAM_{35}$-*co*-$M2_{15}$ and conclude that increase in bisphosphonate addition increases cloud points. Figure 5.21 demonstrates the transmittance to temperature curves of block copolymers synthesized from the same monomer at different ratios as well as different monomers at equal ratios.

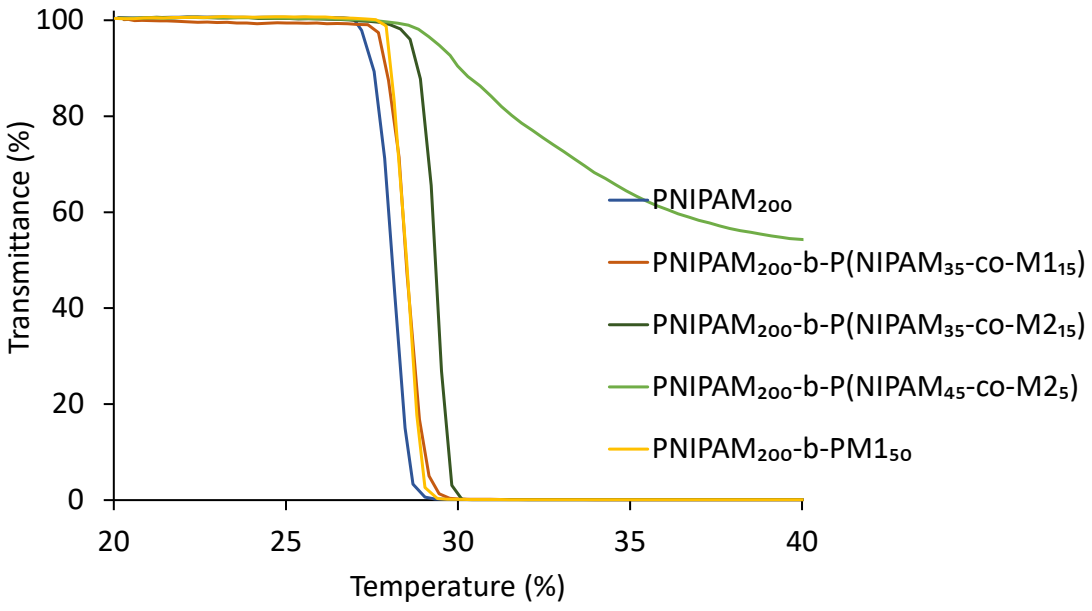

Figure 5.21. Turbidimetry studies of block copolymers of NIPAM and Mx.

5.3.6.3. Aqueous solution behaviours of PNIPAM-b-PAHA and ale-PNIPAM-b-PAHA polymers Turbidimetry measurements of PNIPAM-b-PAHA based polymers were carried out on 3 and 10 g/L polymer solutions prepared in D_2O or in 0.02M $CaCl_2$ solutions. The polymer solutions were placed on a shaker for one day to obtain homogenous solutions since the water solubility of $PNIPAM_{200}$-b-$PAHA_{100}$ and solubility of modified polymers in $CaCl_2$ solution are low. After modification cloud points increase dramatically as shown in Table 5.5. Percent transmittance of PNIPAM-b-PAHA decreases from 100 % to 98.5 % (orange line) in the arranged temperature range with a constant slope as shown in Figure 5.22. However, when the solution was prepared in $CaCl_2$ solution, a sharp transition from transparent to opaque was observed (orange dashed line). Cloud points of ALN-$PNIPAM_{200}$-b-$PAHA_{100}$ were found to be more than 6 °C higher than relevant PNIPAM ($PNIPAM_{200}$) due to the hydrophilic effect of the anionic group. In the presence of Ca^{2+}, a decrease in transmittance is observed earlier as expected. It is not shown but the transitions are not reversible when Ca^{2+} ion is present in the system.

Table 5.5. Cloud points of PNIPAM-b-PAHA (3 g/L polymer concentration).

Polymer	**Cloud points (°C)**		**Cloud points after $CaCl_2$ (°C)**	
	3 g/L	10 g/L	3 g/L	10 g/L
$PNIPAM_{200}$	30.2	27.2	NM*	27.4
$PNIPAM_{200}$-b-$PAHA_{100}$	-	-	26.5	25.7
ale-$PNIPAM_{200}$-b-$PAHA_{100}$	36.7	35.6	35.3	-

*Not measured

To better understand structural and dynamic properties of the synthesized polymers, dynamic light scattering measurements were done. The experiments were performed at scattering angle $\Theta = 173^{\circ}$ (backscattering detection mode) with a high-performance particle sizer equipped with He-Ne laser, and a thermoelectric Peltier element for temperature

control. Aqueous polymer solutions were prepared in water and $CaCl_2$ solutions (0.02M) at 10 g/L concentrations and measured in temperature steps of 1 °C with equilibration time of 2 minutes. Particle sizes of $PNIPAM_{200}$-b-$PAHA_{100}$ and ale-$PNIPAM_{200}$-b-$PAHA_{100}$ are around 90 and 20 nm at starting temperature (15 °C). PNIPAM-b-PAHA polymer shows a different trend than the modified polymer in water. The decrease in the average diameter indicates that the polymers are shrinking between 15 °C and 30 °C which results in an increase in the refractive index of particles and increase mean count rate. ale-$PNIPAM_{200}$-b-$PAHA_{100}$ shows a large increase in mean count rate and average diameter around 36 °C. This trend is also seen in PNIPAM at LCST due to polymer structure transition from random coil to condensed globule. The refractive index of the condensed globule structure is larger than that of the random coil structure. As seen in the right column in Figure 5.23, in 0.02M $CaCl_2$ solution, shrinkage of the polymers was observed again for $PNIPAM_{200}$-b-$PAHA_{100}$ but around LCST a sharp increase in the average diameter was detected for both polymers due to the synergetic effect of thermosensitive block and Ca^{2+}-anionic group interaction. The increase in the count rate as seen in ale-$PNIPAM_{200}$-b-$PAHA_{100}$ indicates particle aggregation. At higher temperatures, also reduction of particle size was observed which might be induced by water expulsion due to Ca^{2+}-anionic group interaction between polymer chains.

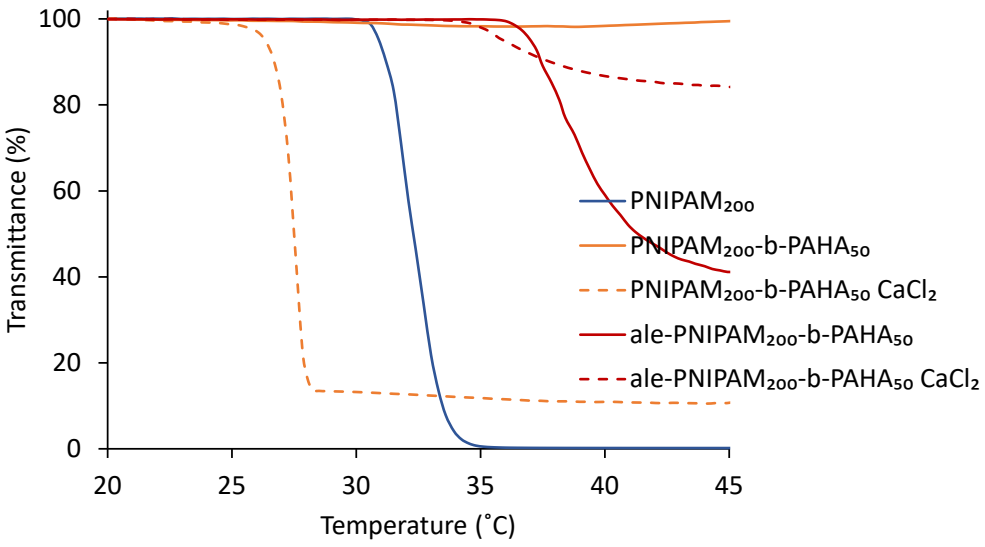

Figure 5.22. Turbidimetry studies of PNIPAM-b-PAHA.

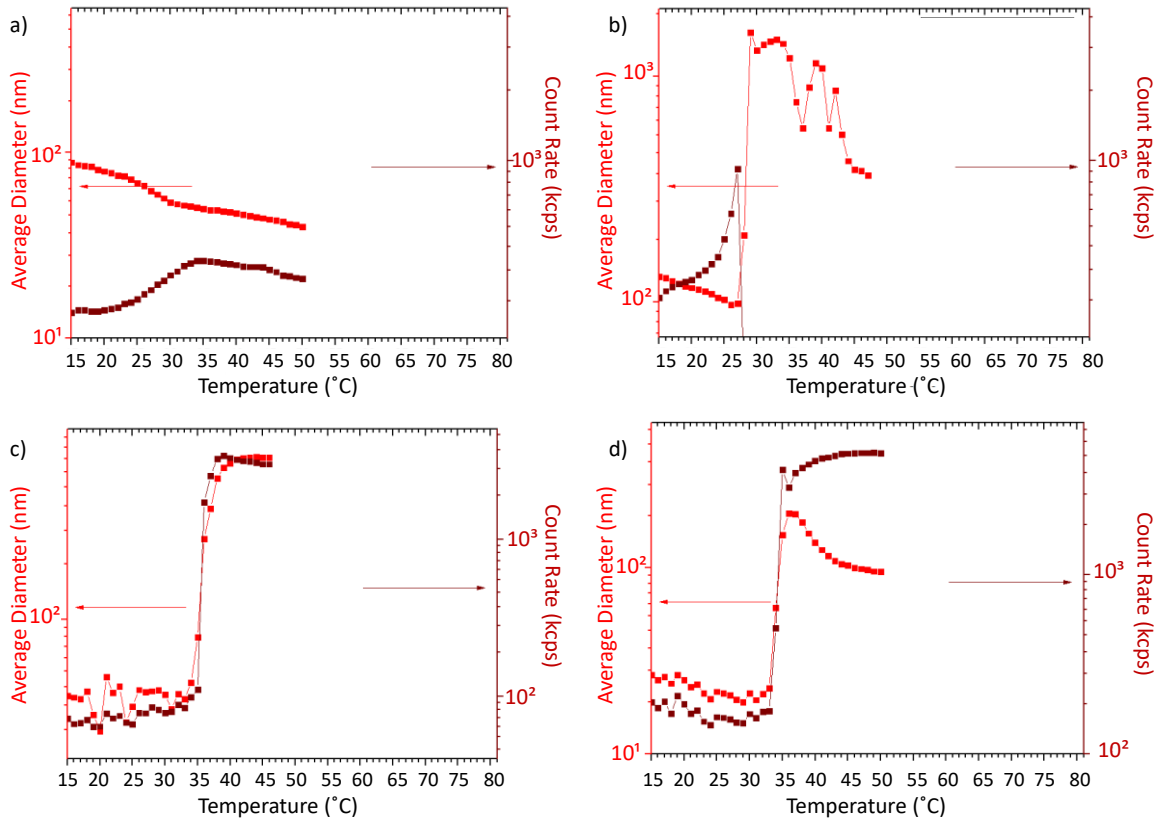

Figure 5.23. Average diameter and count rate vs temperature graphs of 10 g/L solutions of $PNIPAM_{200}$-b-$PAHA_{100}$ (above) and ale-$PNIPAM_{200}$-b-$PAHA_{100}$ (below) (a,c) in water and (b, d) in 0.02 M $CaCl_2$ solution.

5.4. Conclusions

In this chapter, the synthesis and characterization of three novel bisphosphonate functionalized monomers containing different alkyl chains were reported. These monomers were copolymerized with NIPAM at different ratios using FRP and RAFT polymerization to investigate the effect of polymer structure on LCST of polymers in aqueous solution. In addition, bisphosphonic acid functionality was incorporated into carboxylic acid containing NIPAM based polymers via post polymerization modification to understand the influence of hydrophilicity of this group on thermoresponsive behaviour of polymers in water and in $CaCl_2$ solution. Polymers showed cloud points between 27.8 and 36.7 ºC depending on their

structure, interactions with Ca^{2+} and polymer concentration. The cloud point around body temperature implies that bisphosphonic acid containing thermoresponsive polymers can be candidates to be used for bone related biomedical applications.

6. ALENDRONATE INCORPORATION INTO CARBOXYLIC ACID POLYMERS

6.1. Introduction

Bisphosphonic acids show significant bone selectivity rather than other tissues due to their high affinity to Ca^{2+} ions which make them preferable for dental materials, bone targeting systems and the treatment of bone diseases. Polymers are good options to combine bisphosphonic acids with different units like drugs, proteins and imaging agents to enhance their therapeutic uses by diminishing limitations and toxicity. Therefore, design of polymers containing alendronate holds great promise in bioapplications related with bone. In this chapter, two carboxylic acid containing homopolymers were synthesized using ibuprofen functionalized alkyl α-hydroxymethacrylate and 6-acrylamidohexanoic acid via free radical polymerization. Alendronate, a widely used bisphosphonic acid derivative was incorporated into them by electrostatic interaction or covalent bonds formed through activated esters. These polymers are expected to have good interactions with hydroxyapatite. As such, they have potential to be utilized in bone targeting drug delivery systems or remineralization for the therapy of dental caries.

6.2. Experimental

6.2.1. Materials and Methods

Ibuprofen functionalized polymer (p-MA-IBU) was synthesized according to the procedure prepared by our group (M.S. thesis of Burcu Balaban, under preperation). 6-acrylamidohexanoic acid (AHA) was synthesized as described in the literature [277]. 2,2'-azobis(isobutyronitrile) (AIBN), trifluoroacetic acid (TFA), N-(3-dimethylaminopropyl)-N′-ethylcarbodiimide hydrochloride (EDC-HCl), N-hydroxysulfosuccinimide sodium salt (Sulfo NHS), N,N′-dicyclohexylcarbodiimide DCC and solvents were purchased from Sigma-Aldrich or Merck and used without further purification. Sodium alendronate was a

gift from DEVA A.Ş. The chemical structures of polymers were confirmed by ^{1}H NMR (Varian Gemini 400 MHz) and FTIR (Thermo Scientific Nicolet 380) spectroscopies. The molecular weights were determined by gel permeation chromatography (GPC) (Malvern Viscotek) with DMF as eluent using polystyrene standards. The morphologies of the polymer samples were examined using scanning electron microscopy (SEM) (FEI-Philips XL30) under an accelerating voltage of 7.0 kV after sputter coating with a platinium layer. Thermogravimetric analysis (TGA) studies were carried out under nitrogen with a PerkinElmer STA 6000 machine using a heating rate of 10 °C/min.

6.2.2. Homopolymerization of 6-acrylamidohexanoic acid (PAHA)

AHA was synthesized as described in previous chapter. Polymerization of AHA was carried out using standard freeze-pump-thaw procedure in dried EtOH at 68 °C with 1 wt % AIBN addition by adjusting the concentration as 40 w%. The polymer was purified by precipitation from EtOH into water and the yield of PAHA was calculated as 45 % after drying under vacuum.

6.2.3. Alendronate Loading to p-MA-IBU

Alendronate (ALN) loading process was carried out in aqueous medium. A 15 mg/mL solution was prepared by dissolving sodium alendronate in deionized water. The pH of the solution was 4.73 after the alendronate dissolved. p-MA-IBU (10 mg/mL) was added to this solution. After stirring at room temperature for 1 d at 500 rpm, extra ALN was added, adjusting its total concentration as 25 mg/mL. After 2 more days of stirring, the drug loaded particles were isolated from the solution by centrifugation followed by repeated washing with water to remove unreacted alendronate. Then collected particles were freeze dried and the amount of alendronate interacted with polymer was calculated by taking the mass difference of added and remained amount of alendronate.

6.2.4. Functionalization of PAHA with Alendronate

PAHA (42.3 mg, 0.23 mmol), EDC.HCl (86.3 mg, 0.45 mmol) and NHS-Sulfo (99.2 mg, 0.45 mmol) were stirred in water (1.5 mL) under nitrogen for 30 min in an ice bath and extra 30 min at room temperature. Then, ALN (211.9 mg, 0.65 mmol) was dissolved in water by adjusting the pH to 9 and added dropwise into ice-cold heterogeneous activated polymer solution. The pH of the mixture was maintained at 8 and the reaction mixture was stirred for 1 h in an ice bath, meanwhile the solution becomes homogenous, and was stirred for 1 d at room temperature. The product (ALN-PAHA) was purified by dialysis using a membrane with a molecular weight cutoff 14 kDa in water for 5 days to remove the unreacted components.

6.2.5. Interactions of Polymers with HAP

HAP particles (5 wt %) were dispersed in 10 wt % polymer containing polymer/ EtOH/H_2O (10/30/60 or 10/60/30 wt %) solution under stirring. The resulting particles were separated by centrifugation after 24 h and washed several times with ethanol and water depending on the solubility of polymer, then dried under vacuum.

6.2.6. Ibuprofen Release

The drug release studies of ibuprofen prodrug polymers were done in PBS. Briefly, the pre-weighed dry polymer sample (25-30 mg) and 3 mL PBS were transferred to a dialysis membrane (1000 Da) and then was placed into a flask containing 200 mL of PBS, maintained at 37 °C and stirred at 150 rpm for 14 days. At predetermined time intervals 3 mL of external solution was removed and an equal volume of fresh solution was added to the system. Each sample was analyzed by a Lasany UV-Vis double beam spectrophotometer LI-2802 and the amount of released ibuprofen was calculated using the absorbance at 264 nm according to calibration curve. The linear correlation (R^2=0.999) between the absorption and

concentration of ibuprofen was determined using known concentration samples (0.02, 0.05, 0.1, 0.3, 0.4 mg mL^{-1} of ibuprofen in PBS).

6.2.7. Mineralization

Enamel samples were prepared by first embedding clinically removed human teeth into **an** acrylic resin and then cutting the resulting composite into slices. The slices were then etched by 37 % phosphoric acid for 45 s and washed with water for demineralization of enamel. ALN-PAHA solution (25 mg/mL, 100 μL) was dropped onto the etched enamel and dried at room temperature. After washing with water to remove unbound polymer, treated enamel samples were soaked in artificial saliva at 37 ℃ for biomineralization for 14 days, refreshing the solution every day. To prepare artificial saliva, $CaCl_2$ (1.5 mM), KH_2PO_4 (0.9 mM), KCl (130 mM), HEPES (20 mM) and NaN_3 (1 mM) were dissolved deionized water and pH was adjusted to 7 using 1 M KOH. The mineralized enamel samples were washed with water and dried at room temperature.

6.3. Results and Discussion

6.3.1. Synthesis and Characterization of p-MA-IBU:ALN

The blood flow in bone is very low, therefore, combining bone targeting groups and drugs is a common strategy to increase their efficiency. In our work, alendronate was electrostatically linked with p-MA-IBU (synthesized previously by our group) to obtain a bone targeting anti-inflammatory prodrug which can have potential to be utilized for osteoarthritis, one of most common health problems. pH has an important role since the drug loading depends on electrostatic interactions. Therefore, reaction was carried out at pH 4.7, at which alendronate has a positively charged primary ammonium ion and polymer contains negatively charged carboxylic acid moieties. Concentrated alendronate solution and long reaction time were chosen to enable drug loading on the water insoluble polymer. After isolating the particles from alendronate solution, particles were washed with water and

subjected to repeated centrifugation, adding fresh water cycles to remove unreacted alendronate for 2 days.

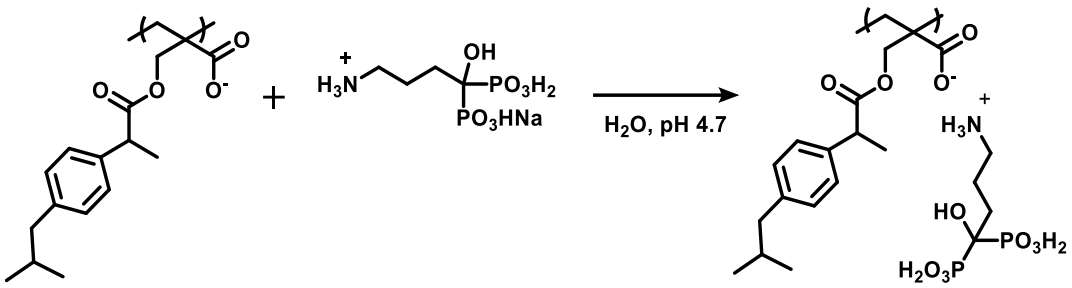

Figure 6.1. Synthesis of p-MA-IBU:ALN.

The FTIR spectrum of washed particles is shown in Figure 6.2. The spectrum contains peaks of both polymer and alendronate showing the success of the interaction. A broad O-H stretching band between 2500 and 3500 cm^{-1}, N-H bending vibration of the primary ammonium ion at 1632 cm^{-1} and P=O, P-O-H, P-O-C stretching and bending vibrations between 1200 and 900 cm^{-1} are observed in the spectrum. A small shift was detected in the N-H bending vibration of the primary ammonium ion of alendronate (1643 to 1634 cm^{-1}) and carbonyl stretching of polymer (from 1713 to 1732 cm^{-1}) compared to their original spectra because of the interaction between them [281]. The stability of electrostatic interaction in water was proven after 2 days of washing process. It was also tested for the acidic medium by stirring the p-MA-IBU:ALN in pH 3 solution for 1 h. As seen from the FTIR spectrum of the collected sample after washing, the intensity of the peaks corresponding to alendronate was dramatically decreased. In acidic environment, the carboxylate ion is protonated, and subsequently the interacted alendronate is liberated. The difference in the morphology of polymer samples is apparent as presented in Figure 6.3. SEM confirmed the deposition of alendronate on p-MA-IBU, crystal structures were observed in the zoomed SEM image of p-MA-IBU:ALN. The smaller crystals measure as 43-92 nm and larger ones are 220-575 nm in diameter.

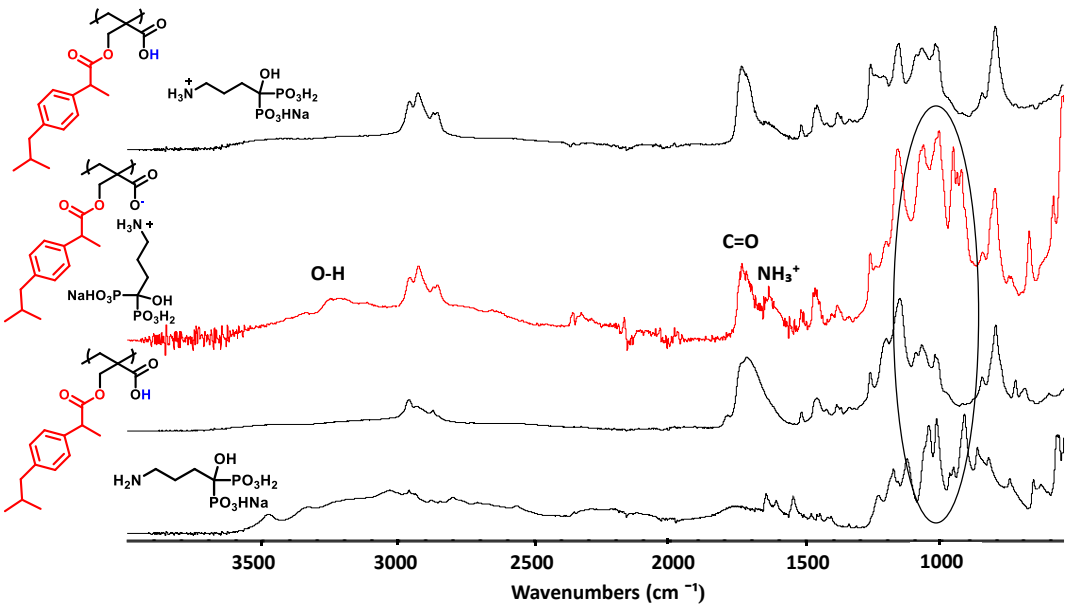

Figure 6.2. FT-IR spectra of p-MA-IBU:ALN at pH 3, p-MA-IBU:ALN, ALN (top to bottom).

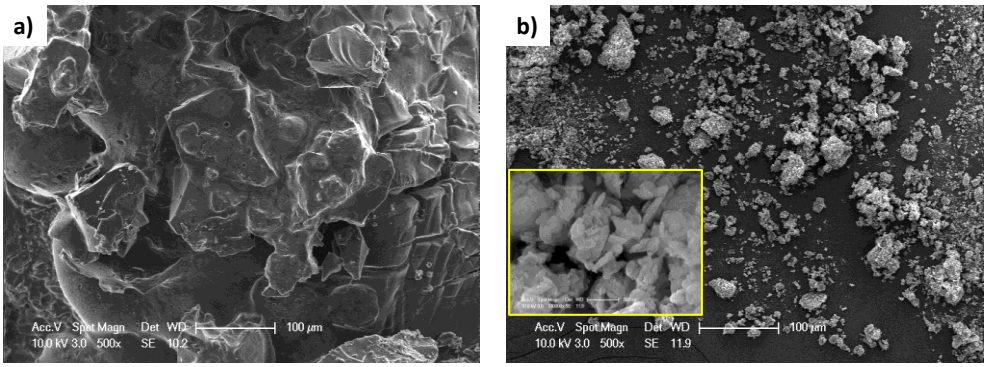

Figure 6.3. SEM micrographs of (a) p-MA-IBU and (b) p-MA-IBU:ALN.

TGA thermogram of the polymers is shown in Figure 6.4. The difference in the char yields of p-MA-IBU (9%) and p-MA-IBU:ALN (47%) obviously shows the presence of an extra moiety. A broad mass loss (15%) was monitored between 132 and 313 °C which may correspond to water and ammonia degradation of alendronate. Alendronate's thermal decomposition occurs in three different stages at 136 (mass loss of three water molecules), 295 (mass loss of ammonia) and 438 °C (complete pyrolysis lead to the formation of $NaH_3P_2O_7$). Goulart da Silva et al. found 55 % char yield for pure alendronate [282]. Loaded

alendronate amount was roughly calculated as 69% by comparison of char yields of pure alendronate and formed structure. Loading efficiency of particles was calculated between 66 and 87 % by taking the ratio of mass difference of added and remained amount of alendronate to initial mass of p-MA-IBU.

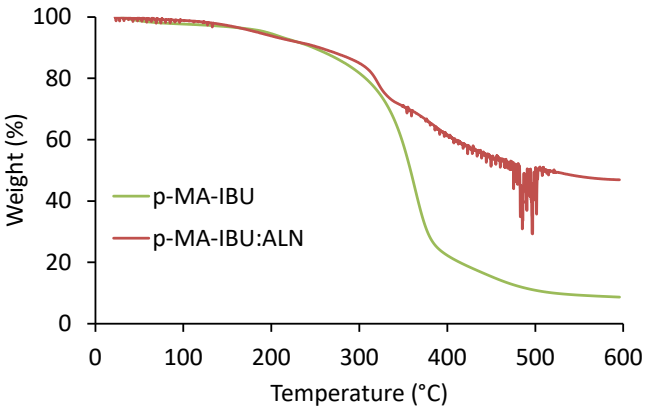

Figure 6.4. TGA thermogram of p-MA-IBU p-MA-IBU:ALN.

6.3.2. HAP Interactions of p-MA-IBU and p-MA-IBU:ALN

Synthesized polymers were mixed with HAP particles to determine their HAP affinity. For this reason, 10 w % polymer was dissolved in EtOH and H_2O mixture (60:30 w%). After 24 h stirring and washing with EtOH, the interaction of the synthesized polymers with HAP was investigated by FTIR as shown in Figure 6.5. The FTIR spectrum of HAP ($Ca_{10}(PO_4)_6(OH)_2$) shows bands of phosphate ions (PO_4^{3-}). The peaks at 1090 and 1017 cm^{-1} are assigned to the triply degenerate asymmetric stretching mode (ν3) and the one at 962 cm^{-1} is associated with the symmetric stretching mode (ν1) of P−O bonds. The bands observed at 600 and 650 cm^{-1} are related with the triply degenerate bending (ν4) mode of O−P−O bonds. Moreover, the peak appearing at 631 cm^{-1} associated with the vibrational mode of the hydroxyl anion [287]. The intensity of polymer peaks in the FTIR spectrum of p-MA-IBU:ALN:HAP is too strong due to the insoluble character of the polymer. Therefore, the discussion was done for p-MA-IBU. In addition to characteristic HAP bands, carbonyl peaks observed at 1732 cm^{-1} for p-MA-IBU:HAP. The presence of carbonyl peaks implies that polymer remained on HAP surface even after it was washed EtOH. Moreover, the blue

shift of the carbonyl peak of p-MA-IBU (from 1714 to 1732 cm^{-1}) shows the strong interaction between C-O^- of the polymer and HAP. The peak corresponding to asymmetric stretching mode (ν3) of phosphate at 1017 cm^{-1} shifted to lower frequency. Acidic group of the polymers could replace inorganic phosphate and chelate calcium ion to form calcium salts of polymers that can end up a shift in wavenumbers [291]. A newly formed small peak at 880 cm^{-1} in the spectrum of p-MA-IBU:HAP indicates that carbonate ions (CO_3^{2-}) that produced by dissolved CO_2 in air are substituted with the site of hydroxyl ion in HAP.

Table 6.1. IR band positions of p-MA-IBU before and after HAP treatment.

	C=O (cm^{-1})	NH (cm^{-1})	PO_4^{3-} (cm^{-1})
HAP	-	-	1017
p-MA-IBU	1714	-	-
p-MA-IBU:HAP	1732	-	1013

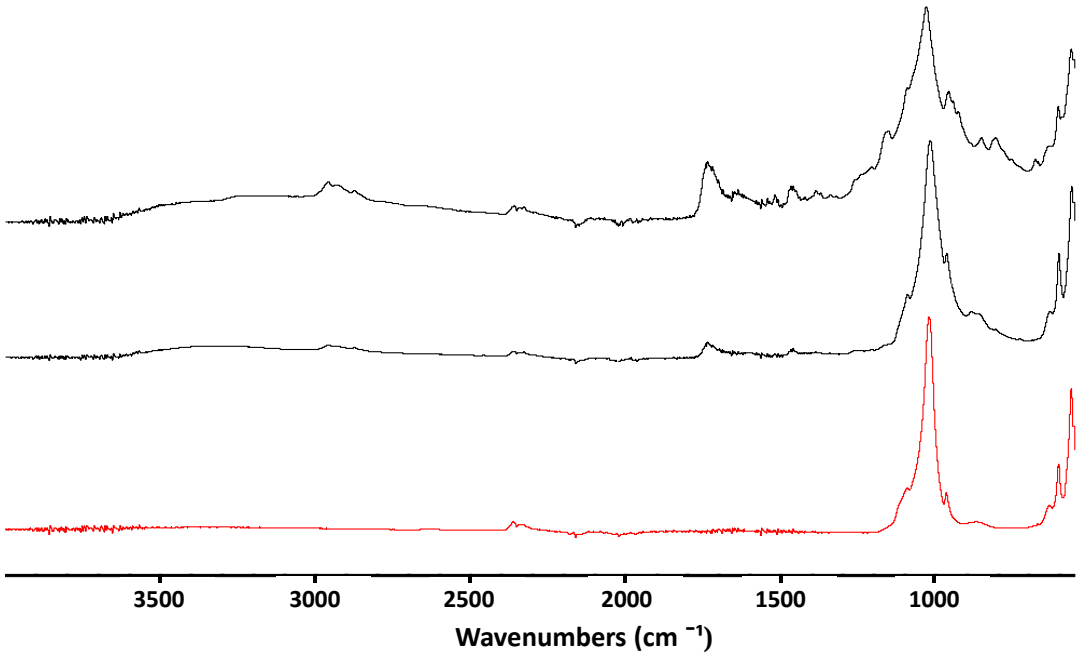

Figure 6.5. FTIR spectra of p-MA-IBU:ALN:HAP, p-MA-IBU:HAP and HAP (from top to bottom).

6.3.3. Ibuprofen Release from Prodrugs

ALN was electrostatically incorporated into p-MA-IBU structure to improve its bone targeting capacity. Although the HAP affinity of p-MA-IBU:ALN could not be determined by FTIR because of its poor solubility, the strong interaction between ALN and bone tissue is very well known. Moreover, after interaction the hydrophilicity of the product changed due to the addition of ionic groups. There are different factors affecting the rate of hydrolysis of a drug such as structure of polymers, the linkage type and hydrophilicity of polymers. IBU is attached to the p-MA-IBU via ester linkages and increase in hydrophilicity enables water diffusion and accelerates release. In order to observe the performance of prodrugs under physiological conditions, drug release studies were performed in PBS at 37 °C under shaking. Since the polymers were not soluble in water, the hydrolysis was performed in a heterogeneous system using dialysis tubing *(MWCO = 1000)* which are permeable to low molecular weight IBU. The amount of the released IBU passing to external solution at different time intervals was determined from its absorbance at 264 nm using a UV spectrophotometer and calculated from the calibration curve.

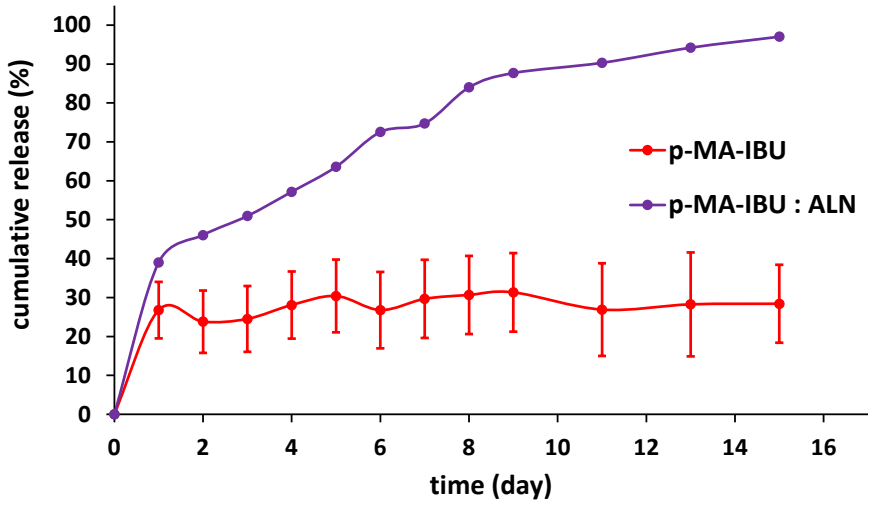

Figure 6.6. The release profiles of ibuprofen from p-MA-IBU and p-MA-IBU:ALN.

Figure 6.6 shows the cumulative IBU release from p-MA-IBU and p-MA-IBU:ALN as a function of time. Approximately 26% of ibuprofen was released from p-MA-IBU in 1

day and it stayed almost constant for 15 days at PBS. Physical interaction between alendronate and p-IBU-MA created a more hydrophilic prodrug resulting higher and more controlled drug release. A faster first day release (39% in 1 day) was observed from p-MA-IBU:ALN, After 84% of IBU release- within 8 days, release rate decelerated from 6.4 to 1.8 % per day. Total amount of released IBU was calculated as 97 % at the end of 15 days. Almost full degradation can be attributed to the fact that ester bonds are more accessible and hydrolysis is facilitated thanks to hydrophilic ALN. Ibuprofen, the degradation product of the release study is a weak acid. Although p-MA-IBU:ALN is not stable in acidic medium, released ibuprofen could not change the pH of the PBS. Even when ALN is liberated due to a disruption in electrostatic interaction, it is a non-chromophoric compound and cannot be detected by UV-Vis spectrophotometric analysis.

6.3.4. Synthesis and Characterization of PAHA and ALN-PAHA

The homopolymer of AHA was synthesized in EtOH using 1 wt% AIBN as the initiator by adjusting the concentration as 40 wt %. After purification by precipitating into water, the yield was calculated as 62 % for the reaction carried out overnight. The polymer is soluble in EtOH and DMF but not soluble in water. GPC analysis was done in DMF (including 1 g/L lithium bromide) as an eluent using light scattering detector. The number average molecular weight (M_n) and polydispersity index of polymer were found to be 346000 g mol^{-1} and 2.59. The ^1H NMR (Figure 6.8) and FTIR (Figure 6.9) spectra of PAHA showed broadened peaks compared to monomer. Disappearance of alkene peaks at 1654 cm^{-1} could not be distinguished because of the broad carbonyl peak. Moreover, the peak at 1634 cm^{-1} corresponding to carbonyl stretching of amide group shifted to 1636 cm^{-1}.

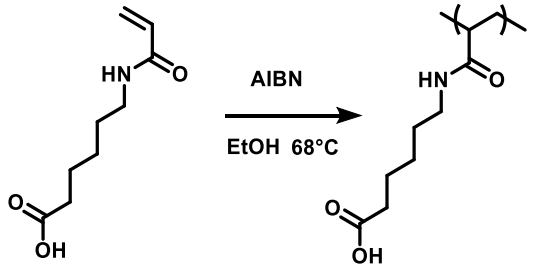

Figure 6.7. Synthesis of PAHA.

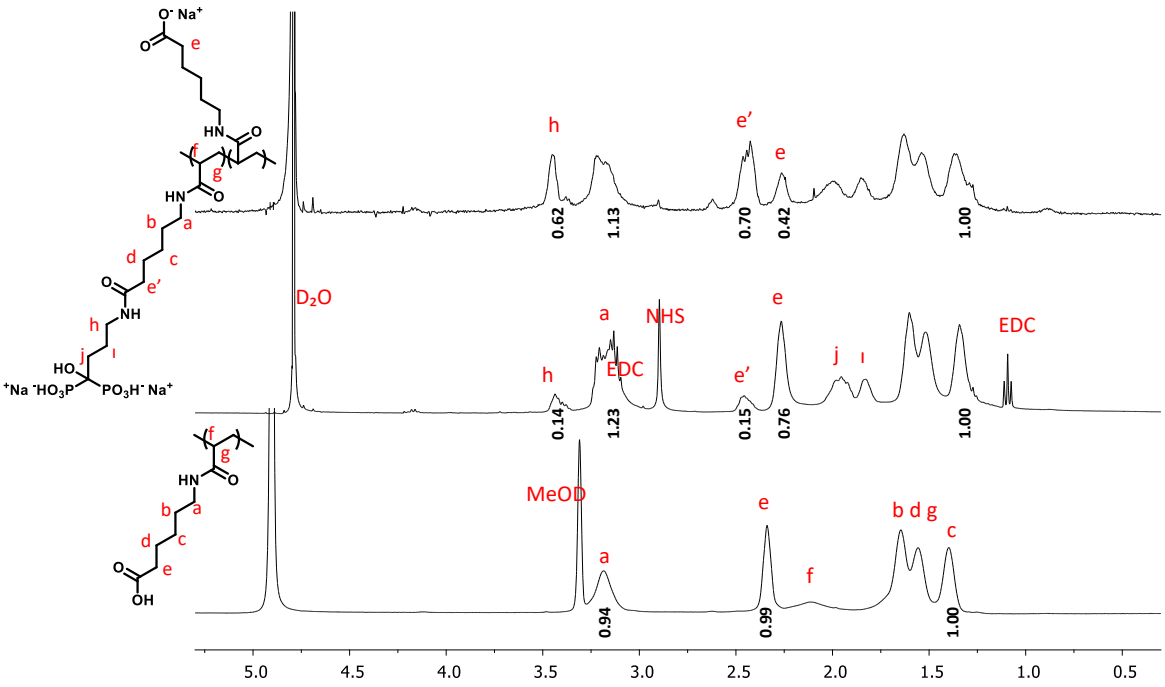

Figure 6.8. ^{1}H NMR spectra of PAHA and ALN-PAHA.

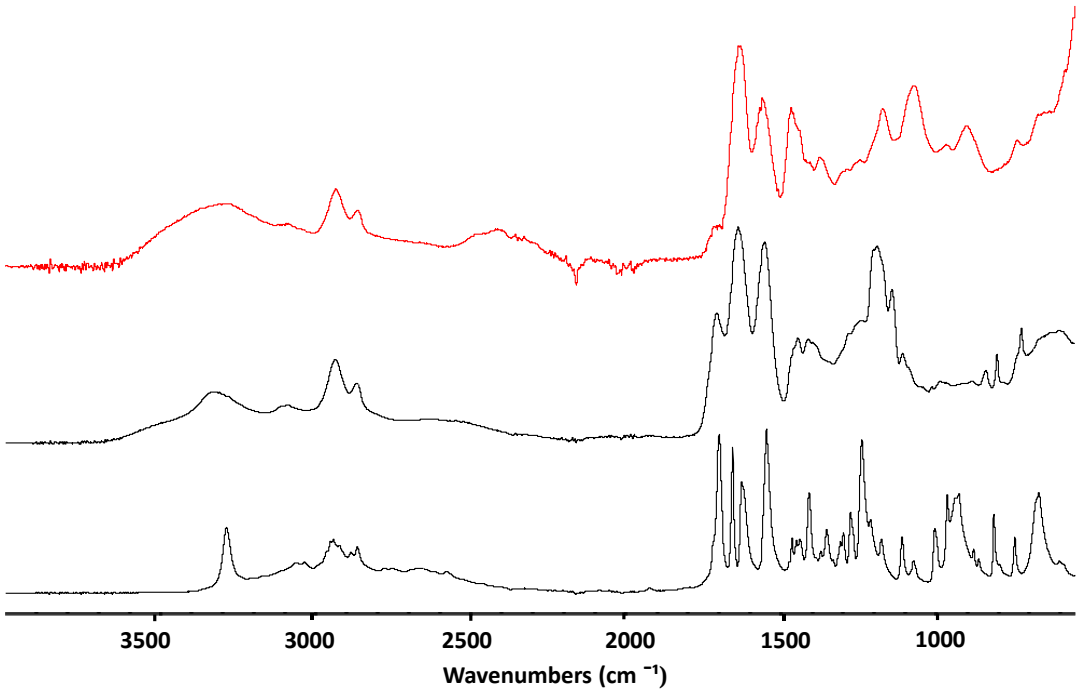

Figure 6.9. FTIR spectra of ALN-PAHA, PAHA and AHA (from top to bottom).

Bisphosphonic acid functionality was incorporated into PAHA structure via amidation. Amide bond formation is a widespread synthetic method and many procedures have been studied up to now. The condensation of carboxylic acid and amine can form an amide bond with the release of water; however, this reaction requires high reaction temperature and nonaqueous solvents. Therefore, activation of the carboxylic acid to convert the -OH of the acid into a good leaving group is necessary before the treatment with the amine. Acyl chloride formation with thionyl chloride or oxalyl chloride as well as activated ester formation with carbodiimides such as EDC and N,N′-dicyclohexylcarbodiimide (DCC) are two of the methods used for carboxylic acid activation [283, 284]. The high reactivity of acid chlorides toward amines makes them preferable for sterically hindered substances. Moreover, a catalytic amount of DMF can be added to accelerate acid chloride formation. Nevertheless, HCl formation is a byproduct, the cleavage of protecting groups and the necessity of anhydrous conditions are the main drawbacks of this method. Alendronate is a water-soluble powder and not soluble in highly polar solvents such as DMSO, DMF and alcohols. Therefore, hydrolysis of formed acid chloride, producing carboxylic acid in alendronate addition step, is the main problem for our aim.

Carbodiimides are a large group of compounds for amide bond preparation. The mechanism for coupling carboxylic acids to amines is demonstrated in Figure 6.10. After O-acylisourea intermediate formation, different products can be produced by mechanisms other than direct reaction with the amine. For example, excess carboxylic acid can react with the intermediate to form an anhydride which also gives the desired amide via aminolysis. Intramolecular acyl transfer of the O-acylisourea caused irreversible formation of N-acylurea byproduct. The workup to remove the urea byproduct depends on the selection of carbodiimide. To illustrate, dicyclohexylurea from DCC can be isolated by filtration due to its very limited solubility in organic solvents while the urea byproduct of EDC is water soluble and can be removed by aqueous workup. The formation of N-acylurea can be diminished and amide coupling rate can be accelerated by addition of auxiliary nucleophile such as 1-hydroxybenzotriazole (HOBt), 4-Dimethylaminopyridine (DMAP) and NHS.

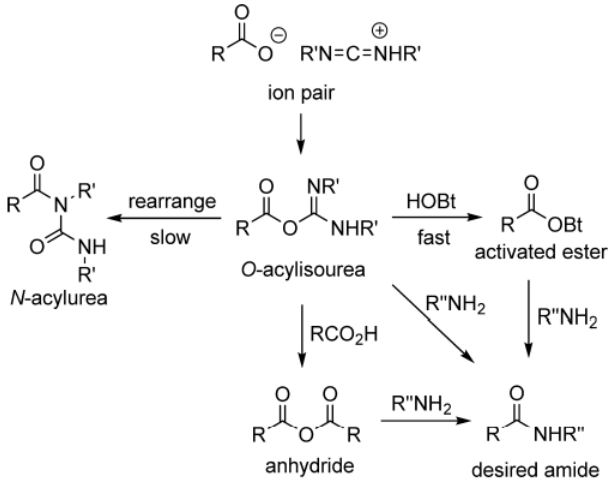

Figure 6.10. Mechanism of amidation via activated esters.

Alendronate incorporation based on activated ester formation was studied in two steps. The main problem of this reaction is mismatched solubility of starting materials. Even small amount of DMF in aqueous ALN solution or water in polymer dissolved in DMF can cause precipitation. Therefore, the reaction was done in DMF and H_2O separately as heterogenous reactions. In the first step, Sulfo NHS or HOBt with catalytic amount of DMAP was dissolved in the relative solvent containing PAHA. After 1 h mixing, EDC.HCl was added to the ice-cold mixture to form O-acylisourea intermediate. Cold temperature reduced the formation of urea by product. Then in the second step, alendronate was added to mixture at 0 °C under nitrogen. The pH of ALN was adjusted by TEA to improve its solubility for the reaction carried out in DMF; however, the goal could not be achieved, and reaction was continued in blurry DMF. Surprisingly, the insoluble PAHA became water soluble within 30 min after ALN addition. After stirring 24 h at room temperature, products were purified by dialysis and freeze dried. The product obtained in DMF became insoluble in DMF, DMSO, EtOH and water after drying. Similar insoluble products were also obtained when the aminolysis reaction was tried by adding ALN aqueous solution into PAHA solution dissolved in DMF. Probably, the carboxylic acid groups on polymer react with the O-acylisourea intermediate to form anhydride when the amine is not present in the same phase with polymer. The vacuum conditions during freeze drying can increase the possibility of crosslinking.

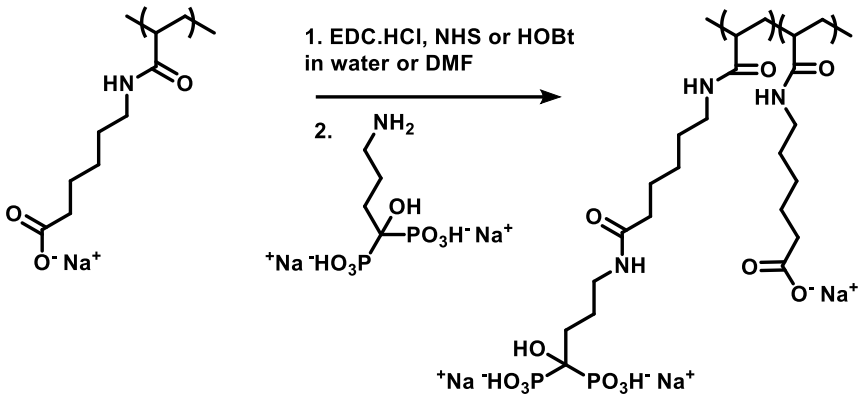

Figure 6.11. ALN incorporation into PAHA.

The alendronate modified polymer obtained in water (ALN-PAHA) was characterized by ^{1}H, ^{13}C NMR and FTIR spectroscopies. The formation peaks at 1.83, 1.96 and 3.44 indicates ALN incorporation. Moreover, an extra peak was observed at 2.46 ppm corresponding to methylene protons next to amide carbonyl formed by alendronate incorporation as seen in Figure 6.8. The methylene protons adjacent to carbonyl of carboxylic acid also showed a 0.07 ppm (from 2.34 to 2.27 ppm) upfield shift after modification because of the interaction with NaOH in basic medium. Even though the product was dialyzed for 5 days, there are some impurities representing EDC (at 1.1 and 3.1 ppm) and NHS (at 2.9 ppm) presence. Therefore, a second dose of alendronate at pH 9 was added onto modified polymer in water and stirred for extra 24 h. As can be seen from the top spectrum in Figure 6.8, the intensity of the peaks corresponding to incorporated ALN increased and impurity peaks disappeared. The modification ratio of alendronate was calculated via comparison of the areas of the methylene protons adjacent to formed amide (labeled as h at 3.44 and e' at 2.46) to methylene protons of AHA (labeled as c at 1.34) and was found as 15 % and 65 % after first and second ALN addition. Alendronate is not a chromophoric compound, but its quantification by UV-Vis spectroscopy is possible after the formation of a complex of bisphosphonic acid with Fe^{3+} ions in perchloric acid [285]. A calibration curve (y=0.686x-0.0104) was prepared using five standard solutions containing 0.324-1.620 mg ALN and 1mM Fe^{3+}. However, ALN-PAHA assembled into insoluble aggregates instead of soluble complexes, which makes the determination of ALN through absorbance impractical. The FTIR spectra of ALN-PAHA (Figure 6.9) showed peaks of P=O

and P-O at 1168, 1065 and 961 cm^{-1}. The intensity of the peak at 1702 cm^{-1} decreased and the peaks representing NH of amide shifted to 1555 from 1549 cm^{-1} due to the added amide functionality. ^{13}C NMR spectrum of modified polymer showed the characteristic quaternary carbon peaks at 72.45, 73.77, 75.06 ppm as well as methylene carbon peaks at 23.48 and 26.20 as shown in Figure 6.12. The methylene carbon next to new amide N showed a peak at 55.18 ppm providing the successful incorporation [286]. The peaks at 160.48, 173.71, 176.49 and 183.13 ppm indicates the carbonyl of NHS, amide bound to the main chain, amide close to ALN and carboxylic acid respectively.

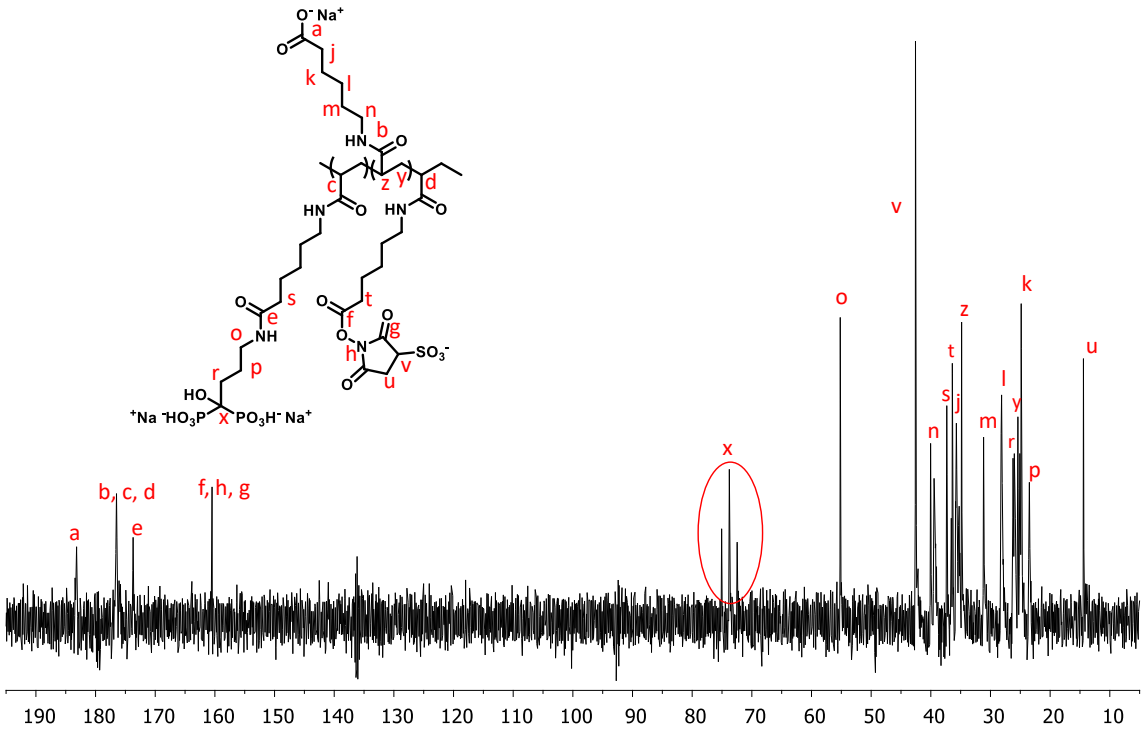

Figure 6.12. ^{13}C NMR spectrum of ALN-PAHA.

6.3.5. Interactions of PAHA and ALN-PAHA with HAP

To investigate HAP affinity of polymers, 10 wt % polymer was dissolved in EtOH and H_2O mixture. The ratio between solvents were adjusted between 30-60 wt% depending on

solubility of the polymers. In other words, H_2O was in larger amount for water soluble ALN-PAHA while the ratio of EtOH is higher to prepare water insoluble PAHA solution. After 24 h stirring and washing with EtOH and H_2O, the interaction of the synthesized polymers with HAP was characterized by FTIR as shown in Figure 6.13.

Table 6.2. IR band positions of PAHA and ALN-PAHA before and after HAP treatment.

	C=O (cm^{-1})	NH (cm^{-1})	PO_4^{3-} (cm^{-1})
HAP	-	-	1017
PAHA	1704, 1634	1548	-
PAHA:HAP	1704, 1634	1557	1012
ALN-PAHA	1636	1543	-
ALN-PAHA:HAP	1634	1557	1019

In addition to characteristic HAP bands, carbonyl peaks observed at 1704 and 1634 cm^{-1} for PAHA:HAP (both for carboxylic acid and amide) and ALN-PAHA:HAP respectively. The presence of carbonyl peaks after washing shows the interaction between polymer and HAP. The shift in the amide II peak (representing NH bending) of PAHA and ALN-PAHA to higher frequency (1557 cm^{-1}) after mixing with HAP indicates the increase in hydrogen bonding [288, 289]. The small red shift in amide I (representing C=O stretching) signifies the weakened C=O due to the formation of bonding between Ca^{2+} ions and unpaired electrons of oxygen [290]. The phosphate band became broader after mixing with polymers as seen in Figure 6.13. The peak corresponding to asymmetric stretching mode (ν3) of phosphate at 1017 cm^{-1} shifted to lower frequency for PAHA and higher frequency for ALN-PAHA. There is not any pyrophosphate peak at 721 cm^{-1} indicating that the adsorption of polymers occurred by electrostatic interaction instead of condensation with PO_4^{3-} of the HAP (covalent binding model) [292].

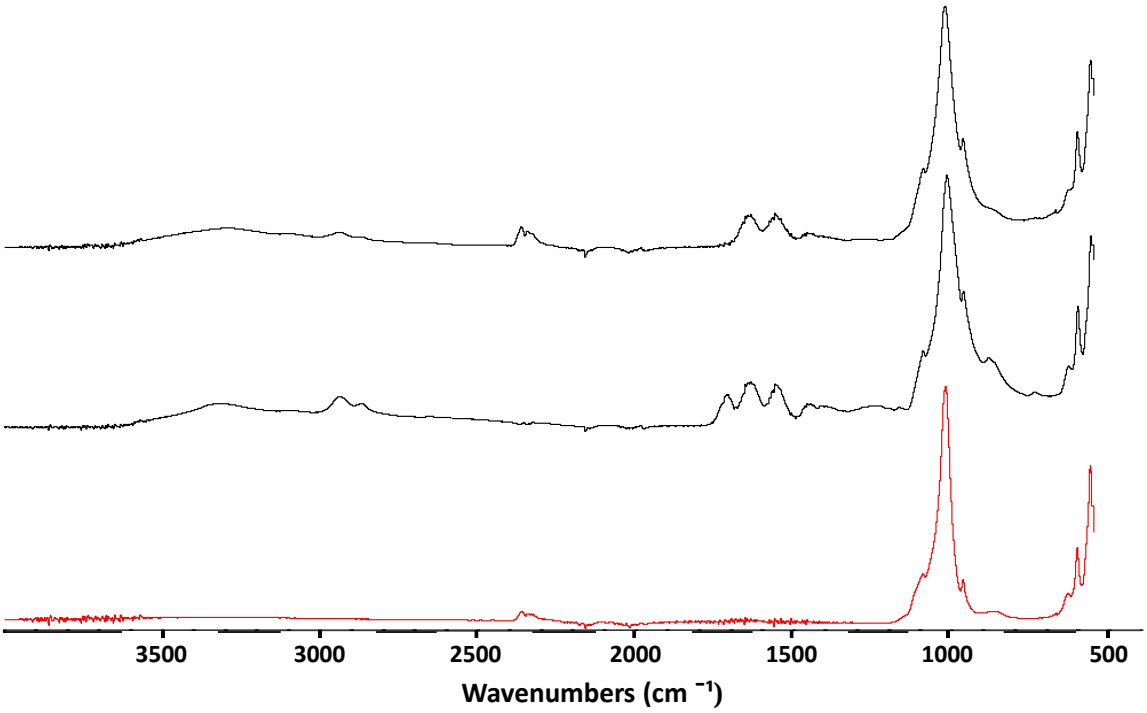

Figure 6.13. FTIR spectra of ALN-PAHA:HAP, PAHA:HAP and HAP (from top to bottom).

Besides the acidic functionality, the spacer group can also determine the interaction potential of polymer with HAP. For example, the intensity of the carbonyl peak is less for p-MA-IBU:HAP (Figure 6.5) than for PAHA:HAP (Figure 6.13) even though they both have carboxylic acid functionality. After washing, the amount of polymer retained on HAP is lower for p-MA-IBU:HAP because the ibuprofen bound to same carbon as well as the absence of spacer group between polymer chain and acidic functionality cause steric hindrance which makes the binding difficult. The long spacer group in PAHA structure enables that high amount of PAHA to be adsorbed on HAP surface, in this case the binding affinity between polymer and HAP is strong enough to resist washing.

6.3.6. Remineralization Studies on Etched Enamel

Mineralization of etched dentin involves new crystal growth in the dentinal tubule and on the dentin surface. Binding strength to the dentin is an important criterion in the remineralization process since the oral cavity contains a lot of flowing fluids. After binding capacities of polymers on HAP were investigated, we decided to study remineralization on enamel using ALN-PAHA due to its water solubility and good interaction with HAP. To prepare the enamel samples they were etched with 37% H_3PO_4 and then treated with polymer. Mineralization was carried out by incubating the treated samples in artificial saliva. The morphologies of acid etched enamel and mineralized sample were observed by SEM. As can be seen in Figure 6.14, the surfaces of etched enamel changed and newly generated crystals with the appearance of prism-like structures were detected after 2 weeks in artificial saliva. The effective mineral regeneration was observed not only on the surface but also in the dentinal tubules and the diameter of dentinal tubules decreased. The ordered appearance of prism-like structures demonstrates the capacity of polymer to control the growth of HAP crystals on enamel. These results indicate that ALN-PAHA can induce remineralization.

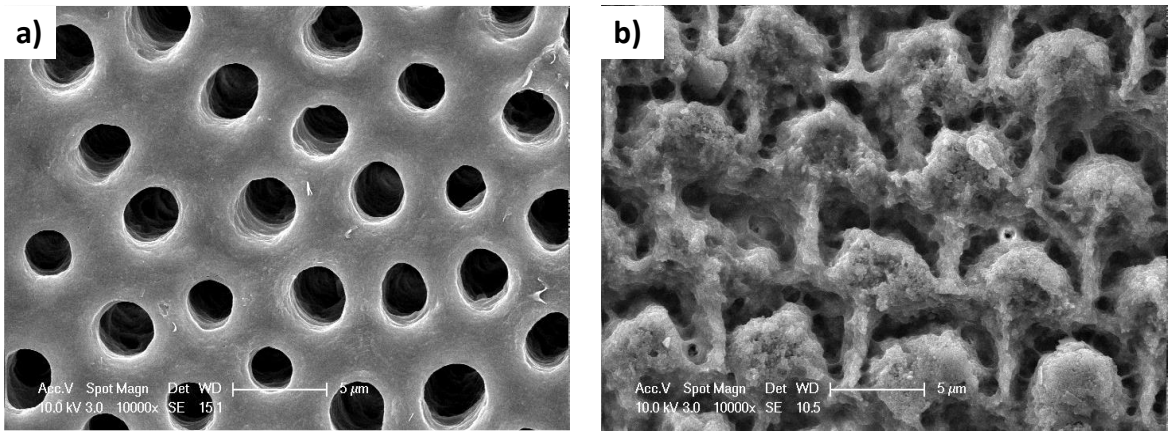

Figure 6.14. SEM micrographs of (a) acid etched tooth enamel and (b) ALN-PAHA treated sample after being immersed in artificial saliva for 14 days.

6.4. Conclusions

In this chapter bisphosphonic acid functionality was incorporated through post polymerization modification reactions of carboxylic acid containing polymers to obtain materials with strong HAP affinity. NMR and FTIR spectra indicated that ALN was successfully incorporated into structure via electrostatic interaction or covalent bonds. The hydrophilicity of polymers increased with ALN addition. The interaction of polymers with synthetic HAP was investigated by FTIR and it was observed that the acidic functionality, spacer group and polymer structure affect the HAP binding. The generation of prism-like crystals on acid etched enamel in artificial saliva supports the potential of the polymer in dental systems. The ibuprofen release studies show the influence of hydrophilicity of the polymer on its release profile and ALN incorporation accelerated the release in a controlled matter. Overall, these two bisphosphonic acid funtionalized polymers can be considered as potential candidates in various bone related biomedical applications.

7. CONCLUDING REMARKS

In this dissertation, (bis)phosphonate functionalized monomers, polymers and networks were successfully synthesized and their properties such as adjustable hydrophobicity, swelling and degradation as well as structure dependent mineralization and binding ability were evaluated for their potential use in various biomedical applications such as tissue engineering scaffolds, dental materials and targeted drug delivery.

Three novel phosphonate/phosphonic acid-functionalized (for biocompatibility and affinity to bone and similar tissues) PBAE macromers with designed hydrophilic/hydrophobic properties (based on PEGDA, HDDA and HDEDA) were synthesized via step-growth polymerization. Their homo- and copolymerization with PEGDA at different ratios (50 and 80 w% PEGDA) gave novel degradable and pH responsive gels. The differences in the hydrophilicity and molecular weight of the macromers enabled the tailoring of swelling, degradation and mechanical properties of final networks. PBAE gels can degrade completely in 2 days. PEGDA gels' degradation is determined by the amount of PBAE macromers and can range from 20-50%. The mechanical properties of phosphonate functionalized PBAEs are studied for the first time in the literature and uniaxial compression tests revealed that the extent of decrease of the gel crosslink density during degradation was strongly correlated with increasing amount and hydrophilicity of the PBAE macromers. The degradation products of the gels showed no significant cytotoxicity on NIH 3T3 mouse embryonic fibroblast cells. We expect the controllable diversity achieved on swelling, degradation and mechanical properties to make these novel non-toxic biomaterials useful for tissue engineering applications.

Three PAA macromers were synthesized through aza-Michael addition of 2-aminoethyl phosphonic acid or its mixture with 5-amino-1-pentanol at different ratios onto N,N-methylene bis(acrylamide) to control the amount of phosphonic acid functionality. The macromers homo- and copolymerized with HEMA at different ratios (25, 50, 72 w% HEMA) to obtain hydrogels with various hydrophilicities. The alteration in the macromer composition and molecular weight of macromers affected the swelling, degradation and

mineralization ability of final hydrogels. The amount of phosphonic acid and pH of the medium affected the swelling behaviour of hydrogels. The mass losses of hydrogels (12-20 % in 4 weeks) are influenced by the crosslink density and hydrophilicity of networks as well as presence of Ca^{2+} ion. The hydrogels showed mineralization ability in SBF and 5xSBF and the extent of mineralization is dependent on the composition of macromers and pre-treatment of hydrogels with $CaCl_2$. Surprisingly the hydrogels containing only 5-amino-1-pentanol have high apatite growth ability. The degradation products of the hydrogels had no effect on U-2 OS, Saos-2 and NIH 3T3 cells, suggesting their cytocompatibility. These results demonstrate that designed materials have potential to be used as nontoxic degradable biomaterials.

Three bisphosphonate containing acrylamide monomers were synthesized using bisphoshonate functionalized amines with different hydrophilicities (propyl, octyl and octadecyl groups). Their random (5, 10, 30 mol% funtionalized monomer in feed ratio) and diblock (2, 6, 16 mol % functionalized monomer in total feed ratio) copolymers with NIPAM were synthesized using FRP and RAFT polymerization to investigate the influence of structure on aqueous solution behaviour of the polymers. However chain transfer reactions caused by labile methine proton and/or steric hindrance of acrylamides resulted in low molecular weight polymers in FRP and also uncontrolled polymerizations in RAFT. The dealkylation of neither bisphosphonate functionalized acrylamides nor their copolymers with NIPAM, using TMSBr to obtain bisphosphonic acid functionalized polymers could not be achieved due to structural reasons. Therefore, another method which involved functionalization of a block copolymer of NIPAM and AHA with TMSP or alendronate was applied and among these two post modifications the second one gave the desired polymers. The synthesized thermoresponsive polymers with bisphosphonate and bisphosphonic acid groups showed cloud points between 27.8 and 36.7 ºC. These LCST values, close to body temperature, show that these polymers may find a use in biomedical applications.

Two carboxylic acid containing homopolymers, ibuprofen functionalized alkyl α-hydroxymethacrylate based p-MA-IBU and 6-acrylamidohexanoic acid based PAHA, were synthesized via free radical polymerization and alendronate was successfully incorporated into the first polymer via electrostatic interactions and the second polymer via covalent

bonds. Polymers` interactions with synthetic hydroxyapatite depending on the acidic group and polymer structure (spacer group) were observed by FTIR. It was found that alendronate loading accelerated the release of ibuprofen in PBS in a controlled manner from p-MA-IBU:ALN due to increased hydrophilicity. The alendronate containing water soluble polymer (ALN-PAHA) promoted the mineral growth on enamel in artificial saliva indicating its potential as a dental material. These outcomes indicates that synthesized polymers may be used in bone/dental related biomedical applications.

In summary, new monomers, polymers and crosslinked networks with (bis)phosphonate functionality were synthesized and the effect of functional group on properties was evaluated to understand their suitability for bone related biomedical applications.

REFERENCES

1. Nair, L. S. and C. T. Laurencin, "Biodegradable Polymers as Biomaterials", *Progress in Polymer Science*, Vol. 32, No. 8-9, pp. 762–798, 2007.

2. Zivic, F., S. Affatato, M. Trajanovic, M. Schnabelrauch, N. Grujovic and K. L. Choy, *Biomaterials in Clinical Practice Advances in Clinical Research and Medical Devices*, Springer, Cham, 2018.

3. Heimann, R. B., *Materials for Medical Application, Appendix B. Current World Market Situation of Biomaterials and Biomedical Devices*, Walter de Gruyter GmbH, Berlin, 2020.

4. Hildebrand, H. F., "Biomaterials - A History of 7000 Years", *BioNanoMaterials*, Vol. 14, No. 3-4, pp. 119–133, 2013.

5. Hassanein, N. and A. Amleh, "Biomaterial Implants: A Gateway to Cancer through Genetics and Epigenetics", *Advances in Modern Oncology Research*, Vol. 04, No. 04, pp. 15–27, 2018.

6. Todros, S., M. Todesco and A. Bagno, "Biomaterials and Their Biomedical Applications: From Replacement to Regeneration", *Processes*, Vol. 9, No. 11, pp. 1949-1968, 2021.

7. Kiran, A. S. K. and S. Ramakrishna, *An Introduction to Biomaterials Science and Engineering*, World Scientific Publishing Co. Pte. Ltd., Singapore, 2021.

8. Raghavendra, G. M., K. Varaprasad and T. Jayaramudu, *Nanotechnology Applications for Tissue Engineering, Chapter 2-Biomaterials: Design, Development and Biomedical Applications*, Elsevier Inc., Oxford, 2015.

9. Gribova, V., T. Crouzier and C. Picart, "A material's Point of View on Recent Developments of Polymeric Biomaterials: Control of Mechanical and Biochemical Properties", *Journal of Materials Chemistry*, Vol. 21, No. 38, pp. 14354–14366, 2011.

10. Ning, C., L. Zhou and G. Tan, "Fourth-Generation Biomedical Materials", *Materials Today*, Vol. 19, No. 1, pp. 2–3, 2016.

11. Kowalski, P. S., C. Bhattacharya, S. Afewerki and R. Langer, "Smart Biomaterials: Recent Advances and Future Directions", *ACS Biomaterials Science and Engineering*, Vol. 4, No. 11, pp. 3809–3817, 2018.

12. Montoya, C., Y. Du, A. L. Gianforcaro, S. Orrego, M. Yang and P. I. Lelkes, "On The Road to Smart Biomaterials for Bone Research: Definitions, Concepts, Advances, and Outlook", *Bone Research*, Vol. 9, No. 1, pp. 1-16, 2021.

13. Nair, L. S. and C. T. Laurencin, "Polymers as Biomaterials for Tissue Engineering and Controlled Drug Delivery", *Advances in Biochemical Engineering/Biotechnology*, Vol. 102, No. October, pp. 47–90, 2006.

14. Ulery, B. D., L. S. Nair and C. T. Laurencin, "Biomedical Applications of Biodegradable Polymers", *Journal of Polymer Science Part B: Polymer Physics*, Vol. 49, No. 12, pp. 832–864, 2011.

15. Shoichet, M. S., "Polymer Scaffolds for Biomaterials Applications", *Macromolecules*, Vol. 43, No. 2, pp. 581–591, 2010.

16. Iqbal, S., Y. Qu, Z. Dong, J. Zhao, A. R. Khan, S. Rehman and Z. Zhao, "Poly (β-amino esters) Based Potential Drug Delivery and Targeting Polymer; An Overview and Perspectives (review)", *European Polymer Journal*, Vol. 141, No. August, pp. 110097-110112, 2020.

17. Ferruti, P., M. A. Marchisio and R. Duncan, "Poly (amido-amine)s : Biomedical Applications", *Macromolecular Rapid Communications*, Vol. 23, No. 5, pp. 332–355, 2002.

18. Lynn, D. M. and R. Langer, "Degradable Poly (β-amino esters): Synthesis, Characterization , and Self-Assembly with Plasmid DNA", *Journal of the American Chemical Society*, Vol. 122, No. 10, pp. 10761–10768, 2000.

19. Akinc, A., D. G. Anderson, D. M. Lynn and R. Langer, "Synthesis of Poly(β-amino ester)s Optimized for Highly Effective Gene Delivery", *Bioconjugate Chemistry*, Vol.

14, No. 5, pp. 979–988, 2003.

20. Anderson, D. G., C. A. Tweedie, N. Hossain, S. M. Navarro, D. M. Brey, K. J. Van Vliet, R. Langer and J. A. Burdick "A Combinatorial Library of Photocrosslinkable and Degradable Materials", *Advanced Materials*, Vol. 18, No. 19, pp. 2614–2618, 2006.

21. Ferruti, P., "Poly(amidoamine)s: Past, Present, and Perspectives", *Journal of Polymers Science Part A: Polymer Chemistry*, Vol. 51, No. 11, pp. 2319–2353, 2013.

22. Zintchenko, A., L. J. Van Der Aa and J. F. J. Engbersen, "Improved Synthesis Strategy of Poly(amidoamine)s for Biomedical Applications: Catalysis by 'Green' Biocompatible Earth Alkaline Metal Salts", *Macromolecular Rapid Communications*, Vol. 32, No. 3, pp. 321–325, 2011.

23. Guven, M. N., G. Demirci, S. Altuncu, U. Gulyuz, O. Okay, H. Yagci Acar and D. Avci, "Alendronate-Functionalized Poly(amido amine) Cryogels of High-Toughness for Biomedical Applications", *Polymer (Guildf)*, Vol. 190, No. February, pp. 122248-122258, 2020.

24. Ou, M., R. Xu, S. H. Kim, D. A. Bull and S. W. Kim, "A Family of Bioreducible Poly(disulfide amine)s for Gene Delivery", *Biomaterials*, Vol. 30, No. 29, pp. 5804–5814, 2009.

25. Cheng, W., D. Wu and Y. Liu, "Michael Addition Polymerization of Trifunctional Amine and Acrylic Monomer: A Versatile Platform for Development of Biomaterials", *Biomacromolecules*, Vol. 17, No. 10, pp. 3115–3126, 2016.

26. Drury, J. L. and D. J. Mooney, "Hydrogels for Tissue Engineering: Scaffold Design Variables and Applications", *Biomaterials*, Vol. 24, No. 24, pp. 4337–4351, 2003.

27. Dang, J. M. and K. W. Leong, "Natural Polymers for Gene Delivery and Tissue Engineering", *Advanced Drug Delivery Reviews*, Vol. 58, No.4, pp. 487–499, 2006.

28. Gualandi, C., N. Bloise, N. Mauro, P. Ferruti, A. Manfredi, M. Sampaolesi, A. Liguori, R. Laurita, M. Gherardi, V. Colombo, L. Visai, M. L. Focarete and E. Ranucci, "Poly-l-Lactic Acid Nanofiber–Polyamidoamine Hydrogel Composites:

Preparation, Properties, and Preliminary Evaluation as Scaffolds for Human Pluripotent Stem Cell Culturing", *Macromolecular Bioscience*, Vol. 16, No. 10, pp. 1533–1544, 2016.

29. Tocchio, A., F. Martello, M. Tamplenizza, E. Rossi, I. Gerges, P. Milani and C. Lenardi, "RGD-Mimetic Poly(amidoamine) Hydrogel for The Fabrication of Complex Cell-laden Micro Constructs", *Acta Biomaterialia*, Vol. 18, No. May, pp. 144–154, 2015.

30. Hawkins, A. M., T. A. Milbrandt, D. A. Puleo and J. Z. Hilt, "Synthesis and Analysis of Degradation, Mechanical and Toxicity Properties of Poly(β-amino ester) Degradable Hydrogels", *Acta Biomaterialia*, Vol. 7, No. 5, pp. 1956–1964, 2011.

31. Rossi, E., I. Gerges, A. Tocchio, M. Tamplenizza, P. April, C. Recordati, F. Martello, I. Martin, P. Milani and C. Lenardi, "Biologically and Mechanically Driven Design of an RGD-Mimetic Macroporous Foam for Adipose Tissue Engineering Applications", *Biomaterials*, Vol. 104, No. October, pp. 65–77, 2016.

32. Chen, S., J. Shi, X. Xu, J. Ding, W. Zhong, L. Zhang, M. Xing and L. Zhang, "Study of Stiffness Effects of Poly(amidoamine)-Poly(N-isopropyl acrylamide) Hydrogel on Wound Healing", *Colloids Surfaces B Biointerfaces*, Vol. 140, No. April, pp. 574–582, 2016.

33. Magnaghi, V., V. Conte, P. Procacci, G. Pivato, P. Cortese, E. Cavalli, G. Pajardi, E. Ranucci, F. Fenili, A. Manfredi and Paolo Ferruti, "Biological Performance of a Novel Biodegradable Polyamidoamine Hydrogel as Guide for Peripheral Nerve Regeneration", *Journal of Biomedical Materials Research - Part A*, Vol. 98A, No. 1, pp. 19–30, 2011.

34. Emilitri, E., F. Guizzardi, C. Lenardi, M. Suardi, E. Ranucci and P. Ferruti, "Novel Poly(amidoamine)-Based Hydrogels as Scaffolds for Tissue Engineering", *Macromolecular Symposia*, Vol. 266, No.1, pp. 41–47, 2008.

35. Mauro, N., A. Manfredi, E. Ranucci, P. Procacci, M. Laus, D. Antonioli, C. Mantovani, V. Magnaghi and P. Ferruti, "Degradable Poly(amidoamine) Hydrogels as Scaffolds for in-Vitro Culturing of Peripheral Nervous System Cells",

Macromolecular Bioscience, Vol. 13, No. 3, pp. 332–347, 2013.

36. Jacchetti, E., E. Emilitri, S. Rodighiero, M. Indrieri, A. Gianfelice, C. Lenardi, A. Podestà, E. Ranucci, P. Ferruti and P. Milani, "Biomimetic Poly(amidoamine) Hydrogels as Synthetic Materials for Cell Culture", *Journal of Nanobiotechnology*, Vol. 6, No. 14, pp. 1–15, 2008.

37. Brey, D. M., J. L. Ifkovits, R. I. Mozia, J. S. Katz and J. A. Burdick, "Controlling Poly(β-amino ester) Network Properties Through Macromer Branching", *Acta Biomaterialia*, Vol. 4, No. 2, pp. 207–217, 2008.

38. Nutan, B., A. K. S. Chandel, D. V. Bhalani and S. K. Jewrajka, "Synthesis and Tailoring The Degradation of Multi-responsive Amphiphilic Conetwork Gels and Hydrogels of Poly(β-amino ester) and Poly(amido amine)", *Polymer (Guildf)*, Vol. 111, No. February, pp. 265–274, 2017.

39. Brey, D. M., I. Erickson and J. A. Burdick, "Influence of Macromer Molecular Weight and Chemistry on Poly(β-amino ester) Network Properties and Initial Cell Interactions", *Journal of Biomedical Materials Research - Part A*, Vol. 85, No. 3, pp. 731–741, 2008.

40. Yao, K., G. Gong, Z. Fu., Y. Wang, L. Zhang, G. Li and Y. Yang, "Synthesis and Evaluation of Cytocompatible Alkyne-Containing Poly(β-amino ester)-Based Hydrogels Functionalized via Click Reaction", *ACS Macro Letters*, Vol. 9, No. 9, pp. 1391–1397, 2020.

41. Yu, L., K. Xu, L. Ge, W. Wan, A. Darabi, M. Xing and W. Zhong, "Cytocompatible, Photoreversible, and Self-Healing Hydrogels for Regulating Bone Marrow Stromal Cell Differentiation", *Macromolecular Bioscience*, Vol. 16, No. 9, pp. 1381–1390, 2016.

42. Wang, Y., Q. Zhao, H. Zhang, S. Yang and X. Jia, "A Novel Poly(amido amine) Dendrimer-Based Hydrogel as A Mimic for The Extracellular Matrix", *Advanced Materials*, Vol. 26, No. 24, pp. 4163–4167, 2014.

43. Martello, F., A. Tocchio, M. Tamplenizza, I. Gergesa, V. Pistis, R. Recenti, M.

Bortolin, M. Del Fabbro, S. Argentiere, P. Milani and C. Lenardi, “Poly(amido-amine)-Based Hydrogels with Tailored Mechanical Properties and Degradation Rates for Tissue Engineering”, *Acta Biomaterialia*, Vol. 10, No. 3, pp. 1206–1215, 2014.

44. Wang, Q. G., I. Wimpenny, R. E. Dey, X. Zhong, P. J. Youle, S. Downes, D. C. Watts, P. M. Budd, J. A. Hoyland and J. E. Gough, “The Unique Calcium Chelation Property of Poly(vinyl phosphonic acid-*co*-acrylic acid) and Effects on Osteogenesis in Vitro”, *Journal of Biomedical Materials Research - Part A*, Vol. 106, No. 1, pp. 168–179, 2018.

45. Akyol, E., M. Tatliyuz, F. Demir Duman, M. N. Guven, H. Y. Acar and D. Avci, “Phosphonate-functionalized Poly(β-amino ester) Macromers as Potential Biomaterials”, *Journal of Biomedical Materials Research - Part A*, Vol. 106, No. 5, pp. 1390–1399, 2018.

46. Babic, M. M. and J. Nikodinovic, “In Vitro and in Vivo Biocompatibility of Novel Zwitterionic Poly (beta amino) Ester Hydrogels Based on Diacrylate and Glycine for Site-Specific Controlled Drug Release”, *Macromolecular Chemistry and Physics*, Vol. 220, No. 17, pp. 1900188- 1900197, 2019.

47. Xu, Q., L. Guo, S. A, Y. Gao, D. Zhou, U. Greiser, J. Creagh-Flynn, H. Zhang, Y. Dong, L. Cutlar, F. Wang, W. Liu, W. Wang and W. Wang, “Injectable Hyperbranched Poly(β-amino ester) Hydrogels with on-Demand Degradation Profiles to Match Wound Healing Processes”, *Chemical Science*, Vol. 9, No. January, pp. 2179-2187, 2018.

48. Buwalda, S. J., A. Bethry, S. Hunger, S. Kandoussi, J. Coudane and B. Nottelet, “Ultrafast in Situ Forming Poly(ethylene glycol)-Poly(amido amine) Hydrogels with Tunable Drug Release Properties via Controllable Degradation Rates”, *European Journal of Pharmaceutics and Biopharmaceutics*, Vol. 139, No. April, pp. 232–239, 2019.

49. Vo, T. N., A. K. Ekenseair, P. P. Spicer, B. M. Watson, S. N. Tzouanas, T. T. Roh and A. G, Mikos, “In Vitro and in Vivo Evaluation of Self-mineralization and Biocompatibility of Injectable, Dual-Gelling Hydrogels for Bone Tissue

Engineering", *Journal of Controlled Release*, Vol. 205, No. May, pp. 25–34, 2015.

50. Wang, J., H. He, R. C. Cooper and H. Yang, "In Situ-Forming Polyamidoamine Dendrimer Hydrogels with Tunable Properties Prepared via Aza-Michael Addition Reaction", *ACS Applied Materials and Interfaces*, Vol. 9, No. 12, pp. 10494–10503, 2017.

51. Peng, B., X. Lai, L. Chen, X. Lin, C. Sun, L. Liu, S. Qi, Y. Chen and K. W. Leong, "Scarless Wound Closure by A Mussel-Inspired Poly(amidoamine) Tissue Adhesive with Tunable Degradability", *ACS Omega*, Vol. 2, No. 9, pp. 6053–6062, 2017.

52. Yang, W., X. Wu, F. Liu, Y. Dou, Z. Hu and W. Hao, "A Fluorescent, Self-Healing and pH Sensitive Hydrogel Rapidly Fabricated from HPAMAM and Oxidized Alginate with Injectability", *RSC Advances*, Vol. 6, No. March, pp. 34254–34260, 2016.

53. Nguyen, M. K., D. K. Park and D. S. Lee, "Injectable Poly(amidoamine)-Poly(ethylene glycol)-Poly(amidoamine) Triblock Copolymer Hydrogel with Dual Sensitivities: pH and Temperature", *Biomacromolecules*, Vol. 10, No. 4, pp. 728–731, 2009.

54. Huynh, C. T., M. K. Nguyen, J. H. Kim, S. W. Kang, B. S. Kim and D. S. Lee, "Sustained Delivery of Doxorubicin Using Biodegradable pH/Temperature-Sensitive Poly(ethylene glycol)-Poly(β-amino ester urethane) Multiblock Copolymer Hydrogels", *Soft Matter*, Vol. 7, No. April, pp. 4974–4982, 2011.

55. Clark, A., T. A. Milbrandt, J. Z. Hilt and D. A. Puleo, "Mechanical Properties and Dual Drug Delivery Application of Poly(lactic-co-glycolic acid) Scaffolds Fabricated with A Poly(β-amino ester) Porogen", *Acta Biomaterialia*, Vol. 10, No. 5, pp. 2125–2132, 2014.

56. Gevorgyan, S., E. Rossi, M. A. Cappelluti, A. Tocchio, F. Martello, I. Gerges, C. Lenardi, P. Milani and S. Argentiere, "Photocrosslinked Poly(amidoamine) Nanoparticles for Central Nervous System Targeting", *Colloids and Surfaces B Biointerfaces*, Vol. 151, No. March, pp. 197–205, 2017.

57. Zhang, Y., R. Wang, Y. Hua, R. Baumgartner and J. Cheng, “Trigger-Responsive Poly(β-amino ester) Hydrogels”, *ACS Macro Letters,* Vol. 3, No. 7, pp. 693–697, 2014.

58. Lin, C. and J. F. J. Engbersen, “Effect of Chemical Functionalities in Poly(amido amine)s for Non-Viral Gene Transfection”, *Journal of Controlled. Release*, Vol. 132, No. 3, pp. 267–272, 2008.

59. Gajbhiye, V. and S. Gong, “Lectin Functionalized Nanocarriers for Gene Delivery”, *Biotechnology Advances*, Vol. 31, No. 5, pp. 552–562, 2013.

60. Lin C., Z. Zhonga, M. C.Lok, X. Jiang, W. E. Hennink, J. Feijen and J. F.J. Engbersen, “Random and Block Copolymers of Bioreducible Poly(amido amine)s with High- and Low-Basicity Amino Groups : Study of DNA Condensation and Buffer Capacity on Gene Transfection”, *Journal of Controlled Release*, Vol. 123, No. 1, pp. 67–75, 2007.

61. Arote, R. B., H. L. Jiang, Y. K. Kim, M. H. Cho, Y. J. Choi and C. S. Cho, “Degradable Poly(amido amine)s as Gene Delivery Carriers”, *Expert Opinion on Drug Delivery*, Vol. 8, No. 9, pp. 1237–1246, 2011.

62. Lin, C., Z. Zhong, M. C. Lok, X. Jiang, W. E. Hennink, J. Feijen and J. F. J. Engbersen “Novel Bioreducible Poly(amido amine)s for Highly Efficient Gene Delivery”, *Bioconjugate Chemistry*, Vol. 18, No. 1, pp. 138–145, 2007.

63. Huang, J.-Y., Y. Gao, L. Cutlar, J. O'Keeffe-Ahern, T. Zhao, F.-H. Lin, D. Zhou, S. McMahon, U. Greiser, W. Wang and W. Wang, “Tailoring Highly Branched Poly(β-amino ester)s: A Synthetic Platform for Epidermal Gene Therapy”, *Chemical Communications*, Vol. 51, No. April, pp. 8473–8476, 2015.

64. Peng, L., Y. Gao, Y. Xue, S. Huang and R. Zhuo, “Cytotoxicity and in Vivo Tissue Compatibility of Poly(amidoamine) with Pendant Aminobutyl Group as a Gene Delivery Vector”, *Biomaterials*, Vol. 31, No. 16, pp. 4467–4476, 2010.

65. Lin, C., C.-J. Blaauboer, M. M. Timoneda, M. C. Lok, M. van Steenbergen, W. E. Hennink, Z. Zhong, J. Feijen and J. F. J. Engbersen, “Bioreducible Poly(amido amine)s with Oligoamine Side Chains : Synthesis, Characterization, and Structural

Effects on Gene Delivery", *Journal of Controlled Release*, Vol. 126, No. 2, pp. 166–174, 2008.

66. Won, Y., M. Ankoné, J. F. J. Engbersen, J. Feijen and S. W. Kim, "Poly(amido amine)s Containing Agmatine and Butanol Side Chains as Efficient Gene Carriers", *Macromolecular Bioscience*, Vol. 16, No. 4, pp. 619–626, 2016.

67. Sun, Y., H. Liu, T. Yang, L. Lang, L. Cheng, H. Xing, L. Yang and P. Ding, "Amphoteric Poly(amido amine)s with Adjustable Balance Between Transfection Efficiency and Cytotoxicity for Gene Delivery", *Colloids and Surfaces B Biointerfaces*, Vol. 175, No. October, pp. 10–17, 2019.

68. Van Der Aa, L. J., P. Vader, G. Storm, R. M. Schiffelers and J. F. J. Engbersen, "Intercalating Quaternary Nicotinamide-Based Poly(amido amine)s for Gene Delivery", *Journal of Controlled Release*, Vol. 195, No. December, pp. 11–20, 2014.

69. Piest, M., C. Lin, M. A. Mateos-Timoneda, M. C. Lok, W. E. Hennink, J. Feijen, J. F. and J.Engbersen, "Novel Poly(amido amine)s with Bioreducible Disulfide Linkages in Their Diamino-Units : Structure Effects and in Vitro Gene Transfer Properties", *Journal of Controlled Release*, Vol. 130, No. 1, pp. 38–45, 2008.

70. Zugates, G. T., N. C. Tedford, A. Zumbuehl, S. Jhunjhunwala, C. S. Kang, L. G. Griffith, D. A. Lauffenburger, R. Langer and D. G. Anderson, "Gene Delivery Properties of End-Modified Poly(β-amino ester)s", *Bioconjugate Chem*istry, Vol. 18, No. 6, pp. 1887–1896, 2007.

71. Anderson, D. G., W. Peng, A. Akinc, N. Hossain, A. Kohn, R. Padera, R. Langer and J. A. Sawicki, "A Polymer Library Approach to Suicide Gene Therapy for Cancer", *Proceedings of the National Academy of Sciences*, Vol. 101, No.45, pp. 16028 – 16033, 2004.

72. Kim, T., M. Lee and S. Wan, "A Guanidinylated Bioreducible Polymer with High Nuclear Localization Ability for Gene Delivery Systems," *Biomaterials*, Vol. 31, No.7, pp. 1798–1804, 2010.

73. Liu, S., Y. Gao, S. A, D. Zhou, U. Greiser, T. Guo, R. Guo and W. W, "Biodegradable

Highly Branched Poly(β-amino ester)s for Targeted Cancer Cell Gene Transfection", *ACS Biomaterials Science and Engineering*, Vol. 3, No. 7, pp. 1283–1286, 2017.

74. Yin, Q., Y. Gao, Z. Zhang, P. Zhang and Y. Li, "Bioreducible Poly(β-amino esters)/shRNA Complex Nanoparticles for Efficient RNA Delivery", *Journal of Controlled Release*, Vol. 151, No. 1, pp. 35–44, 2011.

75. Elzes, M. R., N. Akeroyd, J. F. J. Engbersen and J. M. J. Paulusse, "Disulfide-Functional Poly(amido amine)s with Tunable Degradability for Gene Delivery", *Journal of Controlled Release*, Vol. 244, No. December, pp. 357–365, 2016.

76. Zhao, J., P. Huang, Z. Wang, Y. Tan, X, Hou, L. Zhang, C.-Y. He and Z.-Y. Chen, "Synthesis of Amphiphilic Poly(β-amino ester) for Efficiently Minicircle DNA Delivery in Vivo", *ACS Applied Materials and Interfaces*, Vol. 8, No. 30, pp. 19284–19290, 2016.

77. Zhang, H. and S. V. Vinogradov, "Short Biodegradable Polyamines for Gene Delivery and Transfection of Brain Capillary Endothelial Cells", *Journal of Controlled. Release*, Vol. 143, No. 3, pp. 359–366, 2010.

78. Huang, X., D. Zhou, M. Zeng, F. Alshehri, X. Li, J. O'Keeffe-Ahern, Y. Gao, L. Pierucci, U. Greiser, G. Yin and W- Wang, "Star Poly(β-amino esters) Obtained from The Combination of Linear Poly(β-amino esters) and Polyethylenimine", *ACS Macro Letters*, Vol. 6, No. 6, pp. 575–579, 2017.

79. Demirci, G., M. N. Guven, S. Altuncu, Y. Utku Konca, D. Avci and H. Yagci Acar, "(Bis)phosphonic Acid-functionalized Poly(ethyleneimine)-Poly(amido amine)s for Selective in Vitro Transfection of Osteosarcoma Cells", *ACS Applied Polymer Materials*, Vol. 3, No. 8, pp. 3776–3787, 2021.

80. Hoare, T. R. and D. S. Kohane, "Hydrogels in Drug Delivery: Progress and Challenges", *Polymer (Guildf)*, Vol. 49, No. 8, pp. 1993–2007, 2008.

81. Movassaghian, S., O. M. Merkel and V. P. Torchilin, "Applications of Polymer Micelles for Imaging and Drug Delivery", *Wiley Interdisciplanary Reviews Nanomedicine and Nanobiotechnology*, Vol. 7, No. 5, pp. 691–707, 2015.

82. Wang, H., F. Xu, Y. Wang, X. Liu, Q. Jin and J. Ji, "pH-responsive and Biodegradable Polymeric Micelles Based on Poly(β-amino ester)-graft-phosphorylcholine for Doxorubicin Delivery", *Polymer Chemistry*, Vol. 4, No. 10, pp. 3012–3019, 2013.

83. Englert, C., J. C. Brendel, T. C. Majdanski, T. Yildirim, S. Schubert, M. Gottschaldt, N. Windhab and U. S.Schubert, "Pharmapolymers in the 21st century: Synthetic Polymers in Drug Delivery Applications", *Progress in Polymer Science*, Vol. 87, No December, pp. 107–164, 2018.

84. Zheng, Z., C. Yu and H. Wei, "Injectable Hydrogels as Three-Dimensional Network Reservoirs for Osteoporosis Treatment", *Tissue Engineering - Part B: Reviews*, Vol. 27, No. 5, pp. 430–454, 2021.

85. Sivashanmugam, A., R. Arun Kumar, M. Vishnu Priya, S. V. Nair and R. Jayakumar, "An Overview of Injectable Polymeric Hydrogels for Tissue Engineering", *European Polymer Journal*, Vol. 72, No. November, pp. 543–565, 2015.

86. Ghezzi, M., S. Pescina, C. Padula, P. Santi, E. Del Favero, L. Cantù and S. Nicoli, "Polymeric Micelles in Drug Delivery: An Insight of the Techniques for Their Characterization and Assessment in Biorelevant Conditions", *Journal of Controlled Release*, Vol. 332, No. February, pp. 312–336, 2021.

87. Casolaro, M., I. Casolaro, A. Spreafico, C. Capperucci, B. Frediani, R. Marcolongo, N. Margiotta, R. Ostuni, R. Mendichi, F. Samperi, T. Ishii and Yoshihiro Ito, "Novel Therapeutic Agents for Bone Resorption. Part 1. Synthesis and Protonation Thermodynamics of Poly(amido-amine)s Containing Bisphosphonate Residues", *Biomacromolecules*, Vol. 7, No. 12, pp. 3417–3427, 2006.

88. Franchini, J., E. Ranucci, P. Ferruti, M. Rossi and R. Cavalli, "Synthesis, Physicochemical Properties, and Preliminary Biological Characterizations of A Novel Amphoteric Agmatine-Based Poly(amidoamine) with RGD-like Repeating Units", *Biomacromolecules*, Vol. 7, No. 4, pp. 1215–1222, 2006.

89. Chen, D., M. Wu, J. Chen, C. Zhang, T. Pan, B. Zhang, H. Tian, X. Chen and Junqi Sun, "Robust, Flexible, and Bioadhesive Free-Standing Films for The Codelivery of Antibiotics and Growth Factors", *Langmuir*, Vol. 30, No. 46, pp. 13898–13906, 2014.

90. Min, K. H., J.-H, Kim, S. M. Bae, H. Shin, M. S. Kim, S. Park, H. Lee, R.-W. Park, I.-S. Kim, K. Kim, I. C. Kwon, S. Y. Jeong and D. S. Lee, "Tumoral Acidic pH-responsive MPEG-poly(β-amino ester) Polymeric Micelles for Cancer Targeting Therapy", *Journal of Controlled Release*, Vol. 144, No.2, pp. 259–266, 2010.

91. Filipović, V. V., M. M. Babić, D. Gođevac, A. Pavić, J. Nikodinović-Runić and S. L. Tomić, "In Vitro and in Vivo Biocompatibility of Novel Zwitterionic Poly(beta amino)ester Hydrogels Based on Diacrylate and Glycine for Site-Specific Controlled Drug Release", *Macromolecular Chemistry and Physics*, Vol. 220, No.17, pp. 1900188-1900198, 2019.

92. Qiao, Z. Y., C.-Y. Hou, D. Zhang, Y. Liu, Y.-X. Lin, H.-W. An, X.-J. Li and H. Wang, "Self-Assembly of Cytotoxic Peptide Conjugated Poly(β-amino ester)s for Synergistic Cancer Chemotherapy", *Journal of Materials Chemistry B*, Vol. 3, No. 15, pp. 2943–2953, 2015.

93. Fernando, I. R., D. P. Ferris, M. Frasconi, D. Malin, E. Strekalova, M. D. Yilmaz, M. W. Ambrogio, M. M. Algaradah, M. P. Hong, X. Chen, M. S. Nassar, Y. Y. Botros, de V. L. Cryns and J. F. Stoddart, "Esterase- and pH-Responsive Poly(β-amino ester)-capped Mesoporous Silica Nanoparticles for Drug Delivery", *Nanoscale*, Vol. 7, No. 16, pp. 7178–7183, 2015.

94. Hu, W., L. Qiu, L. Cheng, Q. Hu, Y. Liu, Z. Hu, D. Chen and L. Cheng, "Redox and pH Dual Responsive Poly(amidoamine) Dendrimer-Poly(ethylene glycol) Conjugates for Intracellular Delivery of Doxorubicin", *Acta Biomaterialia*, Vol. 36, No. May, pp. 241–253, 2016.

95. Jeong, I. K., G. H. Gao, Y. Li, S. W. Kang and D. S. Lee, "A Biodegradable Polymersome with pH-Tuning On-Off Membrane Based on Poly(β-amino ester) for Drug Delivery", *Macromolecular Bioscience*, Vol. 13, No. 7, pp. 946–953, 2013.

96. Cheng, W., J. N. Kumar, Y. Zhang and Y. Liu, "pH- and Redox-Responsive Poly(ethylene glycol) and Cholesterol-Conjugated Poly(amido amine)s Based Micelles for Controlled Drug Delivery", *Macromolecular Bioscience*, Vol. 14, No. 3, pp. 347–358, 2014.

97. Bui, Q. N., Y. Li, M. S. Jang, D. P. Huynh, J. H. Lee and D. S. Lee, "Redox- and pH-Sensitive Polymeric Micelles Based on Poly(β-amino ester)-Grafted Disulfide Methylene Oxide Poly(ethylene glycol) for Anticancer Drug Delivery", *Macromolecules*, Vol. 48, No. 12, pp. 4046–4054, 2015.

98. Chen, J., X. Qiu, J. Ouyang, J. Kong, W. Zhong and M. M. Q. Xing, "pH and Reduction Dual-Sensitive Copolymeric Micelles for Intracellular Doxorubicin Delivery", *Biomacromolecules*, Vol. 12, No. 10, pp. 3601–3611, 2011.

99. Lakes, A. L., C. T. Jordan, P. Gupta, D. A. Puleo, J. Z. Hilt and T. D. Dziubla, "Reducible Disulfide Poly(beta-amino ester) Hydrogels for Antioxidant Delivery", *Acta Biomaterialia*, Vol. 68, No. March, pp. 178–189, 2018.

100. Bingol, B., S. Altuncu, F. Demir Duman, A. Ak, U. Gulyuz, H. Yagci Acar, O. Okay and D. Avci, "One-Step Injectable and Bioreducible Poly(β-amino ester) Hydrogels as Controlled Drug Delivery Platforms", *ACS Applied Polymeric Materials*, Vol. 1, No. 7, pp. 1724–1734, 2019.

101. Huang, T., H. Liu, P. Liu, P. Liu, L. Li and J. Shen, "Zwitterionic Copolymers Bearing Phosphonate or Phosphonic Motifs as Novel Metal-Anchorable Anti-Fouling Coatings", *Journal of Materials Chemistry B*, Vol. 5, No. 27, pp. 5380–5389, 2017.

102. Liu, H., L. Liu, X. Jiang, J. Fan, W. Peng, P. Liu, T. Yang, H. Chen, W. Jiang, G. Yin, P. Liu and J. Shen, "Rational Design of A Zwitterionic-Phosphonic Copolymer for The Surface Antifouling Modification of Multiple Biomedical Metals", *Journal of Materials Chemistry B*, Vol. 7, No. 25, pp. 4055–4065, 2019.

103. Kosian, M., M. M. J. Smulders and H. Zuilhof, "Structure and Long-Term Stability of Alkylphosphonic Acid Monolayers on SS316L Stainless Steel", *Langmuir*, Vol. 32, No. 4, pp. 1047–1057, 2016.

104. Kurzak, B., W. Goldeman, M. Szpak, E. Matczak-Jon and A. Kamecka, "Synthesis of N-methyl Alkylaminomethane-1,1-diphosphonic Acids and Evaluation of Their Complex-Formation Abilities Towards Copper(II)", *Polyhedron*, Vol. 85, No. 28, pp. 675–684, 2015.

105. Huang, Y., Y. He, Z. Huang, Y. Jiang, W. Chu, X. Sun, L. Huanga and C. Zhao, "Coordination Self-Assembly of Platinum-Bisphosphonate Polymer-Metal Complex Nanoparticles for Cisplatin Delivery and Effective Cancer Therapy", *Nanoscale*, Vol. 9, No. 28, pp. 10002–10019, 2017.

106. Xu, T., L. Zhang, Z. Cheng and X. Zhu, "A Novel Methacrylate with a Bisphosphonate Group: RAFT Polymerization and Flame Retardant Property of The Resultant Polymers", *Polymer Chemistry*, Vol. 6, No. 12, pp. 2283–2289, 2015.

107. Kemal, E., K. O. Adesanya and S. Deb, "Phosphate Based 2-hydroxyethyl Methacrylate Hydrogels for Biomedical Applications", *Journal of Materiels Chemistry*, Vol. 21, No. 7, pp. 2237–2245, 2011.

108. Yuan, W., Z. Li, X. Xie, Z. Y. Zhang and L. Bian, "Bisphosphonate-Based Nanocomposite Hydrogels for Biomedical Applications", *Bioactive Materials*, Vol. 5, No. 4, pp. 819–831, 2020.

109. Monge, S., B. Canniccioni, A. Graillot and J. J. Robin, "Phosphorus-Containing Polymers: A Great Opportunity for The Biomedical Field", *Biomacromolecules*, Vol. 12, No. 6, pp. 1973–1982, 2011.

110. Ossipov, D. A., "Bisphosphonate-Modified Biomaterials for Drug Delivery and Bone Tissue Engineering", *Expert Opinion on Drug Delivery*, Vol. 12, No. 9, pp. 1443–1458, 2015.

111. Hiranphinyophat, S. and Y. Iwasaki, "Controlled Biointerfaces with Biomimetic Phosphorus-Containing Polymers", *Science and Technology of Advanced Materials*, Vol. 22, No. 1, pp. 301–316, 2021.

112. Giger, E. V., B. Castagner and J. C. Leroux, "Biomedical Applications of Bisphosphonates", *Journal of Controlled Release*, Vol. 167, No. 2, pp. 175–188, 2013.

113. Sedghizadeh, P. P., S. Sun, A. F. Junka, E. Richard, K. Sadrerafi, S. Mahabady, N. Bakhshalian, N. Tjokro, M. Bartoszewicz, M. Oleksy, P. Szymczyk, M. W. Lundy, J. D. Neighbors, R. G. G. Russell, C. E. McKenna and F. H. Ebetino, "Design,

Synthesis, and Antimicrobial Evaluation of A Novel Bone-Targeting Bisphosphonate-Ciprofloxacin Conjugate for The Treatment of Osteomyelitis Biofilms", *Journal of Medicinal Chemistry*, Vol. 60, No. 6, pp. 2326–2343, 2017.

114. Chen G., S. Arns and R. N. Young, "Determination of The Rat in Vivo Pharmacokinetic Profile of A Bone-Targeting Dual-Action Pro-Drug for Treatment of Osteoporosis", *Bioconjugate Chemistry*, Vol. 26, No. 6, pp. 1095–1103, 2015.

115. Chen, S. H., T. I. Liu, C. L. Chuang, H. H. Chen, W. H. Chiang and H. C. Chiu, "Alendronate/Folic Acid-Decorated Polymeric Nanoparticles for Hierarchically Targetable Chemotherapy Against Bone Metastatic Breast Cancer", *Journal Materials Chemistry B*, Vol. 8, No. 17, pp. 3789–3800, 2020.

116. Wang, K., C. Guo, X. Dong, Y. Yu, B. Wang, W. Liu and D. Chen, "In Vivo Evaluation of Reduction-Responsive Alendronate-Hyaluronan-Curcumin Polymer-Drug Conjugates for Targeted Therapy of Bone Metastatic Breast Cancer", *Molecular Pharmaceutics*, Vol. 15, No. 7, pp. 2764–2769, 2018.

117. Liu, T., S. Romanova, S. Wang, M. A. Hyun, C. Zhang, S. M. Cohen, R. K. Singh and T. K. Bronich, "Alendronate-Modified Polymeric Micelles for The Treatment of Breast Cancer Bone Metastasis", *Molecular Pharmaceutics*, Vol. 16, No. 7, pp. 2873-2883, 2019.

118. Hulsart-Billström, G., P. K. Yuen, R. Marsell, J. Hilborn, S. Larsson and D. Ossipov, "Bisphosphonate-Linked Hyaluronic Acid Hydrogel Sequesters and Enzymatically Releases Active Bone Morphogenetic Protein-2 for Induction of Osteogenic Differentiation", *Biomacromolecules*, Vol. 14, No. 9, pp. 3055–3063, 2013.

119. Bansal, G., J. E. I. Wright, C. Kucharski and H. Uludağ, "A Dendritic Tetra(bisphosphonic acid) for Improved Targeting of Proteins to Bone", *Angewandte Chemie - International Edition*, Vol. 44, No. 24, pp. 3710–3714, 2005.

120. Chiminazzo, A., G. Borsato, A. Favero, C. Fabbro, C. E. McKenna, L. G. D. Carbonare and M. T. Valenti, "Diketopyrrolopyrrole Bisphosphonate conjugate: A New Fluorescent Probe for In Vitro Bone Imaging", *Chemistry - A European Journal*, Vol. 25,No. 14, pp. 3617–3626, 2019,

121. Gluz, E., D. M. Mizrahi and S. Margel, “Synthesis and Characterization of New Poly(ethylene glycol)bisphosphonate Vinylic Monomer and Non-Fluorescent and NIR-Fluorescent Bisphosphonate Micrometer-Sized Particles”, *Polymer (Guildf)*, Vol. 54, No. 2, pp. 565–571, 2013.

122. Xie, H., G. Chen and R. N. Young, “Design, Synthesis, and Pharmacokinetics of a Bone-Targeting Dual-Action Prodrug for the Treatment of Osteoporosis”, *Journal of Medicinal Chemistry*, Vol. 60, No. 16, pp. 7012–7028, 2017.

123. Konya, V., G. Marsche, R. Schuligoi and A. Heinemann, “E-Type Prostanoid Receptor 4 (EP4) in Disease and Therapy”, *Pharmacology and Therapeutics*, Vol. 138, No. 3, pp. 485–502, 2013.

124. Furuyama, N. and Y. Fujisawa, “Distinct Roles of Cathepsin K and Cathepsin L in Osteoclastic Bone Resorption”, *Endocrine Research*, Vol. 26, No. 2, pp. 189–204, 2000.

125. Yewle, J. N., D. A. Puleo and L. G. Bachas, “Enhanced Affinity Bifunctional Bisphosphonates for Targeted Delivery of Therapeutic Agents to Bone”, *Bioconjugate Chemistry*, Vol. 22, No. 12, pp. 2496–2506, 2011.

126. Plesselova, S., P. Garcia-Cerezo, V. Blanco, F. J. Reche-Perez, F. Hernandez-Mateo, F. Santoyo-Gonzalez, M. D. Giron-Gonzalez and R. Salto-Gonzalez, “Polyethylenimine Bisphosphonate Cyclodextrin Ternary Conjugates: Supramolecular Systems for the Delivery of Antineoplastic Drugs”, *Journal of Medicinal Chemistry*, Vol. 64, No. 16, pp. 12245–12260, 2021.

127. Rahman, M. A. and B. Ochiai, “A Facile Aqueous Roduction of Bisphosphonated-Polyelectrolyte Functionalized Magnetite Nanoparticles for pH-Specific Targeting of Acidic-Bone Cells”, *RSC Advances*, Vol. 12, No. 13, pp. 8043–8058, 2022.

128. Yamashita, S., H. Katsumi, N. Hibino, Y. Isobe, Y. Yagi, K. Kusamori, T. Sakane and A.Yamamoto, “Development of PEGylated Carboxylic Acid-Modified Polyamidoamine Dendrimers as Bone-Targeting Carriers for The Treatment of Bone Diseases”, *Journal of Controlled Release*, Vol. 262, No. March, pp. 10–17, 2017.

129. Varghese, O. P., W. Sun, J. Hilborn and D. A. Ossipov, “In Situ Cross-Linkable High Molecular Weight Hyaluronan-Bisphosphonate Conjugate for Localized Delivery and Cell-Specific Targeting: A Hydrogel Linked Prodrug Approach”, *Journal of American Chemistry Society*, Vol. 131, No. 25, pp. 8781–8783, 2009.

130. D’Souza, S., H. Murata, M. V. Jose, S. Askarova, Y. Yantsen, J. D.Andersen, C. D.J.Edington, W. P.Clafshenkel, R. R.Koepsel and A. J.Russell, “Engineering of Cell Membranes with A Bisphosphonate-Containing Polymer Using ATRP Synthesis for Bone Targeting”, *Biomaterials*, Vol. 35, No.35, pp. 9447–9458, 2014.

131. Breuksch, I., M. Weinert and W. Brenner, “The Role of Extracellular Calcium in Bone Metastasis”, *Journal of Bone Oncology*, Vol. 5, No. 3, pp. 143–145, 2016.

132. Thamake, S. I., S. L. Raut, Z. Gryczynski, A. P. Ranjan and J. K. Vishwanatha, “Alendronate Coated Poly-Lactic-co-Glycolic Acid (PLGA) Nanoparticles for Active Targeting of Metastatic Breast Cancer”, *Biomaterials*, Vol. 33, No. 29, pp. 7164–7173, 2012.

133. Mehnath, S., K. Karthikeyan, M. Rajan and M. Jeyaraj, “Fabrication of Bone-Targeting Hyaluronic Acid Coupled Alendronate-Bioactive Glass for Osteosarcoma Therapy”, *Materials Chemistry and Physics*, Vol. 273, No. April, pp. 125146, 2021.

134. Bouilhac, C., C. Travelet, A. Graillot, S. Monge, R. Borsali and J. J. Robin, “Synthesis of Fatty Phosphonic Acid Based Polymethacrylamide by RAFT Polymerization and Self-Assembly in Solution”, *Polymer Chemistry*, Vol. 5, No. 8, pp. 2756–2767, 2014.

135. Hu, N., L. M. Johnson, N. Pothayee, N. Pothayee, Y.Lin, R. M. Davis and J. S. Riffle, “Synthesis of Ammonium Bisphosphonate Monomers and Polymers”, *Polymer (Guildf).*, Vol. 54, No. 13, pp. 3188–3197, 2013.

136. Chu, W., Y. Huang, C. Yang, Y. Liao, X. Zhang, M. Yan, S. Cui and C. Zhao, “Calcium Phosphate Nanoparticles Functionalized with Alendronate-Conjugated Polyethylene Glycol (PEG) for The Treatment of Bone Metastasis”, *International Journal of Pharmaceutics*, Vol. 516, No. 1-2, pp. 352–363, 2017.

137. Holzwarth, J. M. and P. X. Ma, “Biomimetic Nanofibrous Scaffolds for Bone Tissue

Engineering", *Biomaterials*, Vol. 32, No. 36, pp. 9622–9629, 2011.

138. Liu, M., X. Zeng, C. Ma, H. Yi, Z. Ali, X. Mou, S. Li, Y. Deng and N. He, "Injectable Hydrogels for Cartilage and Bone Tissue Engineering", *Bone Research*, Vol. 5, No. November, pp. 1-20, 2017.

139. Chen, L., K. Yang, H. Zhao, A. Liu, W. Tu, C. Wu, S. Chen, Z. Guo, H. Luo, J. Sun and H. Fan, "Biomineralized Hydrogel with Enhanced Toughness by Chemical Bonding of Alkaline Phosphatase and Vinylphosphonic Acid in Collagen Framework", *ACS Biomaterials Science and Engineering*, Vol. 5, No. 3, pp. 1405–1415, 2019.

140. Li, Z., T. Du, C. Ruan and X. Niu, "Bioinspired Mineralized Collagen Scaffolds for Bone Tissue Engineering", *Bioactive Materials*, Vol. 6, No. 5, pp. 1491–1511, 2021.

141. Morozowich, N. L., J. L. Nichol and H. R. Allcock, "Investigation of Apatite Mineralization on Antioxidant Polyphosphazenes for Bone Tissue Engineering", *Chemistry of Materials*, Vol. 24, No. 17, pp. 3500–3509, 2012.

142. Yang, X., S. Akhtar, S. Rubino, K. Leifer, J. Hilborn and D. Ossipov, "Direct Click Synthesis of Hybrid Bisphosphonate-Hyaluronic Acid Hydrogel in Aqueous Solution for Biomineralization", *Chemistry of Materials*, Vol. 24, No. 9, pp. 1690–1697, 2012.

143. Lin, Z., S. Cao, X. Chen, W. Wu and J. Li, "Thermoresponsive Hydrogels from Phosphorylated ABA Triblock Copolymers: A Potential Scaffold for Bone Tissue Engineering", *Biomacromolecules*, Vol. 14, No. 7, pp. 2206–2214, 2013.

144. Bleek, K. and A. Taubert, "New Developments in Polymer-Controlled, Bioinspired Calcium Phosphate Mineralization from Aqueous Solution", *Acta Biomaterialia*, Vol. 9, No. 5, pp. 6283–6321, 2013.

145. Huang, J., G. Liu, C. Song, E. Saiz and A. P. Tomsia, "Role of Molecular Chemistry of Degradable pHEMA Hydrogels in Three-Dimensional Biomimetic Mineralization", *Chemistry of. Materials*, Vol. 24, No. 7, pp. 1331–1337, 2012.

146. Ethirajan, A., U. Ziener and K. Landfester, "Surface-Functionalized Polymeric Nanoparticles As Templates for Biomimetic Mineralization of Hydroxyapatite",

Chemistry of Materials, Vol. 21, No. 11, pp. 2218–2225, 2009.

147. Vieira, S., A. S. Morais, E. Garet, J. Silva-Correia, R. L.Reis, Á. González-Fernández and J. M. Oliveira, "Self-Mineralizing Ca-Enriched Methacrylated Gellan Gum Beads for Bone Tissue Engineering", *Acta Biomaterialia*, Vol. 93, No. July, pp. 74–85, 2019.

148. Kumar, A., K. M. Rao and S. S. Han, "Synthesis of Mechanically Stiff and Bioactive Hybrid Hydrogels for Bone Tissue Engineering Applications", *Chemical Engineering Journal*, Vol. 317, No. June, pp. 119–131, 2017.

149. Phadke, A., C. Zhang, Y. Hwang, K. Vecchio and S. Varghese, "Templated Mineralization of Synthetic Hydrogels for Bone-Like Composite Materials: Role of Matrix Hydrophobicity", *Biomacromolecules*, Vol. 11, No. 8, pp. 2060–2068, 2010.

150. Salama, A., "Chitosan Based Hydrogel Assisted Spongelike Calcium Phosphate Mineralization for In-Vitro BSA Release", *International Journal of Biological Macromolecules*, Vol. 108, No. March, pp. 471–476, 2018.

151. Taubert, A., C. Balischewski, D. Hentrich, T. Elschner, S. Eidner, C. Günter, K. Behrens and T. Heinze, "Water-Soluble Cellulose Derivatives Are Sustainable Additives for Biomimetic Calcium Phosphate Mineralization", *Inorganics*, Vol. 4, No. 4, pp. 1-17, 2016.

152. Liu, P., E. Emmons and J. Song, "A Comparative Study of Zwitterionic Ligands-Mediated Mineralization and The Potential of Mineralized Zwitterionic Matrices for Bone Tissue Engineering", *Journal of Materials Chemistry B*, Vol. 2, No. 43, pp. 7524–7533, 2014.

153. Mai, T., K. Wolski, A. Puciul-Malinowska, A. Kopyshev, R. Gräf, M. Bruns, S. Zapotoczny and A. Taubert, "Anionic Polymer Brushes for Biomimetic Calcium Phosphate Mineralization-A Surface with Application Potential in Biomaterials", *Polymers (Basel).*, Vol. 10, No. 10, pp. 1165-1181, 2018.

154. Hamai, R., Y. Shirosaki and T. Miyazaki, "Apatite-Forming Ability of Vinylphosphonic Acid-Based Copolymer in Simulated Body Fluid: Effects of

Phosphate Group Content", *Journal of Materials Science: Materials in Medicine*, Vol. 27, No. 10, pp. 1-8, 2016.

155. Suzuki, S., M. R. Whittaker, L. Grøndahl, M. J. Monteiro and E. Wentrup-Byrne, "Synthesis of Soluble Phosphate Polymers by RAFT and Their in Vitro Mineralization", *Biomacromolecules*, Vol. 7, No. 11, pp. 3178–3187, 2006.

156. Mahjoubi, H., E. Buck, P. Manimunda, R. Farivar, R. Chromik, M. Murshed and M. Cerruti, "Surface Phosphonation Enhances Hydroxyapatite Coating Adhesion on Polyetheretherketone and Its Osseointegration Potential", *Acta Biomaterialia*, Vol. 47, No. January, pp. 149–158, 2017.

157. Wei, P., Z. Yuan, W. Jing, Y. Huang, Q. Cai, B. Guan, Z. Liu, X. Zhang, J. Mao, D. Chen and X. Yang, "Strengthening The Potential of Biomineralized Microspheres in Enhancing Osteogenesis via Incorporating Alendronate", *Chemical Engineering Journal*, Vol. 368, No. February, pp. 577–588, 2019.

158. George, M. N., X. Liu, A. L. Miller, H. Xu and L. Lu, "Phosphate Functionalization and Enzymatic Calcium Mineralization Synergistically Enhance Oligo[poly(ethylene glycol) fumarate] Hydrogel Osteoconductivity for Bone Tissue Engineering", *Journal of Biomedical Materials Research - Part A*, Vol. 108, No. 3, pp. 515–527, 2020.

159. Guven, M. N., B. Balaban, G. Demirci, H. Yagci Acar, O. Okay and D. Avci, "Bisphosphonate-Functionalized Poly(amido amine) Crosslinked 2-hydroxyethyl Methacrylate Hydrogel As Tissue Engineering Scaffold", *European Polymer Journal*, Vol. 159, No. June, pp. 110732-110742, 2021.

160. Liu, L., X. Li, X. Shi and Y. Wang, "Injectable Alendronate-Functionalized GelMA Hydrogels for Mineralization and Osteogenesis", *RSC Advances*, Vol. 8, No. 40, pp. 22764–22776, 2018.

161. Teotia, A. K., D. B. Raina, C. Singh, N. Sinha, H. Isaksson, M. Tägil, L. Lidgren and A. Kumar, "Nano-Hydroxyapatite Bone Substitute Functionalized with Bone Active Molecules for Enhanced Cranial Bone Regeneration", *ACS Applied Materials and Interfaces*, Vol. 9, No. 8, pp. 6816–6828, 2017.

162. Dey, R. E., X. Zhong, P. J. Youle, Q. G. Wang, I. Wimpenny, S. Downes, J. A. Hoyland, D. C. Watts, J. E. Gough and P. M. Budd, "Synthesis and Characterization of Poly(vinylphosphonic acid-co-acrylic acid) Copolymers for Application in Bone Tissue Scaffolds", *Macromolecules*, Vol. 49, No. 7, pp. 2656–2662, 2016.

163. Guven, M. N., M. S. Altuncu, T. Bal, D. C. Oran, U. Gulyuz, S. Kizilel, O. Okay and Duygu Avci, "Bisphosphonic Acid-Functionalized Cross-Linkers to Tailor Hydrogel Properties for Biomedical Applications", *ACS Omega*, Vol. 3, No. 8, pp. 8638–8647, 2018. https://pubs.acs.org/doi/10.1021/acsomega.8b01103

164. Li, A., H. Xu, P. Yu, J. Xing, C. Ding, X. Yan, J. Xie and J. Li,"Injectable Hydrogels Based on Gellan Gum Promotes in Situ Mineralization and Potential Osteogenesis", *European Polymer Journal*, Vol. 141, No. September, pp. 110091-110100, 2020.

165. Furuichi, K., Y. Oaki, H. Ichimiya, J. Komotori and H. Imai, "Preparation of Hierarchically Organized Calcium Phosphate-Organic Polymer Composites by Calcification of Hydrogel", *Science and Technology of Advanced Materials*, Vol. 7, No. 2, pp. 219–225, 2006.

166. Regitsky, A. U., B. Keshavarz, G. H. McKinley and N. Holten-Andersen, "Rheology as A Mechanoscopic Method to Monitor Mineralization in Hydrogels", *Biomacromolecules*, Vol. 18, No. 12, pp. 4067–4074, 2017.

167. Harding, J. L. and M. D. Krebs, "Bioinspired Deposition-Conversion Synthesis of Tunable Calcium Phosphate Coatings on Polymeric Hydrogels", *ACS Biomaterials Scence and. Engineering*, Vol. 3, No. 9, pp. 2024–2032, 2017.

168. Wu, W., Z. Lin, Y. Liu, X. Xu, C. Ding and J. Li, "Thermoresponsive Hydrogels Based on A Phosphorylated Star-Shaped Copolymer: Mimicking The Extracellular Matrix for in Situ Bone Repair", *Journal of Material Chemistry B*, Vol. 5, No. 3, pp. 428–434, 2017.

169. Griffin, D. M., M. A. Kennedy and S. R. Bhatia, "Calcium Phosphate Nanocomposites via in Situ Mineralization in Block Copolymer Hydrogels", *Polymers for Advanced Technology*, Vol. 32, No. 3, pp. 1372–1379, 2021.

170. Tan, J., R. A. Gemeinhart, M. Ma and W. Mark Saltzman, “Improved Cell Adhesion and Proliferation on Synthetic Phosphonic Acid-Containing Hydrogels”, *Biomaterials*, Vol. 26, No. 17, pp. 3663–3671, 2005.

171. Dey, R. E., I. Wimpenny, J. E. Gough, D. C. Watts and P. M. Budd, “Poly(vinylphosphonic acid-co-acrylic acid) Hydrogels: The Effect of Copolymer Composition on Osteoblast Adhesion and Proliferation”, *Journal of Biomedical Materials Research - Part A*, Vol. 106, No. 1, pp. 255–264, 2018.

172. Zheng, Y., L. Liu, L. Xiao, Q. Zhang and Y. Liu, “Enhanced Osteogenic Activity of Phosphorylated Polyetheretherketone via Surface-Initiated Grafting Polymerization of Vinylphosphonic Acid”, *Colloids and Surfaces B Biointerfaces*, Vol. 173, No. May, pp. 591–598, 2019.

173. Kim, S., Z. K. Cui, J. Fan, A. Fartash, T. L. Aghaloo and M. Lee, “Photocrosslinkable Chitosan Hydrogels Functionalized with the RGD Peptide and Phosphoserine to Enhance Osteogenesis”, *Journal of Materials Chemistry B*, Vol. 4, No. 31, pp. 5289–5298, 2016.

174. Dadsetan, M., M. Giuliani, F. Wanivenhaus, M. Brett Runge, J. E. Charlesworth and M. J. Yaszemski, “Incorporation of Phosphate Group Modulates Bone Cell Attachment and Differentiation on Oligo(polyethylene glycol) Fumarate Hydrogel”, *Acta Biomaterialia*, Vol. 8, No. 4, pp. 1430–1439, 2012.

175. Frassica M. T., S. K. Jones, J. Suriboot, A. S. Arabiyat, E. M. Ramirez, R. A. Culibrk, M. S. Hahn and M. A. Grunlan “Enhanced Osteogenic Potential of Phosphonated-Siloxane Hydrogel Scaffolds”, *Biomacromolecules*, Vol. 21, No. 12, pp. 5189–5199, 2020.

176. Nejadnik, M. R., X. Yang, T. Mimura, Z. T. Birgani, P. Habibovic, K. Itatani, J. A. Jansen, J. Hilborn, D. Ossipov, A. G. Mikos and S. C. G. Leeuwenburgh, “Calcium-Mediated Secondary Cross-Linking of Bisphosphonated Oligo(poly(ethylene glycol) fumarate) Hydrogels”, *Macromolecular Bioscience*, Vol. 13, No. 10, pp. 1308–1313, 2013.

177. Cui, Y., T. Zhu, D. Li, Z. Li, Y. Leng, X. Ji, H. Liu, D. Wu and J. Ding,

"Bisphosphonate-Functionalized Scaffolds for Enhanced Bone Regeneration", *Advanced Healthcare Materials*, Vol. 8, No. 23, pp. 1–21, 2019.

178. Wang, H. and S. C. Heilshorn, "Adaptable Hydrogel Networks with Reversible Linkages for Tissue Engineering", *Advanced Materials*, Vol. 27, No. 25, pp. 3717–3736, 2015.

179. Zhang, K., Q. Feng , J. Xu, X Xu, F. Tian, K. W. K. Yeung and L. Bian, "Self-Assembled Injectable Nanocomposite Hydrogels Stabilized by Bisphosphonate-Magnesium (Mg^{2+}) Coordination Regulates the Differentiation of Encapsulated Stem Cells via Dual Crosslinking", *Advanced Functional Materials*, Vol. 27, No. 34, pp. 1701642-1701652, 2017.

180. Shi, L., H. Carstensen, K. Hölzl, M. Lunzer, H. Li, J. Hilborn, A. Ovsianikov and D. A. Ossipov, "Dynamic Coordination Chemistry Enables Free Directional Printing of Biopolymer Hydrogel", *Chemistry of Materials*, Vol. 29, No. 14, pp. 5816–5823, 2017.

181. Lopez-Perez, P. M., R. M. P. Da Silva, I. Strehin, P. H. J. Kouwer, S. C. G. Leeuwenburgh and P. B. Messersmith, "Self-Healing Hydrogels Formed by Complexation between Calcium Ions and Bisphosphonate-Functionalized Star-Shaped Polymers", *Macromolecules*, Vol. 50, No. 21, pp. 8698–8706, 2017.

182. Diba, M., J. An, S. Schmidt, M. Hembury, D. Ossipov, A. R. Boccaccini and S. C. G. Leeuwenburgh, "Exploiting Bisphosphonate–Bioactiveglass Interactions for The Development of Self-Healing and Bioactive Composite Hydrogels", *Macromolecular Rapid Communications*, Vol. 37, No. 23, pp. 1952–1959, 2016.

183. Kim, Y.-H., X. Yang, L. Shi, S. A. Lanham, J. Hilborn, R. O. C. Oreffo, D. Ossipov and J. I. Dawson, "Bisphosphonate Nanoclay Edge-Site Interactions Facilitate Hydrogel Self-Assembly and Sustained Growth Factor Localization", *Nature Communications*, Vol. 11, No. 1, pp. 1-9, 2020.

184. Sánchez-Fernández, M. J., M. R. Immers, R. P. F. Lanao, F. Yang, J. C. M. E. Bender, J. Mecinović, S. C. G. Leeuwenburgh and J. C. M. van Hest, "Alendronate-Functionalized Poly(2-oxazoline)s with Tunable Affinity for Calcium Cations",

Biomacromolecules, Vol. 20, No. 8, pp. 2913–2921, 2019.

185. Nejadnik, M. R., X. Yang, M. Bongio, H. S. Alghamdi, J. J. J. P. van den Beucken, M. C. Huysmans, J. A. Jansen, J. Hilborn, D. Ossipov and S. C. G. Leeuwenburgh, "Self-Healing Hybrid Nanocomposites Consisting of Bisphosphonated Hyaluronan and Calcium Phosphate Nanoparticles", *Biomaterials*, Vol. 35, No. 25, pp. 6918–6929, 2014.

186. Shi, L., Y. Han, J. Hilborn and D. Ossipov, "'Smart' Drug Loaded Nanoparticle Delivery from A Self-Healing Hydrogel Enabled by Dynamic Magnesium-Biopolymer Chemistry", *Chemical Communications*, Vol. 52, No. 74, pp. 11151–11154, 2016.

187. Sánchez-Fernández, M. J., J. Rutjes, R. P. Félix Lanao, J. C. M. E. Bender, J. C. M. van Hest and S. C. G. Leeuwenburgh, "Bone-Adhesive Hydrogels Based on Dual Crosslinked Poly(2-oxazoline)s", *Macromolecular Bioscience*, Vol. 21, No. 12, pp. 1–11, 2021.

188. Shi, L., F. Wang, W. Zhu, Z. Xu, S. Fuchs, J. Hilborn, L. Zhu, Q. Ma, Y. Wang, X. Weng and D. A. Ossipov, "Self-Healing Silk Fibroin-Based Hydrogel for Bone Regeneration: Dynamic Metal-Ligand Self-Assembly Approach", *Advanced Functional Materials*, Vol. 27, No. 37, pp. 1–14, 2017.

189. Catel, Y., U. K. Fischer and N. Moszner, "Monomers for Adhesive Polymers, 13. Synthesis, Radical Photopolymerization and Adhesive Properties of Polymerizable 2-Substituted 1,3-propylidenediphosphonic Acids", *Designed Monomers and Polymers*, Vol. 17, No. 3, pp. 286–299, 2014.

190. Catel, Y., U. K. Fischer and N. Moszner, "Monomers for Adhesive Polymers, 10-Synthesis, Radical Photopolymerization and Adhesive Properties of Methacrylates Bearing Phosphonic Acid Groups", *Macromolecular. Materials and Engineering*, Vol. 298, No. 7, pp. 740–756, 2013.

191. Catel, Y., U. K. Fischer and N. Moszner, "Monomers for Adhesive Polymers: 11. Structure-Adhesive Properties Relationships of New Hydrolytically Stable Acidic Monomers", *Polymer International*, Vol. 62, No. 12, pp. 1717–1728, 2013.

192. Bingol, H. B., A. Altin, T. Bal, S. Agopcan-Cinar, S. Kizilel and D. Avci, “Synthesis and Evaluation of New Phosphonic Acid-Functionalized Acrylamides with Potential Biomedical Applications”, *Journal of Polymer Science Part A Polymer Chemistry*, Vol. 53, No. 23, pp. 2755–2767, 2015.

193. Bilgici, Z. S., S. B. Turker and D. Avci, “Novel Bisphosphonated Methacrylates: Synthesis, Polymerizations, and Interactions with Hydroxyapatite”, *Macromolecular Chemistry and Physics*, Vol. 214, No. 20, pp. 2324–2335, 2013.

194. Kachbi Khelfallah, S., M. Monteil, J. Deschamp, O. Gager, E. Migianu-Griffoni and M. Lecouvey, “Synthesis of Novel Polymerizable Molecules Bearing Bisphosphonate”, *Organic and Biomolecular Chemistry*, Vol. 13, No. 46, pp. 11382–11392, 2015.

195. Van Meerbeek, B., K. Yoshihara, Y. Yoshida, A. Mine, J. De Munck and K. L. Van Landuyt, “State of the Art of Self-Etch Adhesives”, *Dental Materials*, Vol. 27, No. 1, pp. 17–28, 2011.

196. Feitosa, V. P., F. A. Ogliari, B. Van Meerbeek, T. F. Watson, K. Yoshihara, A. O. Ogliari, M. A. Sinhoreti, A. B. Correr, G. Cama and S. Sauro, “Can The Hydrophilicity of Functional Monomers Affect Chemical Interaction?”, *Journal of Dental Research*, Vol. 93, No. 2, pp. 201–206, 2014.

197. Feitosa, V. P., S. Sauro, F. A. Ogliari, J. W. Stansbur, G. H. Carpenter, T. F. Watson, M. A. Sinhoreti and A. B. Correr, “The Role of Spacer Carbon Chain in Acidic Functional Monomers on the Physicochemical Properties of Self-Etch Dental Adhesives”, *Journal of Dentistry*, Vol. 42, No. 5, pp. 565–574, 2014.

198. Catel, Y., S. Schörpf and N. Moszner, “Monomers for Adhesive Polymers, 16. Synthesis of Acidic Dimethacrylates Starting from Thioglycerol”, *Macromolecular Materials and Engineering*, Vol. 300, No. 10, pp. 1010–1022, 2015.

199. Tauscher, S., Y. Catel and N. Moszner, “Monomers for Adhesive Polymers, 17.a Synthesis, Photopolymerization and Adhesive Properties of Polymerizable Phosphonic Acids Bearing Urea Groups”, *Designed Monomers and Polymers*, Vol. 19, No. 1, pp. 77–88, 2016.

200. Altin, A., B. Akgun, O. Buyukgumus, Z. Sarayli Bilgici, S. Agopcan, D. Asik, H. Yagci Acar and Duygu Avci,"Synthesis and Photopolymerization of Novel, Highly Reactive Phosphonated-Ureamethacrylates for Dental Materials", *Reactive and Functional Polymers*, Vol. 73, No. 9, pp. 1319–1326, 2013.

201. Guven, M. N., E. Akyol, F. Demir Duman, H. Yagci Acar, O. Karahan and D. Avci, "Urea Dimethacrylates Functionalized with Bisphosphonate/Bisphosphonic Acid for Improved Dental Materials", *Journal of Polymer Science Part A Polymer Chemistry*, Vol. 55, No. 19, pp. 3195–3204, 2017.

202. Solimando, X., Y. Catel, N. Moszner, J. J. Robin and S. Monge, "Smart Functionalized Phosphonic Acid Based Copolymers: New Structures for Old Purposes", *Polymer Chemistry*, Vol. 11, No. 18, pp. 3237–3250, 2020.

203. Cui, X., Y. Koujima, H. Seto, T. Murakami, Y. Hoshino and Y. Miura, "Inhibition of Bacterial Adhesion on Hydroxyapatite Model Teeth by Surface Modification with PEGMA-Phosmer Copolymers", *ACS Biomaterial Science and Engineering*, Vol. 2, No. 2, pp. 205–212, 2016.

204. Lamont, R. J. and P. G. Egland, "Dental Caries", *Molecular Medical Microbiology Second Edition*, Vol. 2–3, No. 4, pp. 945–955, 2014.

205. Liang, K., M. D. Weir, M. A. Reynolds, X. Zhou, J. Li and H. H. K. Xu, "Poly(amido amine) and Nano-Calcium Phosphate Bonding Agent to Remineralize Tooth Dentin in Cyclic Artificial Saliva/Lactic acid", *Material Science and Engineering C*, Vol. 72, No. March, pp. 7–17, 2017.

206. Liu, J., Y. Gao, X. Zhu, Y. Zhang, H. Xu, T. Wang and G. Zhang, "Phosphorylated PAMAM Dendrimers: An Analog of Dentin Non-Collagenous Proteins, Enhancing The Osteo/Odontogenic Differentiation of Dental Pulp Stem Cells", *Clinical Oral Investigations*, Vol. 26, No. 2, pp. 1737–1751, 2022.

207. Wu, D., J. Yang, J, Li, L. Chen, B. Tang, X. Chen, W. Wu and J. Li, "Hydroxyapatite-Anchored Dendrimer for in Situ Remineralization of Human Tooth Enamel", *Biomaterials*, Vol. 34, No. 21, pp. 5036–5047, 2013.

208. Chang, R., Y.-J. Liu, Y.-L. Zhang, S.-Y. Zhang, B.-B. Han, F. Chen and Y.-X. Chen, "Phosphorylated and Phosphonated Low-Complexity Protein Segments for Biomimetic Mineralization and Repair of Tooth Enamel", *Advanced Science*, Vol. 9, No. 6, pp. 1–16, 2022.

209. Wang, Z., Y. Ouyang, Z. Wu, L. Zhang, C. Shao, J. Fan, L. Zhang, Y. Shi, Z. Zhou, H. Pan, R. Tang and B. Fu, "A Novel Fluorescent Adhesive-Assisted Biomimetic Mineralization", *Nanoscale*, Vol. 10, No. 40, pp. 18980–18987, 2018.

210. Chen, M., J. Yang, J. Li, K. Liang, L. He, Z. Lin, X. Chen, X Ren and J. Li, "Modulated Regeneration of Acid-Etched Human Tooth Enamel by A Functionalized Dendrimer That Is An Analog of Amelogenin", *Acta Biomaterialia*, Vol. 10, No. 10, pp. 4437–4446, 2014.

211. Xu, X., N. Wang, M. Wu, J. Wang, D. Wang, Z. Chen, J. Xie, C. Ding and J. Li, "Programmed Antibacterial and Mineralization Therapy for Dental Caries Based on Zinc-Substituted Hydroxyapatite/Alendronate-Grafted Polyacrylic Acid Hybrid Material", *Colloids and Surfaces B Biointerfaces*, Vol. 194, No. April, pp. 111206-111213, 2020.

212. Matveeva, E. V., P. V. Petrovskii and I. L. Odinets, "Efficient Synthesis of Racemic β-aminophosphonates via Aza-Michael Reaction in Water", *Tetrahedron Letters*, Vol. 49, No. 42, pp. 6129–6133, 2008.

213. Bou Orm, N., Y. Dkhissi, S. Daniele and L. Djakovitch, "Synthesis of 2-(arylamino)ethyl Phosphonic Acids via The Aza-Michael Addition on Diethyl Vinylphosphonate", *Tetrahedron*, Vol. 69, No. 1, pp. 115–121, 2013.

214. Khusainova, N. G., D. N. Tazetdinova, I. D. Shurygin, A. R. Garifzyanov and R. A. Cherkasov, "Synthesis and Acid-Base Properties of New β-diaminophosphoryl Compounds", *Russian Journal of Organic Chemistry*, Vol. 52, No. 11, pp. 1697–1699, 2016.

215. Yeom, C. E., M. J. Kim and B. M. Kim, "1,8-Diazabicyclo[5.4.0]undec-7-ene (DBU)-Promoted Efficient and Versatile Aza-Michael Addition", *Tetrahedron*, Vol. 63, No. 4, pp. 904–909, 2007.

216. Guven, M. N., M. S. Altuncu, F. Demir Duman, T. N. Eren, H. Yagci Acar and D. Avci, "Bisphosphonate-Functionalized Poly(β-amino ester) Network Polymers", *Journal of Biomedical Materials Research - Part A*, Vol. 105, No. 5, pp. 1412–1421, 2017.

217. Kim, M. S., S. J. Hwang, J. K. Han, E. K.Choi, H. J. Park, J. S. Kim and D. S. Lee, "pH-Responsive PEG-poly(β-amino ester) Block Copolymer Micelles with A Sharp Transition", *Macromolecular Rapid Communications*, Vol. 27, No. 6, pp. 447–451, 2006.

218. Song, W., Z. Tang, M. Li, S. Lv, H. Yu, L. Ma, X. Zhuang, Y. Huang and X. Chen, "Tunable pH-Sensitive Poly(β-amino ester)s Synthesized from Primary Amines and Diacrylates for Intracellular Drug Delivery", *Macromolecular Bioscience*, Vol. 12, No. 10, pp. 1375–1383, 2012.

219. Safranski, D. L., J. C. Crabtree, Y. R. Huq and K. Gall, "Thermo-Mechanical Properties of Semi-Degradable Poly(β-amino ester)-co-methyl Methacrylate Networks Under Simulated Physiological Conditions", *Polymer (Guildf).*, Vol. 52, No. 21, pp. 4920–4927, 2011.

220. Gupta, P., C. Lacerda, V. Patil, D. Biswal, P. Wattamwar, J. Z. Hilt and T. D. Dziubla, "Degradation of Poly(β-amino ester) Gels in Alcohols through Transesterification: Method to Conjugate Drugs to Polymer Matrices", *Journal of Polymer Science Part A Polymer Chemistry*, Vol. 55, No. 12, pp. 2019–2026, 2017.

221. Kokubo, T. and H. Takadama, "How Useful Is SBF in Predicting in Vivo Bone Bioactivity?", *Biomaterials*, Vol. 27, No. 15, pp. 2907–2915, 2006.

222. Chou, Y. F., W. A. Chiou, Y. Xu, J. C. Y. Dunn and B. M. Wu, "The Effect of pH on The Structural Evolution of Accelerated Biomimetic Apatite", *Biomaterials*, Vol. 25, No. 22, pp. 5323–5331, 2004.

223. Manfredi, A., E. Ranucci, M. Suardi and P. Ferruti, "Polymerization Kinetics of Poly(amidoamine)s in Different Solvents", *Journal of Bioactive and Compatible Polymers*, Vol. 22, No. 2, pp. 219–231, 2007.

224. Lin, C. and J. F. J. Engbersen, "PEGylated Bioreducible Poly(amido amine)s for Non-Viral Gene Delivery", *Material Science and Engineering C*, Vol. 31, No. 7, pp. 1330–1337, 2011.

225. Mateos-Timoneda, M. A., M. C. Lok, W. E. Hennink, J. Feijen and J. F. J. Engbersen, "Poly(amido amine)s as Gene Delivery Vectors: Effects of Quaternary Nicotinamide Moieties in The Side Chains", *ChemMedChem*, Vol. 3, No. 3, pp. 478–486, 2008.

226. Shkilnyy, A., A. Friedrich, B. Tiersch, S. Schöne, M. Fechner, J. Koetz, C.-W. Schläpfer and A. Taubert, "Poly(ethylene imine)-Controlled Calcium Phosphate Mineralization", Vol. 24, No. 25, pp. 2102–2109, 2008.

227. Shkilnyy, A., S. Schöne, C. Rumplasch, A. Uhlmann, A. Hedderich, C. Günter and A. Taubert, "Calcium Phosphate Mineralization with Linear poly(ethylene imine): A Time-Resolved Study", *Colloid and Polymer Science*, Vol. 289, No. 8, pp. 881–888, 2011.

228. Boyer, C., V. Bulmus, T. P. Davis, V. Ladmiral, J. Liu and S. Perrier, "Bioapplications of RAFT Polymerization", *Chemical Reviews*, Vol. 109, No. 11, pp. 5402–5436, 2009.

229. Keddie, D. J., G. Moad, E. Rizzardo and S. H. Thang, "RAFT Agent Design and Synthesis", *Macromolecules*, Vol. 45, No. 13, pp. 5321–5342, 2012.

230. York, A. W., S. E. Kirkland and C. L. McCormick, "Advances in The Synthesis of Amphiphilic Block Copolymers via RAFT Polymerization: Stimuli-Responsive Drug and Gene Delivery", *Advanced Drug Delivery Reviews*, Vol. 60, No. 9, pp. 1018–1036, 2008.

231. Moad, G., "RAFT Polymerization to Form Stimuli-Responsive Polymers", *Polymer Chemistry*, Vol. 8, No. 1, pp. 177–219, 2017.

232. Moad, G., E. Rizzardo and S. H. Thang, "Radical Addition-Fragmentation Chemistry in Polymer Synthesis", *Polymer (Guildf).*, Vol. 49, No.5, pp. 1079–1131, 2008.

233. Blidi, I., O. Coutelier and M. Destarac, "Well-Defined Phosphonate-Functional Copolymers through RAFT Copolymerization of Dimethyl-p-

vinylbenzylphosphonate", *Journal of Polymer Science Part A Polymer Chemistry*, Vol. 52, No. 18, pp. 2616–2624, 2014.

234. David, G., Z. E. Asri, S. Rich, P. Castignolles, Y. Guillaneuf, P. Lacroix-Desmazes and B. Boutevin, "Peculiar Behavior of Degenerative Chain Transfer Polymerization of A Phosphonated Methacrylate", *Macromolecular Chemistry and Physics*, Vol. 210, No. 8, pp. 631–639, 2009.

235. Xu, T., L. Zhang, Z. Cheng and X. Zhu, "Recent Advances in 'Living'/Controlled Radical Polymerization of Phosphorus-Containing Monomers and Their Potential Applications", *Science China Chemistry*, Vol. 58, No. 11, pp. 1633–1640, 2015.

236. Canniccioni, B., S. Monge, G. David and J. J. Robin, "RAFT Polymerization of Dimethyl(methacryloyloxy)methyl Phosphonate and Its Phosphonic Acid Derivative: A New Opportunity for Phosphorus-Based Materials", *Polymer Chemistry*, Vol. 4, No. 13, pp. 3676–3685, 2013.

237. Steinbauer, P., A. Rohatschek, O. Andriotis, N. Bouropoulos, R. Liska, P. J. Thurner and S. Baudis, "Biomimetic Adhesion Motifs Based on RAFT Polymers with Phosphonate Groups", *European Polymer Journal*, Vol. 143, No. September, pp. 110188-110199, 2021.

238. Tian, C., T. Xu, L. Zhang, Z. Cheng and X. Zhu, "RAFT Copolymerization of A Phosphorus-Containing Monomer with α-hydroxy Phosphonate and Methyl Methacrylate", *RSC Advances*, Vol. 6, No. 41, pp. 34659–34665, 2016.

239. The Ho, H., J. Coupris, S. Pascual, L. Fontaine, T. Lequeux and T. N. Pham, "Synthesis and Characterization of Innovative Well-Defined Difluorophosphonylated-(co)polymers by RAFT Polymerization", *Polymer Chemistry*, Vol. 6, No. 25, pp. 4597–4604, 2015.

240. Falireas, P. G., C. Negrell, and G. David, "Synthesis and Aqueous Solution Properties of An Amino Bisphosphonate Methacrylate Homopolymer via RAFT Polymerization", *Polymers (Basel)*, Vol. 10, No. 7, pp. 22–26, 2018.

241. Hua, D., J. Tang, J. Jiang and X. Zhu, "Synthesis of Phenylphosphinic Acid-

Containing Amphiphilic Homopolymers by Reversible Addition-Fragmentation Transfer (RAFT) Polymerization and Its Aggregation in Water", *Polymer (Guildf)*, Vol. 50, No. 24, pp. 5701–5707, 2009.

242. Pan, H., M. Sima, P. Kopečková, K. Wu, S. Gao, J. Liu, D. Wang, S. C. Miller and J. Kopeček, "Biodistribution and Pharmacokinetic Studies of Copolymer-Alendronate Conjugates", *Molecular Pharmaceutics*, Vol. 5, No. 4, pp. 548–558, 2008.

243. Graillot, A., S. Monge, C. Faur, D. Bouyer and J. J. Robin, "Synthesis by RAFT of Innovative Well-Defined (Co)polymers from A Novel Phosphorus-Based Acrylamide Monomer", *Polymer Chemistry*, Vol. 4, No. 3, pp. 795–803, 2013.

244. Zhang, Q. M. and M. J. Serpe, "Synthesis, Characterization, and Antibacterial Properties of A Hydroxyapatite Adhesive Block Copolymer", *Macromolecules*, Vol. 47, No. 22, pp. 8018–8025, 2014

245. Blidi, I., R. Geagea, O. Coutelier, S. Mazières, F. Violleau and M. Destarac, "Aqueous RAFT/MADIX Polymerisation of Vinylphosphonic Acid", *Polymer Chemistry*, Vol. 3, No. 22, pp. 609–612, 2012.

246. Markiewicz, K. H., L. Seiler, I. Misztalewska, K. Winkler, S. Harrisson, A. Z. Wilczewska, M. Destarac and J.-D. Marty, "Advantages of Poly(vinyl phosphonic acid)-Based Double Hydrophilic Block Copolymers for The Stabilization of Iron Oxide Nanoparticles", *Polymer Chemistry*, Vol. 7, No. 41, pp. 6391–6399, 2016.

247. Seiler, L., J. Loiseau, F. Leising, P. Boustingorry, S. Harrisson and M. Destarac, "Acceleration and Improved Control of Aqueous RAFT/MADIX Polymerization of Vinylphosphonic Acid in The Presence of Alkali Hydroxides", *Polymer Chemistry*, Vol. 8, No. 25, pp. 3825–3832, 2017.

248. Hanisch, A., P. Yang, A. N. Kulak, L. A. Fielding, F. C. Meldrum and S. P. Armes, "Phosphonic Acid-Functionalized Diblock Copolymer Nano-Objects via Polymerization-Induced Self-Asssembly: Synthesis, Characterization, and Occlusion into Calcite Crystals", *Macromolecules*, Vol. 49, No. 1, pp. 192–204, 2016.

249. Cui, X., T. Murakami, Y. Hoshino and Y. Miura, "Anti-Biofouling Phosphorylated

HEMA and PEGMA Block Copolymers Show High Affinity to Hydroxyapatite", *Colloids and Surfaces B Biointerfaces*, Vol. 160, No. December, pp. 289–296, 2017.

250. Bachler, P. R., M. D. Schulz, C. A. Sparks, K. B. Wagener and B. S. Sumerlin, "Aminobisphosphonate Polymers via RAFT and A Multicomponent Kabachnik-Fields Reaction", *Macromolecular Rapid Communications*, Vol. 36, No. 9, pp. 828–833, 2015.

251. Pothayee, N., S. Balasubramaniam, R. M. Davis, J. S. Riffle, M. R. J. Carroll, R. C. Woodward and T.G.St. Pierre, "Synthesis of 'Ready-to-adsorb' Polymeric Nanoshells for Magnetic Iron Oxide Nanoparticles via Atom Transfer Radical Polymerization", *Polymer (Guildf)*, Vol. 52, No. 6, pp. 1356–1366, 2011.

252. Balasubramaniam, S., N. Pothayee, Y. Lin, M, House, R. C. Woodward, T. G. St. Pierre, R. M. Davis and J. S. Riffle, "Poly(N-isopropylacrylamide)-Coated Superparamagnetic Iron Oxide Nanoparticles: Relaxometric and Fluorescence Behavior Correlate to Temperature-Dependent Aggregation", *Chemistry of Materials*, Vol. 23, No. 14, pp. 3348–3356, 2011.

253. Dufils, P. E., G. David, B. Boutevin, G. Woodward, G. Otter, A. Guinaudeau, S. Mazières and M. Destarac, "Phosphonate-Terminated Poly(vinyl acetate) Synthesized by RAFT/MADIX Polymerization", *Journal of Polymer Science Part A Polymer Chemistry*, Vol. 50, No. 10, pp. 1997–2007, 2012.

254. Xu, X., Y. Liu, W. Fu, M. Yao, Z. Ding, J. Xuan, D. Li, S. Wang, Y. Xia and M. Cao, "Poly(N-isopropylacrylamide)-Based Thermoresponsive Composite Hydrogels for Biomedical Applications", *Polymers (Basel)*, Vol. 12, No. 3, pp. 1–22, 2020.

255. Brooks, W. L. A., G. Vancoillie, C. P. Kabb, R. Hoogenboom and B. S. Sumerlin, "Triple Responsive Block Copolymers Combining pH-Responsive, Thermoresponsive, and Glucose-Responsive Behaviors", *Journal of Polymer Science Part A Polymer Chemistry*, Vol. 55, No. 14, pp. 2309–2317, 2017.

256. Graisuwan, W., H. Zhao, S. Kiatkamjornwong, P. Theato and V. P. Hoven, "Formation of Thermo-Sensitive and Cross-Linkable Micelles by Self-Assembly of Poly(pentafluorophenyl Acrylate)-Containing Block Copolymer", *Journal of*

Polymer Science Part A Polymer Chemistry, Vol. 53, No. 9, pp. 1103–1113, 2015.

257. Ward, M. A. and T. K. Georgiou, "Thermoresponsive Polymers for Biomedical Applications", *Polymers (Basel)*, Vol. 3, No. 3, pp. 1215–1242, 2011.

258. Halperin, A., M. Kröger, and F. M. Winnik, "Poly(N-isopropylacrylamide) Phase Diagrams: Fifty Years of Research", *Angewandte Chemie - International Edition*, Vol. 54, No. 51, pp. 15342–15367, 2015.

259. Karimi, M., P. S. Zangabad, A. Ghasemi, M. Amiri, M. Bahrami, H. Malekzad, H. G. As, Z. Mahdieh, M. Bozorgomid, A. Ghasemi, M. R. R. T. Boyuk and M. R. Hamblin, "Temperature-Responsive Smart Nanocarriers for Delivery of Therapeutic Agents: Applications and Recent Advances", *ACS Appl. Mater. Interfaces*, Vol. 8, No. 33, pp. 21107–21133, 2016.

260. Graillot, A., D. Bouyer, S. Monge, J. J. Robin and C. Faur, "Removal of Nickel Ions from Aqueous Solution by Low Energy-Consuming Sorption Process Involving Thermosensitive Copolymers with Phosphonic Acid Groups", *Journal of Hazardous Materials*, Vol. 244–245, No. January, pp. 507–515, 2013.

261. Graillot, A., S. Monge, C. Faur, D. Bouyer, C. Duquesnoy and J. J. Robin, "How to Easily Adapt Cloud Points of Statistical Thermosensitive Polyacrylamide-Based Copolymers Knowing Reactivity Ratios", *RSC Advances*, Vol. 4, No. 37, pp. 19345–19355, 2014.

262. Ren, H., D. Chen, Y. Shi, H. Yu, Z. Fu and W. Yang, "Charged End-Group Terminated Poly(N-isopropylacrylamide)-b-poly(carboxylic azo) with Unusual Thermoresponsive Behaviors", *Macromolecules*, Vol. 51, No. 9, pp. 3290–3298, 2018.

263. Skrabania, K., W. Li and A. Laschewsky, "Synthesis of Double-Hydrophilic BAB Triblock Copolymers via RAFT Polymerisation and Their Thermoresponsive Self-Assembly in Water", *Macromol. Chem. Phys.*, Vol. 209, pp. 1389–1403, 2008.

264. Pasparakis, G. and M. Vamvakaki, "Multiresponsive Polymers: Nano-Sized Assemblies, Stimuli-Sensitive Gels and Smart Surfaces", *Polymer Chemistry*, Vol. 2,

No. 6, pp. 1234–1248, 2011.

265. Kondiah, P. J., Y. E. Choonara, P. P. D. Kondiah, T. Marimuthu, P. Kumar, L. C. du Toit and V. Pillay, "A Review of Injectable Polymeric Hydrogel Systems for Application in Bone Tissue Engineering", *Molecules*, Vol. 21, No. 11, pp. 1-31, 2016.

266. Herfurth, C., A. Laschewsky, L. Noirez, B. von Lospichl and M. Gradzielski, "Thermoresponsive (Star) Block Copolymers from One-Pot Sequential RAFT Polymerizations and Their Self-Assembly in Aqueous Solution", *Polymer (Guildf).*, Vol. 107, No. December, pp. 422–433, 2016.

267. Lin, H. H. and Y. L. Cheng, "In-Situ Thermoreversible Gelation of Block and Star Copolymers of Poly(ethylene glycol) and Poly(N-isopropylacrylamide) of varying Architectures", *Macromolecules*, Vol. 34, No. 11, pp. 3710–3715, 2001.

268. Bivigou-Koumba, A. M., E. Görnitz, A. Laschewsky, P. Müller-Buschbaum and C. M. Papadakis, "Thermoresponsive Amphiphilic Symmetrical Triblock Copolymers with A Hydrophilic Middle Block Made of Poly(N-isopropylacrylamide): Synthesis, Self-Organization, and Hydrogel Formation", *Colloid and Polymer Science*, Vol. 288, No. 5, pp. 499–517, 2010.

269. Zhou, C., M. A. Hillmyer and T. P. Lodge, "Efficient Formation of Multicompartment Hydrogels by Stepwise Self-Assembly of Thermoresponsive ABC Triblock Terpolymers", *Journal of American Chemical Society*, Vol. 134, No. 25, pp. 10365–10368, 2012.

270. Miasnikova, A., A. Laschewsky, G. De Paoli, C. M. Papadakis, P. Müller-Buschbaum and S. S. Funari, "Thermoresponsive Hydrogels from Symmetrical Triblock Copolymers Poly(styrene-block-(methoxy diethylene glycol acrylate)-block-styrene)", *Langmuir*, Vol. 28, No. 9, pp. 4479–4490, 2012.

271. Chassenieux, C., T. Nicolai and L. Benyahia, "Rheology of Associative Polymer Solutions", *Current Opinion in Colloid and Interface Science*, Vol. 16, No. 1, pp. 18–26, 2011.

272. Chen, C. F., C. T. Y. Lin and I. M. Chu, "Study of Novel Biodegradable

Thermosensitive Hydrogels of Methoxy-poly(ethylene glycol)-block-polyester Diblock Copolymers", *Polymer International*, Vol. 59, No. 10, pp. 1428–1435, 2010.

273. Wang, L., M. Zhang, Z. Yang and B. Xu, "The First Pamidronate Containing Polymer and Copolymer", *Chemical Communications*, Vol. 26, No. May, pp. 2795–2797, 2006.

274. Chen, J. P., M. J. Tsai and H. T. Liao, "Incorporation of Biphasic Calcium Phosphate Microparticles in Injectable Thermoresponsive Hydrogel Modulates Bone Cell Proliferation and Differentiation", *Colloids and Surfaces B Biointerfaces*, Vol. 110, No. October, pp. 120–129, 2013.

275. Liao, H. T., M. J. Tsai, M. Brahmayya and J. P. Chen, "Bone Regeneration Using Adipose-Derived Stem Cells in Injectable Thermo-Gelling Hydrogel Scaffold Containing Platelet-Rich Plasma and Biphasic Calcium Phosphate", *International Journal of Molecular Science*, Vol. 19, No. 9, pp. 1–18, 2018.

276. Degenhardt, C. R. and D. C. Burdsall, "Synthesis of Ethenylidenebis(phosphonic acid) and Its Tetraalkyl Esters", *The Journal of Organic Chemistry*, Vol. 51, No. 18, pp. 3488–3490, 1986.

277. Hetzer, M., B. V. K. J. Schmidt, C. Barner-Kowollik and H. Ritter, "Limitations of Cyclodextrin-Mediated RAFT Homopolymerization and Block Copolymer Formation", *Journal of Polymer Science Part A Polymer Chemistry*, Vol. 51, No. 11, pp. 2504–2517, 2013.

278. Galaka, T, M. F. Casal, M. Storey, C. Li, M. N. Chao, S. H. Szajnman, R. Docampo, S. N. J. Moreno and J. B. Rodriguez, "Antiparasitic Activity of Sulfur- and Fluorine-Containing Bisphosphonates Against Trypanosomatids and Apicomplexan Parasites", *Molecules*, Vol. 22, No. 1, pp. 1–22, 2017.

279. Hu, N., A. Peralta, S. Roy Choudhury, R. Zhang, R. M. Davis and J. S. Riffle, "Acrylamide Monomers and Polymers That Contain Phosphonate Ions", *Polymer (Guildf)*, Vol. 65, No. 1, pp. 124–133, 2015.

280. Bailly, T., R. Burgada, T. Prangé and M. Lecouvey, "Synthesis of Tetradentate Mixed

Bisphosphonates - New Hydroxypyridinonate Ligands for Metal Chelation Therapy", *Tetrahedron Letters*, Vol. 44, No. 1, pp. 189–192, 2003.

281. Pasqua, L., I. E. De Napoli, M. De Santo, M. Greco, E. Catizzone, D. Lombardo, G. Montera, A. Comandè, A. Nigro, C. Morelli and A. Leggio, "Mesoporous Silica-Based Hybrid Materials for Bone-Specific Drug Delivery", *Nanoscale Advances*, Vol. 1, No. July, pp. 3269–3278, 2019.

282. Goulart da Silva, T., D. B. Pereira, B. F. de Carvalho Patricio, M. A. Sarcinelli, H. V. A. Rocha, S. Letichevsky, C. E. R. da Silva and R. H. Mendonça, "Polycaprolactone/Alendronate Systems Intended for Production of Biomaterials", *Journal of Applied Polymer Science*, Vol. 138, No. 1, pp. 1–17, 2021.

283. Valeur, E. and M. Bradley, "Amide Bond Formation: Beyond The Myth of Coupling Reagents", *Chemícal Society Reviews*, Vol. 38, No. December, pp. 606–631, 2009.

284. Dunetz, J. R., J. Magano and G. A. Weisenburger, "Large-Scale Applications of Amide Coupling Reagents for The Synthesis of Pharmaceuticals", *Organic Process Research and Developments*, Vol. 20, No. 2, pp. 140–177, 2016.

285. Kuljanin, J., I. Jankovi, J. Nedeljkovi, D. Prstojevi and V. Marinkovi, "Spectrophotometric Determination of Alendronate in Pharmaceutical Formulations via Complex Formation with Fe(III) Ions", *Journal of Pharmaceutical and Biomedical Analysis*, Vol. 28, No. 6, pp. 1215–1220, 2002.

286. Chen, H., G. Li, H. Chi, D. Wang, C. Tu, L. Pan, L. Zhu, F. Qiu, F. Guo and X. Zhu, "Alendronate-Conjugated Amphiphilic Hyperbranched Polymer Based on Boltorn H40 and Poly(ethylene glycol) for Bone-Targeted Drug Delivery", *Bioconjugate Chemistry*, Vol. 23, No. 9, pp. 1915–1924, 2012.

287. In, Y., U. Amornkitbamrung, M. H. Hong and H. Shin, "On The Crystallization of Hydroxyapatite Under Hydrothermal Conditions: Role of Sebacic Acid as An Additive", *ACS Omega*, Vol. 5, No.42, pp. 27204–27210, 2020.

288. Manas, E. S., Z. Getahun, W. W. Wright, W. F. DeGrado and J. M. Vanderkooi, "Infrared Spectra of Amide Groups in α-helical Proteins: Evidence for Hydrogen

Bonding Between Helices and Water", *Journal of the American Chemical Society*, Vol. 122, No. 41, pp. 9883-9890, 2000.

289. Midha, S., R. Tripathi, H. Geng, P. D. Lee and S. Ghosh, "Elucidation of Differential Mineralisation on Native and Regenerated Silk Matrices", *Materials Science and Engineering C*, Vol. 68, No. November, pp. 663–674, 2016.

290. Zhai, Y. and F. Z. Cui, "Recombinant Human-Like Collagen Directed Growth of Hydroxyapatite Nanocrystals", *Journal of Crystal Growth*, Vol. 291, No. 1, pp. 202–206, 2006.

291. Ma, J., M. Xia, S. Zhu and F. Wang, "A New Alendronate Doped HAP Nanomaterial for Pb^{2+}, Cu^{2+} and Cd^{2+} Effect Absorption", Vol. 400, No. December, pp. 123143-123153, 2020.

292. Fukegawa, D., S. Hayakawa, Y. Yoshida, K. Suzuki, A. Osaka and B. Van Meerbeek, "Chemical Interaction of Phosphoric Acid Ester with Hydroxyapatite", Vol. 85, No. 10, pp. 941-944, 2006.

293. Treloar, L. R. G., *The Physics of Rubber Elasticity*, University Press, Oxford, 1975.

294. Flory, P. J., *Principles of Polymer Chemistry*, Cornell University Press, Ithaca, NY, 1953.

295. Wallin, R. F. and E. Arscott, "A Practical Guide to ISO 10993–5: Cytotoxicity" *Medical Device and Diagnostic Industry*, Vol. 20, No. April, pp. 96-98, 1998.

296. Elliott, J. C., *Structure and chemistry of the apatite and other calciumorthophosphates*, Elsevier, Amsterdam, The Netherlands, 1994.

297. Moad, G., E. Rizzardo and S. H. Thang, "Living Radical Polymerization by The RAFT Process—A First Update", *Australian Journal of Chemistry*, Vol. 59, No. September, pp. 669–692, 2006.

298. David, G., C. Negrell, A. Manseri and B. Boutevin, "Poly(MMA)-b-poly (monophosphonic acrylate) Diblock Copolymers Obtained by ATRP and Used as Additives for Anticorrosive Coatings", *Journal of Applied Polymer Science*, Vol. 114,

No. 4, pp. 2213-2220, 2009.

299. El Asri, Z., K. Chougrani, C. Negrell-Guirao, G. David, B. Boutevin and C. Loubat, "An Efficient Process for Synthesizing and Hydrolyzing a Phosphonated Methacrylate: Investigation of The Adhesive and Anticorrosive Properties", *Journal of Polymer Science Part A Polymer Chemistry*, Vol. 46, No. 14, pp. 4794-4803, 2008.

300. Kim, S. Y. and S. C. Lee, "Thermoresponsive Injectable Hydrogel System Based on Poly(N-isopropylacrylamide-co-vinylphosphonic acid). I. Biomineralization and Protein Delivery", *Journal of Applied Polymer Science*, Vol. 113, No. 6, pp. 3460-3469, 2009.

301. Skrabania, K., A. Miasnikova, A. M. Bivigou-Koumba, D. Zehmb and A. Laschewsky, "Examining the UV-Vis Absorption of RAFT Chain Transfer Agents and Their Use for Polymer Analysis", *Polymer Chem*istry, Vol. 2, No. June, pp. 2074-2083, 2011.

302. Catel, Y., M. Degrange, L. Le Pluart, P.-J. Madec, T.-N. Pham, F. Chen and W. D. Cook, "Synthesis, Photopolymerization, and Adhesive Properties of New Bisphosphonic Acid Monomers for Dental Application", *Journal of Polymer Science Part A Polymer Chemistry*, Vol. 47, No. 20, pp. 5258-5271, 2009.

APPENDIX A: SUPPLEMENTARY DATA

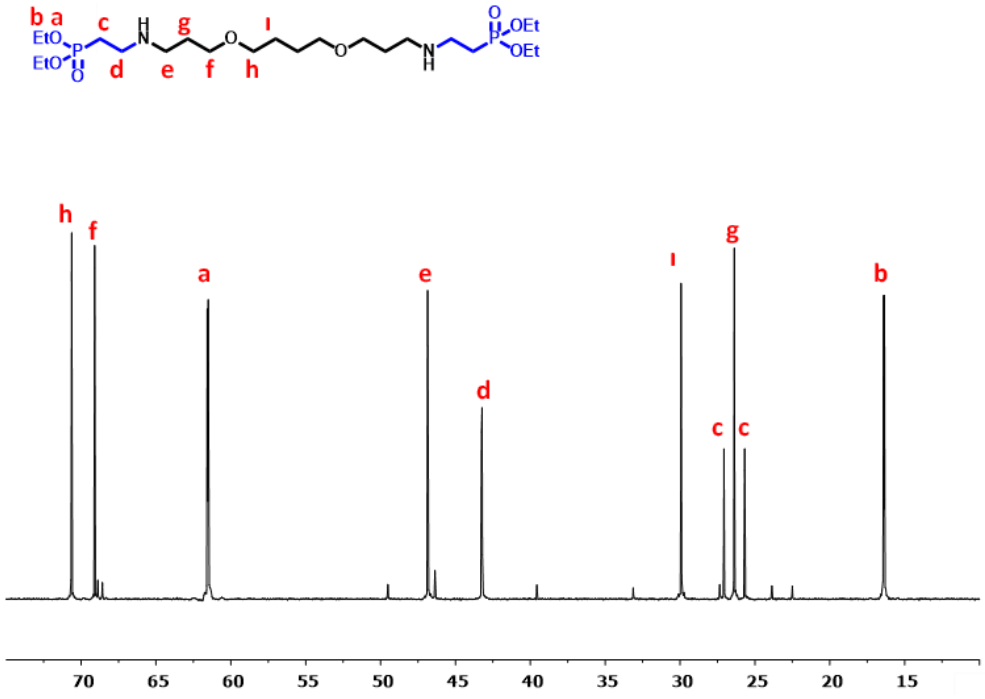

Figure A.1.^{13}C NMR spectrum of PA.

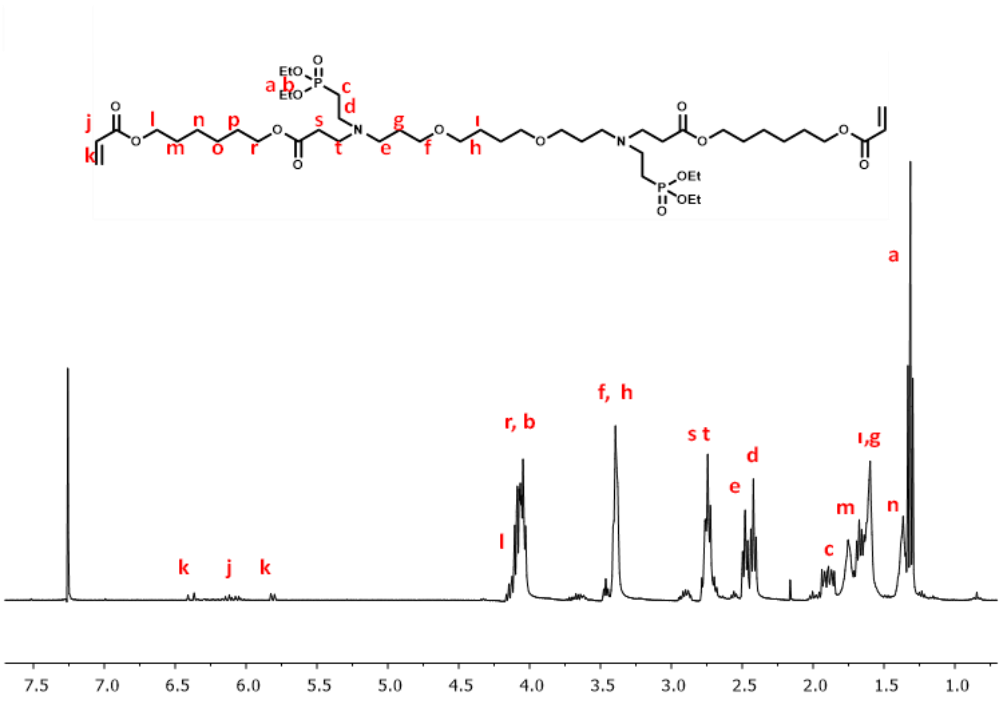

Figure A.2. ^{1}H NMR spectrum of macromer M1.

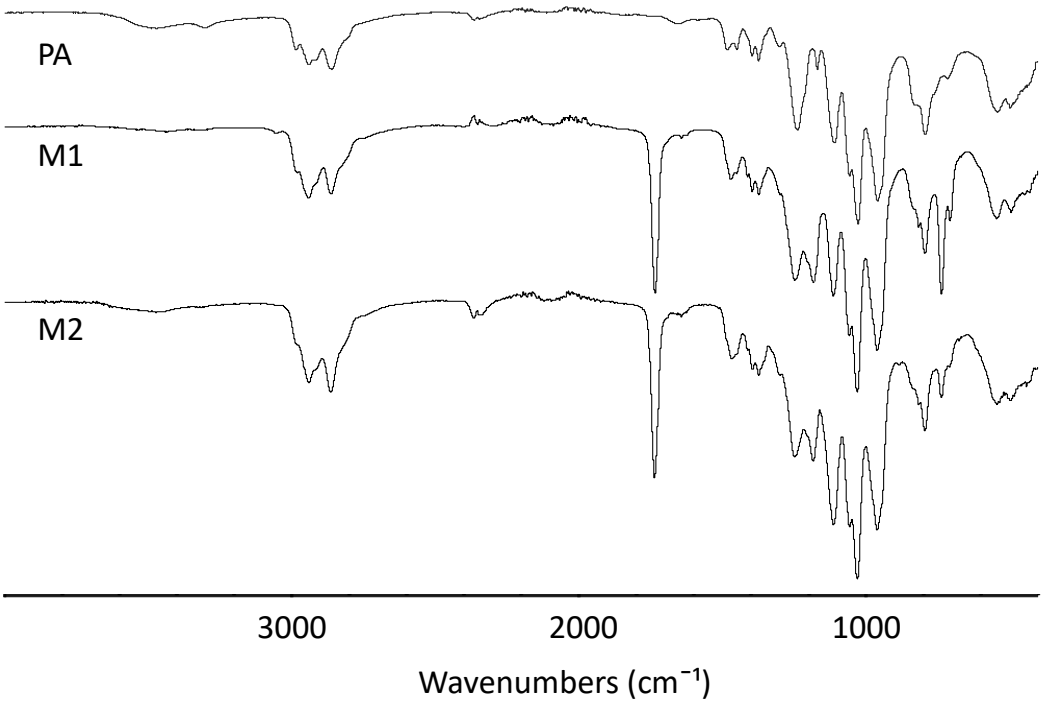

Figure A.3. FTIR spectra of PA, M1 and M2.

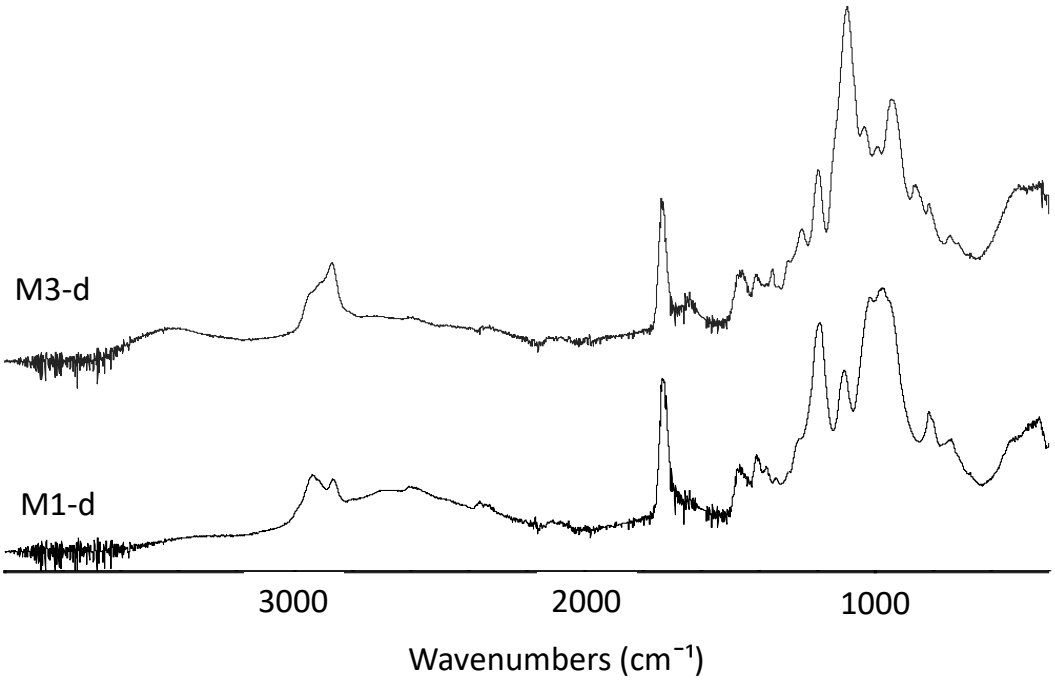

Figure A.4. FTIR spectra of dealkylated macromers M1-d and M3-d.

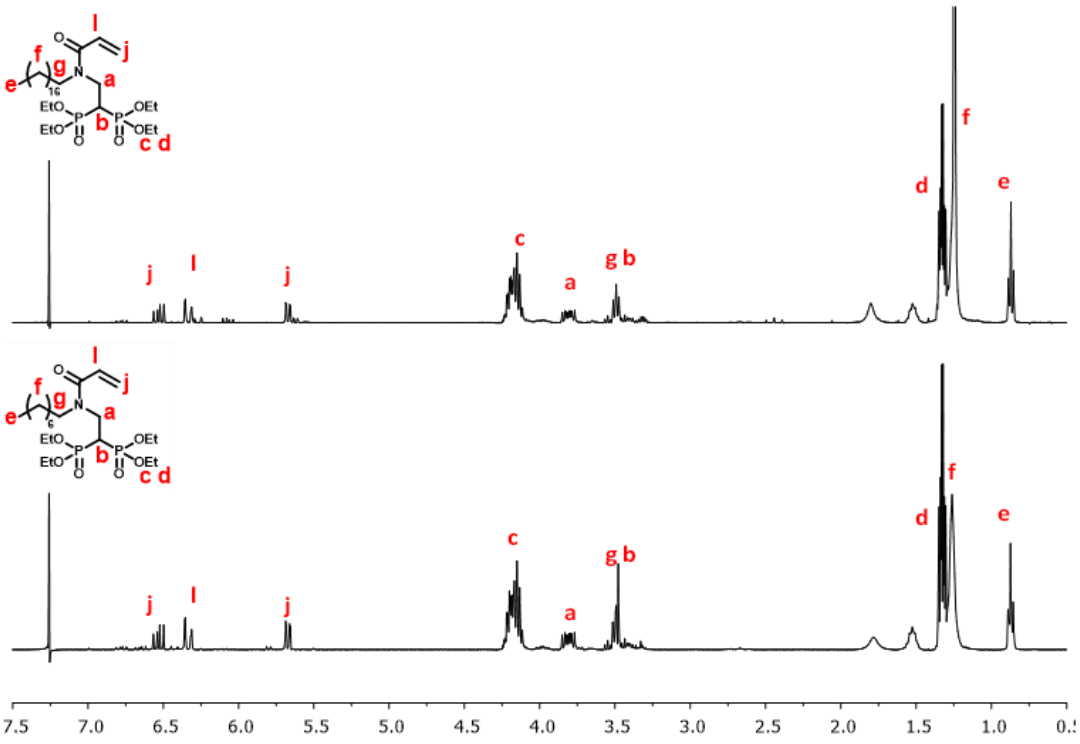

Figure A.5. ^{1}H NMR spectra of acrylamide monomers M2 and M3.

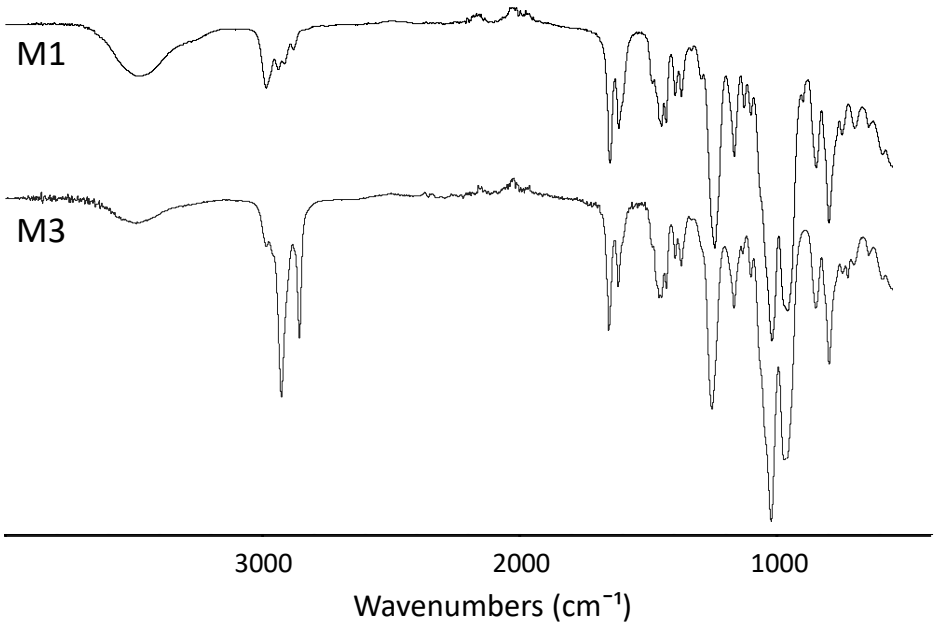

Figure A.6. FTIR spectra of acrylamide monomers M1 and M3.

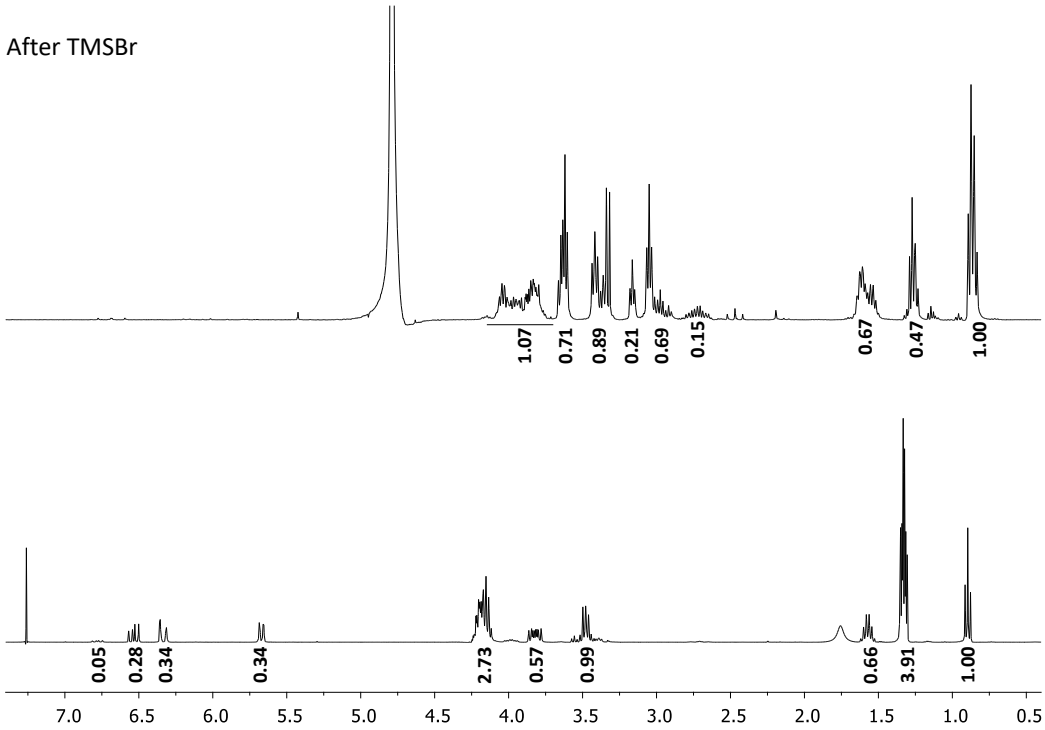

Figure A.7. ^{1}H NMR and integrals of M1 before and after TMSBr dealkylation.

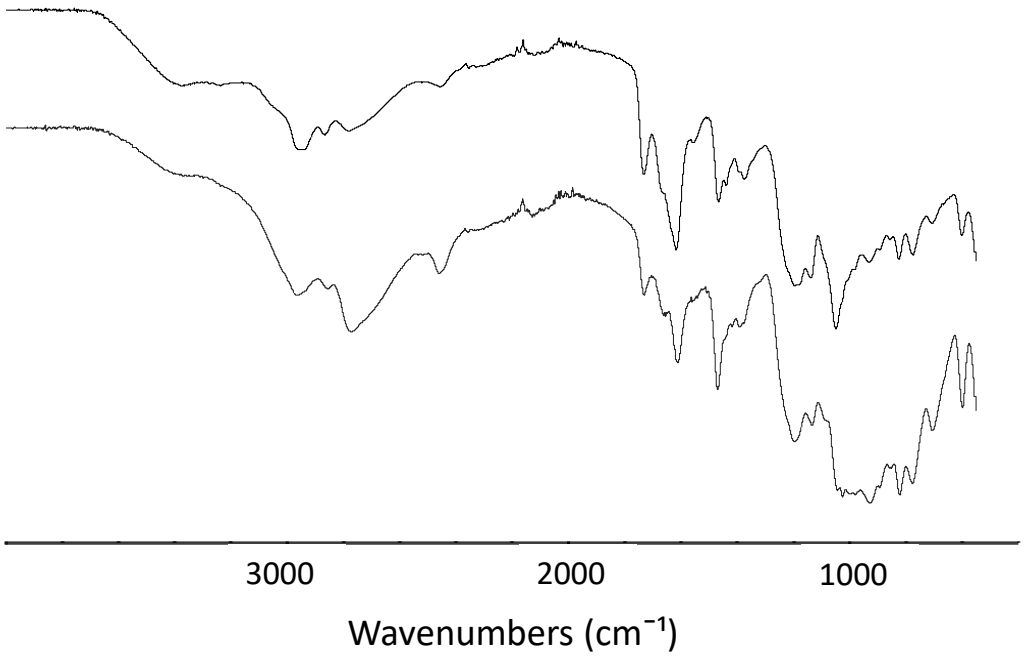

Figure A.8. FTIR spectra of tmsp-P(NIPAM-co-AHA) before and after dialysis (bottom to top).

APPENDIX B: COPY RIGHT LICENCES

Copyrights belonging to figures taken from literature articles can be found below.

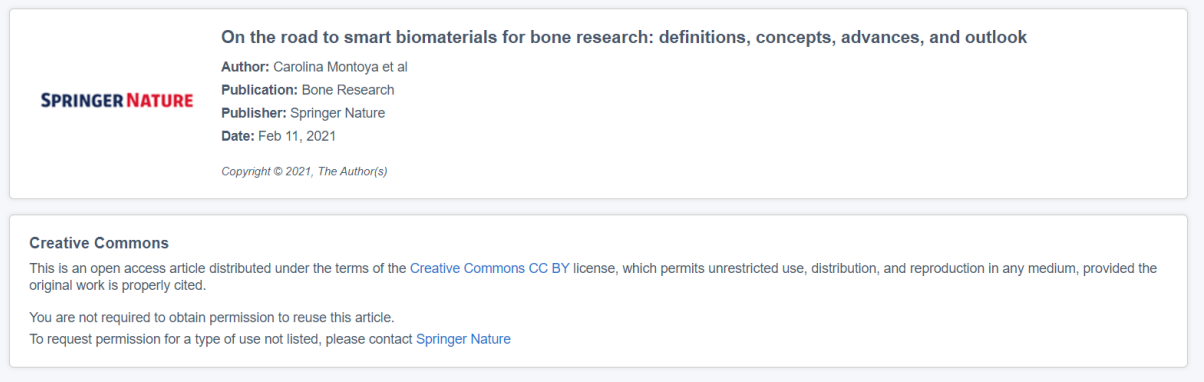

SPRINGER NATURE

On the road to smart biomaterials for bone research: definitions, concepts, advances, and outlook

Author: Carolina Montoya et al
Publication: Bone Research
Publisher: Springer Nature
Date: Feb 11, 2021

Copyright © 2021, The Author(s)

Creative Commons

This is an open access article distributed under the terms of the Creative Commons CC BY license, which permits unrestricted use, distribution, and reproduction in any medium, provided the original work is properly cited.

You are not required to obtain permission to reuse this article.
To request permission for a type of use not listed, please contact Springer Nature

Figure B.1.Permission from [12] Springer Nature, Copyright (2021).

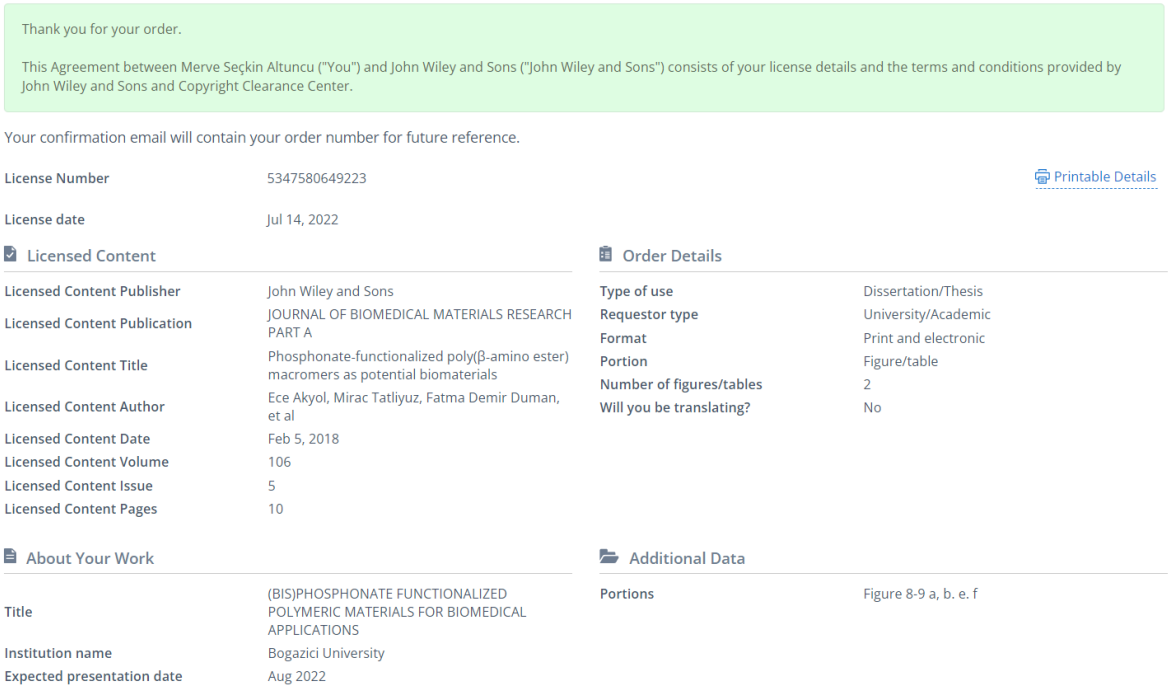

Thank you for your order.

This Agreement between Merve Seçkin Altuncu ("You") and John Wiley and Sons ("John Wiley and Sons") consists of your license details and the terms and conditions provided by John Wiley and Sons and Copyright Clearance Center.

Your confirmation email will contain your order number for future reference.

License Number	5347580649223
License date	Jul 14, 2022

Printable Details

Licensed Content

Licensed Content Publisher	John Wiley and Sons
Licensed Content Publication	JOURNAL OF BIOMEDICAL MATERIALS RESEARCH PART A
Licensed Content Title	Phosphonate-functionalized poly(β-amino ester) macromers as potential biomaterials
Licensed Content Author	Ece Akyol, Mirac Tatliyuz, Fatma Demir Duman, et al
Licensed Content Date	Feb 5, 2018
Licensed Content Volume	106
Licensed Content Issue	5
Licensed Content Pages	10

Order Details

Type of use	Dissertation/Thesis
Requestor type	University/Academic
Format	Print and electronic
Portion	Figure/table
Number of figures/tables	2
Will you be translating?	No

About Your Work

Title	(BIS)PHOSPHONATE FUNCTIONALIZED POLYMERIC MATERIALS FOR BIOMEDICAL APPLICATIONS
Institution name	Bogazici University
Expected presentation date	Aug 2022

Additional Data

Portions	Figure 8-9 a, b. e. f

Figure B.2. Permission from [45] John Wiley and Sons, Copyright (2018).

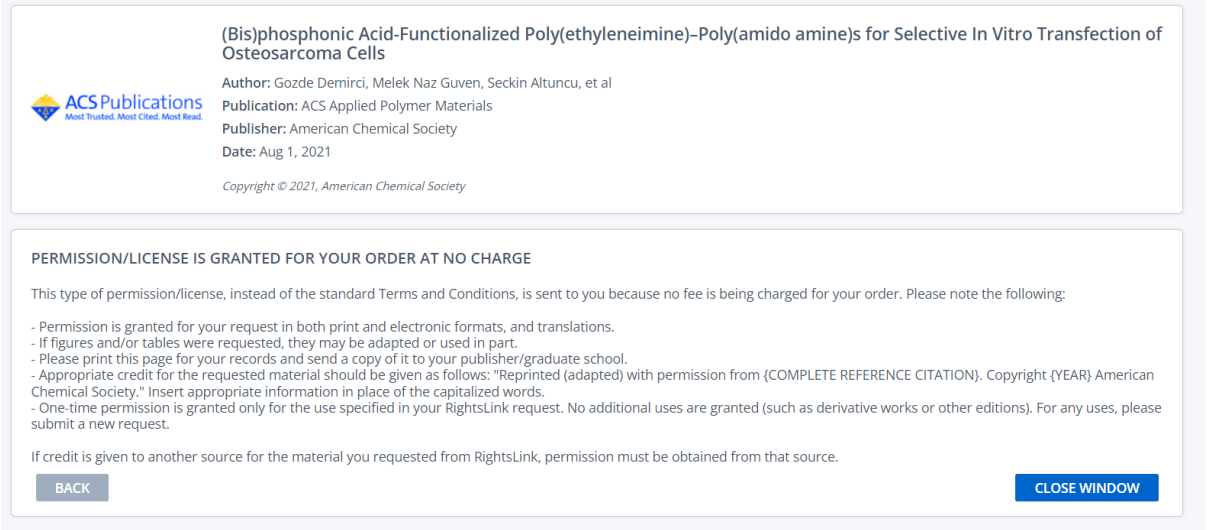

(Bis)phosphonic Acid-Functionalized Poly(ethyleneimine)–Poly(amido amine)s for Selective In Vitro Transfection of Osteosarcoma Cells

Author: Gozde Demirci, Melek Naz Guven, Seckin Altuncu, et al
Publication: ACS Applied Polymer Materials
Publisher: American Chemical Society
Date: Aug 1, 2021

Copyright © 2021, American Chemical Society

PERMISSION/LICENSE IS GRANTED FOR YOUR ORDER AT NO CHARGE

This type of permission/license, instead of the standard Terms and Conditions, is sent to you because no fee is being charged for your order. Please note the following:

- Permission is granted for your request in both print and electronic formats, and translations.
- If figures and/or tables were requested, they may be adapted or used in part.
- Please print this page for your records and send a copy of it to your publisher/graduate school.
- Appropriate credit for the requested material should be given as follows: "Reprinted (adapted) with permission from {COMPLETE REFERENCE CITATION}. Copyright {YEAR} American Chemical Society." Insert appropriate information in place of the capitalized words.
- One-time permission is granted only for the use specified in your RightsLink request. No additional uses are granted (such as derivative works or other editions). For any uses, please submit a new request.

If credit is given to another source for the material you requested from RightsLink, permission must be obtained from that source.

BACK CLOSE WINDOW

Figure B.3. Permission from [79] American Chemical Society, Copyright (2021).

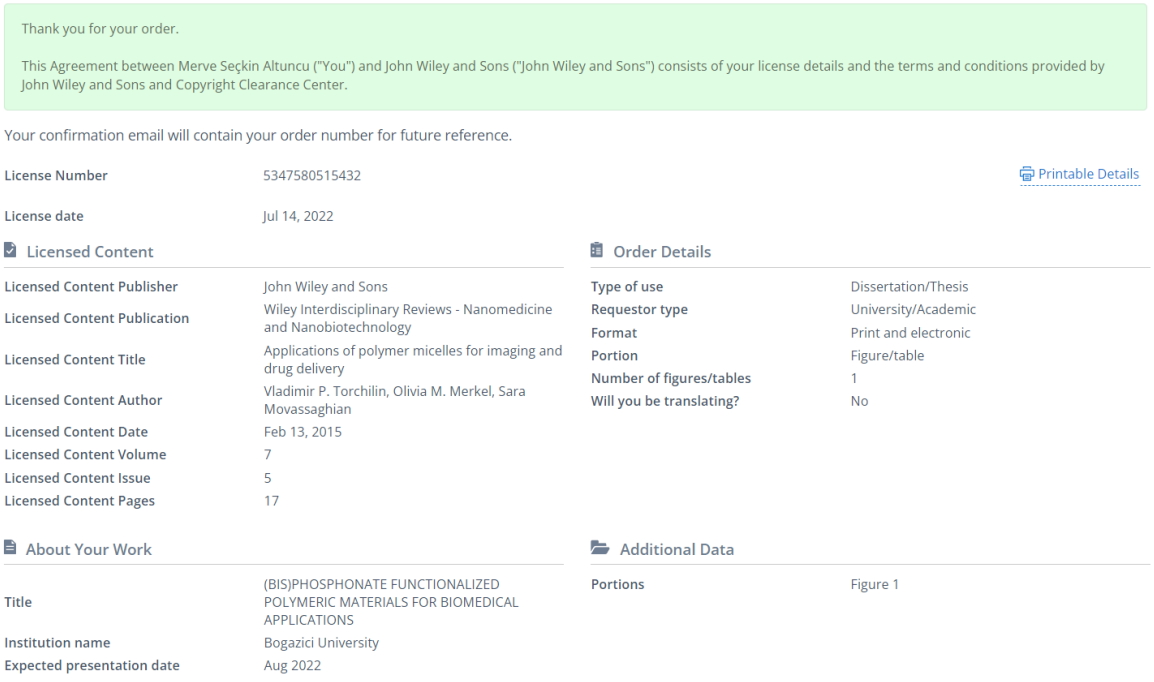

Thank you for your order.

This Agreement between Merve Seçkin Altuncu ("You") and John Wiley and Sons ("John Wiley and Sons") consists of your license details and the terms and conditions provided by John Wiley and Sons and Copyright Clearance Center.

Your confirmation email will contain your order number for future reference.

License Number	5347580515432
License date	Jul 14, 2022

Printable Details

Licensed Content

Licensed Content Publisher	John Wiley and Sons
Licensed Content Publication	Wiley Interdisciplinary Reviews - Nanomedicine and Nanobiotechnology
Licensed Content Title	Applications of polymer micelles for imaging and drug delivery
Licensed Content Author	Vladimir P. Torchilin, Olivia M. Merkel, Sara Movassaghian
Licensed Content Date	Feb 13, 2015
Licensed Content Volume	7
Licensed Content Issue	5
Licensed Content Pages	17

Order Details

Type of use	Dissertation/Thesis
Requestor type	University/Academic
Format	Print and electronic
Portion	Figure/table
Number of figures/tables	1
Will you be translating?	No

About Your Work

Title	(BIS)PHOSPHONATE FUNCTIONALIZED POLYMERIC MATERIALS FOR BIOMEDICAL APPLICATIONS
Institution name	Bogazici University
Expected presentation date	Aug 2022

Additional Data

Portions	Figure 1

Figure B.4. Permission from [81] John Wiley and Sons, Copyright (2015).

LICENSED CONTENT

Publication Title	Nanoscale	**Publication Type**	e-Journal
Article Title	Esterase- and pH-responsive poly(β-amino ester)-capped mesoporous silica nanoparticles for drug delivery.	**Start Page**	7178
		End Page	7183
Author/Editor	National Center for Nanoscience and Technology., Royal Society of Chemistry (Great Britain)	**Issue**	16
		Volume	7
Date	01/01/2009	**URL**	http://www.rsc.org/Publishing/Journal...
Language	English		
Country	United Kingdom of Great Britain and Northern Ireland		
Rightsholder	Royal Society of Chemistry		

REQUEST DETAILS

Portion Type	Chart/graph/table/figure	**Distribution**	Worldwide
Number of charts / graphs / tables / figures requested	1	**Translation**	Original language of publication
		Copies for the disabled?	No
Format (select all that apply)	Print, Electronic	**Minor editing privileges?**	No
Who will republish the content?	Not-for-profit entity	**Incidental promotional use?**	Yes
Duration of Use	Life of current edition	**Currency**	USD
Lifetime Unit Quantity	Up to 499		
Rights Requested	Main product		

NEW WORK DETAILS

Title	(BIS)PHOSPHONATE FUNCTIONALIZED POLYMERIC MATERIALS FOR BIOMEDICAL APPLICATIONS	**Institution name**	Bogazici University
		Expected presentation date	2022-08-23
Instructor name	Merve Seçkin Altuncu		

ADDITIONAL DETAILS

Order reference number	N/A	**The requesting person / organization to appear on the license**	Merve Seçkin Altuncu

REUSE CONTENT DETAILS

Title, description or numeric reference of the portion(s)	Figure 1	**Title of the article/chapter the portion is from**	Esterase- and pH-responsive poly(β-amino ester)-capped mesoporous silica nanoparticles for drug delivery.
Editor of portion(s)	Fernando, Isurika R; Ferris, Daniel P; Frasconi, Marco; Malin, Dmitry; Strekalova, Elena; Yilmaz, M Deniz; Ambrogio, Michael W; Algaradah, Mohammed M; Hong, Michael P; Chen, Xinqi; Nassar, Majed S; Botros, Youssry Y; Cryns, Vincent L; Stoddart, J Fraser	**Author of portion(s)**	Fernando, Isurika R; Ferris, Daniel P; Frasconi, Marco; Malin, Dmitry; Strekalova, Elena; Yilmaz, M Deniz; Ambrogio, Michael W; Algaradah, Mohammed M; Hong, Michael P; Chen, Xinqi; Nassar, Majed S; Botros, Youssry Y; Cryns, Vincent L; Stoddart, J Fraser
Volume of serial or monograph	7		
Page or page range of portion	7178-7183	**Issue, if republishing an article from a serial**	16
		Publication date of portion	2015-04-28

Figure B.5. Permission from [93] Royal Society of Chemistry, Copyright (2009).

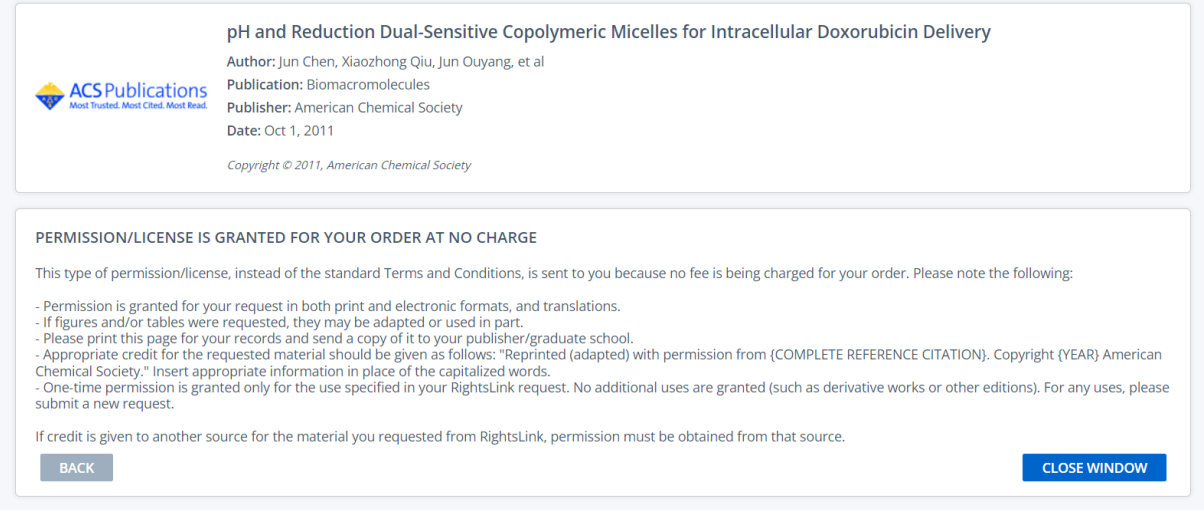

pH and Reduction Dual-Sensitive Copolymeric Micelles for Intracellular Doxorubicin Delivery

Author: Jun Chen, Xiaozhong Qiu, Jun Ouyang, et al
Publication: Biomacromolecules
Publisher: American Chemical Society
Date: Oct 1, 2011

Copyright © 2011, American Chemical Society

PERMISSION/LICENSE IS GRANTED FOR YOUR ORDER AT NO CHARGE

This type of permission/license, instead of the standard Terms and Conditions, is sent to you because no fee is being charged for your order. Please note the following:

- Permission is granted for your request in both print and electronic formats, and translations.
- If figures and/or tables were requested, they may be adapted or used in part.
- Please print this page for your records and send a copy of it to your publisher/graduate school.
- Appropriate credit for the requested material should be given as follows: "Reprinted (adapted) with permission from {COMPLETE REFERENCE CITATION}. Copyright {YEAR} American Chemical Society." Insert appropriate information in place of the capitalized words.
- One-time permission is granted only for the use specified in your RightsLink request. No additional uses are granted (such as derivative works or other editions). For any uses, please submit a new request.

If credit is given to another source for the material you requested from RightsLink, permission must be obtained from that source.

BACK CLOSE WINDOW

Figure B.6. Permission from [98] American Chemical Society, Copyright (2011).

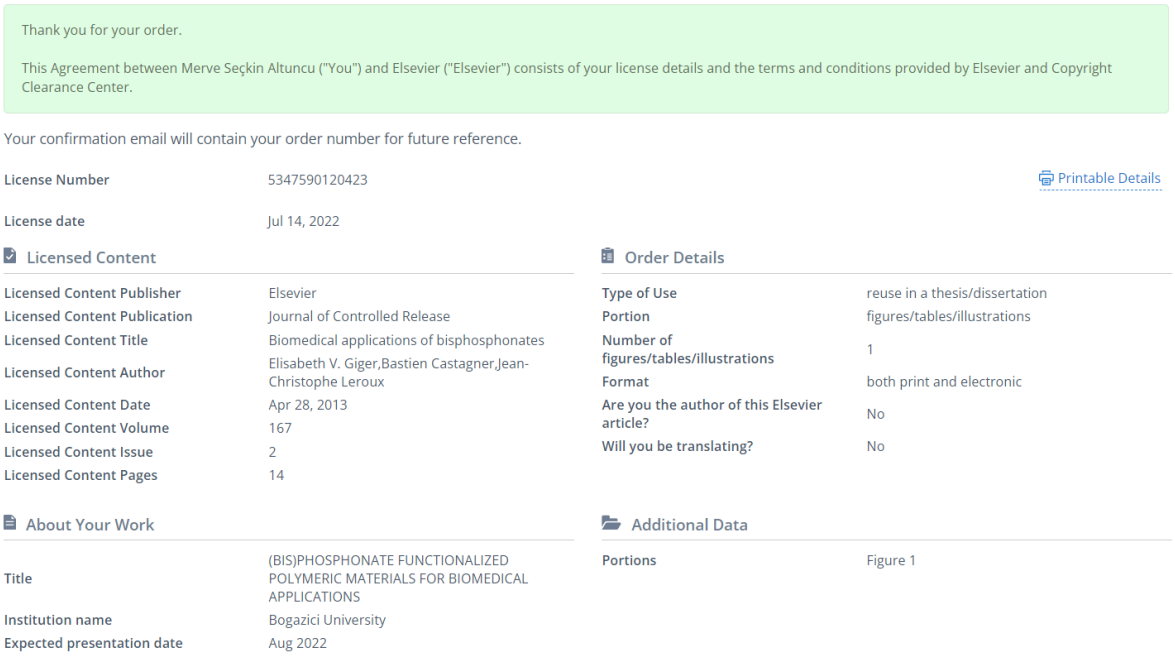

Thank you for your order.

This Agreement between Merve Seçkin Altuncu ("You") and Elsevier ("Elsevier") consists of your license details and the terms and conditions provided by Elsevier and Copyright Clearance Center.

Your confirmation email will contain your order number for future reference.

License Number	5347590120423
License date	Jul 14, 2022

Printable Details

Licensed Content

Licensed Content Publisher	Elsevier
Licensed Content Publication	Journal of Controlled Release
Licensed Content Title	Biomedical applications of bisphosphonates
Licensed Content Author	Elisabeth V. Giger,Bastien Castagner,Jean-Christophe Leroux
Licensed Content Date	Apr 28, 2013
Licensed Content Volume	167
Licensed Content Issue	2
Licensed Content Pages	14

Order Details

Type of Use	reuse in a thesis/dissertation
Portion	figures/tables/illustrations
Number of figures/tables/illustrations	1
Format	both print and electronic
Are you the author of this Elsevier article?	No
Will you be translating?	No

About Your Work

Title	(BIS)PHOSPHONATE FUNCTIONALIZED POLYMERIC MATERIALS FOR BIOMEDICAL APPLICATIONS
Institution name	Bogazici University
Expected presentation date	Aug 2022

Additional Data

Portions	Figure 1

Figure B.7. Permission from [112], Elsevier, Copyright (2013).

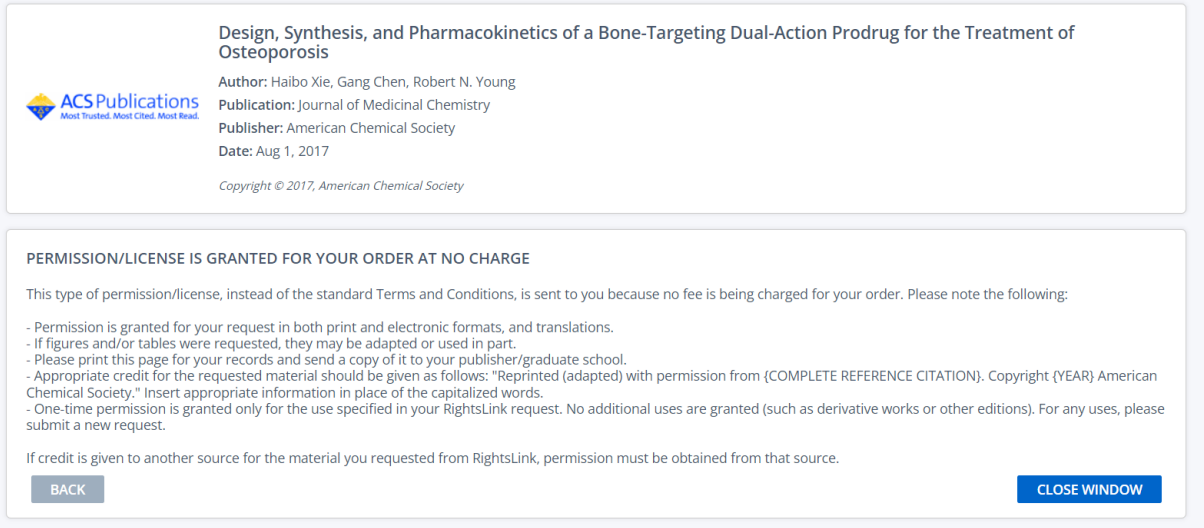

Design, Synthesis, and Pharmacokinetics of a Bone-Targeting Dual-Action Prodrug for the Treatment of Osteoporosis

Author: Haibo Xie, Gang Chen, Robert N. Young
Publication: Journal of Medicinal Chemistry
Publisher: American Chemical Society
Date: Aug 1, 2017

Copyright © 2017, American Chemical Society

PERMISSION/LICENSE IS GRANTED FOR YOUR ORDER AT NO CHARGE

This type of permission/license, instead of the standard Terms and Conditions, is sent to you because no fee is being charged for your order. Please note the following:

- Permission is granted for your request in both print and electronic formats, and translations.
- If figures and/or tables were requested, they may be adapted or used in part.
- Please print this page for your records and send a copy of it to your publisher/graduate school.
- Appropriate credit for the requested material should be given as follows: "Reprinted (adapted) with permission from {COMPLETE REFERENCE CITATION}. Copyright {YEAR} American Chemical Society." Insert appropriate information in place of the capitalized words.
- One-time permission is granted only for the use specified in your RightsLink request. No additional uses are granted (such as derivative works or other editions). For any uses, please submit a new request.

If credit is given to another source for the material you requested from RightsLink, permission must be obtained from that source.

BACK CLOSE WINDOW

Figure B.8. Permission from [122] Elsevier, American Chemical Society (2017).

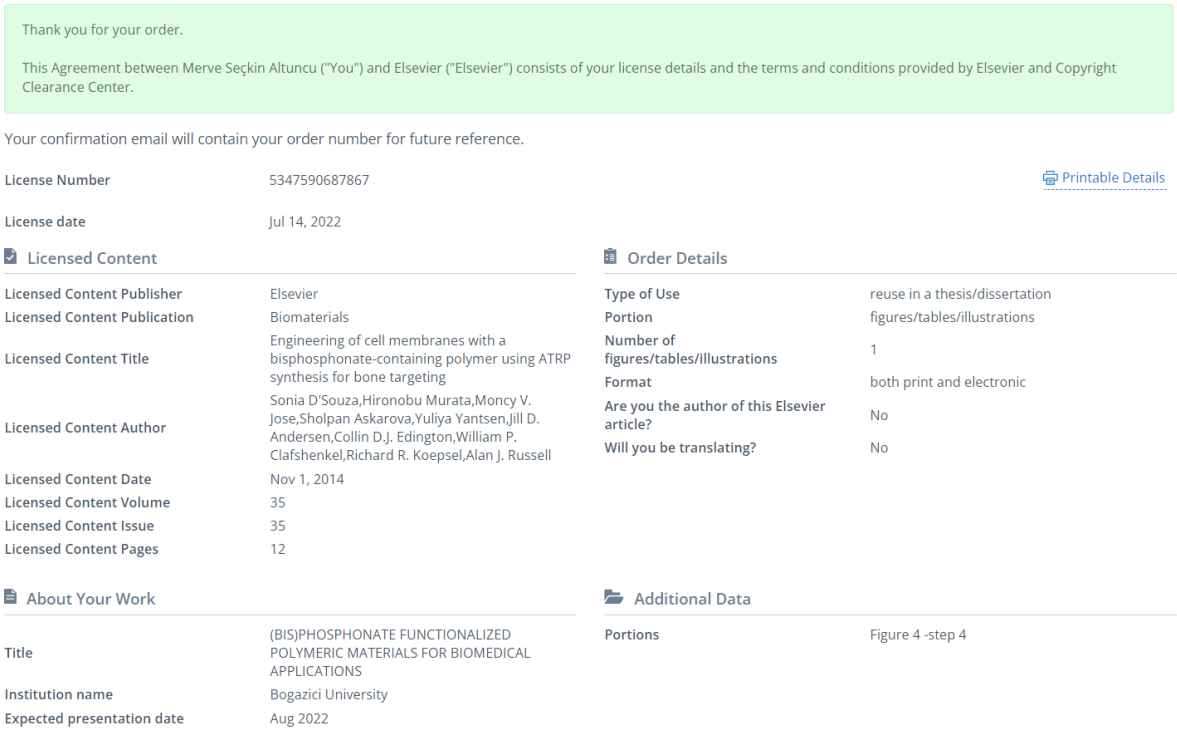

Thank you for your order.

This Agreement between Merve Seçkin Altuncu ("You") and Elsevier ("Elsevier") consists of your license details and the terms and conditions provided by Elsevier and Copyright Clearance Center.

Your confirmation email will contain your order number for future reference.

Printable Details

License Number	5347590687867
License date	Jul 14, 2022

Licensed Content

Licensed Content Publisher	Elsevier
Licensed Content Publication	Biomaterials
Licensed Content Title	Engineering of cell membranes with a bisphosphonate-containing polymer using ATRP synthesis for bone targeting
Licensed Content Author	Sonia D'Souza,Hironobu Murata,Moncy V. Jose,Sholpan Askarova,Yuliya Yantsen,Jill D. Andersen,Collin D.J. Edington,William P. Clafshenkel,Richard R. Koepsel,Alan J. Russell
Licensed Content Date	Nov 1, 2014
Licensed Content Volume	35
Licensed Content Issue	35
Licensed Content Pages	12

Order Details

Type of Use	reuse in a thesis/dissertation
Portion	figures/tables/illustrations
Number of figures/tables/illustrations	1
Format	both print and electronic
Are you the author of this Elsevier article?	No
Will you be translating?	No

About Your Work

Title	(BIS)PHOSPHONATE FUNCTIONALIZED POLYMERIC MATERIALS FOR BIOMEDICAL APPLICATIONS
Institution name	Bogazici University
Expected presentation date	Aug 2022

Additional Data

Portions	Figure 4 -step 4

Figure B.9. Permission from [130] Elsevier, Copyright (2014).

Thank you for your order.

This Agreement between Merve Seçkin Altuncu ("You") and Elsevier ("Elsevier") consists of your license details and the terms and conditions provided by Elsevier and Copyright Clearance Center.

Your confirmation email will contain your order number for future reference.

License Number	5347590855308
License date	Jul 14, 2022

Printable Details

Licensed Content

Licensed Content Publisher	Elsevier
Licensed Content Publication	International Journal of Pharmaceutics
Licensed Content Title	Calcium phosphate nanoparticles functionalized with alendronate-conjugated polyethylene glycol (PEG) for the treatment of bone metastasis
Licensed Content Author	Weijing Chu,Yanjuan Huang,Chanzhen Yang,Yunhui Liao,Xuefei Zhang,Mina Yan,Shengmiao Cui,Chunshun Zhao
Licensed Content Date	Jan 10, 2017
Licensed Content Volume	516
Licensed Content Issue	1-2
Licensed Content Pages	12

Order Details

Type of Use	reuse in a thesis/dissertation
Portion	figures/tables/illustrations
Number of figures/tables/illustrations	1
Format	both print and electronic
Are you the author of this Elsevier article?	No
Will you be translating?	No

About Your Work

Title	(BIS)PHOSPHONATE FUNCTIONALIZED POLYMERIC MATERIALS FOR BIOMEDICAL APPLICATIONS
Institution name	Bogazici University
Expected presentation date	Aug 2022

Additional Data

Portions	Graphical Abstract

Figure B.10. Permission from [136] Elsevier, Copyright (2017).

Thank you for your order.

This Agreement between Merve Seçkin Altuncu ("You") and Elsevier ("Elsevier") consists of your license details and the terms and conditions provided by Elsevier and Copyright Clearance Center.

Your confirmation email will contain your order number for future reference.

License Number	5347591061134
License date	Jul 14, 2022

Printable Details

Licensed Content

Licensed Content Publisher	Elsevier
Licensed Content Publication	Acta Biomaterialia
Licensed Content Title	New developments in polymer-controlled, bioinspired calcium phosphate mineralization from aqueous solution
Licensed Content Author	Katrin Bleek,Andreas Taubert
Licensed Content Date	May 1, 2013
Licensed Content Volume	9
Licensed Content Issue	5
Licensed Content Pages	39

Order Details

Type of Use	reuse in a thesis/dissertation
Portion	figures/tables/illustrations
Number of figures/tables/illustrations	1
Format	both print and electronic
Are you the author of this Elsevier article?	No
Will you be translating?	No

About Your Work

Title	(BIS)PHOSPHONATE FUNCTIONALIZED POLYMERIC MATERIALS FOR BIOMEDICAL APPLICATIONS
Institution name	Bogazici University
Expected presentation date	Aug 2022

Additional Data

Portions	Figure 1

Figure B.11. Permission from [144] Elsevier, Copyright (2013).

LICENSED CONTENT

Publication Title	Journal of materials chemistry. B, Materials for biology and medicine	**Publication Type**	e-Journal
Article Title	Thermoresponsive hydrogels based on a phosphorylated star-shaped copolymer: mimicking the extracellular matrix for in situ bone repair.	**Start Page**	428
		End Page	434
		Issue	3
		Volume	5
Author/Editor	Royal Society of Chemistry (Great Britain)	**URL**	http://pubs.rsc.org/en/journals/journ...
Date	01/01/2013		
Language	English		
Country	United Kingdom of Great Britain and Northern Ireland		
Rightsholder	Royal Society of Chemistry		

REQUEST DETAILS

Portion Type	Chart/graph/table/figure	**Distribution**	Worldwide
Number of charts / graphs / tables / figures requested	2	**Translation**	Original language of publication
		Copies for the disabled?	No
Format (select all that apply)	Print, Electronic	**Minor editing privileges?**	No
Who will republish the content?	Not-for-profit entity	**Incidental promotional use?**	Yes
Duration of Use	Life of current edition	**Currency**	USD
Lifetime Unit Quantity	Up to 499		
Rights Requested	Main product		

NEW WORK DETAILS

Title	(BIS)PHOSPHONATE FUNCTIONALIZED POLYMERIC MATERIALS FOR BIOMEDICAL APPLICATIONS	**Institution name**	Bogazici University
		Expected presentation date	2022-08-23
Instructor name	Merve Seçkin Altuncu		

ADDITIONAL DETAILS

Order reference number	N/A	**The requesting person / organization to appear on the license**	Merve Seçkin Altuncu

REUSE CONTENT DETAILS

Title, description or numeric reference of the portion(s)	Figure 1, 3 b and c	**Title of the article/chapter the portion is from**	Thermoresponsive hydrogels based on a phosphorylated star-shaped copolymer: mimicking the extracellular matrix for in situ bone repair.
Editor of portion(s)	Wu, Wei; Lin, Zaifu; Liu, Yanpeng; Xu, Xinyuan; Ding, Chunmei; Li, Jianshu	**Author of portion(s)**	Wu, Wei; Lin, Zaifu; Liu, Yanpeng; Xu, Xinyuan; Ding, Chunmei; Li, Jianshu
Volume of serial or monograph	5	**Issue, if republishing an article from a serial**	3
Page or page range of portion	428-434	**Publication date of portion**	2017-01-21

Figure B.12. Permission from [168] Royal Society of Chemistry, Copyright (2013).

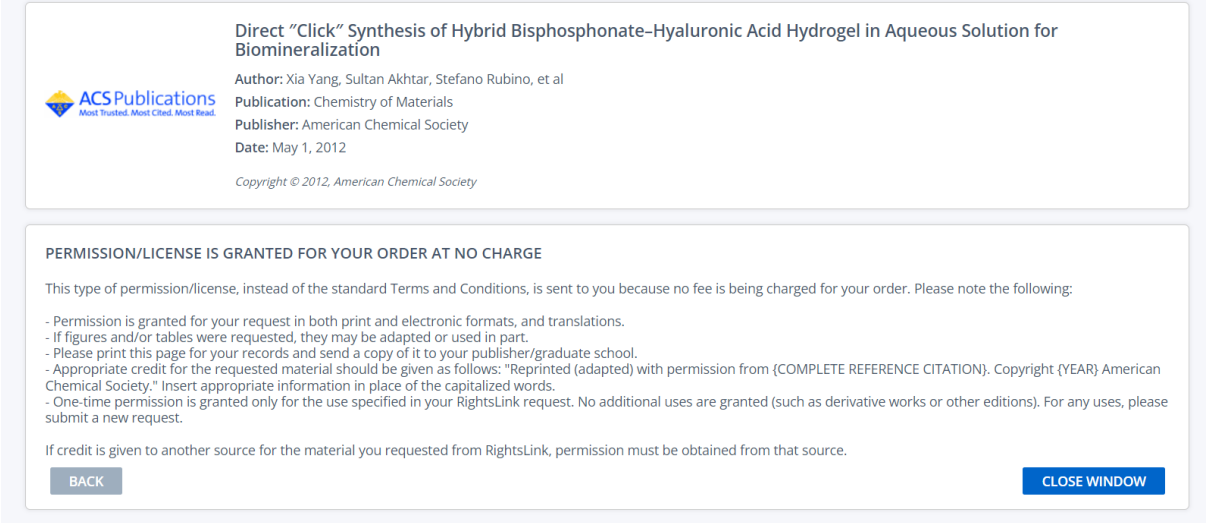

Direct ″Click″ Synthesis of Hybrid Bisphosphonate–Hyaluronic Acid Hydrogel in Aqueous Solution for Biomineralization

Author: Xia Yang, Sultan Akhtar, Stefano Rubino, et al
Publication: Chemistry of Materials
Publisher: American Chemical Society
Date: May 1, 2012

Copyright © 2012, American Chemical Society

PERMISSION/LICENSE IS GRANTED FOR YOUR ORDER AT NO CHARGE

This type of permission/license, instead of the standard Terms and Conditions, is sent to you because no fee is being charged for your order. Please note the following:

- Permission is granted for your request in both print and electronic formats, and translations.
- If figures and/or tables were requested, they may be adapted or used in part.
- Please print this page for your records and send a copy of it to your publisher/graduate school.
- Appropriate credit for the requested material should be given as follows: "Reprinted (adapted) with permission from {COMPLETE REFERENCE CITATION}. Copyright {YEAR} American Chemical Society." Insert appropriate information in place of the capitalized words.
- One-time permission is granted only for the use specified in your RightsLink request. No additional uses are granted (such as derivative works or other editions). For any uses, please submit a new request.

If credit is given to another source for the material you requested from RightsLink, permission must be obtained from that source.

BACK CLOSE WINDOW

Figure B.13. Permission from [142] American Chemical Society, Copyright (2012).

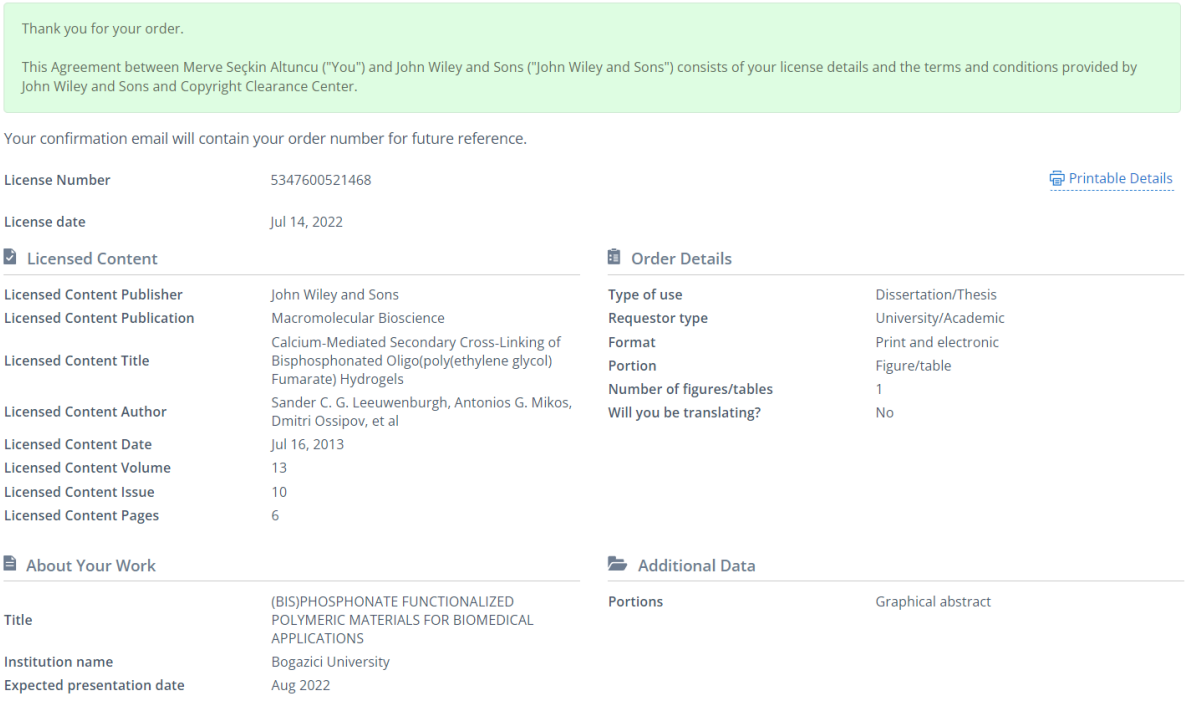

Thank you for your order.

This Agreement between Merve Seçkin Altuncu ("You") and John Wiley and Sons ("John Wiley and Sons") consists of your license details and the terms and conditions provided by John Wiley and Sons and Copyright Clearance Center.

Your confirmation email will contain your order number for future reference.

License Number	5347600521468
License date	Jul 14, 2022

Printable Details

Licensed Content

Licensed Content Publisher	John Wiley and Sons
Licensed Content Publication	Macromolecular Bioscience
Licensed Content Title	Calcium-Mediated Secondary Cross-Linking of Bisphosphonated Oligo(poly(ethylene glycol) Fumarate) Hydrogels
Licensed Content Author	Sander C. G. Leeuwenburgh, Antonios G. Mikos, Dmitri Ossipov, et al
Licensed Content Date	Jul 16, 2013
Licensed Content Volume	13
Licensed Content Issue	10
Licensed Content Pages	6

Order Details

Type of use	Dissertation/Thesis
Requestor type	University/Academic
Format	Print and electronic
Portion	Figure/table
Number of figures/tables	1
Will you be translating?	No

About Your Work

Title	(BIS)PHOSPHONATE FUNCTIONALIZED POLYMERIC MATERIALS FOR BIOMEDICAL APPLICATIONS
Institution name	Bogazici University
Expected presentation date	Aug 2022

Additional Data

Portions	Graphical abstract

Figure B.14. Permission from [176] John Wiley and Sons, Copyright (2013).

LICENSED CONTENT

Publication Title	Chemical communications	Rightsholder	Royal Society of Chemistry
Article Title	"Smart" drug loaded nanoparticle delivery from a self-healing hydrogel enabled by dynamic magnesium-biopolymer chemistry.	Publication Type	e-Journal
		Start Page	11151
		End Page	11154
Author/Editor	Royal Society of Chemistry (Great Britain)	Issue	74
		Volume	52
Date	01/01/1996		
Language	English		
Country	United Kingdom of Great Britain and Northern Ireland		

REQUEST DETAILS

Portion Type	Chart/graph/table/figure	Distribution	Worldwide
Number of charts / graphs / tables / figures requested	2	Translation	Original language of publication
		Copies for the disabled?	No
Format (select all that apply)	Print, Electronic	Minor editing privileges?	No
Who will republish the content?	Not-for-profit entity	Incidental promotional use?	Yes
Duration of Use	Life of current edition	Currency	USD
Lifetime Unit Quantity	Up to 499		
Rights Requested	Main product		

NEW WORK DETAILS

Title	(BIS)PHOSPHONATE FUNCTIONALIZED POLYMERIC MATERIALS FOR BIOMEDICAL APPLICATIONS	Institution name	Bogazici University
		Expected presentation date	2022-08-23
Instructor name	Merve Seçkin Altuncu		

ADDITIONAL DETAILS

Order reference number	N/A	The requesting person / organization to appear on the license	Merve Seçkin Altuncu

REUSE CONTENT DETAILS

Title, description or numeric reference of the portion(s)	Figure 1, 2 a-b	Title of the article/chapter the portion is from	"Smart" drug loaded nanoparticle delivery from a self-healing hydrogel enabled by dynamic magnesium-biopolymer chemistry.
Editor of portion(s)	Shi, Liyang; Han, Yuanyuan; Hilborn, Jöns; Ossipov, Dmitri	Author of portion(s)	Shi, Liyang; Han, Yuanyuan; Hilborn, Jöns; Ossipov, Dmitri
Volume of serial or monograph	52	Issue, if republishing an article from a serial	74
Page or page range of portion	11151-11154	Publication date of portion	2016-09-25

Figure B.15. Permission from [186] Royal Society of Chemisty, Copyright (2016).

Thank you for your order.

This Agreement between Merve Seçkin Altuncu ("You") and John Wiley and Sons ("John Wiley and Sons") consists of your license details and the terms and conditions provided by John Wiley and Sons and Copyright Clearance Center.

Your confirmation email will contain your order number for future reference.

License Number	5347610140167
License date	Jul 14, 2022

Printable Details

Licensed Content

Licensed Content Publisher	John Wiley and Sons
Licensed Content Publication	Advanced Functional Materials
Licensed Content Title	Self-Healing Silk Fibroin-Based Hydrogel for Bone Regeneration: Dynamic Metal-Ligand Self-Assembly Approach
Licensed Content Author	Dmitri A. Ossipov, Xisheng Weng, Yingjie Wang, et al
Licensed Content Date	Aug 2, 2017
Licensed Content Volume	27
Licensed Content Issue	37
Licensed Content Pages	14

Order Details

Type of use	Dissertation/Thesis
Requestor type	University/Academic
Format	Print and electronic
Portion	Figure/table
Number of figures/tables	3
Will you be translating?	No

About Your Work

Title	(BIS)PHOSPHONATE FUNCTIONALIZED POLYMERIC MATERIALS FOR BIOMEDICAL APPLICATIONS
Institution name	Bogazici University
Expected presentation date	Aug 2022

Additional Data

Portions	Figure 1, 3, 4 b and c

Figure B.16. Permission from [188] John Wiley and Sons, Copyright (2017).

Thank you for your order.

This Agreement between Merve Seçkin Altuncu ("You") and Elsevier ("Elsevier") consists of your license details and the terms and conditions provided by Elsevier and Copyright Clearance Center.

Your confirmation email will contain your order number for future reference.

License Number	5347610856967
License date	Jul 14, 2022

Printable Details

Licensed Content

Licensed Content Publisher	Elsevier
Licensed Content Publication	Acta Biomaterialia
Licensed Content Title	Modulated regeneration of acid-etched human tooth enamel by a functionalized dendrimer that is an analog of amelogenin
Licensed Content Author	Mei Chen,Jiaojiao Yang,Jiyao Li,Kunneng Liang,Libang He,Zaifu Lin,Xingyu Chen,Xiaokang Ren,Jianshu Li
Licensed Content Date	Oct 1, 2014
Licensed Content Volume	10
Licensed Content Issue	10
Licensed Content Pages	10

Order Details

Type of Use	reuse in a thesis/dissertation
Portion	figures/tables/illustrations
Number of figures/tables/illustrations	1
Format	both print and electronic
Are you the author of this Elsevier article?	No
Will you be translating?	No

About Your Work

Title	(BIS)PHOSPHONATE FUNCTIONALIZED POLYMERIC MATERIALS FOR BIOMEDICAL APPLICATIONS
Institution name	Bogazici University
Expected presentation date	Aug 2022

Additional Data

Portions	Figure 1

Figure B.17. Permission from [210] Elsevier, Copyright (2014).

LICENSED CONTENT

Publication Title	Polymer chemistry	Publication Type	e-Journal
Article Title	Smart functionalized phosphonic acid based copolymers: new structures for old purposes	Start Page	3237
		End Page	3250
Author/Editor	Royal Society of Chemistry (Great Britain)	Issue	18
		Volume	11
Date	01/01/2010	URL	http://www.rsc.org/Publishing/Journal...
Language	English		
Country	United Kingdom of Great Britain and Northern Ireland		
Rightsholder	Royal Society of Chemistry		

REQUEST DETAILS

Portion Type	Chart/graph/table/figure	Distribution	Worldwide
Number of charts / graphs / tables / figures requested	1	Translation	Original language of publication
		Copies for the disabled?	No
Format (select all that apply)	Print, Electronic	Minor editing privileges?	No
Who will republish the content?	Not-for-profit entity	Incidental promotional use?	No
Duration of Use	Life of current edition	Currency	USD
Lifetime Unit Quantity	Up to 499		
Rights Requested	Main product		

NEW WORK DETAILS

Title	(BIS)PHOSPHONATE FUNCTIONALIZED POLYMERIC MATERIALS FOR BIOMEDICAL APPLICATIONS	Institution name	Bogazici University
		Expected presentation date	2022-08-23
Instructor name	Merve Seçkin Altuncu		

ADDITIONAL DETAILS

Order reference number	N/A	The requesting person / organization to appear on the license	Merve Seçkin Altuncu

REUSE CONTENT DETAILS

Title, description or numeric reference of the portion(s)	Graphical abstract	Title of the article/chapter the portion is from	Smart functionalized phosphonic acid based copolymers: new structures for old purposes
Editor of portion(s)	Solimando, Xavier; Catel, Yohann; Moszner, Norbert; Robin, Jean-Jacques; Monge, Sophie	Author of portion(s)	Solimando, Xavier; Catel, Yohann; Moszner, Norbert; Robin, Jean-Jacques; Monge, Sophie
Volume of serial or monograph	11		
Page or page range of portion	3237-3250	Issue, if republishing an article from a serial	18
		Publication date of portion	2020-01-01

Print License

Figure B.18. Permission from [202] Royal Society of Chemisty, Copyright (2020).

Thank you for your order.

This Agreement between Merve Seçkin Altuncu ("You") and John Wiley and Sons ("John Wiley and Sons") consists of your license details and the terms and conditions provided by John Wiley and Sons and Copyright Clearance Center.

Your confirmation email will contain your order number for future reference.

License Number	5350340823624
License date	Jul 15, 2022

Printable Details

Licensed Content

Licensed Content Publisher	John Wiley and Sons
Licensed Content Publication	Journal of Polymer Science Part B: Polymer Physics
Licensed Content Title	Biomedical applications of biodegradable polymers
Licensed Content Author	Bret D. Ulery, Lakshmi S. Nair, Cato T. Laurencin
Licensed Content Date	May 5, 2011
Licensed Content Volume	49
Licensed Content Issue	12
Licensed Content Pages	33

Order Details

Type of use	Dissertation/Thesis
Requestor type	University/Academic
Format	Print and electronic
Portion	Figure/table
Number of figures/tables	1
Will you be translating?	No

About Your Work

Title	(BIS)PHOSPHONATE FUNCTIONALIZED POLYMERIC MATERIALS FOR BIOMEDICAL APPLICATIONS
Institution name	Bogazici University
Expected presentation date	Aug 2022

Additional Data

Portions	Table 1

Figure B.19. Permission from [14] John Wiley and Sons, Copyright (2011).

Thank you for your order.

This Agreement between Merve Seçkin Altuncu ("You") and Elsevier ("Elsevier") consists of your license details and the terms and conditions provided by Elsevier and Copyright Clearance Center.

Your confirmation email will contain your order number for future reference.

License Number	5350341193133
License date	Jul 15, 2022

Printable Details

Licensed Content

Licensed Content Publisher	Elsevier
Licensed Content Publication	Biotechnology Advances
Licensed Content Title	Lectin functionalized nanocarriers for gene delivery
Licensed Content Author	Virendra Gajbhiye,Shaoqin Gong
Licensed Content Date	September–October 2013
Licensed Content Volume	31
Licensed Content Issue	5
Licensed Content Pages	11

Order Details

Type of Use	reuse in a thesis/dissertation
Portion	figures/tables/illustrations
Number of figures/tables/illustrations	1
Format	both print and electronic
Are you the author of this Elsevier article?	No
Will you be translating?	No

About Your Work

Title	(BIS)PHOSPHONATE FUNCTIONALIZED POLYMERIC MATERIALS FOR BIOMEDICAL APPLICATIONS
Institution name	Bogazici University
Expected presentation date	Aug 2022

Additional Data

Portions	Figure 2

Figure B.20. Permission from [59] Elsevier, Copyright (2013).

LICENSED CONTENT

Publication Title	Australian journal of chemistry	**Country**	Australia
Author/Editor	COMMONWEALTH SCIENTIFIC AND INDUSTRIAL RESEARCH OR, INSTITUTE OF PHYSICS (GREAT BRITAIN)., AUSTRALIAN NATIONAL RESEARCH COUNCIL., AUSTRALIAN ACADEMY OF SCIENCE.	**Rightsholder**	CSIRO Publishing
		Publication Type	Journal
		URL	http://cass.nls.uk/
Date	01/01/1953		
Language	English		

REQUEST DETAILS

Portion Type	Chart/graph/table/figure	**Distribution**	Worldwide
Number of charts / graphs / tables / figures requested	1	**Translation**	Original language of publication
		Copies for the disabled?	No
Format (select all that apply)	Print, Electronic	**Minor editing privileges?**	No
Who will republish the content?	Not-for-profit entity	**Incidental promotional use?**	Yes
Duration of Use	Life of current edition	**Currency**	USD
Lifetime Unit Quantity	Up to 499		
Rights Requested	Main product		

NEW WORK DETAILS

Title	(BIS)PHOSPHONATE FUNCTIONALIZED POLYMERIC MATERIALS FOR BIOMEDICAL APPLICATIONS	**Institution name**	Bogazici University
		Expected presentation date	2022-08-23
Instructor name	Merve Seçkin Altuncu		

ADDITIONAL DETAILS

Order reference number	N/A	**The requesting person / organization to appear on the license**	Merve Seçkin Altuncu

REUSE CONTENT DETAILS

Title, description or numeric reference of the portion(s)	Figure 3	**Title of the article/chapter the portion is from**	Living Radical Polymerization by the RAFT Process—A First Update
Editor of portion(s)	N/A	**Author of portion(s)**	COMMONWEALTH SCIENTIFIC AND INDUSTRIAL RESEARCH OR; INSTITUTE OF PHYSICS (GREAT BRITAIN).; AUSTRALIAN NATIONAL RESEARCH COUNCIL.; AUSTRALIAN ACADEMY OF SCIENCE.
Volume of serial or monograph	59		
Page or page range of portion	669-692	**Issue, if republishing an article from a serial**	N/A
		Publication date of portion	1953-01-01

Figure B.21. Permission from [297] CSIRO Publishing, Copyright (2006).

LICENSED CONTENT

Publication Title	Tissue engineering. Part B, Reviews	Publication Type	e-Journal
Article Title	Injectable hydrogels as three-dimensional network reservoirs for osteoporosis treatment	Start Page	430
		End Page	454
Date	01/01/2008	Issue	5
Language	English	Volume	27
Country	United States of America	URL	http://www.liebertonline.com/teb
Rightsholder	Mary Ann Liebert Inc.		

REQUEST DETAILS

Portion Type	Image/photo/illustration	Distribution	Worldwide
Number of images / photos / illustrations	2	Translation	Original language of publication
		Copies for the disabled?	No
Format (select all that apply)	Print, Electronic	Minor editing privileges?	No
Who will republish the content?	Academic institution	Incidental promotional use?	Yes
Duration of Use	Life of current edition	Currency	USD
Lifetime Unit Quantity	Up to 499		
Rights Requested	Main product		

NEW WORK DETAILS

Title	(BIS)PHOSPHONATE FUNCTIONALIZED POLYMERIC MATERIALS FOR BIOMEDICAL APPLICATIONS	Institution name	Bogazici University
		Expected presentation date	2022-09-12
Instructor name	Merve Seçkin Altuncu		

ADDITIONAL DETAILS

Order reference number	N/A	The requesting person / organization to appear on the license	Merve SeçkinAltuncu

REUSE CONTENT DETAILS

Title, description or numeric reference of the portion(s)	Figure 3 and 4	Title of the article/chapter the portion is from	Injectable hydrogels as three-dimensional network reservoirs for osteoporosis treatment
Editor of portion(s)	Zheng, Zhi; Yu, Cui-Yun; Wei, Hua	Author of portion(s)	Zheng, Zhi; Yu, Cui-Yun; Wei, Hua
Volume of serial or monograph	27	Issue, if republishing an article from a serial	5
Page or page range of portion	430-454	Publication date of portion	2021-10-01

Figure B.22. Permission from [84] Mary Ann Liebert Inc., Copyright (2008).

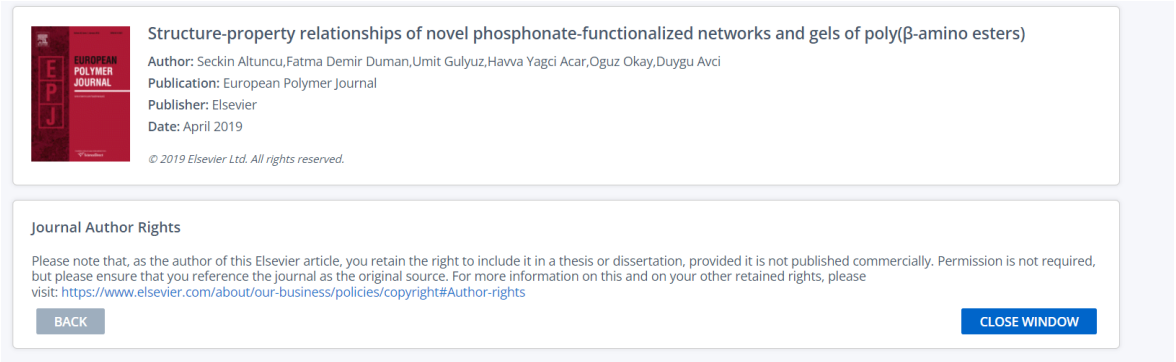

Figure B.23. Permission from (Chapter 3) Elsevier, Copyright (2019).

Thank you for your order.

This Agreement between Merve Seçkin Altuncu ("You") and John Wiley and Sons ("John Wiley and Sons") consists of your license details and the terms and conditions provided by John Wiley and Sons and Copyright Clearance Center.

Your confirmation email will contain your order number for future reference.

Printable Details

License Number	5384901266820
License date	Sep 09, 2022

Licensed Content

Licensed Content Publisher	John Wiley and Sons
Licensed Content Publication	JOURNAL OF BIOMEDICAL MATERIALS RESEARCH PART A
Licensed Content Title	Phosphonic acid-functionalized poly(amido amine) macromers for biomedical applications
Licensed Content Author	Duygu Avci, Havva Yagci Acar, Gozde Demirci, et al
Licensed Content Date	May 4, 2020
Licensed Content Volume	108
Licensed Content Issue	10
Licensed Content Pages	11

Order Details

Type of use	Dissertation/Thesis
Requestor type	Author of this Wiley article
Format	Print and electronic
Portion	Full article
Will you be translating?	No

About Your Work

Title	(BIS)PHOSPHONATE FUNCTIONALIZED POLYMERIC MATERIALS FOR BIOMEDICAL APPLICATIONS
Institution name	Bogazici University
Expected presentation date	Sep 2022

Additional Data

Figure B.24. Permission from (Chapter 4) John Wiley and Sons, Copyright (2020).